THE TENSILE PROPERTIES OF CERTAIN AGE-HARDENING ALUMINIUM - COPPER - MAGNESIUM ALLOYS

A thesis submitted for examination for the degree of Doctor of Philosophy of the University of London by :

Francis Russell Curry

July 1967

Synopsis

Single crystal and polycrystalline specimens of Al, 3.8 wt. % Cu, 0.56 wt. % Mg (7:1, Cu:Mg) and Al, 3.3 wt. % Cu, 1.5 wt. % Mg. (2.2:1, Cu:Mg) alloys, aged at 190°C, have been strained at a constant extension rate, in a tensometer designed to facilitate low temperature testing. The design of the tensometer and the growth of single crystals by the strain-anneal method have been described in detail.

In the early stages of ageing, material containing GPB zones was found to deform in a similar manner to pure aluminium. The yield strength appeared to be determined by the resistance encountered by dislocations shearing the zones, as calculated from current theories. Single crystal yield points and strain ageing serrations on polycrystal stress-strain curves have been explained in terms of dislocation multiplication as a result of magnesium atom pinning.

In peak aged and overaged material, θ' and S precipitates did not appear to deform, initially, with the matrix. The yield strength seemed to be controlled by the Orowan stress.

For alloys in all aged conditions, the strain-hardening characteristics of the polycrystals and the relationship between single crystal and polycrystal deformation in terms of the aggregate theories, have been examined. These results, together with the temperature dependence of the yield stress and the work-hardening rate, have pointed to the importance of the grain-boundary precipitate-free zones during the deformation of polycrystals. Metallographic studies of the fractures of single crystals and polycrystals indicated that apparent intercrystalline failure in well-aged alloys resulted from ductile fracture occurring preferentially in the precipitate-free boundary zones.

CONTENTS

1. INTRODUCTION

The strengthening of aluminium alloys as a result of controlled ageing treatments is well known as an important industrial process. It finds a wide application in aircraft engineering, mainly because of the favourable strength-to-weight ratio in the materials so produced.

The age-hardening phenomenon was discovered more than fifty years ago and attempts have been made ever since to explain the relationship between the strengthening and the microstructures produced by the precipitation processes. It is only recently that success in detail has begun to be reached and this is primarily due to the fact that accurate information about the microstructure of aged alloys, that is, the size, distribution, spacing and morphology of the precipitates can now be obtained directly by the examination of thin foils in the electron microscope. In addition, the details of the interactions between precipitates and dislocations during deformation may also be observed directly. When the results from this type of study are taken in conjunction with complementary information about the mechanical properties of aged alloys from tensile tests, it is then possible to relate the sources of strengthening to the relevant important microstructural features. Of particular value is information about the tensile behaviour of single crystals, from which quantitative tests of theories for the strengthening may be made. One purpose of the present investigation was to obtain information about the tensile properties of the alloys selected for study, with the object of correlating the changes in mechanical behaviour after ageing with

the structural changes as they are currently understood. Other aims will now be considered.

As part of a wider investigation into the role of the main alloying elements on the ageing behaviour of Duralumin-type alloys, several research projects have been undertaken previously in the Department of Metallurgy at Imperial College. These have been concerned with the constitution and age-hardening characteristics of high purity ternary and quarternary aluminium alloys which form the bases of the Duralumin types. Since very little of this previous work has been concerned with mechanical properties other than indentation hardness, another purpose of the present investigation was to initiate a study of the mechanical properties of these high-purity alloys, with the object of determining the strengthening effect associated with each alloying element. Due to the scarcity of data available on the strengths of high-purity aluminium alloys it was necessary to conduct tests initially on binary Al-Cu material, but most of the measurements were made on Al-Cu-Mg ternary alloys. This is the basic alloy system of most of the Duralumin-type alloys.

The choice of alloys used in this investigation was governed by several factors. First, the association of the work with the Duralumin-type alloys suggested that the amounts of copper and magnesium should be in the ratio of 7:1 by weight, respectively. However, the hardening then results from the structures found in the binary Al-Cu system in addition to the ternary ones. In order to separate the effects of these different structures, alloys of α (Al) - S

pseudo-binary composition, with a Cu:Mg ratio of 2.2:1 by weight, were also studied. The values for the copper and magnesium contents of both the alloys were taken from the phase diagram near the solubility limit of these elements at 500°C, which was chosen as the solution treatment temperature. This temperature is similar to that used in commercial practice and is the same as that used in previous age-hardening and X-ray investigations into Al-Cu-Mg alloys.

Alloys of 7:1 and 2.2:1 Cu:Mg ratios have been studied in some detail at the Fulmer Research Institute. The age-hardening and structural ageing characteristics are now well documented and thus the extension to mechanical property measurements is a logical one. The use of alloys of these compositions enables a direct study to be made of the effect of Mg additions to binary Al-Cu alloys. This constitutes a further purpose to the investigation.

It has already been emphasised that mechanical property data from single crystals of these alloys are useful, particularly when allied to information from electron microscope observations. In this connection, the final purpose to the work was to develop a technique for growing single crystals of these two alloys, and to compare their tensile properties with those of polycrystals.

The presentation of this work includes initially a description of the apparatus used and the experimental procedures employed. The design and construction of both the tensile testing machine and the strain-anneal apparatus, together with the determination of the

correct crystal growth conditions, occupied the major part of the time spent and so have been reported in some detail. In particular, a section is included on the method employed and the difficulties experienced in obtaining the critical conditions necessary for single crystal growth. This is followed by a review of the literature dealing with the important aspects of tensile deformation of precipitation hardening alloys, together with a resumé of the precipitation processes occurring in the particular alloys used in this investigation.

The results are mainly presented in graphical form, but a description of the important findings is also included in view of the large amount of data obtained and the number of different aspects of tensile deformation covered. In addition to the yield stress, tensile stress and elongation measurements, the results include the assessment of the work-hardening rate, the effect of temperature and grain size and the study of the fracture characteristics. The majority of these topics have also been studied with both single crystals and with polycrystalline material.

Finally, the discussion of the results is sub-divided into the three main aspects of the work, namely, the relationship between the tensile properties and the microstructures of the two alloys, the effect of Mg on the mechanical properties of Al-Cu alloys and the comparison between the behaviour of single crystals and polycrystals of the two alloys. Within each division, the agreement between observation and theory is examined, explanations are proposed for observations in terms of theory, and the correlation between various

effects is attempted. It is hoped, thereby, that a contribution is made towards a better understanding of the mechanical properties of alloys in the Al-Cu-Mg system.

2. APPARATUS AND EXPERIMENTAL PROCEDURE

2.1 Alloy Preparation

Alloys were cast by a semi-continuous technique at the British Aluminium Research Laboratories, from super-purity aluminium, (99.995%), electrolytic copper, added as an Al, 50% Cu hardener, and 99.9% magnesium. The melt was held at a temperature just above the melting point, and degassed with chlorine for 15 minutes prior to casting. The casting machine launders were designed to provide a non-turbulent flow of metal into the mould, and in this way, the ingots contained a minimum number of inclusions. The as-cast ingots were $2\frac{5}{8}$" in diameter by 3' in length, but only the centre 18" was fabricated for use. The analysis of the metal used in this investigation was as follows:-

	Identification	% Wt.Cu	% Wt.Mg	% Wt.Si	% Wt.Fe
a)	JWY	3.8	0.56	0.007	0.0035
b)	JWZ	3.3	1.58	0.003	0.0055
c)	KLY	3.8	0.55	N.A.	N.A.
d)	KLX	3.3	1.50	N.A.	N.A.

N.A. - not analysed.

Alloys KLY and KLX were made from aluminium of 99.999% purity.

Materials c) and d) and part of a) and b) were hot extruded at 450°C, after 3 hours homogenisation at this temperature. c) and d) were extruded to $\frac{3}{8}$" dia. rods, and a) and b) were extruded to $\frac{1}{4}$" diameter. The remaining portions of a) and b) were homogenised at

450°C for 12 hours, and hot pressed and cold-rolled, with intermediate annealing, to 5/16" thick sheet. Substantial preferred orientation was avoided in some of the material by cross-rolling. No detectable differences in mechanical properties were observed between the extruded and rolled alloys, although single crystals were grown more easily in the extruded samples and in the material which was not cross-rolled.

A binary Al-Cu alloy, of nominal composition Al, 3.5 wt. % Cu, was also manufactured using a similar casting procedure, but fabricated by rolling and cold-drawing. This alloy was not analysed.

2.2 Apparatus

2.2.1 The tensile testing machine

Tests were carried out on a constant extension-rate machine, designed to facilitate straining at low temperatures. Sectional elevations of the machine are shown in Fig. 1. The specimen was mounted in grips within the lower cage of the machine, which could be immersed in liquid coolant contained in a dewar flask. Extension of the specimen was carried out by the upward motion of a jointed central tie-rod and lead-screw, to which was attached the load-measuring dynamometer. The lead-screw thread was ground to an accuracy of 0.0005" per inch length. It was driven through a bronze nut, with anti-backlash device, housed in a straining-head, which was connected through a worm and pinion reduction gear and V-belt drive to a constant-speed induction motor.

The load range of the strain-gauge dynamometer was 0-2000 lbs., with a linearity of ± 1½%. Input was supplied at 18 v. d.c. from lead-acid accumulators, and the mV output was directly connected to a Honeywell electronic recorder. The load measurement accuracy was ± 1½% of any indicated value. The load measurement sensitivity was 0.5 lb.

Total machine elasticity at fullload was 0.135", of which 0.011" was elasticity of the dynamometer. Elongation measurement was made directly from the recorder chart, after correction for machine elasticity, since both the chart speed and extension rate were constant. For a large number of specimens, the % elongation at fracture measured from the chart, and directly on the specimen, agreed to within 2% elongation.

The specimen grips were of the Hounsfield split-chuck pattern.

The machine was calibrated with a proving ring, which had been checked on a Denison machine.

2.2.2 The tensile specimens

Test pieces were of circular cross-section, single shouldered, based on the Hounsfield design, and are shown in Fig. 2. Single crystal specimens were machined to a smaller size, but the ratio of the cross-sectional area of the gauge-length to the contact area between shoulder and grip was maintained at approximately 1:2.5, to minimise deformation at the grips.

Specimens were machined in pairs, using a special tool holder and 1/16" diameter bit supplied by Tensometer Limited.

2.2.3 The strain-anneal apparatus

The apparatus is shown in Fig. 3. It consisted of a salt bath, above which was mounted a mechanism for lowering the specimen into the salt. The bath consisted of a stainless steel container of pure potassium nitrate, maintained at the required temperature in a nichrome-wound pot furnace, insulated with asbestos. The bath temperature was controlled at $\pm$ 1°C from a Kelvin-Hughes controller connected to a chromel-alumel thermocouple located on the furnace windings. An external resistor, in series with the windings helped to reduce temperature variations. Measurement of the bath temperature was made by means of a stainless-steel sheathed chromel-alumel thermocouple immersed 1" below the surface. A water-cooled brass cylinder was suspended just above the salt surface. The specimen was held by a pin in a stainless steel piston, which slides in the cylinder. The piston was held at the end of a tie-rod connected to a rack and pinion; the pinion was driven, through a gearbox, from a synchronous motor. The motor speed was fixed (1 r.p.h.) but there was a choice of several specimen immersion speeds by connecting different gearbox output shafts to the pinion driving the rack.

The position of the water-cooled cylinder above the surface of the salt was adjustable, and this, together with the water flow rate, and the clearance between the piston and the cylinder wall, determined the temperature gradient on the specimen.

2.3 Experimental Procedure

2.3.1 Heat treatment

Specimens were degreased in benzene, prior to heat treatment. Solution treatment was carried out at 500°C ± 1°C for 18 hours, in a salt bath containing a 50% KNO_3 / 50% $NaNO_2$ mixture. The specimens were then quenched into water at 20°C ± 0.5°C, and immediately aged at 190°C ± 0.2°C in a silicone-oil bath, standing in an air-circulating oven. After ageing, they were again water quenched.

2.3.2 Tensile testing

Tensile testing was carried out at room-temperature and at three sub-zero temperatures, with the following mixtures:-

Acetone + solid CO_2	196°K (- 77°C)
40/60 Petroleum ether + liquid nitrogen	148°K (-125°C)
Boiling liquid nitrogen	77°K (-196°C)

When conducting tests the following procedures were carried out:

(i) The specimen gauge length and diameter were checked with a micrometer.

(ii) The recorder was standardised before use.

(iii) The dynamometer input voltage was recorded on the chart by shorting the accumulators across standard resistors, with a total resistance of 2001Ω , and feeding the potential difference across 1 Ω to the recorder. Thus an 18 v accumulator e.m.f. was recorded as 9 mV on the chart.

(iv) A machine deflection curve, using a 1" diameter steel specimen, was obtained for each series of tests at a given temperature, with a given dynamometer input voltage.

(v) The specimen was assembled in the machine with a small load to maintain alignment and to prevent icing in the grips or ball joints, while the coolant was added.

(vi) The machine cage and specimen were immersed in the low temperature bath for several minutes before a test commenced so that the temperatures of the various machine members reached a steady state; in practice, until the alignment load remained constant.

Not more than four consecutive tests could be made at -196°C, since the temperature of the dynamometer was lowered by conduction of heat through the tie-rod. This affected the dynamometer calibration, and further tests were delayed until the machine reached room temperature. When changing specimens after low temperature tests, the grips were de-iced and dried before a new specimen was assembled in the machine. The coolant level in the dewar flask was kept constant, by topping up, during tests which took several minutes to perform.

2.3.3 Grain size control

A range of different grain sizes was produced in extruded 7:1, Cu:Mg alloy by controlled heat treatments. The details are shown in Table 2.1 below.

Table 2.1

Heat Treatment	Grain size Mean Grain Dia. mm.	$d^{-\frac{1}{2}}$
60 mins at 475°C	0.1	3.16
20 mins at 500°C	0.175	2.4
40 mins at 520°C	0.22	2.13
180 mins at 560°C	0.36	1.67
Lowered through 20° - 560°C temp. gradient in the single crystal furnace	approx 0.9	1.2

The maximum grain size was limited to 0.9 mm since this was equivalent to approximately 20 grains per gauge length cross-section. Armstrong [1] has shown that where there is less than this number a specimen "size effect" may occur, which is caused by the orientation dependence of plastic flow in each grain. Although this was unlikely to be important in aged alloys, the limit of 20 grains per cross-section was kept because of the possibility of a "size effect" in quenched specimens.

The minimum annealing temperature which could be used was determined by the subsequent solution treatment temperature. It was found that after 1 hour at the usual solution treatment temperature of 500°C the grain size was greater than 0.2 mm. diameter and the range of grain sizes for studying mechanical property variations was, therefore, too small. In order to extend this range a minimum annealing temperature of 475°C was chosen, which was 10°C below the solid solubility limit of the α - phase for this alloy, so that solution treatment was carried out just inside the 2-phase region. After 1 hour at 475°C, the grain size was 0.1 mm. Thus, a range of grain sizes changing by almost a factor of 10 was examined.

Uniform grain sizes were not obtained even after reductions of almost 100% by rolling or pressing. It was found, however, that the residual stresses in the extruded material produced a uniform grain structure after annealing. This material was used as the starting material for each of the heat treatments in Table 2.1.

Due to the difficulties encountered in producing what was only a limited range of uniform grain sizes in the 7:1 Cu:Mg material, no attempt was made to repeat this for the 2.2:1, Cu:Mg alloy. In this alloy the temperature range for recrystallisation (between the limit of solid solubility and the solidus) was even smaller than that for the 7.1, Cu:Mg material.

2.3.4 The replication of fracture surfaces

Two-stage cellulose acetate - carbon replicas were made of the fracture surfaces of several tensile specimens, for electron microscopical examination. Similar techniques have been described by Kay [2]. Thin cellulose acetate film (0.003" "Bex" film) was laid on the fracture surface, and softened with drops of acetone. When the plastic had moulded to the fracture contours, it was allowed to dry, then stripped and mounted on a glass slide. 8 Å of 60/40 Au-Pd alloy was evaporated on the plastic at a nominal shadowing angle of 25° , followed by a deposit of 50-100 Å of carbon, evaporated normally.

The cellulose acetate was dissolved away in acetone and the carbon replica collected on a specimen grid.

2.4 The Preparation of Single Crystals

2.4.1 Crystal growth

The strain-anneal method [3] was used in this investigation, mainly because of the presence of Mg, with its associated problems of segregation and oxidation using melt methods. Starting with accurately shaped test-pieces, only the gauge-lengths were converted to single crystals, leaving the shoulders polycrystalline, and therefore stronger. This avoided the necessity to use shaping techniques such as spark, or acid machining. Oxidation of the specimens was minimised by annealing in a salt bath.

An as-machined specimen was first degreased and then given a pre-strain anneal, to produce a completely recrystallised, fine grain size structure. It was then strained 1-2% in a Hounsfield Tensometer, and electropolished to remove surface irregularities caused by machining, which might have provided extraneous nuclei. A longitudinal temperature gradient was produced in the specimen by lowering it into the salt bath. When the lower end of the gauge length reached the necessary temperature for recrystallisation one nucleus would then grow at the expense of the surrounding grains. The growth interface travelled up the specimen, and the temperature gradient ensured that the strained material in front of the growth interface was kept below the temperature required to nucleate new crystals.

The experimental conditions necessary for successful crystal growth were determined after a great deal of experimentation, and are listed in Table 2.2 for the two alloys.

Table 2.2

Treatment	7:1, Cu:Mg	2.2:1, Cu:Mg
1. Pre-strain anneal	(i) 30 mins at 500°C (ii) 5 mins at 555°C (iii) air cool	(i) 30 mins at 500°C (ii) 15 mins at 525°C (iii) acetone quench
2. Critical Strain ($\pm\frac{1}{8}\%$)	$1\frac{1}{2}\%$	$1-1\frac{1}{4}\%$
3. Reduction in gauge length dia. by electropolishing	0.003"	0.003"
4. Growth anneal salt bath temp.	555°C	525°C
5. Growth speed	0.17 cms/hour	0.17 cms/hour

The average yield for perfect or nearly perfect single crystals of each composition was about 25%, once the conditions had been established. In order to establish the correct growth conditions, seven major variables and four "constructional" variables were taken into consideration. The seven major variables, which were able to be measured and changed systematically are listed in Table 2.2 above, (there are three variables in the "pre-strain anneal" treatment). The four "constructional" variables contributed towards controlling the temperature gradient along the specimens, and consisted of the dimensions and positioning of the cooling block, the dimensions of the specimen holder and the method of holding the specimen. These were not easily changed and required modifications to the apparatus.

It is clearly impossible to establish the optimum value for each variable in an entirely systematic manner. Instead, it was found necessary to give particular attention to detailed factors, and to alter only one or two variables at a time after a close inspection of the specimen produced after each attempt. The direction in which the variables were altered was generally deduced from the theoretical description of the strain-anneal process by Williamson and Smallman[4].

They have treated the problem of continued single crystal growth as the minimisation of the probability of forming active nuclei for recrystallisation within the sample. The probability of nucleation is given by:-

$$P = \frac{Tg^2 \, e^{-\frac{Q}{KTg}} \, C.V.K.}{S.v.Qn} \qquad 2.1$$

$$\text{or, } P = \frac{(\frac{v}{B})^{\frac{Qn}{Qg}} \, C.V.Qg^2}{S.v.(\ln(B/v)^2) \, K.Qn} \qquad 2.2$$

where,

P = Total probability of nucleation in the entire sample.

Tg = Interfacial growth temperature.

Qn = Activation energy for nucleation.

Qg = Activation energy for growth.

K = Boltzmann's constant.

C = Probability of finding regions of lowest activation energy for nucleation, Qn, per unit volume.

V = Volume of specimen.

S = Temperature gradient.

v = Velocity of steady state growth = furnace velocity.

B = A constant, representing a limiting growth velocity.

Nucleation is associated with the polygonisation of regions of severe lattice bending caused by the accommodation of different slip characteristics in neighbouring grains in a polycrystal. Provided that the nucleus makes a large-angle boundary with the surrounding matrix, it will grow into a new crystal. Polygonisation may lead to recovery without recrystallisation, particularly at lower temperatures, and there is evidence that recovered regions can be stable in the presence of recrystallised grains. If so, these may form active nuclei during a growth anneal.

Although, more recently, different physical concepts of the nucleation of recrystallised grains have been proposed, the factors affecting the probability of extraneous nucleation, used in Williamson and Smallman's equations, probably remain valid. However, regardless of the true physical picture, the use of these equations, as shown below, resulted in successful crystal growth for the two alloys used in this investigation.

In order to minimise P, factors in the numerator of equation 2.1 or 2.2, must be small, and similarly those in the denominator must be large. Several of the factors, however, are interdependent.

(i) The temperature gradient, S, must be large, which means that the temperature must fall off rapidly ahead of the growth interface. This narrows the region ahead of the interface within which recovery can take place, and thus decreases the possibility of extraneous nucleation. In the apparatus described above, suspending the water-cooled cylinder as close as possible to the salt surface, without actually touching it, imposed a high temperature gradient on the specimen. This was further improved by using aluminium packing pieces between the specimen and piston to improve conduction, and by reducing the clearance between the piston and the cylinder wall, until the piston just failed to seize when it was partly immersed in the salt near the end of its travel. Measurement of the gradient along the specimen could not be made easily, but was estimated to be at least $100^{\circ}C/cm$.

(ii) The specimen volume, V, must be small and in this respect the specimens used for single crystal growth had their gauge diameters reduced from 0.179" to 0.110". Attempts were made to grow crystals from the larger specimens, but with less frequent success. This was believed to be due to a lowering of the temperature gradient along the specimen, by virtue of its greater cross-section for conduction.

(iii) Williamson and Smallman identify the factor B as a limiting growth velocity, so that if v approaches B, then P tends to infinity. B is orientation dependent, so that for favourable orientations, where it is large, P is reduced, and crystals are grown more easily.

It is known that a recrystallised grain grows more rapidly when its orientation is related to that of the parent grain by a rotation of 30° - 40° about a <111> axis. In the present investigation it was found that the orientations of the majority of single crystals lay in that region of the stereographic triangle between the centre and the <100> pole. It can be shown that this corresponds to a rotation of approximately 30° about a <111> axis, if it is assumed that the deformation texture of the extruded rod is <111> parallel to the wire axis and that this texture is retained after annealing. Barrett[5] has reported such a texture for extruded aluminium annealed at temperatures up to 500°C.

(iv) The specimen shape is expected to have an effect on nucleation. The majority of the deformation in a polycrystal initially takes place in each grain within a short distance from the grain boundary. Specimens with a large grain size, and a large free surface area deform in a more inhomogeneous fashion than small grain-sized specimens with a minimum of free surface. Totally enclosed grains within the specimen have boundaries over a solid angle 4π, those at the surface are enclosed over 2π, and those at an edge over π. Thus most heterogeneity of deformation is expected in grains which are not totally enclosed. In the present investigation, cylindrical specimens were used in preference to square or rectangular sectioned specimens.

(v) Specimen preparation is important in order to reduce the probability of nucleation. This arises from a consideration of Qn and C. Stress concentrations at defects in the alloy will raise the value of C, and reduce Qn. If the specimen has not fully recrystallised after the pre-strain anneal, recovered regions of the lattice remain, and provide active nuclei for recrystallisation during the higher temperature growth anneal. To reduce this danger a small percentage of impurity may be added to retard dislocation movements necessary for recovery, and this may account for the greater ease with which crystals are grown in less pure metal. For high-purity metals, rapid heating to the recrystallisation temperature prevents recovery at lower temperatures. Also, a very fine recrystallised grain size will absorb any recovered areas more quickly, by slight grain growth, than will a large recrystallised grain size. In the present work, a double annealing treatment was used, which consisted of a relatively low temperature anneal at 500°C to recrystallise the material to a fine grain-size, followed by a rapid anneal at a higher temperature, to allow the recrystallised grains to grow slightly, and absorb the recovered regions.

It was also necessary to quench these materials after the pre-anneal treatment and to introduce the critical strain as rapidly as possible after quenching, in order to minimise age hardening. The optimum quenching treatments were found to be air-cooling for the 7:1 Cu:Mg alloy and acetone quenching for the 2.2:1 alloy.

(vi) The inter-relationships between the factors are also important. The value of P is seen to be influenced by the ratio $^{Qn}/_{Qg}$. It has been shown from a study of the recrystallisation of aluminium[6] that $Qn \simeq Qg$, so that $^{Qn}/_{Qg} \simeq 1$. Since $^{v}/_{B}$ is < 1, then $(^{v}/_{B})^{Qn}/_{Qg}$ will be reduced by an increase in $^{Qn}/_{Qg}$. Such an increase may be effected by increasing Qn by specimen preparation as outlined in paragraph (v), and also by using the minimum value of critical strain. This is because $^{Qn}/_{Qg}$ has been shown to decrease rapidly with increasing strain[6].

A further decrease in P can result from a reduction in v. This decreases the $(^{v}/_{B})^{Qn}/_{Qg}$ term and increases the $\ln (^{B}/_{v})^{2}$ term in the denominator. These terms together outweigh the remaining $^{1}/_{v}$ term in the expression. The temperature of the growth interface, Tg, and v are also related. Low temperatures, which reduce the nucleation rate, must be accompanied by slow speeds to allow time for atomic transfer across the boundary between the growing crystal and the matrix ahead. Too low a temperature, however, will result in failure to produce a single crystal, because B, the limiting growth velocity, must also be temperature dependent. In the extreme, Tg may fall below the temperature necessary for recrystallisation.

In this experiment, practical considerations governed the choice of bath temperature which affects both Tg and S. Although the bath temperature was maintained at 15 - 20°C below the solidus temperature for each alloy, the actual growth interface temperature was less than this due to the high thermal conductivity of the specimen.

This also helped to minimise the change in the temperature gradient, S, as the proportion of specimen immersed increased with time.

(vii) The critical strain is important, although it is not included, as such, in Williamson and Smallman's equation for P. The significance of the critical strain is reflected solely in its effect on Qn and Qg. The presence of dislocations and point defects introduced by straining decreases the value of Qn, but also decreases Qg by increasing the randomness of atoms in the lattice ahead of the growing crystal. It has been observed that single crystals cease to grow at the upper ends of the gauge lengths, when the temperature gradient passes into the specimen shoulders. This may be due to the sharp change in section of the specimen, whereby the growing crystal has to absorb other crystals in directions normal to the temperature gradient, where B may be small due to the texture in the material. In addition, the absence of strain in the shoulder may increase the value of Qg; at the same time, though, Qn is increased, since the grains in the shoulder are strain-free, having recrystallised to a stable size governed by the pre-strain anneal. The critical strain, therefore, must be sufficient to provide a driving force for recrystallisation, but not so high that the value of Qn/Qg becomes too low. The value of the critical strain will vary with the type of material used, its fabrication, and its structure resulting from the pre-strain anneal. In the present investigation, it is noted that the critical strains were different for the two alloy compositions used.

2.4.2 The determination of crystal orientation

Crystal orientations were determined by the back-reflection Laue method, using standard laboratory equipment. This consisted of a Phillips PW.1009 X-ray set, using a sealed tube with Cu target, operated at 40 KV with 20 mA anode current. The specimen-to-film distance was 3 cm, which was set by means of a feeler-gauge.

A Greninger chart was used to measure the angular co-ordinates and inclinations of zone hyperbolae on the film. These were plotted as zone circles on a stereographic projection using a Wulff net. The intersections of the zone circles were indexed using a table of interplanar angles, and the whole projection was rotated to a standard (001) projection.

The accuracy of the method, using a 0.5 mm diameter collimator, which reduced exposure times to 30 mins, was estimated to be $\pm 2^{\circ}$.

A very similar method is described in detail by Cullity[7].

3. PREVIOUS WORK

3.1 Structural Changes During Ageing

The structural changes occurring during ageing have been studied by several different experimental techniques. The ageing kinetics of various alloys are known to be dependent on such variables as the solution treatment temperature, quenching rate, quenching temperature and alloy content. Electron microscopy has shown that these variables govern the defect structure of the supersaturated solid solution.(8)

In pure metals, this structure depends largely on the stacking fault energy, and in quenched aluminium it consists of prismatic dislocation loops, approximately 500 Å diameter, formed by the collapse and shear of condensed vacancy discs, as a result of the supersaturation of vacancies retained at the quenching temperature. In quenched Al alloys, excess vacancies form prismatic dislocation loops in dilute alloys and helices in concentrated alloys. The helices appear to originate at screw dislocations, which are believed to form by the gliding of prismatic loops, or by the action of Frank-Read sources from prismatic loops(9). The screw dislocations become immobilised by vacancy absorption. The change from loops to helices was thought to indicate that the presence of solute atoms reduces the effective vacancy supersaturation, so that nucleation of prismatic loops is prevented, and excess vacancies migrate to dislocations to form helices, or to sinks, e.g., at grain boundaries(9). The number of excess vacancies, deduced from the concentration of loops, is higher in supersaturated solid solutions than in pure metals.

This was believed to be caused by the lowering of the free energy of formation of a vacancy by an amount equal to the binding energy between it and a solute atom.

Thomas and Whelan[9] showed that for an Al, 4 wt.% Cu alloy quenched from 540°C, the volume fraction vacancy concentration was approximately 3×10^{-5}, and the loop diameter approximately 500 - 2000 Å. Embury and Nicholson[10] showed that the growth of loops and helices as a result of a slower quench or a short ageing treatment, may occur by climb.

The very early stages of ageing have been investigated by the changes in electrical resistivity, since continuous measurements are possible following rapid quenching[8]. The measured changes in electrical resistivity were caused principally by solute atom redistribution which overshadowed the contributions from dislocations and point defects. In supersaturated Al-Cu alloys, aged at low temperatures, it was found that the electrical resistivity increased rapidly at first and then more gradually. The fast reaction was attributed to clustering, whereby the majority of Cu atoms formed very small zones throughout the specimen. The reason for an increase in resistivity, which was also observed for Al-Ag and Al-Zn alloys was not known with certainty, but was thought to be caused by critical scattering by the very small zones. The clustering theory was supported by the observation of a large simultaneous evolution of heat, (approximately 3 kcal/gm. atom Cu), but clustering also implied an abnormally large diffusion coefficient.

This was thought to result from the high vacancy supersaturation existing after quenching. The slow reaction was believed to be caused by a gradual decrease in the vacancy concentration to its equilibrium value, after the initial rapid clustering.

The changes occurring during further ageing have been studied extensively by X-ray diffraction, electron diffraction and transmission electron microscopy. In the Al-Cu system, the structures responsible for ageing were first established by X-ray diffraction. GP(1) zones were shown to consist of Cu-rich discs on {100} Al planes, probably only 1 atomic plane thick and up to 100 Å in diameter[11]. They appeared as streaks between the matrix spots on single crystal X-ray photographs. Nicholson and Nutting[12] confirmed this from observations of zones by thin foil electron microscopy. GP(2) zones (or θ'') consisted of plates of ordered Cu and Al atoms, in a tetragonal structure, with an approximate composition $CuAl_2$. Their thickness was $\leq$ 100 Å, and their diameter was approximately 1500 Å. They were found to have, initially, a slightly different c parameter when formed from GP(1), compared with those nucleated directly from the matrix. Nicholson and Nutting[12] showed that coherency strains existed around GP(2) precipitates and extended from one precipitate to the next, near the peak, when the precipitate density was high. The orientation relationship for GP(2) and θ' was {100} precipitate // {100} matrix,

θ' precipitates were established as face-centred tetragonal, consisting of alternate layers of Cu and Al atoms, with a composition near Cu Al_2. The sequence of precipitation, GP(1) → GP(2) (θ") → θ' → θ, was shown to correlate with the hardness curves[13]. The earlier decomposition products were omitted in turn with decreasing supersaturation, which indicated that GP(2) and θ' may nucleate independently. GP(1) was found to be responsible for hardening at room temperature and in the first stage of ageing at 110° and 130°C. GP(2) was responsible for the second rise and was the main structure at the peak. θ' was associated with softening beyond the peak at 110° and 130°C. At lower supersaturations the amounts of θ' increased until it finally became the only hardening precipitate. In the electron microscope, no strain fields have been observed around θ' precipitates and the existence of structural dislocations has been suggested[14]. Replicas showed that θ' was precipitated preferentially on certain sites in the matrix[15], and these were later identified as the helical dislocations formed during the quench[16]. Nicholson[17] showed that only two orientations of θ' nucleated heterogeneously on helices, and that the missing orientation was that in which the Burgers vector of the dislocation was perpendicular to the misfit vector of the precipitate. This was believed to be a general feature of a partially coherent precipitate nucleating on a dislocation. The lattice misfit between precipitate and matrix is best accommodated if the Burgers vector of the dislocation is parallel to the misfit vector of the precipitate.

The dislocation-nucleated θ' accounted for much of the total θ' precipitated, since large precipitates grew from each helix. This produced a very heterogeneous structure in peak aged alloys, which also contained GP(2), and this feature was thought to account for the wide scatter in the mechanical behaviour of crystals aged near the peak, (Section 3.2.1). θ' was also found to be nucleated at other dislocations and sub-boundary sites.

Heterogeneous precipitation of θ at grain boundaries is accompanied by the formation of precipitate-free "denuded" zones. (see Section 3.3). These zones were shown by Kelly and Nicholson[8] to be denuded of vacancies, rather than solute atoms. θ' precipitates were seen growing preferentially near denuded zones and this was believed to be due to the larger atomic volume of the θ' compared with the matrix, so that nucleation and growth of θ' required vacancy emission.

The ageing of Al-Cu-Mg alloys has been extensively studied by hardness measurements[18] and X-ray diffraction[19]. Particular attention has been paid to alloys of 2.2 : 1, Cu:Mg ratio occurring in the pseudobinary Al-S system, and those containing 7:1, Cu:Mg ratio on which some Duralumin-type alloys are based. In the latter alloys, Al-Cu binary precipitates, together with ternary structures, were responsible for hardening. (Note, 2.2:1, Cu:Mg ratio is almost equivalent to the equiatomic ratio, and 7:1 by weight is equivalent to 2.7:1 by atoms).

GP B zones, analogous to GP(1), were found to form very rapidly over a wide range of composition, and to be stable up to 240°C. The diffuse X-ray diffractions produced by them have been indexed as tetragonal. Silcock[19] interpreted the structure in terms of a needle-shaped zone, 10-20 Å diameter, 40-80 Å long. Gerold and Haberkorn[20] interpreted their results as spherical shaped zones, but Brook[21], and Kelly and Nicholson[8] considered needle-shaped to be more feasible.

At high ageing temperatures (> 240°C) a similar structure to GP B, but with sharper diffraction spots, has been observed, termed GP B(2) by Silcock[19]. The structure has not been determined, but it was assumed to be an ordered segregate, since it was discovered in 7:1, Cu:Mg alloys, and also in 1:6 Cu:Mg alloys aged at 190°C.[21]

S phase, of composition approximately Cu Mg Al_2, has a face centred orthorhombic structure. There is some evidence[22] that an S' phase exists, but its structure is very similar to S, with only a slight distortion of the diffraction spots. The orientation relationship between S and the matrix was shown to be $[100]_S$ // $[100]_{Al}$; $[010]_S$ // $[021]_{Al}$; $[001]_S$ // $[012]_{Al}$.

The ageing sequence for Al-S alloys has been shown to be analogous to that of Al-Cu, and to correlate with the hardness curves[19]. An initial plateau, observed at all ageing temperatures up to 240°C, resulted from precipitation of GP B. At the end of the plateau at temperatures > 110°C, S' was formed, and increased

in amount to 25% at the peak. Rapid softening was associated with the disappearance of GP B. At 240°C, the peak was as high as at 130°C, and the structure then consisted of GP B(2) and S'. Softening was again associated with the disappearance of the zones.

In 7:1, Cu:Mg alloys at temperatures up to 130°C, the initial rise to the plateau was due to GP B and GP(1). Both these disappeared on the rise to the peak, which was associated with GP(2) and S'. At the peak, the structure consisted of S' and θ', but no zones. At 165°C, the initial rise and plateau were due to GP B, the rise to the peak was due to GP(2) and S', and the peak was associated with S' and θ' as before. At 190°C, and above, the rise to the peak, and the peak, were due to GP B(2), S' and θ'. S' appeared very early, and GP B(2) persisted well beyond the peak, when S was present.

Since 7:1, Cu:Mg alloys contained a mixture of the precipitates found in Al-Cu and Al-S alloys, Hardy[18] attempted to synthesise the hardness curves from those of the two binary alloys. This was unsuccessful, since the presence of Mg in the 7:1 alloys accelerated the formation of GP(1) and θ', and caused preferential nucleation of θ', responsible for the peak at 130°C and 165°C, instead of GP(2) as in the binary system.

Wilson and Partridge[23] have studied the nucleation and growth of S' precipitates in an Al, 2.5 wt.% Cu, 1.2 wt.% Mg alloy, aged at 190°C. The as-quenched alloy contained a large number of loops

and helices, which grew, after short ageing times, by a climb process as described by Embury and Nicholson[10]. S' was nucleated heterogeneously on the loops and helices and grew as lath-shaped precipitates along <100> directions. The laths lay in $\{210\}_{Al}$ planes with a common <100> axis and so formed corrugated sheets under certain conditions. An attempt was made to show that the morphology of the S' was consistent with the relative values of the interfacial energies at each of its faces. The interfacial energies were estimated from the mismatch between the precipitate and matrix planes at each face. The lath shape of the S' was shown to be consistent with the relative interfacial energies, but some of the details of the analysis, in particular the $\{210\}_{Al}$ interplanar spacings and the choice of matching precipitate and matrix planes, were unsatisfactory. The formation of "corrugated sheets" of laths at dislocations was shown to occur on planes such that the misfit vectors of the precipitates were as near parallel as possible to the Burgers vector of the dislocation. Thus for a dislocation loop lying in a {110} plane, a composite sheet of S' may grow by lath formation on a pair of conjugate {210} planes. The particular pair of planes chosen was shown to be those which produced maximum relief of misfit strain, and at the same time reduced the deviation of the dislocation loop from its {110} plane to a minimum.

Vaughan[24] has studied the precipitation process in an Al, 3.3 wt.% Cu, 1.58 wt.% Mg alloy, aged at temperatures up to 190°C. The structure of the quenched alloy consisted of loops and helices;

more loops being present than helices. In the early stages of ageing, growth of the loops by climb was observed. The presence of GP B zones was detected as streaks on electron diffraction patterns, but the zones themselves could not be resolved on electron micrographs. This was attributed to their shape, or to the absence of an associated strain field. No distinction was possible between S' and S phases on electron micrographs, which appeared as lath-shaped precipitates, nucleated entirely on dislocation loops and helices. Preferential nucleation of S precipitates of certain orientations on the loops and helices was observed. It was shown that the S orientations were such that the Burgers vector of the dislocations lay in the misfit planes of these precipitates. Precipitates of other orientations would not be able to accomodate the misfit so well.

3.2 The Mechanical Properties of Aged Alloys

3.2.1 The change in mechanical properties with ageing

Until recently, the effect of ageing on mechanical properties had been mainly investigated by means of hardness changes. Previous work on tensile properties of relatively impure material showed that yield stress and tensile strength changed with ageing time in a similar manner to hardness, although not at the same rate[25]. Ductility has been known to decrease markedly in Al-Cu and Duralumin alloys after ageing above room temperature[25]. Extensive hardness measurements have been made by Hardy[26] on high purity Al-Cu alloys and Al-Cu-Mg alloys[18].

Tensile tests on single crystals have shown similar changes with ageing. Kelly and Nicholson[8] reported measurements made by Dew-Hughes on Al, 4 wt.%Cu crystals, which showed that critical resolved shear stress, (C.R.S.S.), and hardness values on the same specimens varied in a similar manner with ageing time. The C.R.S.S. reached a peak after the hardness peak. C.R.S.S. ageing curves for Al, 4wt.%Cu crystals aged at 130°C, 165°C, and 190°C have been reported by Dew-Hughes and Robertson[27], Byrne, Fine and Kelly[28] and Bonar[29]. In each case the shapes were characteristic of the corresponding hardness curves. Bonar also showed that the rate of work-hardening in this alloy, aged at 190°C, measured from the slope of the stress-strain curve at 2% strain, changed abruptly from a low value of approximately 50 kg/mm^2 characteristic of as-quenched and lightly aged crystals, to a high value of approximately 300 kg/mm^2 characteristic of over aged alloys, at about the time that the C.R.S.S. reached its peak value.

These mechanical property changes have been shown to have a marked effect on the form of the stress-strain curve as ageing proceeds. Corderoy and Honeycombe[30] illustrated this for polycrystalline Cu, 8.5 wt.% and 10 wt.% In alloys, aged to contain non-coherent Cu_9In_4 precipitates on $\{100\}_{Cu}$ planes. The stress-strain curves were parabolic at all stages of ageing. Initially, the proof stress and rate of work-hardening were small, but they increased steadily with ageing time, and both reached maximum values at the peak aged condition. At room temperature, and below,

the ductility of the alloys decreased with increasing ageing time.

Information on polycrystalline Al, 4wt.% Cu alloys has been obtained by Matsuura, Izumi and Koda[31,32]. Alloys were tested at 77°K in the as-quenched condition and after ageing for times up to the peak at 130°C, to contain GP(1) and GP(2) zones. The stress-strain curves were parabolic and the yield stresses increased up to the peak, although the rates of work-hardening remained very similar to that of the as-quenched alloy. In a later paper[32], Al, 4 wt.% Cu alloys, aged at 240°C to contain θ' precipitates, were shown to have only a slightly larger yield stress, but a very much greater rate of work-hardening than the as-quenched alloy, for the first 5% strain, after which the rate of work hardening decreased to a lower value. Shaw et al[33] have presented stress-strain curves for polycrystalline Al,3,4 and 5 wt.% Cu alloys aged to contain dispersions of θ - Cu Al_2. These curves were all parabolic and showed very large initial rates of work-hardening which decreased markedly by the time the strain reached approximately 5%. This characteristic of dispersion-hardened polycrystalline alloys has been illustrated by Hart[34] who showed that for Al-Cu containing θ precipitates the increase in flow stress of the dispersion-hardened material over that of the matrix solid solution reached a maximum value at 5 - 10% strain. Beyond this, the two curves were almost parallel.

The change in the form of stress-strain curves for single crystals as ageing proceeds was first demonstrated by Carlsen and Honeycombe[35]. Crystals of Al, 3.5 wt.% Cu alloy were tested at room temperature and 77°K in the solution treated, peak-aged at 190°C and overaged conditions. The solution treated crystals had low C.R.S.S. values and very low rates of work-hardening. The peak-aged crystals had large C.R.S.S. values and initially very rapid rates of work-hardening which decreased after 5% strain to the solution treated value. Overaged crystals had similar curves to the peak-aged crystals but the C.R.S.S. was lower than the solution treated value. Greetham and Honeycombe[36] confirmed these trends on Al, 4.5 wt.% Cu and found, in addition, that crystals aged before the peak exhibited stress-strain curves which were similar to those of the solution treated alloy, but with larger C.R.S.S. values.

Stress-strain curves for aged Al, 4 wt.% Cu alloys have been described by Dew-Hughes and Robertson[27], Byrne, Fine and Kelly[28], Price and Kelly[37], Bonar[29] and Matsuura and Koda[38]. When aged at 130°C, this alloy contains only coherent precipitates at all stages up to the peak. Crystals were shown to exhibit no transition in the form of the stress-strain curves, which were similar to those of pure Al crystals with the same orientations. Crystals aged before the peak at 190°C, and containing only coherent precipitates, also deformed in a similar way to pure Al, whereas those aged at and beyond the peak to contain θ' or θ precipitates were shown to have stress-strain curves similar to those of polycrystalline material.

The transition from low to high rates of work-hardening thus corresponded to the stage at which partially or non-coherent precipitates predominated in the material. Bonar[29] pointed out that in the transition region there was a wide scatter in the C.R.S.S. values and the rates of work-hardening.

The stress-strain curves of Al, 20 wt.% Ag alloys aged at room temperature and at 160°C have also been studied[39]. Both these treatments produced coherent precipitates (clusters and GP zones, respectively), and the crystals deformed by single slip in a similar manner to pure Al, with low rates of work-hardening. Price and Kelly[37] confirmed this result for GP zone-hardened crystals aged at 160°C and showed also that crystals aged to the peak at 200°C, containing γ' precipitates, deformed by multiple slip from the start, in a similar manner to Al-Cu crystals containing θ'. Results were also obtained on Al, 15 wt.% Zn alloys, in the solution treated condition, aged at room temperature to produce GP zones and aged at 160°C to produce platelets of the f.c.c. intermediate phase α'. The solution treated and zone-hardened crystals showed deformation characteristics similar to those of the corresponding Al-Cu and Al-Ag alloys. The crystals containing the α' precipitate also deformed in a similar manner to the zone-hardened crystals. It was shown that these precipitates did not provide strong obstacles to dislocation motion and could deform easily with the matrix, since they formed in an identical orientation with only slight differences in the lattice spacing. This was in contrast to the nature of θ' in

Al-Cu and Υ' in Al-Ag, which are hard phases, unlikely to deform with the matrix at low strains. Thus the nature of the precipitates was also shown to determine whether a transition occurred in the stress-strain curves as ageing proceeds.

Price and Kelly[40] also studied the deformation of Cu, 1.8 wt.% Be crystals aged to contain either GP zones of Be-rich plates on $\{100\}_{Cu}$ planes, or overaged to contain Cu-Be intermetallic Υ precipitates. The stress-strain curves were of the two types characteristic of those of Al-Cu alloys containing GP zones or θ' respectively.

A change in the form of stress-strain curves associated solely with testing temperature has been shown by De Luca and Byrne[41] for Mg, 1.2 wt.% Mn crystals in the as-quenched condition and after ageing to peak hardness at 300°C. It was found that the rates of work-hardening for pure Mg, quenched Mg-Mn and hardened Mg-Mn crystals were all low at room temperature, but very high for the hardened Mg-Mn alloy at 77°K. The precipitates were believed to deform since the crystal rotations were consistent with single slip. No detailed explanation has been given.

3.2.2 Strain ageing

Strain ageing effects may take the form of initial yield points, multiple yielding (serrated stress-strain curves or the Portevin - Le Chatelier effect), or flow stress increments in interrupted low temperature tests.

Initial yielding occurs mainly in Al-Mg alloys[42] and experiments on Al, 3 - 7 wt.% Mg alloys showed that initial yield points occurred at temperatures greater than -70°C in suitably heat-treated material. The effects were attributed solely to the Mg atoms, for three reasons. First, they were not observed in pure Al. Second, quench-ageing experiments (measuring the rate of return of the yield point, suppressed by quenching from a high temperature) indicated that the kinetics were controlled by the activation energy for Mg atom diffusion. Third, precipitation of Mg in the 7 wt.% Mg alloy reduced the magnitude of the yield, whereas identical heat treatment of the $3\frac{1}{2}$ wt.% Mg alloy, in which no precipitation occurred, produced no change. A $d^{-\frac{1}{2}}$ dependence of the yield stress suggested that Mg atom segregation at grain boundaries was hindering the propagation of slip from one grain to the next.

Multiple yielding, either during incremental or continuous loading tests, has been observed on commercial Al[42, 43], Al-Cu[43, 44], Al-Mg[44, 45], Duralumin[42,44] and other alloys[42]. The effect, using soft-beam machines, consists of numerous steps along the work-hardening portion of the stress-strain curve, where extension occurs at constant load, and in hard beam machines consists of serrations or oscillations where sudden extensions cause stress relaxations. The magnitude of the effect is strain rate and temperature[44,45,46] dependent, and the kinetics have been studied by means of interrupted low temperature tests,[42,46,47] where a short ageing treatment at a higher temperature produces a transient

increase in flow stress on resuming the test at the lower temperature.

The mechanism of strain ageing in these alloys is thought to be similar to that in steel, namely the Cottrell - locking of dislocations by impurity atom atmospheres.[46,47,48] Since the interaction energy between a substitutional solute atom and a dislocation is less than that for an interstitial atom, the effect is less marked in substitutional alloys. There is good evidence for the Cottrell model. First, strain ageing is not commonly observed in pure Al[43], but appears in commercial Al[42,43]. Second, it is most marked in quenched age-hardening alloys, eg. Duralumin[42]; also, the effect decreases in the lightly aged alloy and is absent in the fully-aged material. Third, it occurs mainly at temperatures near room temperature[43,45,46].

However, in Al-Mg alloys, it was found that the activation energy for strain ageing was about three times smaller than that for Mg diffusion in Al[46]. Furthermore, strain ageing in all alloys only occurred after some plastic deformation had taken place. To account for this, Cottrell[48] suggested that the diffusion rates of solute atoms were greatly increased by the creation of vacancies during deformation, thus accounting for the low observed activation energies for diffusion in Al-Mg, the necessity for prior strain, and the enhanced effect in quenched alloys. Results on Al-Mg by Westwood and Broom[47] supported this idea.

Sperry[49] pointed out that the Cottrell atmosphere theory failed to explain why strain-ageing was so marked in Al-Mg alloys which show a rapid, low temperature recovery from cold-work, whereas, in other substitutional alloys, it only occurs under special conditions. Also, Sperry claimed that it failed to explain why cold rolling suppressed the effect, although, in tensile tests the magnitude of the serrations increased with strain. However, it does not seem to be generally accepted that cold-rolling suppresses strain-ageing in Al-Mg alloys[50].

As an alternative, it was postulated that the elastic interaction between moving dislocations and point defects caused the thermally activated jumps to be directed towards the dislocations. Thus, after the passage of a number of dislocations along a glide plane, a segregation of defects would be produced, and the resulting lattice distortion would ultimately prevent the passage of further dislocations. Diffusion of the defects back to a random distribution would then release a pile-up of dislocations, producing softening. While being able to account qualitatively for various aspects of the Portevin-Le Chatelier effect, no experimental evidence was offered for this model, and no quantitative support was described.

Thomas[51] has recently studied the Portevin-Le Chatelier effect in a quenched commercial Al, 5 wt.% Mg alloy, as a function of strain rate, grain size and testing temperature. Two effects were observed. The first was associated with coarse grain size material (> 0.6 mm. dia.)

at all temperatures in the range -50°C to +50°C, and with fine grain size material below 0°C. Serrations on the stress-strain curve increased in size with increasing strain, and the stress at which the serrations started decreased with increasing temperature. The effect was attributed to the formation of Cottrell atmospheres and the calculated activation energy for the process agreed with that of Westwood and Broom[47].

The second effect was associated with fine grain size material tested above 0°C and was characterised by the sudden appearance of large regular serrations at approximately 5% strain, which formed plateaux on the stress-strain curves. The serrations corresponded to the formation of regular parallel surface markings on the specimen at 53° to the tensile axis. An increase in testing temperature, or a decrease in strain rate, or a decrease in grain size, all delayed the start of the serrations. Due to this reverse temperature dependence, a new mechanism was proposed. At the start of deformation, at temperatures above 0°C, dislocations are readily locked by solute atmospheres. New dislocations are produced and the material work hardens until the stress required to release the locked dislocations is reached. This release occurs at a stress concentration, e.g., near the grips, and triggers similar releases in grains along the line of maximum shear stress in the specimen. Raising the temperature increases the size of the solute atmospheres, and, therefore, the stress required to release the dislocations. Small grain sizes limit the lengths of locked dislocations and decreasing the strain rate

increases the time in which atmospheres may form; both of these increase the stress for catastrophic dislocation release, as observed.

This model is also only able to account qualitatively for certain aspects of the observed effect. It makes no attempt to explain why there is a limiting grain size for the effect at 0.6 mm. dia; nor is the explanation for the observed direction of the surface markings, at 53° to the specimen axis, entirely satisfactory.

3.2.3 Strain-induced precipitation.

It is known that the kinetics of zone formation in supersaturated alloys are sensitive to the perfection of the matrix lattice.(8) Thus the zone structure may be changed during a tensile test as a result of the influence of dislocations introduced by the deformation. This will alter the form of the stress-strain curves.

It was found that for quenched Al-Cu single crystals the stress-strain curves showed higher rates of work-hardening at room temperature than at 77°K(35). The effect was attributed to strain-induced GP(1) formation, and this was supported by observations on the change in electrical resistivity of Al-Cu wires during deformation, which showed anomalous increases at room temperature, which were not observed at 77°K.(52,53)

Investigation of this effect was carried out by means of interrupted tensile tests. To distinguish between strain ageing (Section 3.2.2) and strain-induced precipitation, Greetham and

Honeycombe[36] used different testing procedures on Al, 4.5 wt.% Cu single crystals. Specimens were either rested for a short time (under load, or unloaded) at the testing temperature before restraining, or rested, unloaded, at a higher temperature before restraining. Solution treated crystals exhibited transient yield points (strain ageing) and permanent flow stress increments (strain-induced precipitation) after interrupting tests at 77°K for a short time at room temperature. Only a permanent increase was obtained for reverted Al-Cu crystals[54], since the vacancy concentration was much lower than in the solution treated alloy. Ageing at room temperature, during room temperature deformation, produced only a permanent increase in flow stress[35,36], which was less than that found during deformation at 77°K. This indicated that some strain-induced precipitation had already occurred before the test was interrupted.

Aged crystals containing GP(1) zones and fully aged crystals containing GP(2) and θ' also showed, after testing, both transient and permanent increases in the flow stress, which, however, were smaller than those of the solution treated crystals. Their existence, nevertheless, implied that the matrix was still supersaturated, even in the fully aged condition.

Overaged crystals showed only a strain-ageing effect after resting at room temperature during deformation at 77°K. The matrix was estimated to contain approximately 0.2% Cu at this stage.

3.2.4 Yield points.

In single crystals, yield points have been observed which are associated with the geometrical changes due to slip. The phenomenon is known as geometrical softening, and it occurs in crystals with low work-hardening rates deforming by single slip. It is caused by the rotation of the slip direction in the crystal towards the tensile axis. The yield effects may consist of load drops, or abrupt changes in the direction of the stress-strain curve at the start of plastic flow. Examples of yield point effects have been observed in solution treated Al-Cu crystals tested at room temperature and $77^{o}K$[36] and in crystals containing GP(1) zones tested at $77^{o}K$.[36,37]

Kelly and Nicholson[8] proposed that where the C.R.S.S. for precipitation-hardened crystals was sufficiently large and the work-hardening rate sufficiently small, then an instability would be expected at the yield point. The work-hardening rate on the load-elongation curve was given by:-

$$\frac{dF}{dl} = \frac{A_o}{\cos\varphi_o . l_o}\left(\frac{1}{\cos^2\lambda \,.\, \cos\varphi_o}\cdot\frac{d\tau}{da} - \frac{\tau.\tan^3\lambda}{\sin\lambda_o}\right) \qquad 3.1.$$

where A_o = Initial cross-sectional area of crystal.

φ_o = Initial angle between tensile axis and glide plane normal.

λ_o = Initial angle between tensile axis and slip direction.

τ = Resolved shear stress.

$\frac{d\tau}{da}$ = Rate of work-hardening of resolved shear stress-glide strain curve.

If $\frac{d\tau}{da}$ was not sufficiently large, then an instability, ($\frac{dF}{dl} \leqslant 0$) would result, when,

$$\frac{1}{\cos^2 \lambda . \cos \varphi_o} \cdot \frac{d\tau}{da} \leqslant \frac{\tau \tan^3 \lambda}{\sin \lambda_o}$$

$$\therefore \quad \frac{d\tau}{da} \leqslant \tau \tan^2 \lambda . \cos \lambda . \cos \varphi .$$

For typical values of λ and φ, each equal to approximately 45^o, $\cos \lambda . \cos \varphi$ is approximately 0.5,

thus:-

$$\frac{d\tau}{da} \leqslant \frac{\tau}{2} \qquad 3.2.$$

For pure f.c.c. metals, $\frac{d\tau}{da}$ during easy glide is of the order of 1 kg/mm^2, and the C.R.S.S. is very much less, so that no instability occurs. In alloy crystals, the rates of work hardening during easy glide may still be only approximately 1 kg/mm^2, but the C.R.S.S. is much larger, and tests are unstable.

A second approach was made by Price and Kelly[37] as a result of studying yield points in zone hardened Al-Cu, Al-Ag and Al-Zn crystals. The distinction between geometricl softening and genuine yield-points was made by predicting the course of the load-elongation curves, after yielding, in crystals with zero work-hardening rates, as a result of geometrical softening, then comparing these with the experimental curves. From the Schmid equation[55]:-

$$\tau = \frac{P}{A} . \cos \lambda . \cos \varphi .$$

where τ = shear stress on the glide plane.

P = tensile load

A = cross-sectional area

λ, φ are as above.

it was shown that since the slip plane area, $\frac{A}{\cos\varphi}$ remained constant during single slip, then $\tau = \frac{P.\cos\varphi}{A}\left(1 - \frac{\sin^2\lambda_o}{(1+\varepsilon)^2}\right)^{\frac{1}{2}}$, where the tensile strain, ε, is given by, $1 + \varepsilon = \frac{\sin\lambda_o}{\sin\lambda}$.

Thus, $P = \frac{\tau.A}{\cos\varphi}\left(1 - \frac{\sin^2\lambda_o}{(1+\varepsilon)^2}\right)^{-\frac{1}{2}}$.

and for a zero work hardening rate, τ is independent of ε and is given by:-

$$\tau = \tau_o = \frac{P_o}{A_o}.\cos\varphi_o.\cos\lambda_o. \qquad \text{where Po = load at yield.}$$

$$\therefore P = P_o.\cos\lambda_o\left(1 - \frac{\sin^2\lambda_o}{(1+\varepsilon)^2}\right)^{-\frac{1}{2}} \qquad 3.3$$

It was predicted, therefore, that an initial yield drop occurs in any crystal when there is no work-hardening, regardless of orientation.

The Al-Cu and Al-Zn crystals showed good agreement between the measured load-elongation curve and the calculated one over the region of negative slope after the yield. These yield drops were attributed to geometrical softening. The Al-Ag crystals showed more rapid yield drops than those predicted by geometrical softening, and these were attributed to a genuine yield point.

3.2.5 The temperature dependence of the mechanical properties.

This has been determined from the changes in the yield stress and the form of the stress-strain curves at different testing temperatures, and from measurements of the reversible change of flow stress.

For pure aluminium single crystals, the C.R.S.S. increases markedly at temperatures less than 150 - 200°K.[56] The increase between room temperature and 77°K is approximately 400%. (The increase in elastic modulus over this temperature range is approximately 6%). The temperature dependence is almost 1 kg/mm^2 / 100°K at 77°K.[56] For polycrystals, the temperature dependence of the proof stress is probably very similar, (the temperature dependence for Cu polycrystals is approximately 0.5 - 1 kg/mm^2 / 100°K at 77°K.[57]) It should be noted that these temperature dependences may simply reflect the very large temperature dependence of the rate of work-hardening in f.c.c. metals. This is almost certainly true for polycrystals and may even be true for single crystals, since the temperature dependence of the stress at which plastic deformation is first detected (approximately 10^{-4}% strain) has been found to be about 0.1 kg/mm^2 / 100°K at 77°K for both single crystals and polycrystals of pure aluminium.[58]

In the age hardening alloys, the temperature dependence of the yield stress is highest for solution treated, and lowest for aged material.[28,58] Solution treated or reverted Al, 4 wt.% Cu crystals show a marked increase in C.R.S.S. at temperatures less than 150°K - 200°K[28,54,59], which is of the order of 50% between room temperature and 77°K.[28,29,54,59] The temperature dependence at 77°K is 1.5 - 3 kg/mm^2/ 100°K[28,54,59], for this alloy, but for Al-Zn is only 0.5 kg/mm^2/ 100°K[60]. Polycrystalline aluminium solid solution alloys show very temperature dependent rates of work-hardening

which increase with the solute content in the same way as the proof stresses.[61]

In Al, 4 wt.% Cu crystals containing GP(1) zones, the temperature dependence of the C.R.S.S. is very similar to that of the supersaturated solid solution crystals.[28,54,59] For crystals containing GP(2) zones, the increase in C.R.S.S. between room temperature and 77°K was approximately 20%,[28,37] and the temperature dependence at 77°K was 1 - 2 kg/mm^2 / 100°K.[28,59] For Al-Zn alloys containing zones the respective values were 13% and 1 kg/mm^2 [37,60] and for Al-Ag, the temperature dependence was very small and equal only to that of the elastic constants.[39]

Alloys containing intermediate and equilibrium precipitates (e.g. θ' and θ in Al-Cu[28]) show a temperature dependence of the C.R.S.S. which is similar to that of pure aluminium.

At low temperatures, only Stages I and II appear in the stress-strain curves of pure f.c.c. metal single crystals. As the temperature is increased Stage III becomes more prominent.[62] In solid solution and zone hardened aluminium alloys the extent of Stages I and II is increased and Stage III is steepened relative to pure Al. The effect of temperature is qualitatively the same as in the pure metal.[62] The stress-strain curves of polycrystals consist mainly of Stage III, and for pure Al and Al solid solutions Dorn et al[61] have shown that the work-hardening rate and the ductility both increase as the temperature is lowered.

Single crystals and polycrystals of alloys containing non-deformable precipitates have similar stress-strain curves which, in general, also diverge as the temperature is lowered.

There are two contributions to this divergence, which causes an increase in the flow stress for a given strain at the lower temperature. First, a reversible component, representing the effect of temperature on the flow stress of a given deformed structure (i.e. the distribution and density of dislocations) and second, an irreversible component, which represents the effect of temperature on the deformed structure produced. To separate these, the reversible component is measured by straining at alternate temperatures[63]. For pure aluminium crystals the ratio of the flow stresses was found to be independent of deformation for strains greater than 5%[63]. The ratio at any temperature T, to that at $0^{\circ}K$ (obtained by extrapolation), increased markedly for T less than $200^{\circ}K$. At higher temperatures, the ratio was never less than 0.75[58]. Thus, the true temperature variation of the flow stress is associated principally with the difference in the deformation structures produced.

For reverted Al, 4 wt.% Cu crystals, the flow stress ratio increases with deformation[54] due to strain induced precipitation. Crystals containing GP(1) zones, θ' or θ precipitates behave in a similar way to pure aluminium[28,54], but for those containing GP(2) zones, the flow stress ratio was constant with strain[28].

Kelly[64] and Byrne, Fine and Kelly[28] emphasised the differences between these alloys by plotting the difference in flow stress at 273°K and 77°K ($\sigma_{77} - \sigma_{273}$) as a function of the flow stress at 273°K. For alloys containing GP(1) zones, $\sigma_{77} - \sigma_{273}$ remained constant, for alloys containing GP(2) $\sigma_{77} - \sigma_{273}$ increased slightly and for alloys containing θ' and θ, $\sigma_{77} - \sigma_{273}$ increased markedly with deformation at 273°K. This was interpreted[8,28] as indicating a small increase in dislocation density with deformation for alloys containing GP(1) and GP(2), similar to pure Al, but a large increase in dislocation density, and therefore in the temperature dependence of the reversible flow stress in alloys containing θ' and θ.

3.3 The Metallography of Aged Alloys

This has been carried out by means of optical and electron microscope replica examination of slip lines, and thin foil transmission examination of deformed structures and the dislocation - precipitate interactions responsible for them.

The deformation of Al-Cu single crystals in the supersaturated solid solution condition, or containing GP(1) zones, was shown to occur by single slip on the {111} , <110> system, producing large slip steps,[28,31,35,54]. Details of these slip bands, resolved by using oxide replicas[65], showed that the number of glide lamellae in each band was less than in pure metals, but increased with the volume fraction of zones, in agreement with earlier observations[66] that lamellae formation was hindered by solute

atoms in solid solution. In alloys containing GP(2) zones, deformation was similar, although the slip lines were observed to be finer[27,28,36]. As ageing proceeds and θ' replaces GP(2), oxide replica examination[65] showed that slip only occurred in areas free from precipitates and that the slip displacements decreased until they were unable to account for the total strain. At and beyond the peak, where θ' or θ predominates, no slip lines were visible until the strains were very large, near the fracture[27,36,67]. Oxide replicas[65] showed that most of the slip occurred in grain boundary denuded zones. Slip lines were observed to shear θ' precipitates, and to avoid θ precipitates. By examining replicas taken from sections through the specimens, Koda and Takeyama[68] confirmed that, even after 1 - 2% strain, θ' precipitates were deformed. In Al-Mg alloys, Thomas and Nutting[65] found that β' precipitates were sheared by slip lines in a similar way to θ' precipitates, but that β precipitates were avoided.

Dislocation - precipitate interactions in thin foils of aged alloys have been examined by transmission electron microscopy. In Al-Cu alloys, dislocations were moved in the foils under the action of thermal stresses, and coherent and partially coherent precipitates were observed to be sheared by dislocations[14,29] but non-coherent precipitates were not sheared.[14] Dislocations were held up momentarily at GP(2) zones and θ' precipitates and bowed between them before shearing.[69] Similar observations made on Al-Zn, Al-Zn-Mg[69] and Al-Ag[70] indicated that dislocations sheared all except non-coherent precipitates.

Experiments have also been carried out on Al, 4 wt.% Cu foils obtained from bulk material and deformed in a straining device in the electron microscope[71]. The structure after ageing to the peak at 130°C consisted of GP(2) zones within the grains, with marked depleted zones on either side of θ' boundary precipitates. On straining, dislocations generated at the boundary precipitates moved predominantly within the depleted zones, with some fine slip within the grains. At higher ageing temperatures the denuded zones were less pronounced and more dislocations moved greater distances within the grains. The concentration of slip in denuded zones has also been observed in Al-Ag alloys[72].

The dislocation arrangements in deformed age hardening alloys have been compared with those in pure aluminium.[73] Quenched Al, 4 wt.% Cu alloys had no cell-like substructure, and deformation increased the number of quenched-in loops and, particularly, helices, perhaps by the interaction of screw dislocations with vacancies remaining after the quench, which elongated in < 110 > directions. Quenched Al, 3 wt.% Mg showed a uniform dislocation distribution consisting of elongated dislocation loops, but no helices. The Al, 4 wt.% Ag showed a similar substructure to deformed pure Al consisting of areas of very low dislocation density separated by areas of very high dislocation density (cell walls). In overaged Al-Cu alloys, containing θ precipitates[73] and in internally oxidised Cu alloys containing non-coherent precipitates[74] dense dislocation tangles have been observed forming a cell structure

connecting the precipitates, with relatively dislocation-free areas between. In internally oxidised Cu-Al alloys, prismatic dislocation loops were observed surrounding the particles[75], and were attributed to dislocations cross-slipping past them. Cross-slip of dislocations around non-coherent precipitates in Al, 4 wt.% Cu has also been postulated[71] and claimed to have been observed after large strains[76].

The deformation of θ' precipitates in Al-Cu alloys has received considerable attention because the metallographic evidence[14,32,65] for shearing of these precipitates was incompatible with the deformation characteristics of alloys containing them.[27,28] Nicholson, Thomas and Nutting[14] suggested that θ' precipitates were sheared at low strains in foils, but only after large strains in bulk material. Koda, Matsuura and Takahashi[76], made an examination of dislocation movements in the foils, and dislocation-precipitate distribution in foils obtained from deformed bulk specimens. After small strains (2 - 3%), some dislocations were observed to be held up at θ' precipitates, and Bonar and Kelly[77] observed dislocations bowing between θ' precipitates after 3% strain. After large strains (approximately 5%) slow dislocations were seen to be held up at precipitates, but fast dislocations sheared through them. From bulk material[76] and in thin foils[29] tangled and jogged dislocations and dislocation loops were observed around precipitates. It was concluded that θ' precipitates were effective obstacles to dislocation movement at low strains. Evidence of deformed θ' precipitates from

replica studies[65] and from thin foils[71] suggests that at high strains (not less than 10%[29]), near fracture, θ' is sheared.

In all thin foil investigations of θ', contrast effects, or striations were observed around the precipitates[14,71,76,77,78]. They have been variously interpreted as moiré patterns[14], arrested dislocations, interface dislocations, or "antiphase boundaries"[76], dislocation loops around the precipitates[77], or a Van der Merwe grain boundary dislocation grid[71]. Recently, Pollard and Nutting[78], from a study of primary creep deformation in Al, 4 wt.% Cu containing θ' precipitates, found that striations also develop around θ' during primary creep, when the dislocation density increases to the same value as observed after approximately ½% tensile deformation. The striations were resolved as spirals or loops around the precipitates, with Burgers vectors lying in the habit plane of the precipitate, and therefore could not have been produced by shearing. The large observed dislocation density (approximately $2 \times 10^{10}/cm^2$) was taken to imply that dislocations only moved small distances, of the order of twice the precipitate spacing, and that consequently the dislocation sources must have a similar distribution to the precipitates. It was postulated that the spirals or loops around the θ' precipitates acted as dislocation sources, and it was implied that climb away from the interface was necessary first. Dislocation emmission from networks around θ' had already been observed[71], and suggested as an explanation for the high rates of work-hardening in these alloys.

Pollard and Nutting considered that the spacing between the spirals (100 - 500 Å) and the strain at which they were found, were both too small to support explanations of their origin based on moiré fringes, Lomer-Cottrell dislocations, Orowan loops or interface dislocations left after shearing. Instead, θ' with dislocation spirals was thought to be an intermediate stage in the θ' → θ transformation, which required a volume contraction, close to that calculated from the loop spacing. Since spirals are not observed around θ' in unstrained material, their formation must require some deformation.

The operation of dislocation spirals as sources, requiring climb away from the interface is unlikely to make a large contribution to room temperature deformation. It should be noted that if the precipitate diameters are similar to their spacing, the flow stress by this mechanism would be similar to the Orowan stress, but much more temperature dependent.

The comparative behaviour of bulk material and thin foils will be considered briefly. The uncertainty associated with thin foil observations is in knowing the rearrangement and dislocation losses which occur during thinning. Hirsch[79] estimated that where dislocation networks were small compared with the foil thickness the worst losses would occur with aluminium, where approximately half the dislocations would be lost. Kelly and Nicholson[8] and Wilson[80] believed that in aged alloys the initial distribution was altered considerably by thinning, since dislocations were observed

to cross slip to the surface to avoid θ' precipitates. Swann[73] has pointed out that with pure metals, no cell structure is found in deformed thin foils, in contrast to bulk material.

3.4 Theories and their Application

3.4.1 Theories of the flow stress

One of the earliest theories to account for the strength of age-hardened alloys was that of Mott and Nabarro[81]. They proposed that the elastic accommodation between precipitate and matrix, due to differences in their lattice parameters, produced internal stresses which opposed dislocation movement. The average of these internal stresses was identified with the yield stress. In order for this to be so, the flexibility of the dislocation line had to be taken into account. Unless the dislocation could bend to a radius of curvature equal to or less than the precipitate spacing, and so lie in the 'energy valleys' between the precipitates, then the constraints on either side of the dislocation line would probably cancel out. Mott and Nabarro derived a formula for the shear yield stress of a material containing coherent, spherical precipitates:-

$$\tau = 2.\ G.\ e.\ f. \qquad 3.4$$

Where, G = shear modulus of matrix

e = a misfit parameter, $\frac{r_1 - r_o}{r_o}$

where, r_o = atomic radius of solvent atom,

r_1 = atomic radius of solute atom
= $r_o (1 + \varepsilon)$

f = volume fraction of precipitate

τ thus depended only on the volume fraction of precipitates, and not on their number, size or spacing. The dislocation flexibility criterion for the yield stress to be equal to the mean internal stress was derived by equating 2.G.e.f. to the Orowan stress, (see equation 3.5 below), from which it was shown that the precipitate spacing, d, must be $\geq \frac{b}{4.e.f.}$, where b = Burgers vector of dislocation.
For $d < \frac{b}{4.e.f.}$, the yield stress was less than 2.G.e.f.
For $d = \frac{b}{4.e.f.}$, the yield stress reached a maximum value of 2.G.e.f. and d was then known as the critical dispersion.
For $d > \frac{b}{4.e.f.}$, the strength remained constant at 2.G.e.f.

Hart[34] showed that at the 'critical dispersion' dislocations must pass through the precipitates, since the stress required to expand dislocations between precipitates with that spacing would be twice the Mott and Nabarro stress, i.e. 4 Gef. Kelly and Nicholson[8] have shown that the temperature dependence of the flow stress predicted by this model is small, since the activation energy required for a dislocation to overcome the opposing internal stress is of the order of 250 eV, which is much greater than could be obtained from thermal fluctuations.

An alternative theory, proposed by Orowan[82] associated the yield stress with the precipitate spacing. Dislocations moving in a material containing hard second phase particles are held up at the particles, and an additional stress is required to expand the dislocations between them. Once the dislocations are forced into a semicircular form, they are able to by-pass the particles, leaving encircling dislocation loops. The stress required is the additional yield stress due to the precipitates,

$$\tau = \frac{T}{b.\rho} \qquad 3.5$$

where, T = line tension of dislocation

b = Burgers vector of dislocation

ρ = radius of curvature of dislocation

For a semicircular form, $\rho = \frac{d}{2}$.

where, d = spacing between particles in the slip plane.

therefore, $\tau = \frac{2T}{b.d.}$

Orowan proposed that for overaged alloys, the decrease in yield stress was caused by the increase in d.

The main drawback to the application of this equation is the uncertainty of T. Cottrell[83] used the expression:-

$$T = \frac{G.b^2}{2\pi.(1-\nu)} \cdot \ln \frac{d}{b} .$$

where, G = Shear Modulus

b = Burgers vector of dislocation

ν = Poisson's Ratio

d = Precipitate spacing in the glide plane

Kelly and Nicholson[8] used an adaptation of the Nabarro expression for a circular loop to a semi-circular one, viz.,

$$T = \frac{G.\,b^2}{4\,\pi} \cdot \varphi \cdot \ln \frac{d}{2b}$$

where, φ = a factor describing the mean between an edge and screw dislocation.

Both these expressions are of the form, $T = \alpha . G . b^2$.

Bonar[29] showed that for realistic values of d/b for aged Al alloys (within the range 25 to 3000), α varies only between 0.25 and 0.75 in Kelly and Nicholson's formula, and is usually approximated to 0.5 in calculations. In the Cottrell expression α has about twice this range of values.

The most useful form of the Orowan criterion is then;

$$\tau = \frac{2\,\alpha . G . b}{d} \qquad 3.6$$

where, $\alpha \simeq 0.5$

For an aged alloy, the solid solution contribution (τ_s) is added to this, and Kelly and Nicholson[8] used the formula:-

$$\tau = \tau_s + \frac{G.b}{4\,\pi} \cdot \varphi \cdot \ln \left(\frac{d - 2r}{2b}\right) \cdot \frac{2}{d - 2r} .$$

where $(d - 2r)$ accounts for particle sizes which cannot be neglected compared with their spacing. The temperature dependence of the flow stress predicted from this model is equal only to the variation in the elastic constants.

Although Orowan's theory was derived for spherical particles, the particle size does not appear in the final equation (3.6) when the spacing is large. If the theory still applies where the spacing is small and the size of the non-spherical particles is large, then difficulty arises in assigning realistic average values to d and r.

Ansell and Lenel[84] thought that the plastic strain associated with the Orowan mechanism was too small to produce detectable plastic flow at the yield stress. As an alternative, they identified the yield point with the stress to yield or fracture the precipitate particles, as a result of dislocation pile-ups against them. Kelly and Nicholson[8] have severely criticised this theory on the grounds that the stress on the leading dislocation due to the pile-up will be sufficient to expand it between the particles. Also, the plastic strain associated with shearing the particles was shown to be even less than that associated with dislocations expanding between them, since the particle spacing is always greater than the particle size.

Kelly and Nicholson[8] proposed a theory to account for the strength of aged alloys based on dislocations shearing the precipitates. The work done by the applied stress was equated to the energy change

after shearing. This energy change arises from the creation of two new surfaces during shearing, viz., the increase in contact area between precipitate and matrix and the formation of an internal interface if the precipitate structure is ordered. Considering the slip plane as a whole, the applied stress to move a dislocation was given by:-

$$\tau = \frac{f.\gamma_p}{b} + \frac{\sqrt{6}}{\pi} \cdot \frac{f.\gamma_s}{r} \qquad 3.7$$

where, γ_p = Surface energy of the internal interface

γ_s = Surface energy of the particle/matrix interface

f = Volume fraction of precipitate

b = Burgers vector of dislocation

r = Mean planar precipitate radius

If $\gamma_p > \gamma_s$, then τ is independent of particle size and shape. If the precipitates are not internally ordered, then $\gamma_p = 0$, and

$$\tau = \frac{\sqrt{6}}{\pi} \cdot \frac{f.\gamma_s}{r}$$

This is a lower limit to the applied stress to move a dislocation; the upper limit was obtained by considering the energy balance for one precipitate. τ was then given by:

$$\tau = \frac{\gamma}{b} \cdot \frac{\bar{l}}{\bar{d}}$$

where $\bar{l}$ = Average length of dislocation lying within the precipitate

$\bar{d}$ = Mean planar particle spacing

γ = Total interfacial energies, including disordered internal interface, particle/matrix interface and the creation of interface dislocations.

For coherent spherical precipitates,

$$\tau = \frac{\sqrt{\pi}}{2} \cdot \frac{\gamma . f^{\frac{1}{2}}}{b} \qquad 3.7.(b)$$

The concept of interfacial dislocations was introduced by Fleischer[85], who visualised that if the lattice parameters of the matrix and the precipitate were different, then the passage of a dislocation through the precipitate would produce a misfit dislocation at the precipitate surface. The extra surface energy contribution associated with the production of an interface dislocation was given by Kelly and Nicholson[8] as:-

$$0.6 . G . b . \left(\frac{\Delta b}{b} \right)^2$$

Where, G = Shear Modulus

b = Burgers vector of dislocation in matrix

Δb = Difference between Burgers vector of dislocation in matrix and precipitate.

For the general case of non-coherent, non-spherical precipitates, Kelly and Nicholson derived the hardening due to the cutting of precipitates as:-

$$\tau = \frac{1}{b^2 d} \left\{ \gamma_p . \bar{l} . d + A_i . \gamma_s + \frac{G . b^3}{2} . \cos^2 \alpha \right\} \qquad 3.8.$$

Where, $\bar{l}$ = Average length of dislocation line within the precipitate

A_i = Particle/matrix interface area produced when dislocation moves forward b

α = Angle between dislocation line and its Burgers vector.

The first two terms arise from the formation of an internal disordered interface, and the increase in particle/matrix interface, including the formation of interface dislocations, respectively, during cutting. The third term takes into account the formation of dislocation dipoles formed at the precipitate interface due to the slip planes in matrix and precipitate not being parallel. For thick precipitates, the first term was thought to be the most important. For thin precipitates or those not internally ordered, the second term predominates, and predicts a resistance to dislocation motion which depends on precipitate orientation. For aluminium alloys, the third term has been shown[8,86] to make only a small contribution.

The temperature dependence of the flow stress predicted by this theory has been obtained from the general theory regarding the thermally activated motion of a dislocation through obstacles in its glide plane, having rigid energy profiles.[87] The obstacle is assumed to be cut in a single activated event, and the form of the temperature dependence is given by:-

$$\tau = \frac{U_o}{v} \left[1 - \left(\frac{kT}{U_o} . \ln \frac{\dot{\varepsilon}_o}{\dot{\varepsilon}} \right)^{\frac{2}{3}} \right]$$

where, U_o = Activation energy for cutting at 0^oK in absence of stress

v = Activation volume

k = Boltzmanns constant

T = Absolute temperature

$\dot{\varepsilon}_o$ = Constant

$\dot{\varepsilon}$ = Strain rate

The flow stress is therefore predicted to be a linear function of $T^{\frac{2}{3}}$.

Another strengthening mechanism has been proposed by Hirsch and Kelly[88]. If a dislocation passes through zones or precipitates in which the separation of the partials is increased, then its energy will be lowered and the work done to pull the dislocation away represents an increase in yield strength. This will occur when the stacking fault energy is lower in the zones or precipitates than in the matrix, provided that the elastic modulii of the two materials are similar.

For a constant volume fraction of zones or precipitates, very little strengthening was predicted for sizes much smaller than the stacking fault width in the matrix, but with increasing zone or precipitate size, the strengthening increased up to a maximum, corresponding to sizes of the order of the stacking fault width within the zones or precipitates themselves. For sizes less than this, the yield stress increases as a function of $r^{-\frac{1}{2}}$, (where r = zone or precipitate radius), and beyond this size, as $r^{\frac{1}{3}}$. In the maximum strengthening region, the yield strength is proportional to $\gamma_2 - \gamma_1$,

where, γ_2 = Stacking fault energy of the matrix

γ_1 = Stacking fault energy of the zones of precipitates.

Here, the temperature dependence of the yield stress is governed by that of $(\gamma_2 - \gamma_1)$, which would probably be small for aluminium

alloys. For smaller particle sizes, thermal fluctuations would reduce the strengthening effect, but, in this region, solid solution effects might be more important.

3.4.2 The application of theories in alloys containing coherent precipitates.

Tests of theories for the flow stress of aged alloys have been carried out on single crystals, since the precipitate distribution is more uniform than in polycrystals and grain boundary effects are avoided.

Kelly, Lassila and Sato[39] showed that for Al, 20 wt.% Ag crystals containing spherical GP zones the C.R.S.S. was 7 - 10 Kg/mm^2. On Mott and Nabarro's theory, using values of e.f from the change in lattice parameter with % Ag, the calculated C.R.S.S. was only 2 kg/mm^2. The spacing of the zones was too small for Orowan's theory to apply at the observed values for C.R.S.S. Kelly[89] applied the cutting theory and used a value for Υ estimated from reversion data in the equation: $\tau = \frac{\sqrt{\pi}}{2} \cdot \frac{\Upsilon_p \cdot f^{\frac{1}{2}}}{b}$ to obtain a shear stress of 7 kg/mm^2, in good agreement with the observed value. Williams,[90] assuming that the C.R.S.S. was governed by disordering of the internal interface during cutting, estimated Υ_p from reversion data, and used the equation: $\tau = \frac{f \cdot \Upsilon_p}{b}$ to obtain a shear stress of only 0.5 kg/mm^2. Thus the major part of the flow stress results from particle-matrix interface effects, and not from internal disordering.

Hirsch and Kelly[88] estimated from their model that the C.R.S.S. for peak aged alloys was 7 kg/mm^2, in agreement with Kelly's value[89]. They pointed out, however, that the stacking fault model, unlike the others, predicted a yield strength dependence on zone radius for a constant volume fraction of zones, in agreement with experimental observations.

For Al, 12 at.% Zn alloys containing spherical GP zones, Dash and Fine[60] showed that the C.R.S.S. was 9.5 kg/mm^2 at 0°K. From Mott and Nabarro, the mean internal stress was calculated to be 5 kg/mm^2. The Orowan criterion was not applicable, for the same reason as for Al-Ag. No direct application of the cutting theory has been reported, and there appears to be no systematic study of reversion undertaken on Al-Zn alloys to enable γ to be estimated. Indirect evidence for zone cutting was obtained by Dash and Fine[60] who found, using crystals of several compositions, that the C.R.S.S. varied as a function of $f^{\frac{1}{2}}$ rather than f, as predicted by Mott and Nabarro. Further evidence was obtained by Price and Kelly[37] who found that the C.R.S.S. for fully hardened crystals aged at room temperature was independent of zone size, (which was varied by altering the quenching temperature).

Stacking fault strengthening was also considered to be important in this alloy[88], although quantitative verification was not possible since the elastic modulus and the stacking fault energy of the zones were not known. Jones[91] showed that at 77°K, after very short ageing times, the C.R.S.S. remained independent of zone

radius for values less than approximately 10 Å, but then increased up to a maximum at 30-40 Å radius. This, together with the fact that other workers had shown the volume fraction of zones to be constant over a wide period of ageing, is in qualitative agreement with Hirsch and Kelly's theory, which also predicted a maximum yield stress of the same order as that observed assuming reasonable values for the stacking fault energies of the matrix and zones.

The temperature dependence of the flow stress for both Al-Ag and Al-Zn alloys has been analysed by the method described above to determine the nature of the dislocation / precipitate interactions. Both Mott and Nabarro's theory and Kelly and Nicholson's theory predict a linear dependence of the C.R.S.S. on $T^{\frac{2}{3}}$, but the activation energy, U_o, for a dislocation to overcome the Mott and Nabarro mean internal stress would be of the order of 200 - 300 eV, whereas for cutting, U_o could be smaller. Experimentally, U_o was obtained from the slope and intercept of a plot of C.R.S.S. against $T^{\frac{2}{3}}$. U_o for Al-Zn was approximately 4 eV,[60] and for Al-Ag was approximately 6 eV,[39] which was thought to support the cutting theory,[8].

Although Al-Ag and Al-Zn are both hardened by spherical GP zones, the temperature dependence of the C.R.S.S. was much larger for Al-Zn than for Al-Ag[60]. For the latter alloy the temperature dependence was equal only to that of the elastic constants[39]. Dash and Fine[60] were unable to explain this satisfactorily, but Price and Kelly[37] pointed out that when the temperature dependence

of the C.R.S.S. for the solid solution matrix is subtracted from that of zone hardened Al-Zn, the remaining temperature dependence is very small, and is approximately equal to that of the elastic constants. In the case of Al-Ag, the solid solution strengthening of the Ag atoms in Al is known to be negligible[39]. Although the temperature dependence due to the zones alone in Al-Zn has therefore been overestimated, the conclusion that dislocation cutting is responsible for strengthening remains unaltered.

For Al-Cu alloys containing GP(1) zones the C.R.S.S. is approximately 7 kg/mm^2 at room temperature, rising to approximately 14 kg/mm^2 at 0^oK[28]. The Mott and Nabarro stress has been estimated as 11 kg/mm^2 [8] using e.f values from changes in lattice parameter, and as 8 kg/mm^2 [27] using f values from the metastable equilibrium diagram[29]. Both estimates are good, but since GP(1) zones are not spherical, and their spacing is not $\geq \frac{b}{4.e.f.}$, then the theory cannot be applied. Kelly and Nicholson[8] and Fleischer[86] approximated the elastic stress field around a zone to that of an edge dislocation loop and calculated that the flow stress required to force a dislocation through it was approximately 3 kg/mm^2. Kelly and Nicholson[8] concluded that coherency stresses do not account for the total flow stress.

The zone spacing was shown to be too small for the operation of the Orowan mechanism[93]. The cutting theory has been applied by Kelly and Fine,[93], who estimated the value of γ_s from reversion data. Since there is no internal ordering in GP(1),

$\gamma_p = 0$. Applying Byrne, Fine and Kelly's values of γ_s to Kelly and Fine's calculation, the flow stress ranges from 0.5 - 2.0 kg/mm^2, depending on the reversion data used. Kelly and Nicholson[8] estimated that the additional contribution to γ_s due to interface dislocation formation was very small, although Fleischer[86] had estimated that the flow stress contribution from this was approximately 1.6 kg/mm^2.

Although one of the major arguments for the cutting theory was the temperature and strain rate dependence results of Byrne, Fine and Kelly, considerable doubt has been cast on the validity of the analysis applied to the Al-Cu system as a result of Price and Kelly's[37] observations on Al-Ag and Al-Zn. There is no method for accurately determining the solid solution contribution in Al-Cu alloys, and although disc shaped zones are expected to produce a strong temperature dependence of the flow stress, it has been shown experimentally that solid solutions of Al-Cu, are themselves strongly temperature dependent.[28,37,54]

The strongest evidence for zone-cutting in Al-Cu alloys comes from the metallography and the mechanical property measurements. (Sections 3.2.1 and 3.3). A quantitative assessment of the contributions to the strengthening, caused by GP(1) zones, has been made by Fleischer[86] and Bonar[29].

Fleischer[86] pointed out that only $\frac{1}{3}$ of the zones, i.e., those lying parallel to the Burgers vector of the dislocation, experience a net energy change when sheared. The remainder of the zones, because of their relative orientations undergo energy changes which cancel. The strengthening was attributed to the sum of the interface dislocation effect, coherency stresses and an effect caused by the difference in elastic modulus between matrix and precipitate. Kelly and Nicholson[8] argued that after the passage of the first dislocation, further slip on the same plane would produce a positive net energy change for all the zones after shearing, but Fleischer[86] thought that the presence of interface dislocations would prevent further slip on the same atomic plane. Kelly[94] and Kelly and Nicholson also criticised the fact that the major strengthening contribution arose from long range effects, i.e., coherency and the elastic modulus difference, for which the average was probably zero, since precipitates in front of and behind the dislocation and above and below the slip plane produced effects which cancel. Fleischer[86] thought that when dislocations were pressed against zones, under the applied stress, the nearest zone produced the largest effect and the others could be neglected.

Bonar[29] considered that in order for any long range effect to contribute to the hardening, the precipitates must be spaced so that under the applied stress the dislocation could bend to a radius of curvature equal to, or less than, this spacing, and so lie in regions where the stress field is a minimum. This condition has already been

described for Mott and Nabarro's theory and is given by:-

$$d > \frac{\alpha . G . b}{\tau} \qquad 3.9.$$

Where, d = mean planar precipitate spacing

α = constant in Orowan Criterion, $\simeq 0.5$

G = shear modulus

b = Burgers vector

τ = applied stress

For GP(1) zones, d was shown to be too small to fulfil this criterion, and the strengthening was attributed to the sum of the solid solution effect, determined experimentally, the change in interfacial energy, and the formation of interface dislocations.

Bonar estimated the interfacial energy change from the equation $\tau = \frac{\gamma . I}{b . d .}$, assuming a value of 300 ergs/cm.^{2} for γ, and excluding the interface dislocation contribution because it was thought that only $\frac{1}{3}$ of the zones contributed to the increase in interfacial energy, and the interface dislocation contribution was confined to the remaining $\frac{2}{3}$ of the zones. For Al, 4 wt.% Cu, it was estimated that the solid solution contributed approximately 1 kg/mm^2, the increase in interfacial energy approximately 2 kg/mm^2 and the interface dislocations approximately 5 kg/mm^2 to the C.R.S.S., compared with the measured room temperature value of approximately 6 kg/mm^2. For alloys containing GP(2) zones, the strongest evidence for zone shearing is from metallography and the stress-strain characteristics. (Sections 3.3 and 3.2.1). Bonar[29] predicted

the same sources of strengthening as for GP(1), and for Al, 4wt.% Cu crystals aged at 130°C, estimated the solid solution contribution as approximately 0.5 kg/mm^2, the increase in interfacial energy (assuming γ = 200 ergs/cm^2.) contribution as approximately 7 kg/mm^2 and the interface dislocation effect as approximately 3 kg/mm^2, compared with the room temperature experimental value, 10.4 kg/mm^2. For GP(2) in alloys aged at 190°C, it was found that the spacing near the peak, where some θ' was present, could result in long range constraints also being effective.

As ageing proceeds, Kelly[95] attributed the initial rise in yield stress to the increase in volume fraction of precipitate. Jones[91] has shown that an alternative explanation is more feasible for Al-Zn aged at room temperature, and it is possible that this stacking fault energy mechanism accounts for the initial rise in the yield strength from the solid solution value, in other systems.

For Al-Cu aged at 130°C, the C.R.S.S. remains constant until the rise to the peak, which is associated with the formation of GP(2) zones. Bonar's calculations[29] showed that, as these zones were coarser, the increase in interfacial energy more than compensated for the diminishing interface dislocation contribution, resulting from the decrease in $\frac{\Delta b}{b}$ and the increase in zone separation d. The increase in the interfacial energy contribution arose because, now that the zones were thicker, all three orientations produced a net increase in energy after shearing. For alloys aged at 190°C, the coarsening of the GP(2) zones accounted for the rise to

the peak, together with the formation of some θ' precipitates, which were also believed to be sheared at this stage. As θ' continued to replace GP(2), the spacing increased, and long range effects started to operate, since the condition $\bar{d} > \frac{\alpha.G.b}{\tau}$ was fulfilled. Eventually, d reached a value $= \frac{2\,\alpha.G.b}{\tau}$, which is the Orowan criterion, and the C.R.S.S. then decreases with further precipitate coarsening. Kelly and Nicholson[8] predicted a critical precipitate size for the transition between dislocation shearing and dislocation avoiding. For perfect, non-coherent, precipitates the critical particle size able to be sheared was determined by equating the stress to shear, (assuming the formation of a high-energy interface) to the Orowan stress. The critical particle size was given by $r_c = \frac{2G.b^2}{\pi.\gamma}$, which for realistic values of γ for oxides and intermetallics was approximately 100 Å. Using a similar argument, but smaller values for γ, ordered coherent and partially coherent precipitates up to approximately 200 Å diameter were shown to be sheared. This was thought to explain the observations on θ' in Al-Cu crystals. Large coherent precipitates were generally sheared, and Price and Kelly[37] confirmed this for α' precipitates in Al-Zn.

No quantitative assessment has been made of the interactions giving rise to work-hardening in alloys containing zones. The rates of work-hardening are slightly greater than in pure Al and additional effects which have been suggested are the increasing difficulty of cross-slip due to a lower stacking fault energy in the solid solution[37], the formation of interface dislocations[29,37]

and a decrease in the particle spacing after shearing[29]. In addition, strain induced precipitation has been shown to occur during room temperature deformation in some alloys. (Section 3.2.3).

3.4.3 The application of theories in alloys containing non-coherent precipitates.

The change in the stress-strain characteristics of aged alloys occurs near the peak aged condition. (Section 3.2.1). Metallographic evidence suggests that dislocations do not shear the precipitates, and the Orowan theory would appear to apply under these conditions. Kelly and Nicholson[8] showed that in many previous investigations on dispersion hardened alloys the Orowan theory was wrongly applied. This theory only applied to annealed specimens, for which the solid solution contribution must be included, and that the measurement 'd' in the equation is, in fact, the average of the shortest distances between adjacent particles in the slip plane, and is only equated to the planar interparticle spacing, i.e. the distance between particle centres, when the particle size is very much less than the spacing.

For Al, 4 wt.% Cu crystals containing θ precipitates, Dew-Hughes and Robertson[96] claimed good agreement with the Orowan theory. Ansell and Lenel[84] also claimed agreement between this data and their own theory. Kelly and Nicholson[8] pointed out that Dew-Hughes and Robertson used the Cottrell estimate of the dislocation line tension, and that their analysis gave a fortuitous result, although, in fact, the data did fit the Orowan theory since the C.R.S.S. was

shown to be a linear function of $\ln(\frac{d-2r}{2b})$. $\frac{1}{d-2r}$. The agreement was within a factor of two, which was thought to be good, since the precipitates were not spherical.

Ashby[74] obtained excellent agreement with the Orowan prediction for results from internally oxidised Cu single crystals containing a wide range of particle spacings. However, Ashby's definition of the planar particle separation was different from that used by Kelly and Nicholson,[8] Dew-Hughes and Robertson[96] and others, who assumed that the particles were situated on f.c.c. lattice points. Ashby defined the separation as the radius of the smallest circle surrounding a particle, within which the probability of finding a second particle was equal to one. This value is approximately half that calculated on the lattice point arrangement.

There appears to be very little agreement over the definition of planar particle spacing in dispersed alloys. This arises from the different particle distributions assumed. In addition to those already mentioned, planar particles have been considered to be arranged as if on the lattice points of a simple cubic lattice[97], or as a cubic arrangement in space,[98], from which a random planar separation was calculated. It should be noted that this latter arrangement predicts a yield stress variation with $f^{\frac{1}{3}}$ for Kelly and Nicholson's cutting theory for spherical precipitates, instead of an $f^{\frac{1}{2}}$ dependence[98]. However, experimental data are insufficiently accurate to distinguish between them. Regardless of which particle

distribution is assumed, all estimates for the planar precipitate separation agree within a factor of approximately two. This could contribute to Kelly and Nicholson's conclusions regarding the experimental agreement with the Orowan equation.

Additional contributions to the flow stress of dispersion hardened alloys have been considered. Ashby[74] showed that short range effects due to elastic misfit (Mott and Nabarro) or shear modulus difference, (Fleischer) causing dislocations to 'stand-off' from precipitates and so decrease their effective spacing, were too small to produce detectable hardening in Al-Cu alloys.

Bonar[29] showed that for Al, 4 wt.% Cu crystals containing θ' precipitates, the agreement between the observed C.R.S.S. and the Orowan criterion was excellent. However, particle spacings were estimated from transmission electron micrographs, and a probable error of $\pm$ 50% was placed on the measured values, due to the errors involved in measuring the foil thickness.

The temperature dependence of the yield strength predicted by the Orowan theory is that of the elastic constants. Byrne, Fine and Kelly[28] showed that this was so for Al-Cu alloys. This precluded the operation of cross-slip mechanisms[8,74,99] to account for the yield stress. Thus, the Orowan theory appears to account fairly well for the observed strength of dispersion hardened materials, in the absence of a stronger alternative theory.

3.4.4 Theories of work-hardening and their application.

The work hardening of these alloys was first considered by Fisher, Hart and Pry[100], who supposed that the increment of strain-hardening due to the dispersion was caused by the accumulation of dislocation loops left around the precipitates after the passage of successive dislocations in the glide plane. It was shown that the hardening τ_h was given by:-

$$\tau_h = \frac{c.\ f^{\frac{3}{2}}.\ N.\ G.\ b}{r} .$$

Where, c = constant $\simeq$ 3

f = volume fraction of precipitates

N = No. of concentric loops around each precipitate

G = Shear Modulus

b = Burgers vector

r = planar precipitate radius

After the accumulation of a given number of loops, stress relief occurred by fracture of the precipitate, or slip within the matrix. This represented the maximum hardening condition, given by

$$\tau_{h\ max.} = 3 f^{\frac{3}{2}} . \tau_c$$

Where, τ_c = a critical value of shear stress at the centre of N concentric loops.

Qualitatively, the theory predicts a very rapid initial rate of work-hardening which decreases with strain, reaching a maximum value. The initial rapid rate of work hardening should increase

with $\frac{f^{\frac{3}{2}}}{r}$, i.e., for a given f, with the fineness of the dispersion. Also, residual stresses of opposite sign should exist in precipitate and matrix on unloading. These effects have been observed[8].

Criticisms of the theory are that cross-slip is neglected, and that the temperature dependence of the flow stress is predicted to be that of the elastic constants, although, after large strains it has been observed to be much larger[8]. Also, the model is unable to account for the metallographic observations of multiple slip and the formation of a cell structure (Section 3.3). Dew-Hughes and Robertson[96] found that for Al-Cu crystals containing θ precipitates τ_h was proportional to $\frac{f}{r}$ and not $\frac{f^{\frac{3}{2}}}{r}$. Kelly and Nicholson[8] showed that large values of N were obtained from these results and that a soft matrix would most probably yield before the precipitates fractured.

As an alternative theory[8], cross-slip was proposed to occur readily, resulting in prismatic loops being left around the precipitates and jogs being formed in moving edge dislocations. The operation of many slip systems then produces a large increase in dislocation density, thus accounting for the rapid rate of work hardening, and stress relief in the matrix, without precipitate fracture, then takes place by the operation of the prismatic loops as Frank-Read sources.

Ashby[74] agreed with this model and in order to account for

the formation of cells of a similar size to the precipitate spacing, with wall thicknesses comparable with the precipitate size, he suggested that the prismatic loops elongated in the slip direction and became stabilised by interaction with other loops. From an estimate of the increase in dislocation density caused by the formation of loops, together with a contribution from glide dislocations, it was found that at strains greater than approximately 1%, loops accounted for the major part of the increase. This implied that the average slip distance was large. At small strains the observed dislocation density was greater than that calculated from the loops alone and, in order to explain this, a mechanism for the rapid increase in length of the glide dislocations by a process called 'ribbon slip' was suggested.

Since the slip distance was large after strains greater than 1%, work hardening was associated with the stress to force glide dislocations through the forest of dislocations comprising the cell structure. The increase in flow stress due to work hardening ($\Delta\tau$) was then given by:-

$$\Delta\tau = \tfrac{1}{2} \cdot G \cdot \sqrt{\frac{b.\ f.\ \varepsilon}{r}}$$

Where, G = shear modulus

b = Burgers vector

f = volume fraction of precipitates

ε = tensile strain

r = mean planar precipitate radius

Thus stress-strain curves are predicted to be parabolic and this has been confirmed from Byrne, Fine and Kelly's results for overaged Al-Cu crystals. Ashby's results for internally oxidised Cu crystals were plotted as flow stress vs. $\frac{b.f.\varepsilon}{r}$, and shown to be linear, as predicted. Dew-Hughes and Robertson's[96] results were also shown to support this relationship, since the increase in flow stress at 7% strain was a linear function of $\frac{b.f}{r}$.

3.5 Fracture

Ductile fracture of pure metals and alloys stressed in tension generally takes the form of a cup and cone failure. A cavity is believed to be nucleated in the centre of a necked specimen, and this propagates transversely, to form the fibrous cup portion. A rapid shear then takes place near the specimen surface, forming the cone. Nucleation of cavities has been shown by Tipper[101], Puttick[102] and Rogers[103] for example, to be associated with inclusions in the material, but Beevers and Honeycombe [104] obtained results to suggest that cavities may also be nucleated by dislocations [58]. The coalescence of these cavities to produce transverse growth was once thought to occur under the influence of triaxial stresses in the neck. The fracture path, however, advances along alternate directions of maximum shear stress[58], although its average path is transverse, and Rogers[103] suggested that the regions of heavy localised shear ahead of the cavity, nucleated sheets of voids which

failed under the superimposed tensile stress. The formation of the cone was thought to occur in a similar way, producing a final 45° separation near the surface.[105] This final stage was shown to be absent in inclusion-free material[106] and in some pure metals at room temperature, which exhibited double cup fractures.

Both ductile and brittle fractures have been found in age hardening alloys, and Geisler[25] showed that the mode of fracture changed as ageing proceeds. Ryder and Smale[107] have studied tensile fractures as a function of ageing, in four different Al alloys, viz. superpure Al, 7.3 wt.% Zn, 2.6 wt.% Mg and Al, 3.9 wt.% Cu and commercial Al, 3.9 wt.% Cu, 1.0 wt% Mg (L.65) and Al, 4.7 wt.% Zn, 2.3 wt.% Mg, 1.3 Wt.% Cu (DTD 683).

In superpure Al-Zn-Mg, the solution treated and lightly aged specimens showed considerable grain elongation before fracture, which was of the transcrystalline, double 45°V - shaped type. Longitudinal boundary cracks were evident near the fracture, and these were attributed to the boundary strength being too low to withstand sliding. However, the incidence of cracks increased with ageing time, whereas the boundaries might be expected to be strengthened. This together with the lower ductility after ageing should decrease the amount of boundary sliding. Replicas of the fracture surfaces, examined in the electron microscope, showed a dimpled pattern characteristic of ductile fractures[108]. Alloys aged before the peak exhibited bright facetted intercrystalline failures

Replicas of the fracture surface showed half voids on a featureless background, which was interpreted as brittle fracture initiated by the fracture or loss of cohesion of boundary precipitate particles. This type of fracture occurred until well after the peak, and was thought to indicate that the grain boundaries probably overaged rapidly to an equilibrium state, since the true fracture stress was constant over this period of time. Heavily overaged alloys showed cup and cone fractures and ductile dimpled patterns on electron micrographs of replicas. No grain boundary cracking was observed.

Superpure Al-Cu alloys in the solution treated condition showed 45° transerystalline fractures, but no grain boundary cracking, and in the lightly aged condition (165°C ageing temperature) exhibited double cup fractures. When aged just before the peak, fractures were intercrystalline, with dull facets, and 45° boundary separations were observed behind the fractures. Electron micrographs of replicas showed the characteristic dimpled pattern of a ductile shear, with a small particle in each dimple. This, together with the absence of large precipitates, suggested that shear stresses parallel to the boundaries were more important than the tensile stresses across them, and that failure occurred within the grain boundary precipitate-depleted zone. Both the commercial alloys retained their characteristic banded structure after heat treatment. Solution treated alloys exhibited jerky flow (Portevin-Le Chatelier effect), which produced 45° deformation bands across their gauge lengths. Fracture occurred in a ductile way in one of these bands,

probably by void growth from gas cavities and inclusions as a result of the reorientation of the fibre structure by shearing. Lightly aged Al-Zn-Mg-Cu alloys fractured in the same way, but lightly aged and peak aged Al-Cu-Mg alloys showed cup and cone fractures. This was not fully understood. The aged Al-Zn-Mg-Cu fractured in a brittle manner on active slip planes. Electron micrographs of replicas showed flat plates of precipitate on a featureless background, together with some ductile areas. No detailed fracture mechanism was suggested.

Observations by Forsyth and Wilson[71] on the fracture of Al, 4 wt.% Cu foil in the electron microscope showed that alloys always fractured along precipitate-depleted zones by thinning and multiple slip within the zone, before fracturing within the grains. This agreed with Ryder and Smale's observations on the fracture of peak aged Al, 4 wt.% Cu bulk material. Lerinman et al[72] found very large shear deformation in the danuded zones of deformed Al-Ag alloys.

The fracture of single crystals of age hardening alloys has also been studied. Aged Al-Zn[109] and Al-Ag[39] crystals have been found to fracture along coarse slip bands where large amounts of deformation had taken place, although no necking occurred. Dew-Hughes and Robertson[27] found a similar behaviour in Al, 4 wt.% Cu crystals containing GP(1) or GP(2) zones. The fracture plane was $\{111\}$, which was either the primary or conjugate slip plane, or parts of each, if sufficient rotation occurred. The fracture

of crystals containing θ' or θ precipitates was described as being similar to polycrystals, and appeared to consist of a double 45° V-shaped fracture after necking.

Beevers and Honeycombe[110] studied the fracture of Al, 5.5 wt.% Cu crystals, and Price and Kelly carried out a similar study on Al, 3.7 wt.% Cu, Al, 20 wt.% Ag, Al, 15 wt.% Zn[111] and Cu, 1.5 wt.% Be[40] crystals. Coarse slip band fracture was found at all stages of ageing in the Al, 5.5 wt.% Cu crystals, even in the solution treated and peak aged at 165°C specimens, and in the other alloys aged to contain GP zones. In these other alloys, Price and Kelly found that solution treated crystals ruptured by necking down to a chisel edge, and that crystals containing intermediate precipitates fractured at 45° by necking after the manner of rectangular-sectioned polycrystals. The coarse slip band shearing type of fracture was examined in detail. Beevers and Honeycombe found that the measured fracture stresses resolved on the {111} fracture planes in <110> directions were constant, and Price and Kelly found that the resolved shear stresses for the first visible formation of coarse slip bands was also constant. In both cases, the resolved shear stresses were very temperature dependent. Beevers and Honeycombe interpreted the constant resolved fracture stress as evidence for dislocation pile-ups or dynamic coalescence of dislocations producing cracks in the material. Electron micrographs of the fracture surfaces showed dimples, or cusps, characteristic of ductile shearing. The cusps were attributed to the dislocation-induced cracks and not

to inclusions in the material.

A Petch plot of the fracture stress for solution treated Al, 5.5 wt.% Cu polycrystals tested at 77°K and 293°K over a grain size range of 6.4 grains/mm^2 to 54 grains/mm^2 showed that the fracture stress was proportional to $d^{-\frac{1}{2}}$. This was thought to support a dislocation pile-up, crack initiation model.

Price and Kelly, however, thought that the resolved shear stress for the initial formation of a coarse shear band was a better measure of the stress to initiate fracture. They showed that the formation of coarse slip bands led to localised shearing within a given band, and that a crack started at the edge of this localised shear region and propagated across the narrowest portion of the specimen to produce a ductile fracture. The crack propagation and ductile shear were attributed to the presence of inclusions, as in pure metals, although only 30 p.p.m. impurity was present in the alloys.

Dew-Hughes and Robertson[27] attributed fracture on coarse slip bands to the formation of a weakened plane when zones were sheared. This implies a constant strain to fracture, depending on the shape and size of the zones, and fracture characteristics depending on whether the primary or the conjugate plane sheared. No such conditions were found by Price and Kelly. Possible reasons suggested for the formation of slip bands were that local softening occurred, that the rate of work-hardening became too low, or that a phase

transformation took place. Experiments showed that if the bands were polished off the specimen, they often re-formed in new positions when retested, thus ruling out local softening. Compression tests showed that coarse slip bands formed at approximately the same shear stress as in tensile tests, thus ruling out the low-work-hardening theory. X-ray examination eliminated the possibility of phase transformations.

Price and Kelly postulated that the coarse slip band formation was a property of the matrix. This was supported by experiments on cold-worked pure Al crystals, on which necking occurred at stresses similar to those of the work hardening contribution to coarse slip band formation in the alloy crystals; i.e. the flow stress at which coarse slip bands formed, minus the critical resolved shear stress. Slip bands were thought to result from the thermally activated breakdown of barriers introduced by deformation. The nature of the obstacles was not known, but presumably they must be similar to those forming during stage II of a normal work hardening curve. These barriers are normally avoided by cross-slip during stage III. Why they should suddenly be broken to cause coarse slip band formation is not clear. However, differences in the resolved shear stress for the formation of coarse slip bands for different alloys would be expected to result from differences in the properties of the matrix, the most obvious of which is the difference in stacking fault energy. Price and Kelly demonstrated that the resolved shear stresses for coarse slip band formation for

the four alloys under consideration were in the correct reverse order to the alloy matrix stacking fault energies.

4. RESULTS

4.1 Polycrystals

4.1.1. Mechanical Properties

.1. Al, 3.5 wt.% Cu.

Alloys were tested at room temperature and -196°C after solution treatment at 500°C and ageing for 0.05 day, 2 days and 10 days respectively at 190°C. The ageing times were chosen from the results of Hardy[26] and Silcock, Heal and Hardy[13] to correspond with alloys containing GP zones, alloys aged to peak, and overaged alloys, respectively.

The 0.1% proof stress, tensile strength and % elongation measured at room temperature and -196°C are shown in Table 4.1 below.

Table 4.1

Ageing Time at 190°C	Testing Temperature	0.1% Proof Stress, t.s.i.	Tensile Strength t.s.i.	% Elongation
0.05 day	Room temp.	6.4	15.0	27
	-196°C	7.6	19.7	36
2 days	Room temp.	11.1	17.7	13
	-196°C	13.2	22.6	19
10 days	Room temp.	9.4	17.4	11
	-196°C	11.3	22.4	18

No previous work has been reported on the tensile properties of high purity Al, 3.5 wt.% Cu alloys aged at 190°C.

Ghate and West[112] quote room temperature values for Al, 3 wt.% Cu and Al, 4.5 wt.% Cu alloys, solution treated at 525°C, in the as-quenched condition, and aged to peak at 130°C. These are summarised below:-

	0.1 % Proof Stress t.s.i.	Tensile Strength t.s.i.	% Elongation
Al, 3 wt.% Cu : As-quenched	7.5	14.5	29
Peak at 130°C	13	21	12
Al, 4.5 wt.% Cu : As-quenched	9	19	25
Peak at 130°C	17	28	9

The lower ageing temperature used by Ghate and West account for the superior properties of their Al, 3 wt.% Cu alloy compared with the Al, 3.5 wt.% Cu alloy in Table 4.1.

Rohner[113] has quoted room temperature values for a high purity Al, 4 wt.% Cu alloy, solution treated from 500°C and aged at 160°C.

These are summarised below:-

Ageing Time at 160°C	0.02 % Proof Stress t.s.i.	0.2 % Proof Stress t.s.i.	Tensile Strength t.s.i.	% Elongation
0.01 day	4.8	7.0	15.3	19
0.1 day	6.5	8.5	17.1	13
3 days (Peak)	10.9	13.5	19.8	10
5 days	10.7	13.0	19.7	12

As expected from the higher % Cu and lower ageing temperature used with this alloy, the properties are superior to those of the Al, 3.5 wt.% Cu alloy in Table 4.1.

Ryder and Smale[107] have published ageing curves of tensile strength and % reduction of area for a high purity Al, 3.9 wt.% Cu alloy, solution treated at 520°C and aged at 165°C. The tensile strength of their alloy is slightly greater than that of Rohner for all ageing times.

Matsuura, Nagasaki and Koda[53] have obtained stress-strain curves for an Al, 4 wt.% Cu alloy, aged at 160°C and 200°C. The curves appear to have been plotted as true stress-strain curves, from which only the values of the proportional limit have been estimated.

Ageing time	Proportional Limit t.s.i.
0.16 day 160°C	10
7 days 160°C (Peak)	14
0.04 day 200°C	5
1 day 200°C (Peak)	10

The proportional limits of the alloy aged at 200°C agree with the 0.1% proof stress values of the Al, 3.5 wt.% Cu alloy in Table 4.1. The lower values of the Japanese alloy are probably due to the higher ageing temperature used, together with the inaccuracies in the estimations made from their published curves.

.2. Al, 3.8 wt.% Cu, 0.56 wt.% Mg (7:1, Cu:Mg)

Tensile tests were carried out at room temperature and at -196°C on specimens of this alloy, which had been solution treated at 500°C, and aged at 190°C for times up to 10 days. Solution treated specimens were tested immediately after quenching. Figs. 4 and 5 are graphs of 0.1% proof stress, tensile strength and % elongation as functions of ageing time, measured respectively at room temperature and -196°C. Good agreement was obtained between three specimens tested after each ageing time.

Both at room temperature and at -196°C, the 0.1% proof stress of the peak aged alloy is three times greater than that of the as-quenched alloy, whereas the tensile strength of the peak aged alloy is only 35% greater than that of the as-quenched one.

The % elongation decreases to approximately 5% at room temperature, and 10% at -196°C, from as-quenched values of approximately 40%.

No previous information has been found about the mechanical properties of this alloy aged at 190°C. Rohner[113] has measured room temperature mechanical properties of a high purity Al, 3.99 wt.% Cu, 0.53 wt.% Mg alloy aged at 160°C. These results have been plotted as functions of ageing time in Fig.6. The curves show slower ageing rates, characteristic of a lower ageing temperature, when compared with Fig.4. At the start of ageing, and at the peak, the 0.1% proof stresses and the tensile strengths are similar to the 7:1, Cu:Mg alloy aged at 190°C; it is possible, however, that the peak at 160°C was not reached after only five days ageing. The slightly higher % Cu and the lower ageing temperature used by Rohner should have produced superior properties in his alloy.

In Table 4.2 the 0.1% proof stresses and tensile strengths of the 7:1 Cu:Mg alloy, and the alloy used by Rohner are compared with the hardness changes of a 7:1 Cu:Mg alloy of similar composition, determined by Hardy[18] in two similarly aged conditions.

Table 4.2

Aged Condition	Al, 3.99 wt.% Cu, 0.53 wt.% Mg (Rohner[113], aged at 160°C)		Al, 3.8 wt.% Cu, 0.55 wt.% Mg (7:1 Cu:Mg aged at 190°C)		7:1, Cu:Mg (Hardy[18])	
	0.2% P.S. t.s.i.	T.S. t.s.i.	0.1% P.S. t.s.i.	T.S. t.s.i.	Aged at 160°C D.P.N.	190°C D.P.N.
Aged for 0.02 day	9	18	9	19	90	80
Peak	21	24	19	24	131	120

Hardy's results clearly show that the alloy aged at 160°C has a higher hardness, both at the start of ageing and at the peak, than the alloy aged at 190°C. Rohner's results, on this basis, seem to be low and, in addition, from Fig.6 it is seen that his alloy has an abnormally low ductility at the start of ageing.

.3. Al, 3.3 wt.% Cu, 1.5 wt.% Mg. (2.2:1, Cu:Mg)

Figs. 7 and 8 are graphs of the mechanical properties of this alloy, as functions of ageing time, measured at room temperature and -196°C respectively. Solution treatment and ageing conditions were identical with those of the Al, 3.5 wt.% Cu and 7:1 Cu:Mg alloys.

It is seen that at each testing temperature, the times to the peak are similar to those for the 7:1 Cu:Mg alloy, but the ageing kinetics are different, and the mechanical properties are superior. There is a more rapid rise to the peak and also more rapid overageing.

This comparison with the 7:1, Cu:Mg alloy agrees with the hardness results of Hardy[18], which have been plotted for both alloys in Fig.9.

The 0.1% proof stress of the peak-aged alloy is slightly more than twice that of the as-quenched alloy at room temperature, and slightly less than twice that at -196°C. The tensile strengths, however, only increase by 30% between the as-quenched and peak-aged conditions at room temperature and by only 16% at -196°C. The % elongation decreases to approximately 5% at room temperature and 7% at -196°C from as-quenched values of 30-32% and 25-27% respectively.

No previous information has been published on the mechanical properties of high purity alloys of this composition.

.4. The Effect of Composition

The effect of increasing % Mg in these alloys is shown in Tables 4.3 and 4.4 below. Table 4.3 lists the room temperature and -196°C 0.1% proof stresses for the Al, 3.5 wt.% Cu, 7:1, Cu:Mg, and 2.2:1, Cu:Mg alloys in three conditions, viz., as-quenched, lightly aged, (i.e. at the start of the plateau,) and peak aged. Table 4.4 lists the corresponding changes in tensile strengths.

Table 4.3

Aged Condition	0.1% Proof stress, (t.s.i.) Room Temp.			0.1% Proof stress, (t.s.i.) -196°C.		
	Al, 3.5 wt.% Cu	7:1, Cu:Mg	2.2:1, Cu:Mg	Al, 3.5 wt.% Cu	7:1, Cu:Mg	2.2:1, Cu:Mg
As-quenched		6.5	9.5		8.5	13.0
Aged for 0.02-0.05 day	6.5	9.5	14.5	7.5	14.0	19.0
Aged to peak	11.0	19.0	21.5	13.0	23.5	26.5

Table 4.4

Aged Condition	Tensile Strength (t.s.i.) Room Temp.			Tensile Strength (t.s.i.) -196°C.		
	Al, 3.5 wt.% Cu	7:1, Cu:Mg	2.2.:1, Cu:Mg	Al, 3.5 wt.% Cu	7:1, Cu:Mg	2.2:1, Cu:Mg
As-quenched		17.0	21.5		23.0	27.5
Aged for 0.02-0.05 day	15.0	19.0	24.0	19.5	26.0	28.0
Aged to peak	17.5	24.0	27.0	22.5	31.0	31.5

.5. Load-Elongation Curve characteristics

(i) Al, 3.5 wt.% Cu.

After ageing for 0.015 days at 190°C, and testing at room temperature, small irregular serrations appeared on the load-elongation

curve after approximately 10% elongation and continued up to the point of instability. After this, the serrations became more frequent and regular, reaching a size which represented a nominal stress drop of 0.1 t.s.i., and eventually disappeared before fracture, which occurred at almost zero load.

When tested at -100°C and at -196°C, serrations were barely visible on the load-elongation trace.

After 2 days ageing, room temperature tested specimens showed a few irregular serrations between a point mid-way along the work hardening portion of the curve and the instability point. Here they disappeared, after reaching a size representing a nominal stress drop of 0.1 t.s.i. No serrations appeared on curves obtained at temperatures of -78°C and below.

After 10 days ageing, there were no serrations on the curves obtained at any temperature. At room temperature and -78°C, specimens showed very little extension beyond the instability point prior to fracture, but at -125°C and below, nominal strains of approximately 5% were observed after instability.

(ii) 7:1, Cu:Mg.

At room temperature, as-quenched specimens produced a pattern of irregular serrations between a point mid-way along the work-hardening portion of the curve and the instability point. At this latter point

the serrations became more regular, and progressively increased to a size which represented a nominal stress drop of approximately 0.2 t.s.i. before fracture. Specimens with a small grain size (see Section 4.1.5.) showed serrations reaching sizes of 0.3 - 0.35 t.s.i. Specimens aged for 0.02 day at 190°C showed a similar pattern of small serrations to that of the as-quenched specimens. The serrations did not commence until farther along the work-hardening portion of the curve, however. After 0.06 days ageing, fewer irregular serrations developed on the curves before the instability point. After instability, the regular pattern of serrations, which did not occur for all the specimens tested, reached a value representing a nominal stress drop of only 0.15 t.s.i. After 0.1 day, 6 or 7 widely spaced irregular serrations appeared before the instability point, and a few regular serrations of 0.05 t.s.i. developed beyond this.

Specimens aged for more than 0.1 day showed no serrations and after ageing for 1 day fractured just after the instability point.

At -196°C, no serrations appeared on any of the load-elongation curves.

Specimens aged between 0.03 day and 0.1 day fractured very shortly after the instability point, but after 0.1 day, nominal strains between 2% and 5% were recorded after instability, prior to fracture.

(iii) 2.2:1, Cu:Mg

At room temperature irregular serrations developed on the curves of as quenched specimens shortly before necking. The serrations reached values representing a nominal stress drop of 0.3 t.s.i., at instability. Thereafter, they became very regular, and increased to 0.5 t.s.i. before fracture.

After ageing for 0.015 day, 6 or 7 irregular, widely spaced serrations occurred on the curves before instability. Here they disappeared, but several regular serrations of approximately 0.3 t.s.i. reappeared just before fracture. No serrations appeared on the curves of specimens tested at temperatures of -78°C., or lower.

After ageing for 0.05 day and 0.1 day, 5 or 6 irregular, widely spaced serrations developed along the work-hardening portion of the curve, but these disappeared at instability, and specimens fractured shortly afterwards.

Ageing for more than 0.1 day removed all traces of serrations on the curves. When aged between 0.1 day and peak, specimens fractured very soon after necking. After 10 days ageing, the specimens fractured suddenly while the load was still increasing.

No specimens tested at -196°C exhibited serrated load-elongation curves. As-quenched specimens, and those aged for times up to 0.1 day, fractured almost immediately after reaching the instability point.

When aged between 0.1 day and 1 day, specimens fractured at the instability point, and when aged for 10 days, they fractured suddenly while the load was still increasing.

Ryder and Smale[107] reported discontinuous yielding in solution treated, and solution treated and slightly aged samples of two commercially pure Al alloys, viz. Al, 4.66 wt.% Zn, 2.25 wt.% Mg, 1.35 wt.% Cu (DTD 683) and Al, 3.95 wt.% Cu, 1.0 wt.% Mg, 0.75 wt.% Si, 0.56 wt.% Mn (BS L65). However, they did not report this type of deformation behaviour in two superpure alloys, Al, 3.9 wt.% Cu, and Al, 7.3 wt.% Zn, 2.6 wt.% Mg, and offered no explanation. It is possible that the magnitude of the serrations on the curves of the superpure alloys was too small to be detected on a "soft" beam machine, such as the Hounsfield Tensometer, which was used by Ryder and Smale.

4.1.2. True Stress - True Strain curves

Mechanical properties are best described in terms of the true stress - true strain relationships existing during deformation. The true stress - true strain curve is more informative than the load-elongation curve, since a comparison of plastic behaviour under different stress systems may be made on this basis. Also, as shown in Appendix 1, the strain hardening properties of materials may be related to their true stress - true strain curves.

In this section, the effect of ageing time on the shapes of the true stress - true strain curves is illustrated for the three alloys. True stresses and true strains have been calculated from equations 1 and 2 in Appendix 1. Generally, only one curve has been drawn for each ageing time, since good agreement usually exists between individual specimens, (eg. Figs. 12 and 13).

.1. Al, 3.5 wt.% Cu.

Fig.10 shows true stress - true strain curves for the three aged conditions studied in this alloy and tested, respectively, at room temperature and at -196°C. The curves may be compared with those published by Matsuura, Nagasaki and Koda[53] for an Al, 4 wt.% Cu alloy aged at 200°C. Although there is no indication that their curves are plotted as true stress - true strain up to maximum load, the shapes are very similar to those in Fig.10. From Matsuura, Nagasaki and Koda's results, after ageing for 0.04 day, plastic flow appears to start at 5.5 t.s.i., after 2 days at 9.5 t.s.i. and after 4 days at 9.0 t.s.i. The respective limits of uniform strain are 0.20, 0.08 and 0.10. These values are seen to be very similar to the corresponding values in Fig.10.

.2. Al, 3.8 wt.% Cu, 0.56 wt.% Mg (7 : 1, Cu:Mg)

Fig.11 shows true stress- true strain curves of specimens aged for various times and tested at room temperature and at -196°C respectively.

.3. Al, 3.3 wt.% Cu, 1.5 wt.% Mg (2.2 : 1, Cu:Mg)

Figs. 12 and 13 are true stress - true strain curves of specimens of this alloy in as-quenched and three aged conditions, tested, respectively, at room temperature and at -196°C. Curves for three specimens in each condition have been drawn to demonstrate the agreement between individual test-pieces.

It is clear from Figs. 10 to 13 that the change in form of the true stress - true strain curve, as ageing proceeds, is similar for all three alloys. In each figure the curves are of two types. First, those which are characteristic of "soft" alloys, ie. in the as-quenched condition, or early stages of ageing, which show low proportional limits, gradual work hardening rates and large uniform strains, of the order of 20-30%. Second, those curves which are characteristic of peak and overaged specimens, which have higher proportional limits, rapid work hardening rates, and lower uniform strains, of the order of 5-10%.

This change in the form of the stress - strain curves as ageing proceeds has already been described. (Section 3.2.1.)

4.1.3. The temperature dependence of Mechanical Properties

.1. The temperature dependence of 0.1% proof stress, tensile strength and % elongation.

(a) Al, 3.5 wt.% Cu.

0.1% proof stress, tensile strength and % elongation have been plotted as functions of testing temperature for this alloy in three aged conditions, in Fig.14. It is seen that the 0.1% proof stress changes only very slightly with temperature in all three conditions; the peak-aged alloy shows the largest increase of 2 t.s.i. between room temperature and -196°C. The tensile strength shows a greater temperature dependence, which is similar in all three conditions, and increases by approximately 5 t.s.i. between room temperature and -196°C. The % elongation shows the largest temperature dependence. The ductility of the alloy aged for 0.05 day increases by 10% between room temperature and -196°C, and the ductilities of the peak and overaged alloys increase by 6%.

(b) Al, 3.8 wt.% Cu, 0.56 wt.% Mg (7 : 1, Cu:Mg)

The mechanical properties of this alloy have not been determined at intermediate temperatures. The properties at room temperature and at -196°C are summarised in Table 4.5, below, for as-quenched alloys and alloys in three aged conditions.

Table 4.5

Aged Condition	Room Temp. Tested			-196°C Tested		
	0.1% Proof Stress t.s.i.	Tensile Strength t.s.i.	% Elongation	0.1% Proof Stress t.s.i.	Tensile Strength t.s.i.	% Elongation
As quenched	6.2	17.4	36	8.3	23.2	43
0.2 days 190°C	9.7	19.0	33	14.2	26.6	36
0.4 days 190°C	19.2	24.1	8	23.6	30.8	12
10 days 190°C	16.0	21.8	6	19.5	29.0	12

By comparing the room temperature and -196°C values for this alloy, it is seen that the strength is slightly more temperature dependent than that of the Al, 3.5 wt.% Cu alloy. The 0.1% proof stress increases by 2-3 t.s.i. for as-quenched and overaged alloys and increases by 4-5 t.s.i. for lightly aged and peak-aged alloys. The tensile strength increases by 6-7 t.s.i. for all aged conditions. The % elongation is less temperature dependent than in the Al, 3.5 wt.% Cu alloy. As-quenched and overaged alloys show an increase of 6-7% ductility, whereas the lightly aged and peak-aged alloys increase by only 3-4%. It should be noted that this last increase approaches the accuracy of measurement.

(c) Al, 3.3 wt.% Cu, 1.5 wt.% Mg. (2.2 : 1, Cu:Mg)

Fig.15 shows the temperature dependence of mechanical properties for this alloy. From Figs.7 and 8 it is seen that the 0.1% proof stress for the as-quenched alloy increases by only 3 t.s.i. between room temperature and -196°C, whereas, from Fig.15, the 0.1% proof stress for all three aged alloys increases by approximately 5 t.s.i. These increases are slightly greater than those observed for the 7:1, Cu:Mg alloy.

The tensile strength also shows a greater temperature dependence than that of the 7:1, Cu:Mg alloy. The as-quenched alloy, and the three aged alloys all show increases of between 5 t.s.i. and 7 t.s.i. at -196°C.

The ductility shows a much smaller temperature dependence than that of the 7:1, Cu:Mg alloy. The as-quenched and lightly aged alloys show no temperature dependence, and the % elongation of the peak alloy increases by only 2%, which is similar to the experimental scatter. The overaged alloy shows no change of ductility down to -125°C, but the % elongation increases slightly at -196°C.

These results may be summarised as follows:-

The 0.1% proof stress shows very little temperature dependence, but what there is tends to be slightly higher for lightly aged and peak-aged alloys. This pattern is similar for all three compositions.

The temperature dependence of tensile strength is greater than that of 0.1% proof stress and appears to be similar for all conditions of ageing, except for the high % Mg alloy, where the lightly aged specimens have a slightly greater temperature dependence. The lower % Mg alloy shows a slightly greater temperature dependence than the other two alloys.

The temperature dependence of ductility varies with both ageing time and composition. Although no values are available for as-quenched Al, 3.5 wt.% Cu alloys, the temperature dependence of the as-quenched 7:1, Cu:Mg alloy is fairly small and there is no temperature dependence for the 2.2:1 Cu:Mg alloy. Lightly aged alloys show a marked decrease of temperature dependence with increasing % Mg. The temperature dependence of peak-aged alloys is small for Al, 3.5 wt.% Cu and decreases to a very low value for 2.2:1, Cu:Mg. Overaged alloys show a similar small temperature dependence for all three compositions, which is generally slightly greater than that of the peak-aged alloys.

.2. The effect of testing temperature on true stress - true strain curves.

(a) Al, 3.5 wt.% Cu

Fig.16 shows the effect of testing temperature on the true stress - true strain curves for alloys aged for 0.05 day, 2 days and 10 days. The lightly aged alloys tested at -196°C show only

slightly higher proportional limits than those tested at room temperature, but have much more extensive work-hardening regions. This results in higher values of true stress at maximum load, and longer uniform strains. Although only one curve is drawn at -100°C, it appears from its similarity to the room temperature curves that the deformation behaviour is similar down to -100°C, but changes below this temperature.

The curves in Fig.16 for alloys aged for 2 days are similar at room temperature and -78°C, but there is a progressive increase in the true stress at maximum load and the limit of uniform strain shown at the lower temperatures. There is also more scatter between the curves of duplicate specimens compared with those of alloys aged for 0.05 day or 10 days. A similar scatter has been observed in the critical resolved shear stresses and rates of work-hardening of Al, 4 wt.% Cu single crystals aged to peak, compared with under- and over-aged specimens[29]. Kelly and Nicholson[8] attribute this to the heterogeneous structure of peak-aged alloys, caused by preferential precipitation of θ' on dislocations.

Overaged alloys show a progressive increase in the true stress at maximum load with decreasing temperature. The limit of uniform strain remains the same down to -125°C, but increases below this temperature. There is much less scatter between duplicate specimens at each temperature, than that shown by alloys aged for 2 days.

(b) Al, 3.8 wt.% Cu, 0.56 wt.% Mg (7:1, Cu:Mg)

True stress - true strain curves of this alloy have been replotted on Fig.17, to compare the room temperature tested and -196°C tested alloys. Both the as-quenched alloy and that aged for 0.02 day show more marked increases in the true stress at maximum load and the limit of uniform strain at -196°C, than the lightly-aged Al, 3.5 wt.% Cu alloy in Fig.16. The peak-aged and overaged alloys also show more marked divergences between the curves at room temperature and -196°C, than the corresponding Al, 3.5 wt.% Cu alloy, but this results partly from a more marked increase in the elastic limit at low temperature for the 7:1, Cu:Mg alloy.

Excellent reproducibility of the curves is seen for all ageing times and at each testing temperature.

(c) Al, 3.3 wt.% Cu, 1.5 wt.% Mg (2.2:1, Cu:Mg)

Figs.18 and 19 show the temperature dependence of the true stress - true strain curves in three aged conditions. All the curves show excellent reproducibility at each testing temperature. Specimens aged for 0.015 day have very similar curves at room temperature and at -78°C, but the curves diverge below this temperature. Peak-aged and overaged specimens have divergent curves at all temperatures; this divergence is most marked for the overaged alloy.

The effect of temperature on the true stress - true strain curves for the three alloys may be summarised as follows:-

In general, lowering the testing temperature causes an increase in the proportional limit, and a greater increase in the true stress at maximum load. This results from a higher rate of work hardening. The consequent increase in uniform strain is predicted from equation 6, Appendix 1, which shows that the strain-hardening coefficient, n , is equal to the limit of uniform strain. Tests carried out at intermediate temperatures between room temperature and -196°C for the Al, 3.5 wt.% Cu, and 2.2:1, Cu:Mg alloys, show that the curves for lightly aged and peak aged Al, 3.5 wt.% Cu alloys and lightly aged 2.2:1 Cu:Mg alloy only diverge below some temperature between -78°C and -125°C. Curves of overaged Al, 3.5 wt.% Cu alloy and peak-aged and overaged 2.2:1, Cu:Mg alloy diverge at each testing temperature below room temperature.

4.1.4. Strain Hardening

Attempts have been made to described the changes in plastic behaviour of these alloys by means of a single parameter related to the work-hardening characteristics.

.1. The work hardening rate

On load-elongation or nominal stress-strain curves this varies

with strain from a value equal to Young's Modulus at the elastic limit, to zero at the instability point. A comparison between the work hardening rates of different alloys may be made by measuring the average slope of the load-elongation trace over some convenient portion of the plastic region. Following a method described by Bonar[29], this was measured directly from the chart trace on the testing machine, and was chosen to be 1" of the pen recorder chart at a distance equal to 1" beyond the elastic limit, where any initial transient flow phenomena had disappeared. The rate of work hardening was then defined as $\frac{\sigma_{0.038} - \sigma_{0.019}}{\sigma_{0.019}}$

Where, $\sigma_{0.038}$ = nominal stress at 0.038 nominal strain

$\sigma_{0.019}$ = nominal stress at 0.019 nominal strain

Since 1" of the recorder chart was equivalent to 0.019 nominal strain. This method of measurement has no fundamental significance.

(a) Al, 3.5 wt.% Cu.

Table 4.6 shows values of work hardening rate obtained by this method.

Table 4.6

Ageing Treatment	Rate of Work-hardening = $\frac{\sigma_{0.038} - \sigma_{0.019}}{\sigma_{0.019}}$, t.s.i.	
	Tested at room temp.	Tested at -196°C
0.05 day at 190°C	95	93
2.0 days at 190°C	99	152
10 days at 190°C	134	193

The change in work hardening rate as ageing proceeds is seen to be similar to that observed for Al, 4 wt.% Cu alloys aged at 190°C (Section 3.2.1.). At room temperature and -196°C, the values for overaged alloys are much larger than those for lightly aged ones, and values for peak aged alloys fall within the wide scatter band previously observed near the peak.

Results obtained by Bonar[29] on Al, 4 wt.% Cu single crystals, using a definition of work hardening rate = $\frac{\sigma_{0.0254} - \sigma_{0.0127}}{\sigma_{0.0127}}$, showed that the values for lightly aged alloys were 40 t.s.i., and for overaged alloys 190 t.s.i., both at room temperature and -196°C.

(b) Al, 3.8 wt.% Cu, 0.56 wt.% Mg (7:1 Cu:Mg)

Rates of work hardening (from tests at room temperature and -196°C) are plotted in Fig.20, as a function of ageing time. The shapes of the two curves are very similar to those reported for Al, 4 wt.% Cu single crystals,[8,29] and show the rapid increase

in the rate of work-hardening near the peak. As observed also for polycrystalline Al, 3.5 wt.% Cu alloy, the rates of work hardening are similar for the lightly aged specimens at the two testing temperatures, but at -196°C, the overaged specimens have higher rates of work hardening compared with those tested at room temperature. Quenched alloys, and those in the very early stages of ageing have relatively higher rates of work hardening than specimens aged for 0.05 day to 0.1 day, just before the rise to the peak; this feature is more marked at -196°C. This is believed to be due to quenching strains in the specimens, caused by the generation of excess dislocations as a result of sudden thermal contraction. These dislocations may anneal out during ageing, or, more probably, accelerate precipitation initially, but then exert a progressively decreasing influence on the rate of work-hardening, as the volume of precipitate in the matrix increases with time. Although this was not observed for Al-Cu single crystals, it should be noted that no values for these were obtained after very short ageing times.

(c) Al, 3.3 wt.% Cu, 1.5 wt.% Mg (2.2:1, Cu:Mg)

Fig.21 shows the rates of work-hardening plotted as functions of ageing time, for this alloy, when tested at room temperature and at -196°C. There is considerable scatter in the room temperature results at each ageing time, but the two curves are very similar, in other respects, to those of the 7:1, Cu:Mg alloy.

A comparison between the respective rates of work-hardening of the ternary alloys, with those of the Al, 3.5 wt.% Cu alloys in three corresponding aged conditions is given in Table 4.7 below:-

Table 4.7

Aged Condition	Rate of work-hardening = $\frac{\sigma_{0.038} - \sigma_{0.019}}{\sigma_{0.019}}$, t.s.i.					
	Tested at room temp.			Tested at - 196°C		
	Al, 3.5 wt.% Cu	7:1, Cu:Mg	2.2:1, Cu:Mg	Al, 3.5 wt.% Cu	7:1, Cu:Mg	2.2:1, Cu:Mg
Lightly aged	95	75	75	93	65	65
Peak aged	99	100	105	152	120	105
Over aged	134	115	115	193	150	140

For each of the alloys in this Table the rate of work-hardening increases markedly near the peak, in the same way as that of Al, 4.wt.% Cu single crystals. However, there is no evidence of a large scatter in values as observed for the single crystals. Triplicate results for polycrystalline specimens (Figs.20 and 21) show very little scatter, and the two ternary alloys show a progressive increase in work hardening rate over a wide ageing period near the peak.

It should also be noted that the Al, 3.5 wt.% Cu alloy shows higher work hardening rates than either of the ternary alloys, for which the values are very similar.

An alternative measurement of the work hardening rate is from the slope of the true stress-true strain curve at a given value of true strain. At all values of strain, the true stress - true strain curve is steeper than the corresponding load elongation curve, so that work hardening rates measured this way are larger than those obtained from the load-elongation curves.

The slopes of the true stress - strain curve at 2% true strain are shown in Table 4.8.

Table 4.8

Ageing time at 190°C	Rate of work-hardening = $\frac{d\bar{\sigma}}{d\bar{\varepsilon}}$ at $\bar{\varepsilon}$ = 0.02, t.s.i.					
	Tested at room temp.			Tested at - 196°C		
	Al, 3.5 wt.% Cu	7:1, Cu:Mg	2.2:1, Cu:Mg	Al, 3.5 wt.% Cu	7:1, Cu:Mg	2.2:1, Cu:Mg
As-quenched		92	115		116	127
0.02/0.05 day	117	88	114	109	106	112
0.4/2.0 days (Peak)	131	139	127	187	165	120
10 days	185	145	145	247	215	193

These results are the averages of two or three specimens in each aged condition. Similar trends in the rates of work hardening with ageing time are observed. The increase in work hardening rate near the peak is less marked, and there appears to be no advantage in using this method to illustrate the changes which occur with ageing.

.2. The work hardening coefficient

In plasticity theory, the shape of the entire plastic curve is fitted to an equation relating true stress and true strain. The work hardening characteristics are then described in terms of a parameter in the equation. The simplest relationship is that proposed by Ludwik[114]:-

$$\bar{\sigma} = k.\bar{\varepsilon}^{n}$$

Changes in work-hardening characteristics are described by changes in values of 'n', the strain-hardening coefficient.

Using the relationships derived in Appendix 1, viz:-

$$n = \bar{\varepsilon} \quad \text{at maximum load,}$$

and, $$\log \bar{\sigma} = \log k + n \log \bar{\varepsilon} .$$

n has been determined from the values of true strain at instability and from the slope of the $\log \bar{\sigma} - \log \bar{\varepsilon}$ plot.

It should be noted that 'n' and the rate of work hardening (Section 4.1.4.1.) are not equivalent, although they are related.

Thus, diffrentiating Ludwik's equation,

$$\bar{\sigma} = k\,\bar{\varepsilon}^{\,n}$$

$$\frac{d\bar{\sigma}}{d\bar{\varepsilon}} = n.\,k.\,\bar{\varepsilon}^{\,(n-1)} = \frac{n.k.\,\bar{\varepsilon}^{\,n}}{\bar{\varepsilon}}$$

$$= n\,\frac{\bar{\sigma}}{\bar{\varepsilon}}$$

Values of n have also been obtained from this equation for true strain values, $\bar{\varepsilon} = 0.02$. These are all shown in Table 4.9. for the 7:1, Cu:Mg alloy tested at room temperature.

Table 4.9

Ageing time	$n = \bar{\varepsilon}$ at max. load	$n = \frac{\log \bar{\sigma}}{\log \bar{\varepsilon}}$ at $\bar{\varepsilon} = 0.03$	$n = \frac{d\bar{\sigma}}{d\bar{\varepsilon}} \cdot \frac{\bar{\sigma}}{\bar{\varepsilon}}$ at $\bar{\varepsilon}=0.02$
As quenched	0.24	0.31	0.20
0.02	0.21	0.19	0.14
0.2	0.08	0.13	0.07
0.4	0.06	0.13	0.11
1.0	0.06	0.13	0.13
10.0	0.06	0.18	0.15

In column 2, $\bar{\varepsilon}$ at maximum load was calculated from $\bar{\varepsilon} = \ln.\,(1 + \varepsilon)$ where ε = Nominal strain at maximum load. In column 3, the slope of the $\log\bar{\sigma} - \log\bar{\varepsilon}$ plot was taken at $\bar{\varepsilon} = 0.03$, since the graphs were not linear (Fig.22). The departure from linearity is most marked for the as-quenched and lightly aged alloys. In previous investigations[57,61] where non-linearity was observed, the slope was

taken at a particular value of the true strain.

Very little agreement is seen between the values for 'n' measured by each method, with the exception of the peak aged and overaged alloys. Here, there is fair agreement between the 'n' values in columns 3 and 4 of Table 4.9., and the log $\bar{\sigma}$ - log $\bar{\varepsilon}$ graphs for these alloys are quite linear. However, the true strains at maximum load are very much smaller than those predicted from Ludwik's equation. Similar results are obtained for Al, 3.5 wt.% Cu alloys and 2.2:1, Cu:Mg alloys.

A second relationship, Swift's equation, (see Appendix 1)

$$\bar{\sigma} = A(B + \bar{\varepsilon})^n$$

has been examined in order to investigate the wide discrepancy between n and $\bar{\varepsilon}$ at maximum load when applying Ludwik's equation to these alloys.

For 2.2:1, Cu:Mg alloys, tested at -196°C in the lightly aged, peak and overaged conditions, data from the stress-strain curves were fitted to equations of the type, $\bar{\sigma} = A(B + \bar{\varepsilon})^n$, to evaluate A, B and n. Evaluation was carried out using the London University 'Pegasus' computer. The programme was written for curve fitting to Swift's equation by the least squares method. The values obtained are shown in Table 4.10.

Table 4.10

Ageing treatment	A	B	n
0.015 day at 190°C	68.31	0.062	0.442
0.4 day at 190°C	51.73	0.009	0.149
10 days at 190°C	53.06	0.005	0.216

The experimental curves and the computed curves, using Swift's equation for the three alloys, are shown in Fig.23.

Using the relationship derived in Appendix 1, viz:- $\bar{\varepsilon}$ instability = (n - B), values of the true strain at maximum load from the experimental curves and (n - B) are shown in Table 4.11.

Table 4.11

Ageing treatment	(n - B)	True strain at maximum load
0.015 day at 190°C	0.380	0.234
0.4 day at 190°C	0.140	0.072
10 days at 190°C	0.211	0.069

In each case, the true strains at instability are less than those predicted by the values of (n - B). The strain hardening characteristics of these alloys therefore do not appear to obey Swift's empirical relationship. Fig.23, however, shows the excellent agreement between the observed and calculated true stress - strain

curves up to the instability point. This suggests that the observed instability represents the point of departure of the actual strain hardening characteristics of these materials from the ideal case. Thus the onset of fracture in these alloys most probably governs the tensile strengths attainable.

.3. The temperature dependence of work-hardening.

The rate of work hardening, measured from the load-elongation curve by the method described in Section 4.1.4.1., exhibits a temperature dependence which varies with alloy composition and heat treatment.

Fig.24 shows the temperature dependence of the work-hardening rate for Al, 3.5 wt.% Cu alloy in three aged conditions. The lightly aged alloy shows no temperature dependence, but peak and overaged alloys show strong temperature dependence.

Although no 7:1, Cu:Mg alloys were tested at intermediate temperatures, Fig.20 shows that this alloy exhibits a similar temperature dependence of work-hardening rate to that of the Al, 3.5 wt.% Cu. The behaviour of the 2.2:1, Cu:Mg alloy is different and is also shown in Fig.24. The overaged alloy has a less marked temperature dependence, compared with the other two alloys, and both the peak and lightly aged alloys have no temperature dependence.

4.1.5. The Grain Size Dependence of Mechanical Properties

A brief survey was made of the effect of grain size on the room temperature mechanical properties of the 7:1, Cu:Mg alloy.

The effect of grain size on the true stress - true strain curves is illustrated in Fig.25 for as-quenched alloys, and those aged slightly beyond the peak. The curves for as-quenched alloys show that decreasing the grain size increases the work hardening rate and the true stress at maximum load, but has no effect on the initial flow characteristics. The curves for the slightly overaged alloys show that there is no grain size dependence of plastic behaviour. Dorn et al[61] have shown that the true stress - true strain curves for pure aluminium of different grain sizes have similar features to those for the as-quenched alloys in Fig.25.

Fig.26 shows the effect of grain size on the 0.1% proof stress, and tensile strength for alloys in the as-quenched and approximately peak aged and overaged conditions. No grain size sensitivity of the 0.1% proof stress is seen for any of the alloys, and no sensitivity of the tensile strength for the two aged alloys. The as-quenched alloys show a slight grain size dependence of tensile strength.

Fig.27 shows that for all the alloys, there is a grain size dependence of % elongation, which is similar for all aged conditions.

The work-hardening rate, defined as $\frac{\sigma_{0.038} - \sigma_{0.019}}{0.019}$ and measured from the load-elongation curves (Section 4.1.4.1) has been

plotted as a function of grain size in Fig.28. The as-quenched alloy shows a distinct grain size dependence, but the aged alloys appear to be insensitive to grain size differences.

4.1.6. Fracture

.1. True Fracture Stress

The change in true fracture stress with ageing time is shown in Figs.29 and 30. True fracture stress was calculated from the load at which the specimen separated, divided by the cross sectional area of the fracture surface. This was measured with a planimeter from tracings made on the microscope with the specimens positioned as shown in Figs.31 - 34.

For the 7:1, Cu:Mg alloy in Fig.29, the fracture stresses of specimens tested at room temperature, decrease markedly with ageing time, and do not appear to have reached a minimum value even after 10 days ageing. There is a close similarity with the % elongation curve in Fig.4, and this is in qualitative agreement with the results of Ryder and Smale[107] on superpure Al, 3.9 wt.% Cu aged at 165°C. The values of the true fracture stress for the 7:1, Cu:Mg alloys aged at 190°C, and the Al, 3.9 wt.% Cu alloys aged at 165°C, are very similar, for ageing times up to one day.

In Fig.30, the 2.2:1, Cu:Mg alloy also shows a decrease in true fracture stress with ageing time, although the results are

very scattered in the early stages of ageing. The fracture stress curve is similar to the % elongation curve in Fig.7. In the quenched condition and after short ageing times, the true fracture stresses are much lower than those of the 7:1, Cu:Mg alloy, but after approximately 0.2 day, the values are almost identical.

Both the 7:1 and 2.2:1 alloys tested at -196°C show almost constant values of true fracture stress with ageing time, although the values for the 2.2:1 alloy are slightly smaller than those of the 7:1 alloy. In the as-quenched condition, the 2.2:1 alloy appears to have a higher true fracture stress at -196°C than at room temperature, but there is considerable scatter in the results for this alloy during the early stages of ageing. This constant true fracture stress at -196°C is not reflected in the % elongation curves for the two alloys, (Figs.5 and 8).

.2. Fracture appearance

7:1, Cu:Mg. Photomicrographs of the fracture surfaces of specimens tested at room temperature and at -196°C are shown in Figs.31 and 32 respectively. At each testing temperature, as-quenched alloys and those aged up to 0.06 day at 190°C, exhibited shear fractures, consisting of fairly dull flat surfaces, inclined at approximately 45° to the tensile axis. After 0.06 day ageing, a few bright facets were visible within the shear surfaces of the low temperature tested specimens. Fewer bright facets were visible in the room temperature tested specimens, but are just discernable in Fig.31(c).

After 0.1 day ageing, the number of bright facets on the surfaces increased with ageing time, although the fractures generally remained at approximately 45° to the axis, and always contained a small sheared area near the periphery.

Sections through the fractures showed that at room temperature, specimens aged up to 0.06 day were 100% transcrystalline, with considerable grain elongation, and no grain boundary separations. An example is shown in Fig.35(a). After 0.06 day ageing, only the grains in the vicinity of the fracture have elongated and the fracture is partly intercrystalline. Some boundaries behind the fracture, which make angles $\geq 45^{\circ}$ to the tensile axis, are seen to be separated. Sometimes, grain boundaries intersecting the fracture surface, and parallel to the tensile axis, are separated for a short distance back into the specimen. These features are shown in Fig.35(b). Peak aged and overaged specimens show no grain elongation, and the fractures consist of approximately equal amounts of grain boundary separation and transcrystalline shearing, Fig.35(c). Marked boundary separations extending back from the fracture surface are also observed, (see Fig.35(d)).

At -196°C, the as-quenched alloy fractured in a similar manner to those tested at room temperature. After only 0.02 day ageing, there was evidence of grain boundary separations at angles $\geq 45^{\circ}$ to the tensile axis behind the fracture, which, however, appeared to be still 100% transcrystalline. After 0.06 day, the fractures

were 50% transcrystalline and 50% intercrystalline; boundary separations were visible extending back into the specimen from the fracture surface. This type of fracture did not change appreciably up to 10 days ageing time. An example is shown in Fig.35(e).

2.2:1, Cu:Mg. Figs.33 and 34 respectively, show the appearance of the fracture surfaces of this alloy when tested at room temperature and at -196°C. In Fig.33, the as-quenched specimen and that aged for 0.015 day show dull, flat, 45° shear fractures, similar to the 7:1 alloy. After 0.1 day, however, the fractures are bright and facetted and remain at 45° to the tensile axis up to 10 days ageing. In Fig.34, the specimens tested at -196°C have bright facetted fracture surfaces even in the as-quenched condition and after lightly ageing. After 0.05 day, the fractures appear very brittle and take place on planes which are more normal to the tensile axis.

Sections through the fractures are shown in Fig.36. Alloys in the as-quenched condition, and after ageing for 0.015 day showed almost identical features, which are illustrated in Figs.36(a), (b), (c) and (d). On specimens tested at room temperature, marked grain elongation has occurred only in the necked region, (Fig.36(a)), and the fracture was entirely transcrystalline, (Fig.36(b)). Very little grain contrast is observed since the deformation has rotated the grains into similar orientations. Decorated slip markings are observed in the heavily deformed grains near the fracture.

Specimens tested at -196°C showed very little grain elongation and the fracture plane is jagged, (Fig.36(c)). At higher magnification the fracture appears to be partly intercrystalline, with these areas separated by areas of transcrystalline failure. (Fig.36(d)). Boundary separations behind the fracture surface, making angles $\geq 45^{\circ}$ to the tensile axis, are observed both in Figs.36(c) and 36 (d).

After ageing for 0.05 day and 0.1 day, room temperature fractures were partly transcrystalline and partly intercrystalline, the intercrystalline portions being generally in the centres of the specimens. Specimens tested at -196°C exhibited only intercrystalline failures, with isolated boundary separations behind the fracture surface, together with numerous separations of boundaries intersecting the fracture and lying parallel to the specimen axis. Specimens aged for more than 0.25 day showed entirely different etching characteristics in Keller's reagent. The grains etched darkly and the boundaries remained light coloured. At high magnification, no precipitates were resolved, as shown in Fig.37(a).

Specimens aged between 0.25 day and the peak (0.5 day), and tested at room temperature, showed predominantly intercrystalline fractures, with small amounts of transcrystalline failure regions across the corners of grains, as shown in Fig.37(b). The amount of this type of transcrystalline fracture increased with ageing time, so that between approximately 0.6 day and 1 day, the fractures were 50% intercrystalline and 50% transcrystalline. After 10 days,

the fractures were entirely intercrystalline.

Specimens tested at -196°C, after ageing for times greater than 0.25 days, also showed transcrystalline fractures, together with some intercrystalline fracture, (Fig.37(c)). After ageing for 10 days, the fractures were entirely intercrystalline and similar to the room temperature tested specimens. An example is shown in Fig.37(d).

Electron Micrographs.

Shadowed carbon replicas of the fracture surfaces of several specimens have been examined. Fig.38 shows results for as-quenched, peak-aged and overaged specimens of 7:1, Cu:Mg alloys tested at 77°K. In each case, the fracture surfaces consisted of cusps which are known to be characteristic of ductile failure. The as-quenched alloy cusps (Fig.38) were generally very large and irregularly shaped, unlike the overaged alloy cusps (Fig.38(c)), which were very small, regularly spaced and of uniform size. Within a given grain, the cusps were generally aligned in one direction. The peak-aged alloy cusps were a mixture of very large and very small as shown in Fig.38(b), but the large cusps were more regular, than those of the as-quenched alloy.

Fractographs from 2.2:1, Cu:Mg alloys are shown in Figs.39 and 40. At both temperatures, the as-quenched and lightly aged alloys exhibit large irregular cusps. There is some evidence of small

cusps as well on the lightly aged alloys. Peak-aged and overaged alloys are characterised by small regular cusps. The change in direction of the cusps at a grain boundary is clearly seen in Fig.39(d). There is some evidence in this photomicrograph and in Fig.40(d) for the existence of particles (0.1 - 0.2μ diameter) in the cusps. These were not generally observed over the whole specimen, however. The grain boundaries observed in Figs.40(c) and 40(d) appear to be 'denuded' of cusps, but particles are clearly visible (Fig.40(c)). These featureless boundary areas could be associated with poor replication of, for example, the boundary separations parallel to the tensile axis (see Fig.35(c)), or simply, deep 'valleys' on the fracture surface. The majority of the boundaries visible in the electron microscope resembled Fig.39(d).

4.2 Single Crystals

Complementary results to those already described have been obtained from tensile tests on aged single crystals of the two ternary alloys. These were carried out in order to correlate the mechanical behaviour of the alloys with the existing theories of the strength of materials containing dispersed particles. The necessity for testing single crystals arises because the effects of grain boundaries on both precipitation and deformation are not yet properly understood, and the bulk of previous work, on which the theories are based, has been carried out on Al-Cu single crystals.

Only a limited number of crystals was available for testing, and no control of orientation was possible during growth. It was therefore important to minimise the effect of orientation dependence of the critical resolved shear stress (C.R.S.S.) and flow characteristics. Specimens tested in the as-quenched and lightly-aged conditions, which would be expected to show the most marked dependence, were always chosen from the centre of the unit stereographic triangle. The remaining crystals, in the more extreme orientations, were tested in the fully aged and overaged conditions, where little orientation dependence would be expected.[28,36]

Single crystal results are generally plotted as resolved shear stress-glide strain curves. Both these quantities are calculated from load-elongation data, as shown in Appendix 2. However, crystals in the peak aged and overaged conditions, which

behave more like polycrystals, and which slip on several systems from the start of deformation, are more conveniently plotted as true stress - true strain curves. As-quenched and lightly aged crystals, which initially show easy glide have been plotted as resolved shear stress against glide strain. The formula used to calculate these quantities does not hold once the tensile axis has rotated across the stereogram to the symmetry position, so that the calculated glide strains after large deformations are not strictly correct. To compare the behaviour of these crystals with that of the peak and overaged crystals and the polycrystals, true stress - true strain curves have also been plotted. These, too, are incorrect, since the calculation of true strain assumes no anisotropy, whereas these soft crystals deform predominantly by single slip.

4.2.1. Stress - Strain Curves

.1. 7:1, Cu:Mg alloy

Resolved shear stress - glide strain (τ-a) curves obtained at various temperatures are shown in Figs.41, 42 and 43 for crystals tested in the quenched condition and aged for 0.01 day and 0.1 day at 190°C, respectively. Each curve has been plotted to the instability point. On the load-elongation traces, obtained from the testing machine, very small serrations after instability were seen only for the as-quenched crystal and those aged for 0.01 day, when tested at room temperature. Unlike the corresponding polycrystals,

no serrations were observed before instability.

Corresponding true stress - true strain curves are shown in Figs.44, 45 and 46, together with those for peak and overaged alloys. The form of the curves changes markedly as ageing proceeds. The as-quenched and lightly aged alloys have low yield stresses and work-hardening rates and large elongations, whereas peak and overaged alloys have high yield stresses and work-hardening rates, and low elongations. These characteristics are similar to those shown by Al, 3.7 wt.% Cu alloys aged at 190°C,[29]. Similar changes in the curves of other Al-Cu alloys aged at different temperatures have also been reported[27,28,36,37].

.2. 2.2:1, Cu:Mg alloy

Resolved shear stress - glide strain curves for as-quenched crystals, and those aged for 0.015 day and 0.1 day at 190°C are shown in Figs.47,48 and 49, respectively. These curves are similar in form to the 7:1, Cu:Mg curves in Figs.41 and 43.

On the load-elongation traces, small serrations appeared after instability only at room temperature for these three alloys. Prior to instability there were no serrations, but the chart trace was wavy in form, indicating discontinuous yielding. The curves of the corresponding polycrystalline specimens showed large serrations before instability, and only the quenched alloys showed serrations after instability.

True stress - true strain curves for as-quenched crystals, and crystals in four aged conditions are plotted in Figs.50, 51 and 52. These show a similar change in form, as ageing proceeds, to the 7:1, Cu:Mg alloy, and the Al-Cu alloys, already described.

.3. Yield Points.

Single crystals of both compositions exhibited discontinuities at yield, in all aged conditions. At room temperature there were no yield drops, but the curves changed abruptly from their elastic to plastic regions; these changes frequently consisted of points of inflection on the curves.

Below room temperature, the curves for as-quenched and lightly-aged crystals showed marked yield points, and the curves for peak and overaged crystals showed either yield extensions or distinct points of inflection at yield. Only overaged 2.2:1, Cu:Mg alloy crystals with orientations near <100> produced smooth curves similar to those of polycrystalline specimens.

Kelly and Nicholson's criterion for a geometrical softening yield point:-

$$\frac{d\tau}{da} \leqslant \tau . \tan^2 \lambda . \cos \lambda . \cos \varphi \qquad \text{(Section 3.2.4.)}$$

has been tested on crystals of 7:1 and 2.2:1, Cu:Mg alloys which show yield drops. In Table 4.12, values of $\tau . \tan^2 \lambda . \cos \lambda . \cos \varphi$ have been calculated at yield for as-quenched and lightly aged crystals.

Table 4.12

Crystal Identification	Ageing Treatment	Testing Temperature	$\tau_o \tan^2 \lambda_o . \cos \lambda_o . \cos \varphi_o$: (kg/mm^2)
R2	As-quenched	-196°C	4.5
R15	0.01 day at 190°C	-196°C	4.4
Y	0.01 day at 190°C	-196°C	4.4
AN	As-quenched	-196°C	5.7
M	0.015 day at 190°C	-74°C	6.2
AB	0.015 day at 190°C	-125°C	3.2
B	0.015 day at 190°C	-196°C	6.8
G	0.015 day at 190°C	-196°C	8.3

Values of $\frac{d\tau}{da}$ for the easy glide regions of these crystals are difficult to measure from the curves, in Figs.42 and 48, but are estimated to be less than 2 kg/mm^2, so that Kelly and Nicholson's instability condition is fulfilled in each case. Crystals 'N' and '16' in Fig.42 do not show yield drops. Calculated values of $\tau_o . \tan^2 \lambda_o . \cos \lambda_o . \cos \varphi_o$ for these two crystals are 2-3 kg/mm^2 and 5-8 kg/mm^2 respectively. Corresponding values of $\frac{d\tau}{da}$ during easy glide, estimated from Fig.42, are 3 kg/mm^2 and 6.5 kg/mm^2, so that the instability conditions are not fulfilled. Easy glide regions were generally absent in room-temperature tested crystals, and this was probably due to strain-induced ageing during the early stages of deformation, as suggested by Greetham and Honeycombe[36].

Price and Kelly[37] have distinguished between geometrical softening yield points, and those due to other effects, by plotting theoretical load-elongation curves after yield, based on a zero work-hardening rate, using the equation:-

$$P = P_o \cdot \cos \lambda_o \left[1 - \frac{\sin^2 \lambda_o}{(1+\varepsilon)^2} \right]^{-\frac{1}{2}} , \qquad \text{(See Section 3.2.4.)}$$

Where P = load,

P_o = load when yielding occurs,

ε = nominal tensile strain,

λ_o = angle between slip direction and tensile axis at yield.

The geometrical softening effect is clarified by considering stress-strain curves, rather than load-elongation curves. The resolved shear stress over a slip plane in a crystal is given by the Schmid equation:-

$$\tau = \frac{P}{A} \cdot \cos \varphi \cdot \cos \lambda .$$

where P = tensile load

A = cross-sectional area

φ = angle between tensile axis and glide plane normal

λ = angle between tensile axis and slip direction.

Price and Kelly have emphasised that the true geometrical factor in this expression is $\frac{\cos \varphi \cdot \cos \lambda}{A}$ and that $\frac{A}{\cos \varphi}$, being the area of the slip plane, remains constant during single slip.

Thus since λ decreases with strain, $\frac{\cos\varphi_0 \cos\lambda}{A}$ must increase for all crystal orientations.

It is clear from the expression $\tau = \frac{P}{A} \cdot \cos\varphi_0 \cos\lambda$, that if the rate of work-hardening is small, (i.e. τ does not increase very much with strain), then P must decrease to compensate for the increase in $\frac{\cos\varphi_0 \cos\lambda}{A}$, and a load drop will appear in the load-elongation trace. This is geometrical softening. Price and Kelly have considered the special case where the work-hardening rate is zero, (i.e. τ remains constant), and have derived an expression for the theoretical decrease in P with strain. Thus, although P decreases, due to geometrical softening, this cannot, by itself, cause a decrease in τ, which must result from some alternative yield-point effect.

To summarise, if the load-elongation curve for a crystal having a low work-hardening rate shows a fall in load after yield, this may or may not be caused by geometrical softening. If the resolved shear stress-glide strain curve still shows a drop in τ after yield, this cannot then be caused by geometrical softening.

Price and Kelly's theoretical curve for the fall in load, based on a zero work-hardening rate, will then be less steep than the actual measured load decrease.

In the present investigation, the crystals listed in Table 4.12 all showed yield drops on their resolved shear stress-glide strain

curves, which were therefore not caused by geometrical softening. This has been confirmed by comparing theoretical geometrical load drops derived from Price and Kelly's equation, with the measured load-elongation curves. Examples for four of the crystals are shown in Fig.65. It is seen that for three of these crystals, the measured load drops are steeper than the theoretical softening curves. The fourth crystal, 2 AN and the other quenched crystal, R2, do not show steeper load drops than the theoretical, but, this might be caused by an increased rate of work-hardening as a result of quenching strains or strain-induced precipitation.

.4. Orientation dependence

There has been no systematic work on the orientation dependence of stress-strain curves of aged Al alloys. Greetham and Honeycombe[36] found that air-cooled Al-Cu crystals tested at 77°K showed the greatest orientation dependence; crystals orientated near <111> or <100> had higher work-hardening rates. Crystals aged to contain zones also showed a similar but smaller orientation dependence. This disappeared after further ageing. Crystals tested at room temperature showed no orientation dependence in any aged conditions.

Data from Kelly and Chiou[54], Dew-Hughes and Robertson[27], Price and Kelly[37] and Greetham and Honeycombe[36], suggest that quenched crystals and those containing GP(1) and GP(2) zones have

low critical resolved shear stresses when oriented near <111>.

In the present investigation, duplicate specimens were generally chosen with similar orientations, and since only a small number of crystals was available for testing, no discussion of orientation dependence is possible.

4.2.2. The effect of ageing

.1. Critical Resolved Shear Stress (C.R.S.S.)

For each crystal, the critical resolved shear stress was calculated from the initial flow stress, i.e. the stress at which the curve deviated from its linear elastic region. Where yield extensions or yield drops occurred, the initial flow stress is often defined as the point at which the plastic flow curve, when extrapolated back, intersects the elastic line. In the present work it was found that this intersection generally coincided with the initial departure of the curve from its elastic region. The method has been referred to by Kelly and Chiou[54].

Fig.53 shows ageing curves of C.R.S.S. for 7:1, Cu:Mg alloy crystals, tested at room temperature and -196°C. As-quenched values are also indicated. Although only a few different ageing times were used, the form of the curves is similar to the corresponding 0.1% proof stress curves for polycrystalline specimens, shown in Figs.4 and 5. The C.R.S.S. of the peak alloy is twice that of the

as-quenched alloy at -196°C, and four times as great at room temperature. This fractional increase in C.R.S.S. as a result of ageing is larger than the corresponding fractional increase in proof stress and hardness for polycrystalline specimens, and thus the change in C.R.S.S. is a more sensitive measure of the degree of ageing. This point was first made by Dew-Hughes and Robertson[27].

Fig.54 shows C.R.S.S. ageing curves for the 2.2:1, Cu:Mg alloy. These, too, are seen to be similar in form to the 0.1% proof stress curves for the polycrystals in Figs.7 and 8. At each temperature, the C.R.S.S. of the peak alloy is approximately $2\frac{1}{2}$ times that of the as-quenched crystals.

Dew-Hughes and Robertson have shown that the C.R.S.S. of unaged Al, 4 wt.% Cu crystals is strongly dependent on the severity of the quench. Thus a water-quenched crystal had a C.R.S.S. of 4.6 kg/mm^2, whereas air-cooled crystals had C.R.S.Stresses of only 2.5 - 3.0 kg/mm^2. In the present investigation, at room temperature, the C.R.S.S. of the as-quenched 7:1, Cu:Mg alloy was 3.5 kg/mm^2, and for the 2.2:1, Cu:Mg alloy, 4.8 kg/mm^2. It is thought that the excess vacancies present after a rapid quench, allow very rapid diffusion, and almost instantaneous formation of G.P. zones. If this is true, the higher value of C.R.S.S. for the Al-Cu alloy, compared with the ternary alloys, might be caused by the higher solution treatment temperature (540°C) used by Dew-Hughes and Robertson.

The influence of a change in quenching treatment on the mechanical properties of Al-Cu single crystals decreases progressively with increase in ageing time. This is shown by comparing the results for the C.R.S.S. and the work hardening rate of Al-Cu crystals aged at 130°C and 190°C obtained by previous workers[27,28,29,35,36,37,59]. Good agreement is found between the properties of crystals with similar compositions, in the same aged conditions, although different quenching techniques were used in each case.

C.R.S.S. - ageing curves have been obtained for Al, 3.7 wt.% Cu crystals, aged at 190°C and tested at room temperature and at -196°C[29]. These have been compared with Figs.53 and 54 and in Table 4.13 a comparison is made between the C.R.S.Stresses of binary and ternary crystals in similar aged conditions. "Lightly aged" refers to alloys on the plateau of the age-hardening curve just before the rise to the peak.

Table 4.13

Aged Condition	C.R.S.S. at Room Temperature kg/mm^2			C.R.S.S. at -196°C kg/mm^2		
	Al, 3.7% Cu	7:1, Cu:Mg	2.2:1, Cu:Mg	Al, 3.7% Cu	7:1, Cu:Mg	2.2:1, Cu:Mg
Lightly aged	4.0	5.9	8.3	6.0	8.4	12.0
Peak	8.0	13.2	13.3	8.5	14.5	17.0
Overaged (10 days)	5.0	10.7	9.5	7.0	12.0	11.0

.2. Mechanical Properties

Ageing curves of yield strength, tensile strength and % elongation for single crystals of both compositions are shown in Figs.55, 56, 57 and 58. Although crystals were tested in only four aged conditions, the values lie on curves which are very similar to those for the polycrystals shown in Figs.4, 5, 7 and 8. The properties of the single crystals and polycrystals are shown together in Table 4.14. To facilitate comparisons, all values are given in units of t.s.i. The values of 0.1% proof stress for the polycrystals have been listed in the "yield strength" columns. Percentage elongation has not been included in the table, since the single crystals in the as-quenched and lightly aged conditions deformed by single slip, and elongations were orientation dependent.

After longer ageing time, the single crystals and polycrystals of the 7:1, Cu:Mg alloy tested at -196°C and the 2.2:1, Cu:Mg alloy tested at room temperature had very similar elongations, whereas for the 7:1 alloy tested at room temperature, and the 2.2:1 alloy tested at -196°C, the elongations of the single crystals were approximately twice those of the corresponding polycrystals.

Table 4.14

Aged Condition	Tested at room temp.				Tested at -196°C			
	Yield Strength t.s.i.		Tensile Strength t.s.i.		Yield Strength t.s.i.		Tensile Strength t.s.i.	
	Single crystal	Poly-crystal	Single crystal	Poly-crystal	Single crystal	Poly-crystal	Single crystal	Poly-crystal
1. 7:1, Cu:Mg								
As-quenched	4.5	6.0	10.0	17.5	9.0	8.0	15.0	23.0
0.01 days at 190°C	7.5	9.0	12.0	18.5	11.0	14.0	15.5	26.0
Peak aged	18.0	19.0	24.0	24.0	20.0	23.0	27.0	31.0
10 days at 190°C	15.5	16.0	22.0	22.0	17.5	20.0	26.0	29.0
2. 2.2:1, Cu:Mg								
As-quenched	6.5	10.0	13.0	21.0	9.0	13.0	14.5	27.5
0.015 days at 190°C	11.0	13.5	14.5	24.0	15.5	19.0	20.0	28.0
Peak aged	18.0	22.0	23.5	27.0	23.5	26.5	27.5	32.0
10 days at 190°C	13.0	16.0	19.0	21.0	15.5	19.5	25.0	27.0

The changes in yield strength and tensile strength, with ageing, for the single crystals follow a similar pattern to the changes for the polycrystals, although the values are generally slightly lower. The quenched and lightly aged materials show the largest differences in strength between single and polycrystals. The strengths of peak and overaged alloys are closer, and are identical for the 7:1 alloy tested at room temperature.

4.2.3. The Temperature Dependence of Properties

.1. Stress-strain curves.

Figs.41 to 52 show the effect of temperature on the stress-strain curves for both alloys. With decreasing temperature, yield strengths increase in all aged conditions, and work hardening rate and uniform strain increase in the peak and overaged conditions. The quenched and lightly aged crystals show little change in work hardening rate with temperature, but, generally, the glide strain at maximum load is greater at lower temperatures.

.2. Critical resolved shear stress.

Fig.59 shows the variation of C.R.S.S. with temperature for 7:1, Cu:Mg alloy crystals in three aged conditions. Values for quenched crystals are also shown at 77°K and 295°K.

Quenched and lightly aged crystals, which increase in strength by 2.5 - 3 kg/mm^2 between room temperature and -196°C, show the

greatest temperature dependence (30 - 50%). Peak and overaged crystals show a smaller temperature dependence (10 - 15%) and increase by only 1.5 kg/mm^2 at -196°C.

In Fig.60, for the 2.2:1, Cu:Mg alloy, the temperature dependence of quenched crystals is similar (30%), but rises to 50%, (4 kg/mm^2 increase) for lightly-aged crystals, and is still 4.5 kg/mm^2, (30%) at the peak; overaged crystals have a temperature dependence of only 1.5 kg/mm^2, (15%).

In Al, 4.wt.% Cu, reverted[28,54] and air-cooled crystals[38] show an increase of 1 - 1.5 kg/mm^2, i.e. 25 - 30%, in C.R.S.S., between room temperature and -196°C. Crystals aged at 130°C to contain GP(1) zones show a corresponding increase of 3 kg/mm^2 (50%) [28,38,54]; those aged at 165°C to contain GP(2) zones, an increase of 2 kg/mm^2, (20%)[37], and those aged at 190°C to contain GP(2) zones, an increase of 1 kg/mm^2 (15%)[29] between room temperature and 77°K. Crystals aged to the peak at 190°C showed very little temperature dependence, (approximately 5%)[28,29], but for overaged crystals the C.R.S.S. increased by approximately 1 kg/mm^2, which, since the C.R.S.S. is decreasing rapidly, was of the order of 20% increase[28,29].

Comparing the above results with those for the ternary alloys, the temperature dependence in the as-quenched condition is similar, i.e. there is approximately a 30% increase in C.R.S.S. at 77°K (It should be noted, however, that only two ternary alloy specimens of each composition were tested in the as-quenched condition.)

In the lightly aged condition, both the ternary alloys contain GPB zones, and it is more appropriate to compare these with Al-Cu alloys containing GP(1) zones, since the zone sizes are more similar. The temperature dependences are then seen to be very similar, (30 - 50% increase in C.R.S.S. at 77°K). Al-Cu, and 7:1, Cu:Mg crystals in the peak aged condition, and all three alloy crystals in the overaged condition show similar temperature dependences, within experimental error (ranging from 5 - 15% increase in C.R.S.S. at 77°K), but the peak-aged 2.2:1, alloy appears to have a very much larger temperature dependence (30%) than the other two alloys.

.3. Other mechanical properties.

To facilitate a comparison between the temperature dependence of the properties of single crystals and polycrystals, yield strength, tensile strength and % elongation have been plotted as functions of temperature in Figs.61 and 62. Values for as-quenched crystals are shown in the ageing curves of Figs.55, 56, 57 and 58.

It should be noted that the strengths and ductilities of quenched and lightly aged alloys deforming by single slip are orientation dependent. The increases in yield strength and tensile strength at -196°C are shown in Table 4.15., together with the corresponding values for polycrystals.

Table 4.15

Aged Condition	% Increase in properties at -196°C			
	Single Crystals		Polycrystals	
	Yield Strength	Tensile Strength	0.1% Proof Stress	Tensile Strength
7:1, Cu:Mg				
As-quenched	100	47	34	33
Lightly aged	38	28	46	40
Peak aged	11	10	23	28
Overaged	13	18	22	33
2.2:1, Cu:Mg				
As-quenched	40	13	30	31
Lightly aged	41	38	38	29
Peak aged	28	20	21	22
Overaged	24	28	30	34

With the exception of the as-quenched single crystals (only one crystal of each alloy was tested at room temperature and -196°C) the percentage increases in yield and tensile strengths at low temperature are similar, within experimental error, for single and polycrystals of each composition.

4.2.4. The Rate of work-hardening

As seen in Section 3.2.1., the work-hardening rate shows a marked increase when the peak value of the yield strength is reached. Kelly and Nicholson[8] suggest that this behaviour is probably general for all precipitation-hardening systems where the final precipitate is an intermetallic compound. Figs.20 and 21 show that such a transition in the value of the work-hardening rate is detectable in polycrystalline material.

Values of the work-hardening rate for single crystals have been measured directly from the load-elongation traces by the method already described in Section 4.1.4.1. Although only four different ageing times have been used, the results have been plotted as ageing curves in Figs.63 and 64. It is seen that the work-hardening rate increases from approximately 20 kg/mm^2 to 300 kg/mm^2 as ageing proceeds. The wide scatter in the values for crystals aged near the peak, observed by Bonar[29] for Al, 3.7 wt.% Cu, is suggested even with the small number of crystals used in this investigation.

For both alloys, the initial work-hardening rates at each temperature are lower than those obtained by Bonar, who reports 60kg/mm^2 for Al, 3.7 wt.% Cu. At room temperature, the work-hardening rates for overaged crystals, 300 kg/mm^2, are similar to those found for Al-Cu, but at -196°C the values are larger (approximately 350 kg/mm^2). This difference has already been noted for polycrystalline material.

Work-hardening rates are shown below in Table 4.16, together with those for Al- 3.7 wt.% Cu obtained by Bonar, to compare with the polycrystalline values in Table 4.7.

Table 4.16

Aged Condition	Rate of work-hardening t.s.i,					
	Tested at room temperature			Tested at -196°C		
	Al, 3.7 wt.% Cu	7:1 Cu:Mg	2.2:1 Cu:Mg	Al, 3.7 wt.% Cu	7:1 Cu:Mg	2.2:1 Cu:Mg
Lightly aged	40	12	12	40	12	12
Overaged	190	175	195	190	220	225

The temperature dependence of the work-hardening rate is similar to that described for polycrystals. It is clear from Figs.63 and 64 that lightly aged crystals show no change in work-hardening rate with temperature, and that overaged crystals are strongly temperature dependent. At the peak, the exact position of the curves is not known, and the apparent negative temperature dependence is not significant.

4.2.5. Fracture

.1. Fracture appearance

Figs.66, 67, 68 and 69 are low magnification photomicrographs of the fractures exhibited by crystals in four aged conditions, when

tested at room temperature and -196°C.

At room temperature, as-quenched crystals and lightly-aged crystals of each composition, necked down to form double chisel-edged fractures, or 'crocodile' fractures as termed by Beevers and Honeycombe[110] for Al, 4 wt.% Cu crystals. These consist of deep V-shaped voids in the centres of the necks, which is thought to be consistent with Orowan's model of slipping apart in single crystals, by an alternating slip mechanism,[114]. In the peak aged condition, the 2.2:1, Cu:Mg crystals showed fractures which appeared to lie on planes parallel to the primary slip plane, together with coarse localised slip bands nearby. This type of fracture has been described by Price and Kelly[111] for zone-hardened Al alloy crystals. They termed the slip band portion the 'shear' region and the final separation portion the 'crack' region, although it was, in fact, entirely ductile. The 7:1, Cu:Mg crystals in the peak aged condition exhibited similar fractures, with larger proportions of 'shear' region and less 'crack' region.

After 10 days ageing, the fracture of the 7:1, Cu:Mg crystals consisted of a final shearing, following large reductions of area resulting from uniform necking. The 2.2:1, Cu:Mg crystal showed very little necking and it was believed that this was an imperfect specimen.

At low temperatures, the as-quenched and lightly aged crystals showed fractures which consisted of heavy localised slip bands,

with the final separations in regions lying almost parallel to these slip bands, as described for peak aged crystals tested at room temperature. The relative amounts of 'shear' region and 'crack' region appeared to vary more with crystal orientation than with alloy composition or testing temperature. Lightly aged crystals were tested at -78°C and -125°C, and showed similar fractures to those at -196°C.

Peak aged crystals, tested at low temperatures, exhibited fractures which were similar to those of the room temperature tested crystals. The 2.2:1 alloy showed very little shearing and the two halves of the crystal appeared to have slid apart along a slip plane, producing a smooth fracture surface. After 10 days ageing, the crystals tested at low temperature generally necked uniformly and formed double cup fractures, after very large reductions in area. Two of the 7:1, Cu:Mg crystals tested at low temperatures fractured in a similar manner to the peak aged crystals, but it is thought that the double cup fracture is more typical of the overaged condition.

Fractographs from 2.2:1, Cu:Mg alloy crystals in the lightly aged, peak-aged and overaged conditions are shown in Fig.70. The lightly-aged and peak aged crystals showed 'shear' and 'crack' regions on their fracture surfaces. Fig.70(b) shows large irregular cusps on the 'crack' region of the lightly aged crystal, which are very similar to the cusps seen on lightly aged

polycrystalline alloy. Fig.70(a) shows the boundary between the 'shear' and 'crack' regions, and slip steps are visible on the 'shear' region. On the peak-aged crystal, Fig.70(c), the cusps are very shallow, but regular, and are elongated over the whole of the 'crack' region. The 'shear' region was not visible on this replica.

The overaged crystal exhibited a double cup fracture, and in Fig.70(d) it is seen that the fracture surface consists of irregular cusps of widely different sizes. This type of cusp pattern is different from the overaged polycrystalline material.

5. DISCUSSION

5.1 The Relationship between Mechanical Properties and Structure.

Precipitation hardened alloys are divided into two groups, depending on whether, or not, the particles are sheared by dislocations at small strains; the groups are distinguishable by the forms of their stress-strain curves[8].

5.1.1 Group 1 alloys

The important characteristics of these alloys have been described in Section 3.2., for several aluminium-based systems. They are typified by the behaviour of Al-Cu alloys aged to contain GP(1) or GP(2) zones. In the case of single crystals, these characteristics are :

(a) critical resolved shear stresses at room temperature of the order of 5-10 kg/mm^2.

(b) work-hardening rates, during Stage 2, within the range 5-15 kg/mm^2.

(c) deformation initially by single slip.

Figs.41, 42, 47, 48 show that as-quenched and lightly aged Al-Cu-Mg alloys fulfil the first two conditions, and the slip line appearance of these soft crystals is consistent with single slip.

If dislocations cut through the particles, then the strengthening has been shown[8] to arise from three contributions, in addition to the strength of the solid solution matrix and any long range

constraints. First, the increase in the particle-matrix interfacial area; second, the formation of a disordered internal interface, if the particle is ordered; third, the formation of an interface dislocation, if the particle and matrix lattice spacings are different. The estimation of the magnitudes of these contributions has been described fully in section 3.4.

Before testing the various strengthening models on the group 1 alloys, it is necessary to estimate values for the metallographic data which are used in the formulae. One of the most important parameters is the volume fraction, f, of GPB zones. In the early stages of ageing (0.01 or 0.015 day at 190°C) the zones have been observed only as streaking in the diffraction patterns from thin foils;[24,115] consequently no direct calculation of volume fraction is possible, based on observed numbers and sizes of zones. A rough estimate has been made by applying the lever rule to the metastable phase diagram proposed by Beton and Rollason[92]. It was necessary to make certain assumptions regarding the structure of the GPB zones, in order to estimate their density (S.G.). Using the Gerold[20] model for GPB, i.e. consisting of alternate layers of Cu and Mg atoms lying on $\{100\}_{Al}$ planes, it was further postulated that there were equal numbers of Cu and Mg atoms in a zone and that these atoms occupied the Al lattice sites. Such a model is feasible, without excessive lattice distortion, since the average of the atomic diameters of Cu (2.55 Å) and Mg (3.24 Å) is 2.89 Å, which is very close to the atomic diameter of Al (2.86 Å). (There is evidence, however,

that the apparent atomic diameter of Al in solid solution is nearer 2.71 Å [116].) The GPB zone density (S.G.) was then taken as the average of the densities of Cu and Mg. For the 7:1 alloy, f for GPB zones was found to be approximately 0.011 and for the 2.2:1 alloy, approximately 0.018.

At a later stage of ageing in the 2.2:1 alloy, between 0.01 and 0.1 day at 190°C, Sen[115] has observed needle-shaped zones in thin foils. This ageing period corresponds to that in which Silcock[19] observed what she termed 'GPB with streak', from X-ray studies. Sen[115] has suggested that the zones termed GPB by Silcock are spherical zones as proposed by Gerold[20], and the 'GPB with streak' are needle-shaped zones, after the model proposed by Silcock, and that the latter only exist for a short period of ageing, whereas the spherical zones persist from immediately after quenching right up to the peak. Sen has measured the number per unit volume and the size of these needle-shaped zones; viz. approximately 10^{17}/cc. and approximately 15 Å diameter and 200 Å long. This agrees with Siloock's lower limit values of 10 - 20 Å diameter, and 80 Å long, and with Kelly and Nicholson's[8] figure of 10^{17} - 10^{18} for the number of GP(1) zones per unit volume in Al, 4 wt.% Cu.

The calculated value for f from Sen's figures is 0.0035, which is almost an order of magnitude less than the value from the metastable phase diagram. There are two possible reasons for this. First, if spherical GPB zones persist throughout this ageing period

as suggested by Sen, then the value of 10^{17} is too low, since this is based solely on the needle-shaped zones, which are visible in electron micrographs. Second, there is a large error (probably 50%) in the estimation of foil thickness, on which the value of 10^{17} is based. It is necessary to be more precise about the zone density than Kelly and Nicholson's approximation of $10^{17} - 10^{18}$.

In applying the formulae of Section 3.4., f values calculated from the metastable phase diagram have been assumed.

A second important parameter is the mean planar interparticle spacing. In the absence of metallographic measurements, because the zones are not visible on electron micrographs, an estimate of the spacing has been made from the volume fraction. Apart from the considerable errors in estimating volume fraction, it has already been mentioned in Section 3.4.3. that the calculation of spacing depends on which particle distribution is assumed. This point has received further attention recently[117]. The calculated spacings vary, approximately, by a factor of 2, as a result.

For spherical zones, the mean planar particle radius, $r_p = \frac{2}{3}$ x radius[74], so that for spherical GPB, r_p is approximately 13 Å[20]. Using Ashby's formula[74] for randomly distributed particles, the mean planar particle separation, d, ($= \frac{1}{2}\sqrt{\frac{\pi}{f}} \cdot r_p - 2r_p$) is approximately 80 Å for the 7:1 alloy and approximately 60 Å for the 2.2:1 alloy. Using the expression for non-randomly distributed particles, which would produce the largest separation ($= \sqrt{\frac{4}{f}}\, r_p - 2r_p$).

the values are 220 Å and 170 Å respectively. It is thought that the two smaller values are more realistic, bearing in mind that the measured spacing[29] for GP2 zones in Al, 4 wt.% Cu aged at 190°C is approximately 70 Å in the early stages of ageing.

The third important parameter is surface energy. Two separate surface energies need to be identified, viz. the particle matrix interfacial energy and the energy of the disordered internal interface if the particle is ordered. Neither of these can be estimated if the details of the structure of the particle are not known. Kelly and Nicholson[8] have derived an equation for the upper limit to the stress required to shear a particle by considering an overall interfacial energy which includes both the surface energy terms above, together with the interface dislocation term. (Equation 3.7 (b), Section 3.4.1.). Kelly[89] and Kelly and Fine[93] used the heat of reversion of zones to estimate this overall surface energy. It was assumed that the energy of an atom at the surface of a zone was one half the value of the energy of solution for an atom calculated from the reversion energy. The physical basis for this is uncertain, and values of surface energy derived for zones in Al-Cu and Al-Ag were in the range 100-200 ergs/cm^2.

Using the values for heats of reversion of 7:1 and 2.2:1, Cu:Mg alloys containing GP zones, from Beton and Rollason[92], viz. 4.75 kcal/gm-mol. of Mg and 6.5 kcal/gm-mol. of Mg respectively, and applying Kelly's formula,[89]

$$\gamma = \frac{\Delta E}{3 b^2}$$

where ΔE = heat of reversion/atom Mg

b = nearest neighbour separation, taken as 3 Å.

then the calculated surface energies are 135 ergs/cm^2 and 185 ergs/cm^2 respectively. These values are slightly higher than expected, but not unrealistic. Bonar[29] has used a value of 300 ergs/cm^2 for γ for GP(1) zones, as an upper limit.

The solid solution contribution to the strength cannot be estimated accurately, but Dew-Hughes and Robertson[27] have shown that for unaged Al-Cu crystals, the C.R.S.S. increases by 1.53 kg/mm^2 per at.% Cu. This value provides a lower limit in the case of Al-Cu-Mg alloys; taking the % Cu remaining in solid solution from Beton and Rollason's metastable phase boundaries. For 7:1 alloys the solid solution composition is 2 wt.% Cu, 0.25 wt.% Mg, for which the Cu contribution to the C.R.S.S. is approximately 1.2 kg/mm^2, and for 2.2:1 alloys, the solid solution is 1 wt.% Cu, 0.5 wt.% Mg for which the Cu contribution to the C.R.S.S. is approximately 0.6 kg/mm^2. The small amount of Mg present will increase these values slightly so that the solid solution contribution to the C.R.S.S. is estimated at 1.5 kg/mm^2 for 7:1 crystals and 1 kg/mm^2 for 2.2:1 crystals at room temperature.

Applying equation 3.9., long range effects will be expected if:-

$$d > \frac{\alpha G b}{\tau}$$

where $\alpha = 0.25$[29] for $\frac{d}{b} = 25$.

$G = 2.5 \times 10^3$ kg/mm^2

$\tau = 6$ kg/mm^2 (7:1) or 9 kg/mm^2 (2.2:1)

i.e., $d \geq 100b$ or $70b$.

Since the estimated d values, (approximately 80 Å (27b) for 7:1 alloys and 60 Å (20b) for 2.2:1 alloys) are less than those calculated from the equation, no long range contribution to hardening is expected.

Applying equation 3.7(b) to estimate the contribution from cutting;

For 7:1 alloys, $\tau = \frac{\sqrt{\pi}}{2} \cdot \frac{\gamma}{b} \cdot f^{\frac{1}{2}}$

where $\gamma = 135$ ergs/cm^2

$b = 2.86 \times 10^{-8}$ cms.

$f = 0.011$

then, $\tau = 42$ kg/mm^2

For 2.2:1 alloys, $\gamma = 285$ ergs/cm^2

$b = 2.86 \times 10^{-8}$ cms.

$f = 0.018$

then, $\tau = 77.9$ kg/mm^2

It is not possible to separate the effects due to increasing the particle-matrix interfacial area and due to disordering the internal interface, because of lack of basic information about the zones, e.g. the type and degree of order, and the disordering

temperature, if any. Regarding the contribution due to interface dislocation formation, Kelly and Nicholson[8] have shown that unless $\frac{\Delta b}{b} \geq 0.1$, where $\Delta b = b_{matrix} - b_{particle}$

b = interatomic spacing,

the contribution is very small. It was shown earlier that the strain associated with GPB is probably small so that the strengthening from interface dislocation formation is likely to be negligible.

Other possible contributions to the strength are the elastic modulus effect of Fleischer[86] and the stacking fault width effect of Hirsch and Kelly[88], considered in Section 3.4.2. Kelly and Nicholson[8] believed that the modulus effect was long-ranged and therefore should not apply here. In any case, its magnitude cannot be estimated because the elastic modulus of a zone is not known.

The zone size is large enough to provide a strengthening effect based on a change in the separation of partial dislocations as they pass through the zones, particularly since the coherency strains are probably small[88]. Low stacking fault energy precipitates of diameter ≥ 20 Å in Al would be expected to contribute to the yield stress, and using the analysis of Hirsch and Kelly this contribution would be approximately 2 kg/mm^2 for 7:1 alloys and approximately 3 kg/mm^2 for 2.2:1 alloys.

The relevant equations, giving upper and lower limits to τ , are:-

$$\tau = 0.04 \ (\Upsilon_2 - \Upsilon_1)^{4/3} . \ f^{\frac{2}{3}}$$

$$\text{and} \quad \tau = 0.23 \ (\Upsilon_2 - \Upsilon_1) \ . \ f^{\frac{2}{3}}$$

where Υ_2 = SFE of matrix

Υ_1 = SFE of zone

f = Vol. fraction of zones

$(\Upsilon_2 - \Upsilon_1)$ was assumed to be 200 ergs/cms^2, as typical for metastable phases in Al.(88)

Summing the contributions from solid solution strengthening, from cutting and from stacking fault effects, the calculated C.R.S. Stresses are 7.7 kg/mm^2 for 7:1 crystals, and 11.9 kg/mm^2 for 2.2:1 crystals, compared with room temperature values of 6 kg/mm^2 and 9 kg/mm^2 respectively. In each case the calculated values are about 30% too large, but taking into account the uncertainty of some of the assumptions made, the agreement is fairly good.

The temperature dependence of group 1 alloys has been described in Section 3.2.5. and discussed in Section 3.4.2. Essentially, the obstacles to dislocation motion (GP zones) are assumed to be cut in a single activated event, whence the flow stress is predicted to be a linear function of $T^{\frac{2}{3}}$; where T° K is the testing temperature. The equation is described in Section 3.4.1. and is repeated here :-

$$\tau = \frac{U_o}{v} \left[1 - \left(\frac{KT}{U_o} \cdot \ln \frac{\dot{\varepsilon}_o}{\dot{\varepsilon}} \right)^{\frac{2}{3}} \right]$$

Values for U_o, the activation energy for cutting at 0^oK, and v, the activation volume have been calculated for Al-Ag, Al-Zn and Al-Cu crystals containing GP zones,[95] from the intercepts and slopes of the graphs of τ as a function of $T^{\frac{2}{3}}$. For Al-Cu crystals containing GP(1), a graph with two different slopes was obtained[28], with two different Uo and v values, termed U_{oH} and v_H and U_{oL} and v_L, corresponding to the high and low temperature branches, respectively. Each was associated with the cutting of zones of different orientation in the slip plane.

Critical resolved shear stresses for the Al-Cu-Mg crystals containing GPB zones have been plotted as functions of $T^{\frac{2}{3}}$ in Fig.71. The interpretation, in the case of 2.2:1 alloys, is uncertain because of scatter and lack of data, but assuming that the plot consists of two straight line portions, values for U_o and v have been calculated, as shown in Table 5.1. together with results for the 7:1 alloy and for binary Al alloys.

Table 5.1. (see page 164)

These ternary alloy values are seen to be consistant with those for the binary alloys. The small values for U_o are in accordance with the small size and strain-free nature of the zones.

Table 5.1.

Alloy	Uo , eV	v , cm^3
Al-Cu GP(1) (28)	0.2 (U_{OL})	7×10^{-22} (v_L)
	6 (U_{OH})	10^{-20} (v_H)
Al-Cu GP(2) (28)	5	6×10^{-21}
Al-Ag (95)	6	10^{-20}
Al-Zn (95)	3.7	6×10^{-21}
7:1, Cu:Mg GPB	2	3×10^{-21}
2.2:1, Cu:Mg GPB	0.1 (U_{OL})	6×10^{-22} (v_L)
	3 (U_{OH})	3.6×10^{-21} (v_H)

The two branches on the $\tau - T^{\frac{2}{3}}$ graphs, for the 2.2:1 alloys, similar to Al-Cu containing GP(1), is not expected to result from an orientation dependence of dislocation-zone interaction, since GPB zones at this ageing stage are believed to be mainly spherical. Two alternative explanations can be put forward.

First, it is possible that in the 2.2:1 alloys a few needle-shaped zones have formed after 0.015 day. Sen(115) has observed streaking on electron diffraction patterns indicative of needle-shaped zones after 15 minutes (0.011 day) at 190°C, although Silcock(19) shows a minimum ageing period of approximately 0.03 day before 'GPB with streak' was detected. The presence of needle-shaped zones might provide an orientation dependence of cutting energy for those zones with their axes parallel to the Burgers

vector of the dislocation, in a somewhat analogous way to GP(1) zones. The smaller value of U_o (0.1 eV) is in accordance with the smaller stress field surrounding GPB zones, compared with GP(1). The higher temperature U_{OH} and v_H values then represent the effects of these GPB zones oriented in different directions (there are 3 different orientations) together with the spherical zones.

It must be emphasised that the points on the $\tau - T^{\frac{2}{3}}$ graph may not, in fact, represent two straight lines, but only an upward curve on a single line. Such a curve has been found for Al-Cu aged at 190°C to contain GP(2), where an appreciable amount of θ' is also present. It is possible that S may be present in the 2.2:1 alloy, particularly if any quenching strains exist to provide nucleating sites.

Values of activation volume, v, have also been estimated from the distribution of the zones. For 7:1 alloys, assuming the zone radius, r, is 8 Å [20] and the spacing, l, 80 Å, then v (given by 2rbl[8], where b is the atomic spacing) is equal to 3.7×10^{-21} cm^3., in excellent agreement with the value of 3×10^{-21} cm^3 in Table 5.1. For 2.2:1 alloys, v is equal to 2.8×10^{-21} cm^3., for spherical zones in reasonable agreement with the value for v_H of 3.6×10^{-21} cm^3., in Table 5.1. No estimation can be made for v_L.

Although considerable doubt has been cast on this type of analysis for Al-Zn and Al-Ag by Price and Kelly[37], who showed that the temperature dependence of the C.R.S.S. arose from the

temperature dependence of the matrix solid solution, this is not necessarily true for Al-Cu. Bonar[29] has shown that the solid solution contribution to the strength of Al-Cu crystals is only 5-10% of the total, so that the temperature dependence of this contribution cannot account for the observed temperature dependence. Similar indications have been found for the Al-Cu-Mg crystals. Thus, although no allowance has been made for the temperature dependence of the matrix solid solution, the analysis is consistent with that of other alloys where zone cutting is believed to control the yield strength.

5.1.2. Group 2 alloys

These alloys are characterised by having parabolic shaped, single crystal stress-strain curves, with high initial work-hardening rates, similar to polycrystals. X-ray examination of deformed specimens indicates that slip occurs on several systems from the start.[28,118] This, together with the observed interaction of dislocations with the precipitates in thin foils[29] indicates that initially the particles are not sheared, unlike the group 1 alloys.

.1 Yield strength

Two models for the yield strength of group 2 alloys have been proposed. Kelly and Nicholson[8] favour the Orowan model, whereby the yield stress is identified with the stress required to expand a dislocation between two adjacent particles[77,]. Ansell and Lenel[84] identify the yield with shearing of the particle under the stress

concentration caused by successive loops formed around it. Most of the evidence appears to favour the Orowan model, as discussed in Section 3.4.1., and this model seems to be obeyed, within a factor of 2. Much of the discrepancy can be accounted for by differences in the estimation of the planar inter-particle spacing in different investigations, particularly for non-spherical particles and under conditions where cross-slipping may occur readily.

In addition to the solid solution strength, long range constraints may also contribute, since the spacing of the particles is now large enough for dislocations to lie in the energy 'valleys' between them. The condition for this is

$$d \geq \frac{\alpha G b}{\tau}$$

For $\alpha \simeq 0.5$ [29]

$G = 2.5 \times 10^{3}$ kg/mm^2.

$b = 2.86 \times 10^{-8}$ cms.

$\tau = 13$ kg/mm^2 (peak)

or 10 kg/mm^2 (overaged)

then $d \geq 100\ b$ (peak)

or $\geq 125\ b$ (overaged)

In the case of peak aged and overaged 7:1 and 2.2:1 alloys, where the major hardening precipitate is S in the form of laths, the interparticle spacing is very difficult to measure due to the high density of precipitation of the laths.[115] Measurements at higher ageing temperature have been made, as part of a study of

coarsening of S precipitates[115]. These measurements suggest that the density of precipitation of the laths after 10 days at 190°C is approximately 7×10^{13}/cc. and that the average size of a lath is approximately 5000 Å x 600 Å x 250 Å. These dimensions agree roughly with estimates made from electron micrographs of 2.2:1· alloys aged for 6 days at 190°C [24]. From these figures an estimate of the spacing between the laths has been made, assuming that the separation is the same in the direction of each measured dimension of the lath. It has also been assumed, to simplify the calculation, that the laths are all aligned parallel to each other. This is not believed to introduce a greater error than those associated with the other assumptions. The value obtained is 1100 Å, i.e. about 400 b. Thus, long range constraints are expected to contribute to the strength. Bonar[29] has discounted long range effects in Al, 4.wt.% Cu alloys containing θ' as a result of observations of dislocations being unaffected by or attracted towards the precipitate particles. This is not necessarily so in the case of S precipitates. Two types of long range stress have been identified.

First, the long range coherency constraints, the magnitude of which is estimated from Mott and Nabarro[81], using equation 3.4.:-

$$\tau = 2 G e f$$

Nabarro[119] has shown that for solid solutions, ef may be estimated from the change in lattice parameter $\frac{\Delta a}{a}$, where

Δa is the difference between the lattice parameters of the solid solution and the solvent metal and 'a' is the lattice parameter for the solvent metal. In the case of aged alloys containing a dispersion, the strain in the matrix due to the particles may be estimated from the change in lattice parameter, provided that the strain arising from the residual solute content in the matrix is low. This assumption has been made for alloys aged for 10 days. Pearson[120] has reviewed X-ray data for these alloys, which show that for 2:1, Cu:Mg alloys annealed at 200°C, the lattice parameter is almost identical with that for pure Al. Consequently there are negligible coherency strains in the overaged alloy. No information about the change in lattice parameter with ageing time has been found, however.

Second, the effect due to the difference in shear modulus between matrix and precipitate particle.[74,86] In the region of an abrupt change in modulus, such as near a large non-coherent precipitate, a dislocation will be attracted or repelled (depending on whether the modulus of the particle is greater or less than that of the matrix) by a force which varies inversely as the distance of approach from the particle. The stress required to overcome this, in the case of a repulsive force, is of the form:

$$\tau = \frac{Gm\,(Gp - Gm)\,b}{4\pi\,(1 - \nu)\,(Gp + Gm)} \cdot \frac{1}{x}$$

where Gm = shear modulus of matrix

Gp = shear modulus of particle

b = Burgers vector of dislocation

ν = Poisson's ratio

x = distance between dislocation and precipitate

For Gp = 2 Gm, then:

$$\tau = \frac{280}{x} \text{ kg/mm}^2 \text{ , where x is in Å}$$

This contribution can be large when dislocations are pressed against precipitates. However, under conditions where the Orowan mechanism applies, such an effect will simply decrease the interparticle separation. Ashby[74] has estimated that x is then only approximately 0.1 r, where r is the particle radius, for intermetallic precipitates in metals, so that the Orowan stress is not affected significantly.

As a contribution to the long range back stresses acting on dislocations[86], the modulus effect is very much less than the Orowan stress,[74] as shown below by the calculation for the mean back stress, which is given by[74] :-

$$\tau = \frac{(Gp - Gm)\ b.f.}{4.\pi} \cdot \frac{1}{d}$$

for $Gp = 5 \times 10^3$ kg/mm^2

$Gm = 2.5 \times 10^3$ kg/mm^2

b = 2.86 Å

f = 0.053

d = 1100 Å

$$\tau = 0.026 \text{ kg/mm}^2$$

The value for f has been calculated from the estimated dimensions and density of precipitation of S laths.

The solid solution contribution is estimated at not more than 0.5 kg/mm^2.

The Orowan stress is given by:-

$$\tau = \frac{2\,\alpha\,Gb}{d} \qquad \text{(equation 3.6.)}$$

This is a simplified form compared with Kelly and Nicholson's equation, and does not take into account the size of the precipitates, compared with their spacing. In the present case the uncertainty attached to the estimation of the spacing does not warrant a more precise expression.

Taking $\alpha = 0.5$

$G = 2.5 \times 10^3\ kg/mm^2$

$b = 2.86$ Å

$d = 1100$ Å ,

then, $\tau = 6.5\ kg/mm^2$

The total calculated yield stress is then approximately 7 kg/mm^2, which agrees well with the measured value of approximately 10 kg/mm^2 for overaged crystals. The errors involved in calculating the interparticle spacing could readily account for the discrepancy.

In the case of peak aged alloys, the number of S precipitates is greater and consequently their spacing smaller. The Orowan stress is therefore larger, and the rapid work-hardening rate immediately after yielding suggests that this is what governs the yield stress.

However, the structure of the peak aged alloy is heterogeneous and there are areas between growing laths of S phase which contain only GPB zones.[115] These areas were observed on electron micrographs to be as large as 1500 Å square. They must offer a similar or slightly greater resistance to dislocation movement than the areas containing S, or S and θ' precipitates. Since the GPB zones are visible in the electron microscope they must be larger than those in lightly aged alloys, so that long range effects, in addition to the cutting resistance and stacking fault energy contributions of Section 5.2.1. are probably responsible for the higher strength in these S and θ' free regions. Such regions will also be expected to influence the work-hardening in these alloys.

As predicted by the Orowan theory, the temperature dependence of the C.R.S.S. for peak and overaged crystals is equal only to that of the shear modulus, together with a small contribution from the matrix solid solution. Figs.59 and 60 show small temperature dependences for 7:1 peak and overaged alloys and for 2.2:1 overaged alloys, but the 2.2:1 peak aged alloy shows a large temperature dependence, similar to that of the lightly aged alloy. This suggests that there is greater heterogeneity in the structure of the 2.2:1 peak aged alloy so that dislocations moving in areas free from S precipitates contribute largely to the deformation. This suggestion is supported by the work-hardening characteristics of the 7:1 and 2.2:1 peak-aged alloys, shown in Figs.63 and 64. The 7:1 crystals are seen to have much higher work-hardening

rates at the peak than those of 2.2:1 crystals, which (particularly at 77°K) are similar to lightly aged crystals.

.2 Work-hardening

The rapid work-hardening rate observed in group 2 alloys has been shown to result from a large increase in dislocation density arising from turbulent slip.[28] The marked temperature dependence of the work-hardening and the increase in the reversible change of flow-stress with strain[28] has emphasised the importance of cross-slip[8], so that a modification of Fisher, Hart and Pry's mechanism for the formation of dislocation loops around the precipitates has been proposed[8]. (Section 3.4.4). Ashby's equation (equation 3.10.) for the increase in flow stress due to work-hardening, $\Delta\tau = \frac{G}{2}\sqrt{\frac{b.f.}{r}}$, predicts a parabolic hardening curve[74]. Figs.45, 46, 51 and 52 show that this generally appears to be true for Al-Cu-Mg crystals at different stages of ageing, although experimental verification cannot be made due to lack of precise values for f and r. The change in work-hardening rate with ageing is shown in Figs.63 and 64. The marked increase near the peak is thought to be associated with the formation of dislocation loops around the S and θ' precipitates, in the same way as that observed in Al-Cu alloys[29] containing θ' or θ. The values of the work-hardening rates in overaged 7:1 and 2.2:1 crystals are equal to or smaller than those in overaged Al-Cu at room temperature, but greater at 77°K. (Table 4.16) Fisher, Hart and Pry showed that the initial work-hardening rate was proportional

to $\frac{f}{r}^{3/2}$ where f is the volume fraction of precipitate and r is the mean radius of the precipitates intersecting the slip plane (the planar particle radius) and Ashby showed that the hardening was proportional to $(f/r)^{\frac{1}{2}}$. In each case a greater hardening rate is predicted by a large volume fraction of precipitate, and a small particle radius. In both the 7:1 and 2.2:1 alloys, the higher total alloy content (Cu+Mg) and faster ageing probably result in a larger volume fraction of precipitate after 10 days ageing, compared with Al, 3.7% Cu, and the lath-shaped S precipitates have a smaller equivalent r value than that for θ' discs, resulting in the higher work-hardening rates observed at -196°C. At room temperature, however, the slightly lower hardening rate for the 7:1 alloy compared with Al-Cu probably represents the greater ease of cross-slip around the lath-shaped S precipitates in this alloy; the 2.2:1 alloy probably contains more precipitates and the closer spacing therefore compensates for the easier cross-slip giving a higher work-hardening rate than in the 7:1 alloy. An alternative explanation, based on the yielding of S precipitates is unlikely at this early stage of deformation, although it is probable that the precipitates are sheared at higher strains. (Section 5.3.4.)

The work-hardening of polycrystals has been described fully in Section 4.1.4. The increase in work-hardening rate with ageing time, corresponding to the change from group 1 to group 2 characteristics in single crystals, is also observed for polycrystals as shown in Figs.20 and 21. The relatively high values for the as-quenched and

lightly aged alloys, together with the parabolic shape of the stress-strain curves, emphasise the marked influence of the grain boundaries on the deformation of these alloys. This is discussed more fully in Section 5.3. In the case of peak and overaged alloys, the influence of the grain boundaries is equally marked but in a different manner. The work-hardening rates of polycrystals are less than those of the corresponding single crystals. (Tables 4.7 and 4.16).

The analysis of work-hardening in polycrystals in Section 4.1.4. showed that the strain-hardening coefficients for alloys in the same aged condition, when measured by different methods, did not agree with one another. (e.g. for 7:1 alloys in Table 4.9.). In the case of as-quenched and lightly aged alloys the true stress - true strain curves are not parabolic over their entire length and cannot be described by a single equation[121]. Log $\bar{\sigma}$ - log $\bar{\varepsilon}$ graphs show three distinct regions (Fig.22), consisting of a short linear portion with non-linearity at lower and higher strains. The low strain non-linearity is associated with transience following yielding, but the high strain non-linearity represents a major departure from the Ludwik equation. The physical significance of this behaviour is not known, but it appears to be a characteristic of pure Al[121] and Al solid solution alloys[61]. These departures from the simple Ludwik equation account for the failure of the expressions $n = \bar{\varepsilon}_u$ and $n = \left.d\bar{\sigma}/d\bar{\varepsilon}\right/\bar{\sigma}/\bar{\varepsilon}$ (Section 4.1.4. and Appendix 1) to describe the strain hardening of the soft alloys.

Peak and overaged alloys have true stress - true strain curves which tend to obey a single parabolic law. This is seen from the log $\bar{\sigma}$ - log $\bar{\varepsilon}$ curves (Fig.22), which, after initial transience associated with yielding, are linear. However, the values of n from the slopes of the log $\bar{\sigma}$ - log $\bar{\varepsilon}$ plots do not agree with the values obtained from the true strain at maximum load (Table 4.9.) These latter values are always too low. Even after correction, using Swift's equation, whereby $\bar{\varepsilon}_u$ was computed from (n-B), (Section 4.1.4 and Appendix 1) the values do not agree. It is proposed that the discrepancy arises because the limit of uniform strain is reached too soon due to non-uniform deformation within the specimen. In the peak and overaged alloys deformation takes place preferentially in the grain boundary precipitate - free zones, which work harden rapidly as a result of boundary generated dislocations moving only short distances within the zones. As a consequence of this, fracture occurs preferentially within the precipitate-free zone. (Section 5.3.4.) This premature failure before the uniform strain potential of the alloy, (as predicted by the Ludwik or Swift equation) has been reached, is supported by the observations that on certain overaged alloys, fracture occurred on a rising stress strain curve. This point is discussed more fully in Section 5.3.4.

5.2. The Effect of Mg

Metallographic studies[19,115] have shown that the effect of Mg on the ageing characteristics of Al-Cu alloys is to speed up

the ageing kinetics, and to alter the precipitate structure by introducing additional kinds of zones and precipitates. Consequently, a direct comparison between the mechanical properties of Al-Cu and Al-Cu-Mg alloys after the same ageing treatments is not meaningful because the precipitate structures are different. A comparison between as-quenched and peak aged alloys has been made, however, to provide information about the improvements in strength brought about by the addition of Mg to Al-Cu.

5.2.1. Supersaturated solid solution alloys

Table 5.2. shows yield stress and tensile stress values for Al-Cu, 7:1 and 2.2:1 alloys. Critical resolved shear stresses for Al-Cu crystals have been estimated from previous work[27,35,36]. Values for as-quenched Al, 3.5 wt.% Cu polycrystalline material have been assumed to be the same as those after 0.05 day at 190°C, since Hardy[26] has shown that no increase in hardness occurs until 0.1 day at 190°C in this alloy.

Table 5.2

Testing Temperature, °K.	Mechanical Property kg/mm^2	Al, 3.5 wt. % Cu (Al, 1.6 at. % Cu)	Al, 3.8 wt. % Cu, 0.56 wt.%Mg (Al, 2.4 at. %Cu + Mg)	Al, 3.3 wt. % Cu, 1.58 wt.%Mg (Al, 3.2 at.% Cu + Mg)
77	C.R.S.S.	4.5	6.7	6.1
	0.1% proof stress	12.0	13.4	20.6
	tensile stress	31.0	36.2	43.3
295	C.R.S.S.	2.8	3.5	4.8
	0.1% proof stress	10.1	9.9	15.3
	tensile stress	23.6	27.6	33.9

There is evidence (see Table 5.4 and Fig.59) that the C.R.S.S. for the 7:1 crystal at 77°K is incorrect and should be approximately 1.5 kg/mm^2 less than the measured value. In which case the increase in C.R.S.S. with % Mg is approximately linear at both temperatures. The rate of increase is 1.25 kg/mm^2 per wt.% Mg, which ignores any effect due to slight differences in the % Cu in each alloy. This has been taken into account, by calculating the increase in C.R.S.S. as a function of atomic % (Cu and Mg), which is approximately 1.25 kg/mm^2 per at.% (Cu and Mg). This is lower than the value of 1.52 kg/mm^2 per at.% Cu found by Dew-Hughes and Robertson for air-cooled Al-Cu crystals[27]. Again, assuming that the C.R.S.S. of the 7:1 crystal at 77°K is incorrect, the temperature dependence of the C.R.S.S. appears to be similar for all three alloys. Thus the increase in strength of the crystals with increasing amounts of solute from Al, 1.6 at.% Cu, to Al, 2.4 at.% (Cu and Mg) to Al, 3.2 at.% (Cu and Mg) is less than it would be for corresponding increases in % Cu alone, but it has the same temperature dependence. This is also borne out by Beevers and Honeycombe's[122] results on solution treated Al, 2.4 at.% Cu, which has a C.R.S.S. of approximately 4.5 kg/mm^2 at 295°K, compared with the 7:1, Cu:Mg value of 3.5 kg/mm^2 in Table 5.2.

In the case of Al-Cu supersaturated solid solutions, elastic interactions between dislocations and the strain fields of the smaller Cu atoms in the matrix, together with the presence of vacancy loops and helices and Cu atom clusters provide the major

contributions to the strength. If some of the Cu atoms were replaced by Mg, the strain fields of Mg and Cu atom pairs would be very small, since the sum of their atomic diameters is approximately the same as twice the atomic diameter of Al. (Section 5.1.1.) Furthermore, Mg atoms which form Mg-vacancy pairs would also have smaller strain fields than single Mg atoms. Thus the strengthening due to elastic strains surrounding Cu atoms in solid solution should be reduced by these two effects. Since the Al-Cu-Mg crystals are stronger than Al-Cu crystals with the same Cu content, then the higher strength must result from other contributions. The vacancy loop density is probably higher in the case of the Al-Cu-Mg crystals, since these were water-quenched, whereas the Al-Cu crystals were air-cooled. Dew-Hughes and Robertson[27] have shown that water-quenching can produce an increase of approximately 2 kg/mm^2 in the C.R.S.S. of water-quenched Al-Cu crystals, compared with air-cooled or acetone-quenched ones. Wilson and Forsyth[123] have found that the dislocation arrangement in quenched alloys depended on the severity of the quench.

The higher retained vacancy concentration in quenched Al-Cu-Mg alloys and more rapid diffusion might enhance the solute clustering contribution to strengthening. In this case, although elastic strain in the matrix is still small, the strengthening would be controlled by the interfacial energy and stacking fault energy contributions in a similar way to GPB zone hardened alloys already described. (Section 5.1.1.).

Table 5.2 shows also that the 0.1% proof stress and tensile strength changes reflect these increases in the shear strength of the matrix. They also increase approximately linearly with % Mg.

5.2.2. Peak-aged alloys

The changes in C.R.S.S., 0.1% proof stress and the tensile strength with % Mg are shown in Table 5.3.

Table 5.3

Testing Temp. ^{o}K	Mechanical Property Kg/mm^2	Al,3.5wt.% Cu (Al,1.6at.% Cu)	Al,3.8wt.% Cu 0.56wt.% Mg (Al,2.4at.%Cu+Mg)	Al,3.3wt.%Cu 1.58wt.% Mg (Al,3.2at.%Cu+Mg)
77	C.R.S.S.	8.5	14.5	17.2
	0.1% proof stress	20.8	37.1	41.7
	Tensile strength	35.6	48.3	50.0
295	C.R.S.S.	8.0	13.2	13.5
	0.1% proof stress	17.5	30.5	34.2
	Tensile strength	27.9	37.9	42.6

The increase in C.R.S.S. is almost linear with atomic % (Cu and Mg), at $77^{o}K$ and the rate of increase is very high, being approximately 7.5 kg/mm^2 per atomic % (Cu and Mg). This rapid increase is due to the smaller interparticle separation of the S precipitates compared with θ' as a result of their lath-shape. This increases the Orowan stress to expand dislocations between the precipitates.

At 295°K the C.R.S.S. increases equally rapidly from Al, 3.7 wt. % Cu to the 7:1, Cu:Mg alloy, but the 2.2:1 alloy then has the same C.R.S.S. value. An explanation, taking into account the heterogeneity of the structure in this alloy is given in Section 5.1.2.

The increase in 0.1% proof stress and tensile strength of the polycrystalline material with % Mg is non-linear and this follows the same trend as the change in hardness with composition discovered by Hardy[18]. Both the proof stress and tensile strength measurements are influenced by the work-hardening rate of the material, which is greatly influenced by the nature of the precipitate particles. In the case of the 2.2:1 alloys, where the structure is heterogeneous and the work hardening rate of peak-aged crystals is low, (Section 5.1.2) the measured proof stress and tensile strength are less than would be predicted if the material were homogeneous.

5.3 The Comparison between Single Crystal and Polycrystal Mechanical Properties.

5.3.1 The aggregate theory.

Attempts[124,125,126] to relate the plastic properties of polycrystalline material to the basic deformation behaviour of single crystals have not been entirely satsifactory in the case of tensile deformation. Apart from the fact that dislocation movements in single crystals are not precisely known, the constraints imposed by a grain in a polycrystal on its differently oriented neighbours can induce additional deformation mechanisms, such as localised slip,

the operation of additional slip systems, and the formation of grain boundary pile-ups. Consequently, most theories have been based on macroplasticity concepts, assuming only deformation by crystallographic slip.

Taylor's analysis[124] dealt with a polycrystal, composed of randomly oriented f.c.c. crystals, under uniaxial tension. He assumed that the grains were rigid-plastic, (i.e., no elastic deformation and a sharp yield point with no work-hardening) and underwent the same homogeneous strain as the aggregate in order to retain boundary continuity. He also assumed that the operative slip systems were those for which the sum of their separate magnitudes were least, in order to calculate the amounts of slip in each crystal. An allowance was made for the von Mises criterion that constant volume strain requires the operation of five independent slip systems. Shear stress and shear strain in a single crystal were then related to the tensile stress and strain in an aggregate by means of an average orientation factor, M, equal to 3.06.

Thus $\bar{\sigma} = M\tau$

and $\bar{\varepsilon} = a/M$

where, $\bar{\sigma}$ = true tensile stress

$\bar{\varepsilon}$ = true tensile strain

τ = single crystal shear stress

a = single crystal glide strain

The factor M is analogous to the Schmid factor $m = \frac{1}{\cos \lambda . \cos \varphi}$

(see Appendix 2) relating the applied tensile stress, σ, acting on a single crystal to the shear stress, τ, on the operative slip plane through the relationship,

$$\sigma = \frac{\tau}{\cos \lambda . \cos \varphi}$$

Confirmation of Taylor's findings has been obtained through more rigorous analysis by Bishop and Hill[125] and by Kocks[126] who has also examined the physical assumptions which were made.

First, grain boundary continuity requires simultaneous slip on at least five systems. Polyslip must therefore be the basic mechanism of polycrystal deformation. Only single crystals with <100> or <111> orientations are able to deform in tension by simultaneous slip on five or more systems (8 and 6 respectively). Good agreement has been shown between polycrystal and aggregate stress-strain curves, derived, using Taylor's formulae, from shear stress-glide strain curves for <111> Al crystals[126,127]. In the case of <100> crystals, agreement was only obtained during the early stages of plastic strain[127].

Second, each grain was assumed to deform homogeneously, ie. uniform slip over the whole grain. Bishop and Hill[125] and Kocks[126] maintained that this assumption was unnecessary, although the deformation may be dealt with, mathematically, as though it were homogeneous. Richards[128] claimed experimental confirmation for this point of view from deformation studies on textured Cu material.

Third, an implicit assumption in Taylor's theory was that all slip systems, latent and active, hardened equally during deformation. This is clearly invalid, since it implies that the stress-strain curves for single crystals are orientation independent. However, Hosford[129] has pointed out that the assumption only needs to apply to polyslip deformation, since this is a prerequisite of the Taylor theory. From plane-strain compression tests on Al single crystals, representing ten different combinations of four or more active slip systems, Hosford showed in each case that the shear stress-glide strain curves were similar to each other and to a polycrystal curve. This implied that the shear stress depended primarily on the amount of prior slip and not on the particular combination of active systems, in support of Taylor's assumption. Kocks and Brown[130] carried out compression tests on Al single crystals, previously deformed into Stage 3. The flow stresses required to activate secondary slip on each of the 24 possible systems were then found to be very similar. This meant that the anisotropy of the yield surface was small, under these conditions, and the Taylor assumption justified. However in tensile tests, <100> Al crystals have shown anomalously low work-hardening behaviour after 5% strain, compared with <111> crystals[131]. The suggestion has been made that this is caused by mutual work-softening of the primary and cross-slip systems[132].

Fourth, Taylor and Bishop and Hill both assumed rigid-plastic material. This assumption is valid only when elastic strains are

very small compared with plastic strain. Lin[133] and Budiansky and Wu[134] have considered the effect of elastic strains, and shown that near the yield point, where plastic strains are small, the value of M can be reduced well below 3.06. Their analysis, which is entirely theoretical, predicts that M is equal to 2.2 when the plastic strain is only 7% of the elastic strain, but increases rapidly to reach the Taylor and Bishop and Hill value after plastic strains of the order of 0.1 - 0.5%. One of the assumptions made is that any interference between the grains can be ignored at low strains, and this corresponds to the physical picture envisaged by Kocks[126] of slip starting on a single system within a few favourably oriented grains, and spreading to two, three and more systems after further deformation. An early aggregate theory, by Sachs[121], also ignored interactions between grains, M being calculated from the average of the Schmid factors for all 24 slip systems in a f.c.c. crystal. It is interesting to note that the value obtained for M was equal to 2.24.

The effect of work-hardening was also considered by Budiansky and Wu[134], who showed that M is increased after large strains, reaching a value as high as 3.6. The physical validity of the assumptions made was not discussed and there is no experimental evidence for the analysis.

5.3.2 Tests of the aggregate theory

.1 The yield stress

Previous results for Al crystals suggest that agreement between aggregate and polycrystal stress-strain curves is not very good at small strains,[124, 127] using the Taylor factor M = 3.06. Only Kocks[126] has shown good agreement at the yield point for an aggregate curve based on a <111> Al crystal.

Table 5.4 shows yield point parameters from single crystals and corresponding polycrystals of Al-Cu-Mg alloys used in the present investigation. Values of 3.06 τ_o, (where τ_o is the C.R.S.S. of the single crystal) are in column 3, and the values of the proportional limit, $\sigma_o(P)$, for polycrystals with corresponding ageing treatments are in column 5. For as-quenched alloys, with the exception of the 7:1 alloy tested at 77°K, there is agreement between the values of 3.06 τ_o and $\sigma_o(P)$. (There is evidence (Table 5.2 and Fig 59) that the C.R.S.S. for this 7:1 crystal is incorrect, so that the 3.06 τ_o value is high.) For aged alloys, 3.06 τ_o values are significantly greater than the $\sigma_o(P)$ values. To ascertain whether, or not, these differences might be caused by errors in measuring $\sigma_o(P)$, values of 0.1% proof stress for the polycrystals ($\sigma_{0.1}(P)$) are shown in column 6. These, too, are significantly smaller than the corresponding values of 3.06 τ_o.

It is concluded that aged alloys show no agreement with the Taylor theory at the yield point. As-quenched alloys show approximate agreement, (with the exception of the 7:1 alloy at 77°K) taking into account the fact that only one crystal of each composition was tested at each temperature.

Table 5.4

Aged Condition		τ_o kg/mm^2	3.06 τ_o kg/mm^2	σ_o(S) kg/mm^2	σ_o(P) kg/mm^2	$\sigma_{0.1}$(P) kg/mm^2	$\sigma_o(P)/\tau_o$ = M
7:1, Cu:Mg							
AQ.	295°K	3.5	10.7	7.0	8.4	9.8	2.4
	77°K	6.6	20.2	13.7	11.5	13.1	1.7
0.01d	295°K	5.8	17.8	11.7	12.9	15.3	2.2
	77°K	8.4	25.7	16.5	20.5	22.4	2.4
0.1d	295°K	11.3	34.6	26.2	21.3	24.4	1.9
	77°K	13.1	40.0	31.6	28.8	31.0	2.2
0.5d	295°K	13.2	40.4	28.6	27.9	30.2	2.1
	77°K	14.5	44.3	31.2	34.6	37.2	2.4
10d	295°K	10.7	32.7	24.5	23.3	25.2	2.2
	77°K	12.0	36.7	27.8	29.3	31.0	2.4
2.2:1, Cu:Mg							
AQ	295°K	4.7	14.4	9.8	13.1	15.3	2.8
	77°K	6.1	18.7	13.6	18.8	21.2	3.1
0.015d	295°K	8.7	26.6	17.5	20.1	21.7	2.3
	195°K	9.3	28.4	19.0	21.9	23.4	2.3
	148°K	10.9	33.3	22.5	25.4	26.6	2.3
	77°K	12.3	37.6	24.7	29.1	31.2	2.4
0.1d	295°K	10.5	32.1	26.0	22.4	24.6	2.1
	77°K	13.9	42.5	32.7	32.5	34.3	2.3
0.4d	295°K	13.2	40.4	28.5	31.4	33.6	2.4
	195°K	14.4	44.0	30.1	34.2	35.6	2.4
	148°K	15.8	48.3	34.4	36.6	38.2	2.3
	77°K	17.0	52.0	33.2	38.4	40.9	2.3
10d	295°K	9.5	29.1	20.9	22.5	24.3	2.4
	195°K	8.8	26.9	19.8	23.8	25.7	2.7
	148°K	11.1	34.0	24.8	26.0	27.6	2.3
	77°K	11.0	33.7	24.6	27.3	29.8	2.5

In column 7, values of the ratio $\sigma_o(P)/\tau_o$ (= M) have been calculated, to see how they compare with the Taylor value, 3.06. They are seen to be consistent and reasonably close to the minimum value of 2.2 calculated by Budiansky and Wu[134], taking elastic strains into consideration in the Taylor theory. The mean of the values in column 7 is 2.35, and the difference between this and 2.2 represents a plastic strain of only 0.025%, on the Budiansky and Wu analysis. This is within experimental error, since it is of the same order as the width of the pen trace on the recorder chart. There appears to be some experimental support, therefore, for a model based on an elastic correction to the Taylor theory.

As an alternative, values of the engineering yield stress, $\sigma_o(S)$, for single crystals, in column 4, have been compared with $\sigma_o(P)$ values. In the case of the 7:1 alloys, the differences between $\sigma_o(S)$ and $\sigma_o(P)$ are fairly random, but for 2.2:1 alloys, there is a trend for $\sigma_o(P)$ to be 10-15% greater than $\sigma_o(S)$. In both alloys the differences are outside the limits of experimental error for stress measurements, estimated to be 3% maximum.

A statistical analysis of the data for all the alloys in Table 5.4 has been made to try to distinguish between the two possibilities, viz., $\sigma_o(P) = 2.2\,\tau_o$ or $\sigma_o(P) = \sigma_o(S)$. Regression analyses produced correlation coefficients of 0.93 for $\sigma_o(P) = 2.2\,\tau_o$ and 0.90 for $\sigma_o(P) = \sigma_o(S)$. The slope of the regression lines were compared with a slope of 1, which was shown to lie within the 95% confidence limits of the regressions. No significant difference (by Student's t test) was found between them.

Using only the data for well-aged alloys, (greater than 0.1 day),

since single slip has been shown to be unrepresentative of polycrystal deformation, similar analyses were carried out. The correlation coefficients obtained were 0.87 for $\sigma_o(P) = 2.2\ \tau_o$ and 0.79 for $\sigma_o(P) = \sigma_o(S)$. Comparing regression line slopes, it was shown that a line of slope equal to 1 was significantly different from the $\sigma_o(P) = \sigma_o(S)$ slope, at the 95% level, whereas for $\sigma_o(P) = 2.2\ \tau_o$ there was no significant difference. This suggests that the yield stresses of aged single and polycrystal alloys support the aggregate theory predictions, taking into account corrections for elasticity. Furthermore, $\sigma_o(P)$ equal to $\sigma_o(S)$ would mean that there was a strong orientation dependence of the C.R.S.S. for aged single crystals. This has not been observed in previous work on Al alloys (Section 4.2.1.4), nor in the present work.

.2. Beyond the yield point

Results for pure Al[126] show that aggregate curves calculated from 'soft' (non-polyslip) orientation single crystal curves, have lower work-hardening rates than the corresponding polycrystal curves. Both as-quenched and GP zone-hardened crystals of Al alloys show similar work-hardening characteristics to pure Al, (Section 4.2.1.4.) since solutes and GP zones introduce an additional 'frictional' resistance to dislocation movement but work-hardening interactions remain similar. Thus in Figs. 72 and 73 the aggregate curves for as-quenched and GPB zone-hardened crystals respectively, using Taylor's theory, have lower work hardening rates than the corresponding polycrystal curves. The agreement between the two curves at the yield point for as-quenched alloys, is consistent with Kocks' results for pure Al, where the C.R.S.S. is orientation independent[126]. The

Budiansky and Wu correction may not be so important here since the yield stress is low and consequently the elastic strain is small. The 7:1 as-quenched alloy at 295°K shows good agreement up to 12% strain, but the 7:1 alloy at 77°K is similar to the lightly aged alloys, examples of which are shown in Fig. 73. Here the aggregate curves start at higher yield stresses but still have lower work hardening rates. Consequently the curves intersect at approximately 4% strain in the case of the two 7:1 alloy specimens and at approximately 8% strain for the four 2.2:1 alloy specimens. These features can be explained qualitatively.

The higher yield stress values, compared with as-quenched alloys, result in larger elastic strains, so that the Budiansky and Wu correction becomes significant, as seen by the ratios $\sigma_o(P)/\tau_o$ in Table 5.4, being approximately equal to 2.3. Beyond the yield the rate of work hardening is low since both the as-quenched and lightly aged crystals have 'soft' orientations. This is consistent with results for pure Al[126]. The explanation is not supported quantitatively, however, since the Budiansky and Wu analysis predicts that the elastic correction becomes less important as the plastic strain increases, until after only 0.5% strain M has increased to 3.06. The aggregate and polycrystal curves should therefore intersect before 0.5% strain, instead of between 4% and 8% as observed.

The load-elongation curves for peak and overaged crystals are parabolic and many of the specimens retain their circular cross-sections after straining. The rapid initial work-hardening has been attributed to slip on many systems (Section 3.4.4.) This suggests that good agreement should be obtained using the Taylor, Bishop and Hill theory for which polyslip is a prerequisite. However, without knowing the operative slip

systems it is not possible to calculate the shear stress and shear strain values for each crystal. As a first approximation it was assumed for crystals with initial orientations near the <100> - <111> boundary that slip takes place equally on primary and conjugate systems, and that glide strains are equivalent to those calculated for <112> crystals. Other crystals used had orientations near <100> or <110> . Relationships between true stress, $\bar{\sigma}$, true strain, $\bar{\varepsilon}$, and resolved shear stress, glide strain for these orientations have been given by Mukherjee, Mote and Dorn[135] assuming octahedral slip on the most favoured systems and no lattice rotation as :-

Tensile axis	cos λ	cos φ	Resolved shear stress, τ .	Total glide strain
<112>	$\sqrt{3}/2$	$\sqrt{2}/3$	$1/\sqrt{6} \cdot \bar{\sigma}$	$\sqrt{6} \cdot \bar{\varepsilon}$
<100>	$1/\sqrt{2}$	$1/\sqrt{3}$	$1/\sqrt{6} \cdot \bar{\sigma}$	$\sqrt{6} \cdot \bar{\varepsilon}$
<110>	$\frac{1}{2}$	$\sqrt{2}/3$	$1/\sqrt{6} \cdot \bar{\sigma}$	$\sqrt{6} \cdot \bar{\varepsilon}$

Values of resolved shear stress and glide strain have then been multiplied by the appropriate Taylor factor (M and $\frac{1}{M}$ respectively) to produce aggregate true stress and true strain.

Comparing aggregate and polycrystal curves for 16 alloys aged between 0.1 day and 10 days, it was found that the work hardening rates of the aggregate curves were generally twice as large as those of the polycrystal curves. It should be noted that the method used to estimate the resolved shear stress and glide strain produces a minimum value for the slope of the aggregate curve.

Since there was no agreement between aggregate and polycrystal curves, true stress - true strain curves for single and polycrystals have been

compared directly, and examples are shown in Fig. 74. The curves are parallel to each other right up to the limit of uniform strain. For the 7:1 alloys, the single crystal curves lie above the polycrystal curves at 295°K, but below them at 77°K. In each case the difference in stress between the curves was never greater than 3 kg/mm^2. For 2.2:1 alloys, the single crystal curves are always below the polycrystal curves. For peak aged alloys the difference in stress between them was as large as 6 kg/mm^2, but for overaged alloys, less than 3 kg/mm^2. The observed differences between the curves must represent the grain boundary contribution to the strength of the alloys. With the exception of the peak aged 2.2:1 alloys, these differences are very small and are constant throughout the work-hardening period. Taking into account the errors in stress and strain measurements for each curve, it may be concluded that the work hardening in single crystals and polycrystals of overaged 2.2:1 alloys and peak and overaged 7:1 alloys is identical.

.3. Summary

(i) As-quenched and lightly-aged alloys.

Yield stresses for aggregates calculated using the Taylor formula are approximately equal to the corresponding polycrystal yield stresses for as-quenched alloys. This agrees with certain results on pure Al[126]. The aggregate yield stresses calculated for lightly aged crystals are greater than the corresponding polycrystal yield stresses. The differences can be accounted for by the Budiansky and Wu[134] analysis which takes elastic strain into consideration. This may result from the larger elastic strains in these alloys due to their higher yield stresses.

For both as-quenched and lightly aged material, the work hardening rates of the aggregates are less than those of the corresponding polycrystals. The single crystals all had 'soft' orientations, (deforming initially by single slip), for which low work hardening rates in aggregate curves have also been found for pure Al[126]. Other minor effects, which might contribute to the work-hardening rate differences are the grain size and degree of preferred orientation of the polycrystals.

(ii) Peak and overaged alloys.

Yield stresses for the aggregates are greater than those of the polycrystals. The differences can be accounted for by the Budiansky and Wu correction to the Taylor factor. However, the work hardening rates of the aggregates are much greater than those of the polycrystals, suggesting that the aggregate theory does not apply. This is most likely to be because the deformation of the single and polycrystals is very similar. With the exception of peak aged 2.2:1 alloys, this is confirmed by comparing true stress - true strain curves, which are substantially the same for the single and polycrystals. The grain boundaries, therefore, do not appear to affect the deformation of these alloys between the yield stress and the limit of uniform strain.

5.3.3. Yield points and serrated yielding

.1. Initial yield points

In Al-Cu and 7:1 and 2.2:1 Al-Cu-Mg alloys, yield points are observed only with single crystals. The results obtained for Al-Cu-Mg alloys in the present investigation are summarised below :-

In as-quenched and lightly aged crystals the yield point becomes sharper with decreasing temperature (see Figs. 41, 42, 47, 48). Yield

drops are observed at low temperatures, as shown in Table 5.5.

Table 5.5

Crystal	Cu:Mg ratio	Ageing treatment	Testing temp.	Yield drop kg/mm^2	% Yield drop $\frac{\tau_{UYP} - \tau_{LYP}}{\tau_{LYP}}$
R2	7:1	As quenched	77°K	0.03	0.25%
R15	7:1	0.01 day	77°K	0.31	1.7%
Y	7:1	0.01 day	77°K	0.47	2.5%
2AN	2.2:1	As quenched	77°K	0.16	1.2%
2M	2.2:1	0.015 day	199°K	0.63	3.2%
2AB	2.2:1	0.015 day	148°K	0.63	2.4%
2G	2.2:1	0.015 day	77°K	0.85	3.1%
2B	2.2:1	0.015 day	77°K	0.95	3.8%

In alloys aged for 0.1 day the yield point becomes sharper with decreasing temperature. (See Figs. 43, 49)

In alloys aged to peak and overaged the yield discontinuity appears to be unaffected by decreasing temperature. Peak aged alloys show more marked discontinuities and overaged alloys less marked discontinuities with increased % Mg, (comparing Figs. 45, 51 and 46, 52 respectively).

Thus, although changes in the slope of the load-elongation curve at the start of plastic deformation are observed in Al-Cu-Mg crystals at all stages of ageing, actual load drops only occur with as-quenched and lightly aged specimens, tested at low temperatures. In the case of Al-Cu alloys, no precise details about the initial yield points of solution treated Al-Cu crystals have been reported,[35,36] but Price and Kelly[37] have shown that the yield drops exhibited by GP zone-hardened Al-Cu

single crystals tested at 77°K result from geometrical softening. For the Al-Cu-Mg crystals in which yield drops have been observed, (Table 5.5) it has been shown in Section 4.2.1.3 that the yield points do not result from geometrical softening.

Other mechanisms for discontinuous yielding which might be expected to apply here have been considered by Cottrell[136]. Where a sharp yield point occurs, there is a sudden increase in the number of mobile dislocations at the start of plastic flow. This may result from the creation of dislocations in the lattice, the multiplication of dislocations, or the unpinning of immobilised dislocations. Yield drops caused by dislocation creation are generally only observed in whiskers, but Cottrell[136] considers that in the vicinity of inclusions etc., stress concentrations can cause dislocation creation in materials where all the dislocations are immobilised by solute pinning, even though the applied stress is below the unpinning stress. Dislocation multiplication as a yield point mechanism has been studied in LiF[137] and other materials. The plastic strain rate in a crystal, $\dot{\varepsilon}$, is expressed by the equation,

$$\dot{\varepsilon} = n b v$$

where,

- n = number of mobile dislocations and is a function of strain
- b = Burgers vector
- v = dislocation velocity, and is a function of stress

It is postulated that at the start of plastic deformation there are only a few dislocations which have to move quickly and therefore at relatively high stress to accommodate the applied strain rate. When the dislocations multiply, their velocity decreases in order to maintain a

constant strain rate, thus causing a fall in stress, provided that v is sufficiently stress sensitive. Johnston[138] has shown that, on this model, the magnitude of the yield drop is diminished if the initial density of mobile dislocations is increased, if the initial work-hardening rate is high, or if the stress dependence of dislocation velocity is small. He also showed that machine stiffness, applied strain rate and dislocation multiplication rate had little effect on the load drop. It is generally considered[121, 136] that this mechanism is unlikely in f.c.c. metals since the dislocation velocity is relatively insensitive to stress (v proportional to τ^{200} for Cu, compared with v proportional to τ^{25} for Li F) . However, if there were no mobile dislocations at the start of plastic deformation(eg. as a result of pinning) and the work-hardening rate was very low, then a small yield drop might be predicted, on this model, for some f.c.c. crystals. Dislocation unpinning, that is, a dislocation being torn away from its atmosphere of impurity atoms and defects has, until recently, been postulated as the basic mechanism for most yield points and strain-ageing behaviour. However, the upper yield point will only be equal to the unpinning stress if the pinning is relatively weak, otherwise dislocation creation or multiplication may take place first. The magnitude of the pinning effect is governed by the interaction (or binding) energy between the dislocation and the solute atom and/or defect, together with their distribution about the dislocation line. In f.c.c. metals, edge dislocations are more strongly bound to solute atoms and vacancies than are screw dislocations.[139]

The binding energies are in the range 0.02 - 0.1 eV per solute atom or vacancy, compared with 0.5 - 1 eV for interstitial atoms in b.c.c. metals.[139] However, for Al-Mg, Westwood and Broom[47] have estimated that the binding energy between a dislocation and a Mg atom in Al is as high as 0.2 eV.

It is most probable that the initial yield points observed on curves of as-quenched and lightly aged single crystals are caused by a dislocation creation and multiplication effect, as a result of strong dislocation pinning. The strength of the pinning is an important aspect of both the Cottrell-locking and dislocation multiplication models of yielding. In each case it affects the magnitude of the yield drop, either by determining the unpinning stress or by controlling the initial density of mobile dislocations. In Table 5.5 the magnitudes of the yield drops are seen to be temperature and composition dependent ; lower temperatures and higher Mg content increase the size of the drops. The temperature effect is caused by the diminishing effect of thermal fluctuations in assisting dislocation breakaway from atmospheres. The effect of Mg in the supersaturated solid solution crystals is caused by the higher concentration of solute atoms around the dislocations. This results from the migration of Mg-vacancy pairs to dislocations, where the vacancies condense, leaving the Mg atoms forming atmospheres around the dislocations. There is a possibility of a higher density of GPB zones forming in the vicinity of dislocations because of the greater concentration of solute atoms there.

Since the single crystal yield points are small, and there is no yield discontinuity on the corresponding polycrystal curves, then it is unlikely that the load drops are caused solely by dislocation unpinning. If there were a catastrophic release of locked dislocations at a stress in the polycrystals corresponding to the upper yield stress in the single crystals, then some trace would be expected on the load-elongation curve. Despite the very rapid initial rate of work-hardening in any polycrystal, yield drops are indeed observed in Al-Mg polycrystalline alloys[45,51]. On the dislocation multiplication model, however, Johnston[138] has shown that increasing the rate of work-hardening markedly reduces the magnitude of the yield point. In the present investigation the work-hardening rate of a polycrystal is almost 10^3 times the stage I hardening rate of the single crystal. (see Figs.18 and 50 for example). Furthermore, at the start of the plastic deformation, the rapid increase in dislocation density in the polycrystal, due to dislocation creation and multiplication at the boundaries would overshadow any dislocation multiplication effect as a result of a low initial density of mobile dislocations due to pinning. The absence of yield points in the polycrystals can, therefore, be satisfactorily explained on this model.

It is proposed that the following mechanisms are operative. In as-quenched alloys, dislocations are pinned by solute atoms or clusters after quenching. When tested at room temperature, yielding is gradual in single crystals, (Figs.41 and 47) because thermal fluctuations assist in unpinning portions of locked dislocations.

When tested at 77°K, the crystals show sharp yield points, because thermal fluctuations are unable to assist in unpinning and there is a rapid multiplication of dislocations, probably by dislocation creation at stress concentrations near the grips. The effect is more marked in the 2.2:1 alloys where there are more Mg atoms than in the 7:1 alloys, which pin dislocations more strongly, possibly because the atmospheres around the dislocations are larger.

After light ageing, dislocations are pinned at frequent intervals along their length either by GP zones or intermediate precipitates, depending on whether the precipitates are preferentially nucleated on dislocations, or not. In the case of Al-4% Cu crystals, aged for 2 days at 165°C[37], the dislocations are almost certainly decorated with θ' precipitates, yet the yield points at 77°K were shown to result only from geometrical softening. This suggests that there is very little dislocation pinning by θ'. The 7:1 alloy aged for 0.01 day should contain only GPB zones, but it is probable that small amounts of θ' and S are also present,[19] in which case the dislocations will be decorated with θ' and S, since these are both preferentially dislocation-nucleated. At room temperature, yielding is smooth (Fig.42) because of thermally assisted dislocation breakaway. As the temperature is lowered, the yield points become sharper, until at 77°K, a yield drop occurs, which is shown in Fig.65 to be steeper than that predicted solely by geometrical softening. This could result from stronger dislocation locking by GPB zones or S precipitates compared with θ'. Alternatively it could mean that the

solid solution matrix is stronger, so that the operation of dislocation sources requires a higher stress than in the case of Al-Cu.

The 2.2:1 crystals aged for 0.015 day should contain GPB zones[19], with S precipitates probably decorating the dislocations. Room temperature yield points are fairly sharp (Fig.48), and lowering the temperature to only 199°K is sufficient to produce a yield drop which becomes larger as the temperature is lowered to 77°K (Fig.65). Again, in order to explain these more marked yield drops compared with the 7:1 alloy, it is not possible to distinguish between more effective dislocation pinning by GPB or S precipitates, or more difficult dislocation creation and multiplication due to a stronger matrix solid solution. In as-quenched and lightly aged polycrystals, no yield points are observed because the strain is accommodated by rapid dislocation multiplication and interaction due to the grain boundaries. The consequent high work-hardening rate also assists in masking any dislocation multiplication within the grains due to dislocation pinning. Crystals of each alloy aged for 0.1 day, also show more marked yield points at 77°K. (The particularly large yield drop observed for the 2.2:1 alloy (Fig.49) may be a spurious result since there was reason to suspect this particular crystal). Although the structures present are probably complex at this stage, the 7:1 alloy contains an appreciable amount of S precipitate,[19] so that the dislocations should be more strongly locked than in the case of the lightly aged alloys. At the same time, the matrix is more depleted of solutes, so that the smaller yield point in the 7:1 alloy (Fig.43)

seems to represent an easier dislocation multiplication process in the matrix, compared with the alloy aged for 0.01 day. In the case of the 2.2:1 alloy, 0.1 day ageing represents the end of the hardness plateau, just before the rise to the peak, which is associated with S precipitation. It is probable that the dislocations are decorated with S precipitates at this point, and it is possible that the matrix contains a maximum number of GPB zones. Thus, pinning is strong, and dislocation multiplication could be more difficult than for lightly aged crystals. This might account for the very large observed yield drop, if it is a real effect associated with this degree of ageing.

In the peak and overaged crystals, yield discontinuities are observed at all testing temperatures, and their characteristics appear to be independent of temperature. It is proposed that these discontinuities are caused by a dislocation multiplication process as a result of a few dislocations becoming unpinned from their precipitates. The yield points are small, and show no load drops because the work-hardening rate is so high in these alloys. (See Figs.45,46,51,52). The precipitates are partially coherent, so that in order for dislocations to become unpinned, segments must be able to expand, locally, between them, e.g. by the Orowan mechanism (Section 3.4.1.). This has been shown to be insensitive to temperature. (Section 3.4.3.). Alternatively, if new dislocation sources operate at the yield stress, dislocation loops still have to expand between precipitates, so that the temperature dependence is small, also. Two other observations are consistent with this model. The yield

discontinuities decrease with overageing and with increasing % Mg. In both cases the matrix is more depleted of solute, so that dislocation multiplication is easier and the yield 'drop' smaller.

As before, polycrystals show no yield discontinuities, because the strain is accommodated by grain boundary generated dislocations. These interact with the precipitates according to the Orowan mechanism, and the resulting high work-hardening rate masks any discontinuity.

.2. The Portevin - Le Chatelier effect.

As-quenched and lightly aged polycrystals tested at room temperature exhibited serrations along the work-hardening portions of their stress-strain curves. The values of true stress ($\bar{\sigma}_{P.L.}$) and true strain ($\bar{\varepsilon}_{P.L.}$) at which serrations started are shown in Table 5.6.

Table 5.6.

Alloy	Ageing Treatment	True stress $\bar{\sigma}_{P.L.}$	True stress $\bar{\varepsilon}_{P.L.}$
7:1	As-quenched	7.2	0.005
7:1	0.02 day	11.1	0.01
7:1	0.06 day	14.9	0.01
7:1	0.1 day	17.1	0.01
2.2:1	As-quenched	12.1	0.01
2.2:1	0.015 day	16.4	0.02
2.2:1	0.05 day	19.6	0.03
2.2:1	0.1 day	21.6	0.05

For a given ageing treatment the magnitude of the serrations increased with strain, but decreased as ageing proceeded.

As-quenched and lightly aged single crystals tested at room temperature also exhibited serrations on their stress-strain curves. These were very small in magnitude and only occurred after the maximum load position.

The Portevin-Le Chatelier effect has been reviewed in Section 3.2.2. and it was seen that dislocation unpinning has been widely postulated to explain the behaviour of Al-Mg and other alloys. During deformation, mobile dislocations become pinned by solute atmospheres which form as a result of strain-enhanced solute diffusion. The increase in applied stress causes unlocking and subsequent dislocation motion at a lower stress. The cycle is then repeated.

There is some evidence that the Portevin-Le Chatelier effect can be explained by a dislocation multiplication process. It has been proposed[140] that plastic deformation may take place until dislocations are sufficiently immobilised by tangling to become locked by solute atmospheres. The applied stress than rises until localised yielding by dislocation multiplication occurs in another part of the specimen, causing a load drop. Bailey et al[141], studying the strain rate dependence of the strain at which serrations start on curves for commercial Al, Al-1% Mg and Al 0.2% Cu alloys have shown that at low strain rates ($< 10^{-4}$ sec^{-1}) the relationship is the inverse of that predicted by the Cottrell-locking model.

They claim that an explanation based on dislocation multiplication can account for this. Thomas[51] has also found that for fine-grained Al, 5% Mg alloys tested above 0°C the delay in the strain at which the serrations start increased with decreasing strain rate and also with increasing temperature, in the reverse manner to the predictions of the Cottrell-locking model. He has accounted for this by a mechanism based on dislocation creation at stress-concentrations near the specimen grips. (See Section 3.2.2.)

The important features of the observed Portevin-Le Chatelier effect in the present alloys suggest an explanation based on dislocation multiplication as a result of dislocation pinning by solute atmospheres. It is proposed that during straining, mobile dislocations become sufficiently tangled to allow them to become pinned by solute atmospheres. The stress rises until localised yielding, by dislocation creation or multiplication, takes place in other parts of the specimen[140]. Dislocation pinning only occurs if the solute diffusion rate is large enough, so that, as observed, serrations only appear at room temperature, after a finite strain (Table 5.6) sufficient to produce defects to enhance diffusion; in the case of single crystals, not until after the maximum load. Only the solutes remaining in solution after zones and precipitates have formed, control the pinning of these mobile dislocations. This explains why the magnitude of the serrations decreases as ageing proceeds. The matrix becomes more depleted in solutes, so that, either the number of mobile dislocations remaining increases (and

so the magnitude of the drop decreases), or the immobilised dislocations are only weakly locked.

The size of the serrations is observed to increase with strain, and this is a consequence of more dislocations becoming immobilised, so that the number remaining to produce the yield drop decreases.

In the case of the 7:1 Cu:Mg alloys, there is no significant increase in the strain at which the serrations first appear (Table 5.6) after the initial ageing period of 0.01 day. This suggests that the solute concentration in the matrix remains approximately constant. During the ageing period of 0.01 - 0.1 day there is an increase in GPB (2), S and θ' in the structure, accompanied by the disappearance of GPB zones[19]. The dissolution of GPB might maintain the solute concentration at an approximately constant level.

The 2.2:1 alloys, aged between 0.015 and 0.1 day show an increase in the strain at which serrations first appear. (Table 5.6). In this case, there is only an increase in GPB zones as ageing proceeds, so that solute depletion of the matrix occurs and pinning becomes weaker. Thus, higher strains are required before the pinning is sufficient to produce a load drop.

No serrations were observed in either alloy after ageing for 0.1 day. This must be due to further solute depletion in the matrix, below the level at which locking can occur. It is also possible that the increasing work-hardening rate assists in masking any small

serrations. In Al, 3.5% Cu, serrations are observed even after ageing to the peak at 190°C. This implies that solute depletion is much less marked in Al-Cu, and Greetham and Honeycombe[36] suggest that the matrix is still supersaturated in Al, 4.5% Cu alloys aged to peak at 190°C.

In single crystals, only as-quenched and lightly aged alloys (0.01, 0.015 day) show small serrations after maximum load. These crystals deform by single slip, and it is not until beyond stage III, at the maximum load, that sufficient numbers of defects have been generated to enhance the solute diffusion rate to a level where mobile dislocations can be pinned. In crystals aged for 0.1 day, only the 2.2:1 alloy showed serrations after the maximum load. No serrations were visible on the curve for the 7:1 crystal which had a higher work-hardening rate than the 2.2:1 crystal. The 7:1 polycrystals aged for 0.1 day only formed serration steps on their curves with difficulty. It is possible that the degree of matrix depletion at this ageing stage required a level of dislocation generation, in order to enhance diffusion rates, which only the polycrystals, with their higher work-hardening rate, could provide. The 2.2:1 alloy after 0.1 day still contained only GPB zones, and the matrix was sufficiently saturated to produce dislocation pinning.

5.3.4 Fracture.

.1. Single crystals.

(a) As-quenched and lightly aged.

Both as-quenched and lightly aged crystals tested at room temperature show similar fractures (Section 4.2.5.). They have been termed 'crocodile' fractures[110] although Rosi and Abrahams[142] have described similar fractures in pure metal <100> crystals as 'V-type'. The specimens neck down to large reductions in area and show traces of slip on two systems near the fracture, with voids in the centre of necked regions. Orowan[114] attributed the void formation to successive slip on primary and conjugate planes. The initiation of the central void was not described. Rosi and Abrahams[142] attributed the voids to vacancy condensation as a result of intense local multiple glide in the neck. Rogers (discussion to[110]) believed that this type of fracture was the single crystal equivalent to a double cup failure, and that it was formed, after a central crack had been initiated, by slipping apart of the planes at the crack tip.[143] Void formation was not necessary for this process and the fracture surface had a characteristic striated appearance[103]. Unfortunately, replica fractographs of 'crocodile' fractures could not be obtained, due to the depth of the void.

At low temperatures crystals in corresponding aged conditions show the coarse shear band type of fracture (Section 3.5.). The transition between 'crocodile' fracture and coarse shear band fracture corresponds to the disappearance of serrations on the load-elongation

traces; for example, it was observed that in alloys aged for 0.1 day, tested at room temperature, the 2.2:1 crystal which showed serrations, had a 'crocodile' fracture, whereas the 7:1 crystal, with no serrations, showed a coarse shear band fracture. The transition between 'crocodile' and coarse shear band fractures with temperature, suggests that inclusions do not play a major role in the 'crocodile' fracture mechanism and in this respect, Beevers and Honeycombe[104] have associated very low temperature discontinuous yielding behaviour with the formation of crack nuclei by avalanches of dislocations. The transition with decreasing temperature, also suggests that the two types of fracture are closely related. This is further supported by similarities in the later stages of the load-elongation curves. At the maximum load position, the as-quenched and lightly aged alloys of both compositions, at all temperatures, show a load drop. This was observed by Price and Kelly[111] to mark the initiation of the coarse shear bands which formed on GP-zone hardened Al-Cu, Al-Ag and Al-Zn crystals. It was proposed that these bands resulted from the thermally activated breakdown of barriers to dislocation glide, which had formed during work-hardening. This mechanism provides an explanation for both the 'crocodile' and coarse shear band fractures and for the transition between them. The coarse shear band is initiated, generally on the conjugate slip system[111], when the tensile axis reaches or overshoots the [100] - [111] boundary. It is proposed that in the case of the as-quenched and lightly aged alloys at room temperature, mobile dislocations on the conjugate system become immobilised by pinning. The stress rises, until either unpinning

takes place, assisted by thermal fluctuations, or new dislocations are generated elsewhere in the specimen, as described in Section 5.3.3. The resulting dislocation multiplications and repinning occur alternately on the primary and conjugate planes, due to the already symmetrical deformation pattern giving rise to the Portevin-Le Chatelier effect. A crack is then readily formed at the intersection of the two glide bands[121], and this provides an explanation for the initiation of the central void following which the crystal slips apart as described by Orowan[114]. The serrations on the load-elongation curves of these alloys always start immediately after the load drop which marks the initiation of the coarse shear bands.

At low temperatures, the coarse slip band fractures are composed of relatively large areas of shear, with small 'crack' regions (Fig. 67(a) and 69(a)). This corresponds to considerable strain after the initiation of coarse slip bands, as observed on the load-elongation curves, where, after the load drop associated with coarse slip band formation, regions of constant load extend for several % strain before decreasing rapidly prior to fracture. The constant load portion represents localised shear near the coarse slip band, accompanied by work-hardening. This behaviour contrasts markedly with that observed by Beevers and Honeycombe[110] on Al, 5.5 wt.% Cu crystals, where the load-elongation curves terminated abruptly (in some cases fracture occurred on a rising curve) and there was negligible necking of the specimen. For this reason, the fracture mechanism proposed by Beevers and Honeycombe is not applicable to Al-Cu-Mg alloys showing

coarse slip band fractures, Price and Kelly[111], however, showed that subsequent to coarse slip band formation and localised shear, a crack was nucleated at the edge of the shear band region, and propagated across it, via inclusion-nucleated voids.

Beevers and Honeycombe's criterion of a constant resolved shear fracture stress is not applicable, since the fracture planes are not parallel to slip planes. The parameters measured by Price and Kelly, however, for Al, 3.7 wt.% Cu crystals have also been determined for the Al-Cu-Mg alloys and are shown in Table 5.7 They are τ_{CSB}, which is the resolved shear stress at which coarse slip bands form, and $(\tau_{CSB} - \tau_o)$, where τ_o is the C.R.S.S., which Price and Kelly have called the work-hardening contribution to the stress for coarse slip band formation. Price and Kelly postulated that the coarse slip bands resulted from the thermally activated breakdown of dislocation barriers formed during work-hardening and that differences in the work-hardening stresses $(\tau_{CSB} - \tau_o)$ for coarse slip band formation arose from differences in the stacking fault energy of the matrix.

Table 5.7 shows that, as ageing proceeds from as-quenched to 0.1 day, the values of $\tau_{CSB} - \tau_o$ decrease (eg. 7:1 crystals at 295°K, from 6.1 to 4.8 kg/mm^2). This is consistent with Price and Kelly's model, because as the matrix is being depleted of solute, the stacking fault energy is increasing and the barrier breakdown stress is decreasing. Similar trends exist for 7:1 crystals tested at 77°K and 2.2:1 crystals tested at 295 and 77°K. In the same way, Price and Kelly observed that at room temperature $\tau_{CSB} - \tau_o$ decreased from

Table 5.7

Aged Condition	Testing Temperature, ^{o}K	τ_{CSB} kg/mm^2	$\tau_{CSB} - \tau_o$ kg/mm^2
7:1, Cu:Mg			
As quenched	295	9.6	6.1
" "	77	14.6	8.1
0.01 day	295	11.5	5.5
" "	195	12.2	5.3
" "	148	13.9	6.4
" "	77	15.3	6.9
0.1 day	295	16.0	4.8
" "	77	17.6	4.4
2.2:1, Cu:Mg			
As quenched	295	11.5	6.8
" "	77	15.3	9.2
0.015 day	295	12.9	4.2
" "	195	15.3	5.8
" "	148	15.3	4.4
" "	77	19.4	7.1
0.1 day	295	14.1	3.8
" "	77	19.8	5.9

9.6 kg/mm^2 for GP(1) hardened crystals to 7.4 kg/mm^2 for GP(2) hardened crystals. The higher values of $\tau_{CSB} - \tau_o$ for these Al-Cu crystals suggests that the stacking fault energies of the matrices of GP(1) and GP(2) hardened Al, 3.7 wt.% Cu crystals are lower than those of 7:1 and 2.2:1 Cu:Mg crystals aged to contain GPB zones. This is consistent with the more rapid ageing of the Mg containing alloys, depleting the matrix to a greater extent than in the Al-Cu alloys. Since the dislocations in these alloys cut through GP zones,

then the effect of the stacking fault energy of the zone must also be considered. Hirsch and Kelly[88] have shown that where the size of the zone is smaller than the width of the extended dislocation in the matrix, the strengthening effect is small. GPB zones in the Al-Cu-Mg alloys are smaller than GP(2) zones in Al-Cu, and this could also contribute to the smaller temperature dependence of $\tau_{CSB} - \tau_o$, compared with Al-Cu.

Price and Kelly suggested that the temperature dependence of a barrier breakdown mechanism should be approximately equal to 2, between 77°K and 295°K and obtained values between 1.5 and 2.5 for Al-Cu, Al-Zn and Al-Ag containing GP zones. From table 5.7., values of $\frac{(\tau_{CSB} - \tau_o)\ 77^oK}{(\tau_{CSB} - \tau_o)\ 295^oK}$ are found to vary between 1.3 and 1.7 with the exception of the 7:1 alloy aged for 0.1 day, where the ratio is approximately 1. In this alloy, matrix depletion is greatest as shown by the absence of a Portevin-Le Chatelier effect. (Section 5.3.3.)

(b) Peak aged alloys.

Peak aged 7:1 crystals showed considerable necking and extensive coarse slip band development on one system near the fracture region. The load-elongation curves showed gradually decreasing loads extending over several % strain, beyond the maximum load and prior to fracture. Two or more slip line systems were observed on the specimen but the fractures took place across the narrowest part of the coarse slip band region. No abrupt load drop marking the coarse slip band initiation, was observed in these crystals.

The 2.2:1 crystals showed very much less necking, and narrower coarse slip bands, although the load-elongation curves decreased gradually for several % strain after the maximum load in much the same way as the 7:1 crystals. This implies that during coarse slip band formation, deformation was concentrated on fewer slip planes. The final failure occurred parallel to the slip planes comprising the coarse shear band, and appeared to be similar to the planar fractures observed by Beevers and Honeycombe. Similar fractures have also been found in overaged Cu-Be crystals containing γ' precipitates[40]. On the other hand, Al, 3.7 wt.% Cu crystals aged to contain θ' and Al-Ag crystals containing γ' precipitates did not fracture by coarse slip band formation. Instead, the crystals showed considerable necking and fractured at approximately 45° to the tensile axis in a similar manner to polycrystals[37]: a few short wavy slip lines being visible near the fracture.

Peak aged structures in the 7:1 and 2.2:1 Cu:Mg crystals consist of GPB(2), S, θ' and GPB, S respectively[19]. It is proposed that during the initial stages of plastic deformation, dislocations are able to cut through only the GPB or GPB(2) zones. The rapid work-hardening is therefore caused by bowing out of dislocations between the S and θ' precipitates by the Orowan mechanism, leaving dislocation loops around them which may cross slip and act as dislocation sources, as described in 3.4.4. After a certain amount of strain, the number of loops increase until the shear stresses acting on the precipitates reach a value where the dislocations are able to cut through the S precipitates. This

corresponds to a decrease in the work-hardening rate (eg. in Fig.48, after 2-3% strain). In the case of the 7:1 alloys, the stress is then transferred to the θ' precipitates, so that further extensive slip takes place on other parallel planes. After many planes have slipped and a wide coarse shear band has formed, fracture occurs by crack initiation at the edge of the band, which propagates by inclusion-nucleated voids across the band, as envisaged for the zone hardened alloys[111]. In the case of the 2.2:1 alloys, a similar deformation mechanism is proposed, except that once the S precipitates have sheared, there are no θ' precipitates on which the stress is transferred, so that slip continues on the same planes, forming a narrow coarse shear band. Fracture occurs as before. The fracture surface (Fig.70(c)) shows very elongated cusps, indicative of void coalescence producing shear rupture or tearing, as described by Beachem[144]. The formation of cracks by dislocation pile-ups[110] is not thought to be likely in the 2.2:1 alloys, despite the planar fractures and the absence of very marked necking, because the load-elongation curves show an extensive and gradual load decrease after maximum load and before fracture.

(c) Overaged alloys.

These show similar deformation behaviour to the peak aged alloys. The high initial work-hardening is caused by rapid dislocation multiplication by loops being left around the precipitates. The work-hardening rate decreases after only a few % strain, and the load reaches a maximum, thereafter decreasing gradually prior to

fracture. The types of fracture appear to be very dependent on the initial orientations of the crystals, which tended to be towards the [100] or [110] corners, or near the [100] - [111] boundary in these alloys. Those oriented near <100 > showed double cup fractures, illustrated in Figs. 67(d) and 69(d), as a result of the large number of simultaneously operating slip systems, (up to 8, for a perfectly oriented <100 > crystal). This, together with the multiple slip induced by the presence of the precipitate particles, produces an axially symmetrical deformation. The crystals oriented near the [100] - [111] boundary show two equally developed, intersecting coarse slip bands, (eg. Fig.66(d)) and the remaining crystals show single coarse slip bands, similar to the 7:1 peak-aged crystals, consisting of many operative slip planes. Overaged 7:1 alloys should contain GPB(2), θ' and S and 2.2:1 alloys only S precipitates[19]. Both the θ' and S precipitates are coarser and more widely spaced than in the peak aged condition[24,115]. It is proposed that the deformation and fracture mechanisms are the same as those described for the peak aged crystals, except that the larger size and spacing of the precipitates results in lower yield stresses and consequently lower stresses at which the S precipitates are sheared, because there are fewer of them.

Very recently, Jones and Kelly[118] have found that γ precipitates in overaged Cu- 1.5% Be crystals, which initially do not deform, are sheared after a small strain. Their evidence rests mainly on the observation of a delayed lattice rotation, indicative of single slip

taking place after a period of initial strain when there was no rotation. At 77°K, the onset of lattice rotation occurred at a higher strain than at 295°K. Several slip line traces were observed, and the fractures were planar, confirming Price and Kelly's observations (40).

.2. Polycrystalline alloys.

As described in 4.1.6.2., as-quenched and lightly aged alloys showed 45° shear-type fractures. Such fractures have been observed primarily in sheet specimens where it has been postulated that no active zone of triaxiality exists(145). However, tests on round specimens of quenched or lightly aged Al-Cu alloys(107) and Al-Zn-Mg-Cu alloys(146) have also shown shear type fractures. No detailed mechanism for their formation has been given, but they have been associated in some cases with serrated load-elongation curves(146). In the present investigation, 7:1 Cu:Mg alloys, tested at room temperature, showed serrated load-elongation curves and shear type fractures when aged up to 0.1 day. Shear fractures are not exclusively associated with serrated curves, however, because as-quenched and lightly aged, (up to 0.02 day) 7:1 alloys also showed shear fractures at 77°K, where there are no serrations. In the same way, the 2.2:1 alloys, as-quenched or lightly aged, when tested at room temperature showed serrations up to 0.1 day, but shear fractures only up to 0.015 day. At low temperatures, no shear fractures (or serrations) are observed even in as-quenched alloys.

Ryder and Vian[146] have observed heavy slip bands, associated with serrations, at approximately 45° to the tensile axis, in commercial Al-Zn-Mg-Cu alloys. This material had a fibre or banded structure, which became kinked or reoriented, away from the tensile axis in the heavy slip regions. Fracture occurred parallel to the slip bands by void growth, the voids being initiated as a result of higher stress concentrations from the reoriented cavities and inclusions comprising the fibre structure.

No similar heavy slip bands were observed in the Al-Cu-Mg alloys, showing shear fractures, but within each grain, prominent slip lines were observed parallel to the fracture surface. These are seen clearly in Fig.36(b), and appear to be the dominant slip directions in each grain, the other slip systems maintaining boundary continuity between the grains, which have undergone considerable rotation.

It is proposed that each serration on the load-elongation curve is associated with the propagation of slip across the specimen as a result of a sudden release or generation and multiplication of dislocations, due to strain ageing, as described in Section 5.3.3. Each multiplication produces slip bands in several grains and the propagation into adjacent grains results partly from the stress concentration of piled up dislocations at the head of the slip bands and partly from the applied stress, tending to produce slip along the direction of maximum shear stress, i.e. at 45° to the axis. The process is similar to that occurring in the single crystals of

as-quenched and lightly aged alloys with V-shaped or coarse slip band fractures. In polycrystals, the slip bands in each grain are predominant on planes closest to the direction of the maximum applied shear stress, aided by the fact that the grains in the neck have rotated to similar orientations due to the large strains. Fracture may then take place by the propagation of a ductile crack, probably starting at a stress concentration at the surface[107] and proceeding via inclusion-nucleated voids within the heavy slip bands of each grain.

Where shear fractures are observed in the absence of serrations, ie. in 7:1 alloys, tested at 77°K, it is proposed that the fracture mechanism is modified in the following way. Since there is no rapid dislocation multiplication due to strain ageing, the directions of the slip bands in each grain result primarily from boundary continuity considerations, but are still influenced by the direction of the maximum applied shear stress. This requires greater elongations (See Figs.4 and 5) to concentrate strain within the slip bands lying approximately at 45° to the axis, thus producing a shear band across the whole specimen, and fracture as before. In Section 4.1.6. it was seen that fractures observed in specimens aged for longer times showed increasing amounts of intercrystalline failure. This corresponded to the approximately constant true fracture stress in alloys tested at 77°K, and to a linear decrease, with ageing time, of the true fracture stress at 295°K, (c.f. Figs. 29, 30). Furthermore, ductile cusp patterns were always observed on fractographs, (Figs.38,39,40).

The existence of these ductile features in an apparently intercrystalline fracture provides strong evidence for the existence of a precipitate-free boundary region in all these alloys, along which fracture takes place preferentially. Similar fracture characteristics have been observed in Al, 4% Cu alloys[107], where the existence of a precipitate-free zone has been well documented[8, 71].

In aged 2.2:1 alloys, Sen[115] has found narrow ($\leq 1\mu$ width) precipitate-free regions in thin foils, which are believed to arise because the boundaries act as sinks for vacancies, so that after quenching there is a deficiency of loops in their vicinity and hence no S (which is dislocation nucleated). GPB, however, is nucleated homogeneously and forms readily in this region, where the solute concentration is unchanged. Ultimately, S precipitates grow into the region from those nucleated on loops just outside. There is also grain-boundary nucleated S which is not lath shaped. This has been observed also by Vaughan[24] in alloys aged for as little as 0.1 day. In accordance with this, the metallographic observations of 2.2:1 alloys show evidence of precipitate-free boundary zones in specimens aged for more than 0.25 day. Thus in Fig.37, aged alloys show denuded zones, approximately 1 - 2μ wide (Fig.37(a)). This is wider than the zones observed in thin foils, possibly as a result of the slower quenching rate in the tensile specimens.

In specimens aged for less than 0.25 day, Sen's observations show that there is always a zone near the boundary which is denuded of vacancies and also, therefore, of dislocation loops. This zone

is expected to be weaker than the interior of the grains, and suggests a reason why even 2.2:1 as-quenched alloys show an intercrystalline fracture when tested at 77°K. As-quenched alloys still retain a large number of vacancies in solution, (since the loop density is found to increase on ageing) and the strengthening effect of these is strongly temperature dependent. At room temperature, thermal fluctuations assist moving dislocations to overcome the pinning effect of vacancies, which are probably condensing to form loops during the tensile test. At 77°K, the vacancies strengthen the matrix and deformation tends to be easier in the vacancy-free regions near the boundaries. These regions work-harden more rapidly and it is likely that dislocation pile-up nucleation of cracks or voids, as envisaged by Beevers and Honeycombe[110] takes place, since there is very little necking, and fracture occurs almost immediately after the maximum load. Fracture occurs most likely by the joining up of dislocation pile-up cracks by shear rupture sometimes across the corner of the grain. Boundary separations behind the fracture are observed (Figs. 36(c) and 36(d)), but the fracture path is partly transcrystalline and the whole fracture surface shows ductile cusps. (Fig. 40(a) and 40(b)). The % elongation at 77°K is less than that at 295°K (Figs. 7 and 8) in accordance with this picture.

The 7:1 alloy is also expected to have precipitate-free zones near the boundaries, although these will be different from the 2.2:1 alloy. Vacancy depletion within the zones will prevent the nucleation of S precipitates, but Θ' may form preferentially in

these regions, because it has a smaller atomic volume than the matrix, so that nucleation and growth requires the emission of vacancies[8]. Thus most vacancy-free zones will be denuded of S and may contain an excess of θ'. In alloys aged beyond 0.05 day, when the structure consists of GPB(2), S, and θ', some boundary zones could be as strong as the grain interiors and others could be weaker. This would explain why in all alloys aged for more than 0.06 day, the fractures are approximately 50% intercrystalline and 50% transcrystalline, but the fracture surfaces are entirely ductile (Fig.38). The observation that several boundaries normal to the fracture surface have separated (e.g. Fig.35(b)), supports the idea that some boundaries are weaker than others. In this case the stress across the boundaries probably resulted from relaxation in the neck due to fracture.

In the 2.2:1 alloy, it was observed that fractures after 10 days ageing were entirely intercrystalline, and this is also in accordance with the precipitate-free zone model. After 10 days, S precipitates have grown into the vacancy-free region, but their density is probably still less than in the grain interiors. Strain may therefore be concentrated in a very narrow region between the boundary precipitate and the S laths growing towards the boundary. The S laths will rarely meet the boundary precipitates which will have removed solutes from their immediate vicinities.

The values of the true fracture stresses of peak aged and overaged polycrystals and single crystals, in Table 5.8 are in accordance with these ideas.

Table 5.3

Aged condition	Testing Temperature	True Fracture Stress, t.s.i.	
		Single crystals	Polycrystals
7:1 Cu:Mg			
0.5 day	295°K	56	23
	77°K	32	34
10 days	295°K	38	23
	77°K	26	32
2.2:1 Cu:Mg			
0.4 day	295°K	21	27
	77°K	36	32
10 days	295°K	17	22
	77°K	*	29

* Double-cup fracture, <100> crystal.

In general, the polycrystal fracture stresses are approximately equal to those of the corresponding single crystals. If the true surface areas of the polycrystal fractures were taken into account, the polycrystal values would be smaller than those shown. This is consistent with fracture occurring preferentially in boundary denuded zones, which are weaker than the grain interiors. The difference in strengths between the zones and grain interiors is not very large, since 7:1 alloys and some of the 2.2:1 alloys show transcrystalline failures. This suggests that shearing of the precipitates, as proposed for the later stages of single crystal deformation also takes place

in those polycrystalline alloys showing partly transcrystalline fractures. This view is supported by the decrease in the work-hardening rates of these alloys after several % strain, in the same way as the single crystals (see Fig.74).

5.3.5. The temperature dependence of mechanical properties

.1. Yield stress

The difficulty in determining the stress at which plastic deformation starts has been emphasised in Section 3.2.5. Consequently the temperature dependence of the measured stress for plastic flow, particularly in the case of polycrystals, will also reflect the temperature dependence of the very high work-hardening rate. This is difficult to predict. On polycrystal curves there is a transience from elastic to plastic deformation, which corresponds to the progression of slip from one or two slip systems in a few crystals to many slip systems in all the crystals. It is in this region that initial flow stress measurements are made. The temperature dependence of work-hardening in this region may be small (since it corresponds to stage 1 or stage 2 hardening), but is probably influenced by the type of deformation taking place after the transience. In the case of polycrystalline Al and Al solid solutions, there is a period of linear hardening[121] (e.g. Figs. 11 and 13) which corresponds to stage 2 deformation in single crystals. At room temperature, the polycrystal curve consists entirely of stage 3, whereas single crystals still show stage 2 regions on their curves[121].

Thus, the temperature dependence of the measured flow stress of polycrystals is probably higher than that of the C.R.S.S. of single crystals.

Table 5.9 shows the ratios of C.R.S.S. between 295°K and 77°K, $\frac{\tau_o\ 77}{\tau_o\ 295}$ together with the ratios of the proportional limits for corresponding polycrystals, $\frac{\sigma_o\ 77}{\sigma_o\ 295}$.

Table 5.9

Ageing Treatment	$\frac{\tau_o\ 77}{\tau_o\ 295}$	$\frac{\sigma_o\ 77}{\sigma_o\ 295}$
7:1 Cu:Mg		
As quenched	1.9	1.37
0.01 day	1.45	1.6
0.1 day	1.16	1.35
0.5 day	1.1	1.24
10 days	1.1	1.25
2.2:1 Cu:Mg		
As quenched	1.3	1.44
0.015 day	1.4	1.45
0.1 day	1.3	1.45
0.4 day	1.3	1.22
10 days	1.16	1.21

The increase in shear modulus is approximately 9%[28] and the increase in Young's modulus approximately 12%[54] over this temperature range. Thus, as-quenched and lightly aged alloys show

temperature dependences larger than the changes in elastic constants; polycrystals generally having larger temperature dependences than single crystals. In the case of pure Al, the temperature dependence is believed to arise from short range interactions between glide dislocations and forest dislocations, resulting in jog production. These also take place in solid solutions and GP zone-hardened alloys, but the magnitude of this depends on the stacking fault energy of the matrix. In addition, short range interactions between glide dislocations and GP zones and solute clusters contribute to the temperature dependence in aged alloys.

The 7:1 crystals aged for 0.1 day and beyond and the 2.2:1 crystals aged beyond the peak have temperature dependences very similar to the change in shear modulus, in agreement with the Orowan model for yielding. The peak aged 2.2:1 crystals show a larger temperature dependence, similar to that of the as-quenched and lightly aged crystals. It has been proposed, (Section 5.1.2.) that this is because of the heterogeneous structure of this alloy, whereby slip takes place initially in the volumes of material containing only GPB zones. The polycrystals of both compositions have temperature dependences equal to twice the change in Young's modulus, which suggests that initial yielding is probably associated with dislocation movement in boundary precipitate-free zones.

.2. Work hardening.

The work-hardening rates have been measured at 2-3% strain (or in Stage 2 for single crystals showing easy glide) as described

in 4.1.4.1. The results are shown in Sections 4.1.4.2. and 4.2.4. and Figs. 20, 21, 24, 63 and 64.

The as-quenched and lightly aged materials show no temperature dependence of the work-hardening rate, although the magnitude for polycrystals is 5-6 times greater than that of the single crystals. This follows directly from a consideration of hardening in pure Al. During Stage 2, single crystals with orientations near the centre of the stereographic triangle deform only on the primary and conjugate systems, and have hardening rates which are approximately 1/6 those of crystals of corner orientations[121]. No temperature dependence of Stage 2 hardening is observed for pure Al. Alloys aged for approximately 0.1 day show an apparent negative temperature dependence in both single and polycrystal form. This is most probably due to strain-induced precipitation during the tensile test.

Peak-aged 2.2:1 crystals also show an apparent negative temperature dependence and this might be due to strain-induced precipitation, or due to the small number of crystals tested. The corresponding polycrystals show no temperature dependence (Fig.24.) This behaviour is different from that of peak and overaged Al-Cu (Fig.24) and 7:1 (Figs.20, 63) alloys and overaged 2.2:1 alloys and indicates that work-hardening in peak aged 2.2:1 material probably takes place by dislocations continuing to move preferentially in the regions free from S precipitates and containing only GPB zones. The low work-hardening rates observed in peak aged 2.2:1 crystals (Fig.64) support this view.

Peak and overaged Al-Cu and 7:1 alloys and overaged 2.2:1 alloys show a marked temperature dependence of work-hardening rate. This is consistent with the deformation mechanism described in Section 3.4.4., whereby, during work-hardening in alloys containing precipitates, cross-slip was proposed to occur readily, resulting in prismatic loops being left around the precipitates. Thus the mechanisms of work-hardening appear to be similar with regard to their temperature dependence in the single crystals and polycrystals, although the magnitudes of the work-hardening rates are different. A comparison of Tables 4.7 and 4.16. shows that the single crystals work harden at a higher rate than the polycrystals. This suggests that in the polycrystals slip is taking place within the precipitate-free zone, with cross-slip of dislocations, as in Stage 3, giving rise to the temperature dependence. However, the shortage of precipitates within the zone means that work-hardening is not so marked as if the precipitate density was as high as in the grain interior, i.e. as it is in the single crystal.

5.3.6. The grain size dependence.

The Hall-Petch relationship, viz.,

$$\sigma_{LYP} = \sigma_i + k_y d^{-\frac{1}{2}}$$

where σ_{LYP} = lower yield stress

σ_i, k_y are constants

d = mean grain diameter

which was discovered empirically, has also been derived theoretically

from a consideration of the propagation of slip from one grain to another (see Tegart[121]). σ_i is identified with the stress required to propagate slip within the initial grain, and k_y is associated with the creation of dislocations at the grain boundary, or the unpinning of dislocations in the adjacent grain, when a slip band is blocked by a boundary. The operative process may be determined from the temperature dependence of k_y. Since the barrier effect is general at all strains, the Hall-Petch relationship has been generalised[147].

$$\sigma_\varepsilon = \sigma'_o + k' d^{-\frac{1}{2}}$$

where σ_ε = flow stress at strain ε

σ'_o, k' are new constants dependent on strain

d = mean grain diameter

σ'_o has been shown to be equal to $M \tau_o$, where M = Taylor's orientation factor, and τ_o is the C.R.S.S. for a free single crystal. k' has been shown to be small in f.c.c. materials, where there is no dislocation locking, but may change with strain, depending on whether dislocation locking is altered, whether strain hardening alters the stress required to operate a dislocation source, whether obstacles are formed which prevent slip band penetration to grain boundaries, whether the slip band width changes, or whether the strain hardening change in σ_o' has a grain size dependence. The interpretation of changes in k' with strain may sometimes indicate physical changes in the material.

Fig.26 shows that for as-quenched 7:1 Cu:Mg alloys, there is

little or no grain size dependence of the 0.1% P.S., but there is a small dependence of tensile strength. This is illustrated by the divergence of the true stress - true strain curves in Fig.25 and the grain-size dependence of the work-hardening rate in Fig.28, suggesting that dislocation pinning becomes stronger with increasing strain. This view is in accordance with the observations on serrations in this alloy (Section 5.3.3.), which first appear after 0.5% strain(Table 5.6), and increase in size as straining proceeds.

Fig.75 shows Petch plots for the grain size dependence of the initial flow stresses of pure Al, Al 3.5% Mg and the as-quenched 7:1 Cu:Mg alloy. The k' values for pure Al (0.5% proof stress) and the 7:1 alloy (0.1% proof stress) are similar and small in magnitude (approximately 0.24 $kg/mm^{3/2}$). The larger k' value (0.86 $kg/mm^{3/2}$) for the Al-Mg alloy lower yield stress, is in accordance with observations of yield points in this alloy[45,51]. After several % strain, however, the Petch plot for pure Al shows a decrease in k', whereas the k' values for Al-Mg alloy after approximately 6% strain, (from Thomas[51]), and the 7:1 alloy after 10% strain have increased to 1.3 and 1.6 respectively. (The increase for Al-Mg is also indicated from the results of Phillips et al[45]). This is consistent with an explanation based on increased effectiveness of dislocation pinning after straining.

The grain size dependence of % elongation, in Fig.27, is not reflected in the limits of uniform strain in Fig.25, and suggests

that most of the grain size effect occurs after necking. In the case of as-quenched alloys, the fine grain size material deforms more homogeneously, whereas coarse grained specimens need to develop slip bands along the direction of maximum shear stress in fewer grains across the section before fracture occurs. In the case of aged alloys, the fracture mechanism proposed in Section 5.3.4., of dislocation pile-up nucleated voids forming in the precipitate-free zones, is expected to be grain size dependent. Smaller grain sizes, with more boundary area, require greater strains to produce the necessary void density in the precipitate-free zones for the propagation of ductile cracks.

Some support to the idea of dislocation pile-up nucleated voids in the aged alloys is provided by the grain size dependence of the true fracture stress. Values are shown in Table 5.10.

A large k' value has been interpreted by Beevers and Honeycombe [122] as evidence for a dislocation pile up mechanism for fracture. They obtained $k' = 7.3$ kg/mm$^{3/2}$ for fully aged Al, 5.4 wt.% Cu alloys. The k' value for peak-aged 7:1 Cu:Mg alloy is seen to be higher than this, although the true fracture stresses at 77°K and 295°K are similar to the Al, 5.4 wt.% Cu alloy; in each case, between 30 and 40 t.s.i. (Fig.29 and ref.122). This might be due to grain boundary precipitates as a result of the low solution treatment temperature used for the 7:1 alloy (Section 2.3.3.), or might indicate that the strain in the precipitate-free zones of the 7:1 alloy is greater than that in the Al-Cu alloy, just prior to

Table 5.10

Aged Condition	True fracture stress, kg/mm^2	$d^{-\frac{1}{2}}$ $mm^{-\frac{1}{2}}$	k' $kg/mm^{3/2}$
0.3 day	84.0	1.95	
	87.1	2.13	14.3
	96.5	2.4	
	105	3.16	
1 day	39.7	1.95	
	45.0	2.13	16.5
	48.5	2.4	
		3.16	
10 days	36.5	1.95	
	37.0	2.13	3.6
	38.1	2.4	
	40.1	3.16	

fracture. This might occur if the precipitate-free zones in the 7:1 alloy were narrower than those in Al-Cu. No firm conclusions, however, may be drawn.

5.3.7. Summary of single crystal and polycrystal deformation.

.1. As-quenched and lightly aged alloys.

The major difference in yield behaviour between single crystals and polycrystals is the occurrence of dislocation multiplication yield points in the single crystals. These are believed to be a consequence of dislocation pinning, and a low Stage 1 work-hardening rate. No yield discontinuities are observed in polycrystals, and it is proposed that dislocation creation at boundaries at the start of the deformation produces multiple slip within the vacancy-depleted zones near the boundaries. This occurs regardless of dislocation pinning within the grains. Support for this view is found in the grain size dependence of the 0.1% proof stress for as-quenched 7:1 alloys tested at room temperature, where k' is very low, approximately equal to that of pure Al, and less than that of Al-Mg alloys. Furthermore, the higher temperature dependence of the yield stress for polycrystals compared with single crystals, suggests that the yield mechanisms are slightly different in each case. The aggregate analysis results also tend to support these ideas, since the polycrystal yield stresses are smaller than the Taylor aggregate yield stresses, which is consistent with dislocation creation at boundaries being easier than dislocation unpinning or creation within individual crystals.

After yielding, the deformation of the single crystals is similar to that of pure Al. Since the orientations are near the centre of the stereographic triangle, the derived aggregate curves have a lower slope than the corresponding polycrystal curves. The work-hardening rate is independent of temperature, as expected during stage 2 deformation. The polycrystals also deform like pure Al; the work-hardening rates are independent of temperature, but higher than those in single crystals, suggesting that linear hardening, such as occurs in <100> or <111> single crystals during stage 2, is taking place. Deformation is probably by the formation of slip bands across grains, from dislocation sources at stress concentrations in the boundaries, e.g. at triple points.

After several % deformation at room temperature, strain ageing serrations appeared on the load-elongation curves. It is postulated that the effect results from dislocation immobilisation by tangling and subsequent solute pinning, enforcing dislocation multiplication elsewhere. The temperature and composition dependence of the Portevin-Le Chatelier effect, and the delay in its occurrence in single crystals are in good agreement with this model. The grain size dependence results support the view that pinning occurs after straining, since k' increases with strain, in the same way as Al-Mg, whereas for pure Al, k' decreases with strain.

In both single crystals and polycrystals, the Portevin-Le Chatelier effect influences the fracture mode. In the former case, dislocation avalanches along primary and conjugate slip planes as a result of

strain-ageing produce crocodile fractures, instead of the more usual coarse slip bands. In the case of polycrystals, dislocation avalanches as a result of strain ageing occur preferentially in slip bands aligned nearest to the maximum shear stress direction, so producing 45° shear fractures.

.2. Peak and overaged.

The major difference between the yielding characteristics in single crystals and polycrystals is the discontinuity observed in the single crystals. Dislocation multiplication, as a result of few mobile dislocations being present at the start of plastic flow, due to solute pinning, is proposed to account for this. No yield drop is observed because the work-hardening rate in the material is high. Polycrystals show no yield discontinuities, and it is proposed that grain boundary generated dislocations move within the precipitate-depleted zone at the start of deformation. This is supported by the temperature dependence results, which show a greater dependence for the polycrystals than for the single crystals. The single crystal temperature dependence is similar to that of the elastic constants, which is in accordance with the Orowan theory for yielding in these alloys. The results of the Taylor aggregate analysis, which show that the aggregate yield stresses are much higher than those of the polycrystals, do not contradict the view that deformation takes place preferentially in the precipitate-free zones. However, there is some evidence for correlation between the polycrystal yield stress and the elastically-corrected aggregate yield stress.

After yielding, the precipitate-free zones play a major part in the subsequent deformation of the polycrystals. It is thought that these zones work-harden rapidly, so that deformation soon takes place simultaneously within the zones and within the grains. The dislocation interactions with the precipitates within the grains are then the same for single crystals and polycrystals. This view is supported by the observation that the true stress - true strain curves are almost parallel for single and polycrystals, whereas the aggregate and polycrystal curves are very different. It is also supported by the similar temperature dependences of the work-hardening rates of single and polycrystals of overaged alloys. The magnitude of this temperature dependence is relatively large, and being similar for single and polycrystals, agrees with the work-hardening model of dislocations cross-slipping around precipitates and forming prismatic loops which act as dislocation sources. The slight displacement of the polycrystal true stress - true strain curves from those of the single crystals, together with the slightly higher initial work-hardening rate of the single crystals, suggests that the precipitate-free boundary zone is also deforming simultaneously with the grain interiors.

Erratic results for the temperature dependence of the work-hardening rate of peak-aged single crystals arise partly from the heterogeneous structure of these materials and partly from the extreme orientations of some of the crystals used. The small temperature dependence of peak aged polycrystals is probably because of the wider precipitate-free zones, within which linear hardening (like stage 2

of extreme orientations of single crystals) takes place.

The precipitate-free zones markedly influence the fracture characteristics. True fracture stresses for single crystals are generally higher than those of polycrystals, suggesting that the precipitate-free zones are weaker than the grains. Metallographic observations confirm that the majority of fractures occur within the zones. The absence of necking, particularly at low temperatures, suggests that dislocation pile-up nucleated voids are responsible for the ductile fracture mechanism. Single crystals still show coarse shear band fractures, the bands being wider in 7:1 crystals, suggesting that S precipitates might be sheared at higher strains.

6. GENERAL CONCLUSIONS

1. The changes in mechanical properties of 7:1 and 2.2:1, Cu:Mg alloys, aged at 190°C, have been found to follow the established changes in hardness[18].

2. The strengthening effect of Mg in the Al-Cu-Mg supersaturated solid solution alloys is less than would be produced if the Mg were replaced by an equivalent atomic percentage of Cu. This is explained on the basis of the relatively small lattice strain associated with Mg-Cu atom pairs or Mg-vacancy pairs. The relatively high vacancy and dislocation loop density caused by the presence of Mg, gives some strengthening and the overall effect of Mg is therefore greater than expected purely from lattice strain considerations.

3. In 7:1 and 2.2:1, Cu:Mg alloys aged for short times to contain GPB zones, dislocations cut through the zones from the start of deformation. This is shown by :-

(a) the low work-hardening rates of single crystals;

(b) the reasonable agreement between the measured critical resolved shear stresses and the strengths calculated from the resistance encountered by dislocations cutting through the zones;

(c) the temperature dependence of the C.R.S.S. being consistent with the theory of thermally activated cutting of obstacles by dislocations.

4. In peak aged and overaged alloys, containing intermediate or equilibrium precipitates, dislocations do not initially cut through

the precipitates. This is shown by :-

(a) the rapid initial work hardening rates of the single crystals;

(b) the reasonable agreement between the measured critical resolved shear stresses and the Orowan strengthening calculated for dislocations bowing between precipitates;

(c) the temperature dependence of the critical resolved shear stress being approximately equal to that of the elastic modulus as predicted by the Orowan model.

5. The heterogeneous structure of peak aged 2.2:1, Cu:Mg alloys enables dislocations to move through regions in the material which contain no precipitates but only GPB zones. As a result, the deformation characteristics differ from those of peak-aged Al-Cu and 7:1, Cu:Mg alloys, in single crystal form, in the following ways :-

(a) the work hardening rate is lower;

(b) the temperature dependence of the critical resolved shear stress is larger than that of the elastic modulus, and is similar to that of as-quenched or lightly-aged crystals.

6. In both 7:1 and 2.2:1, Cu:Mg alloys, weak pinning of dislocations by Mg atoms takes place. This produces yield drops on the stress-strain curves of as-quenched and lightly aged crystals tested at low temperatures, and a Portevin-Le Chatelier effect on the stress-strain curves of as-quenched and lightly aged single crystals and polycrystals at room temperature. The grain size dependence of the flow stress of as-quenched 7:1 alloys is shown to be consistent with a dislocation pinning model. The yield drops and strain-ageing serrations are explained by dislocation

multiplication processes.

7. The fracture of single crystals having 'soft' orientations, at all stages of ageing, occurs by localised shear on slip planes. In the case of as-quenched and lightly aged crystals a fall in load marks the initiation of the localised shear band and this occurs at a shear stress which is temperature and composition dependent. The large strain subsequent to this and prior to fracture, together with the fracture appearance, are inconsistent with a ductile failure model based on the coalescence of dislocation-nucleated voids.

Peak and overaged crystals deform and fracture in a similar manner, but the planar fractures and the differences in the widths of the shear bands for 7:1 and 2.2:1 alloys are interpreted as evidence for dislocations shearing the S precipitates after several per cent strain.

8. The deformation of well-aged polycrystals is strongly influenced by the presence of grain boundary precipitate-free zones. Initially, dislocations move preferentially in these zones, so that the observed temperature dependence of the initial flow stress for polycrystals is higher than that of single crystals, where it is governed only by the change in elastic modulus. Also, the work hardening rate, being governed by dislocation interactions within the zones, is lower in overaged polycrystals than in single crystals. As a result of non-uniform straining, the instability points on the stress-strain curves occur after smaller strains than those predicted from the Ludwik or Swift relationships.

9. The fractures of well-aged polycrystals are governed by the presence of grain boundary precipitate-free zones. In appearance, the fractures are intercrystalline, but fractographs indicate that they are also ductile. Over the ageing period when these fractures occur, the true fracture stresses at low temperature are approximately constant. This is consistent with an explanation based on a ductile failure mechanism in the precipitate-free zones as a result of dislocation-nucleated voids being formed there. The following features provide additional evidence for this :-

(a) the grain size dependence of the true fracture stress for aged 7:1, Cu:Mg alloys;

(b) observations of fractures occurring on rising stress-strain curves.

10. The comparison between single crystal and polycrystal stress-strain curves using the Taylor aggregate theory is not successful for aged Al-Cu-Mg alloys. A correction for elasticity produces approximate agreement between polycrystal and aggregate curves at the start of plastic deformation. For well aged alloys, the aggregate curves after the yield are much steeper than the polycrystal curves. The rapid work hardening of the polycrystals is reduced by the effect of deformation occurring preferentially in the precipitate-free zones. This explanation accounts for the similarity between the true stress - true strain curves for single crystals and polycrystals.

Acknowledgements

The helpful advice and encouragement received from Dr. D.R.F. West are gratefully acknowledged. Also, acknowledgements are made to the Ministry of Aviation for financial assistance, to the British Aluminium Company for the manufacture and analysis of some of the alloys, and to Professor J.G. Ball for the provision of laboratory facilities at the Metallurgy Department, Royal School of Mines.

Appendix 1.

The True Stress Strain Curve in Simple Tension

True stress, $\bar{\sigma} = \frac{P}{A_i}$

where P = load

A_i = Instantaneous cross sectional area.

For uniform strain, the volume change during tensile testing is negligible, so that,

$$A_o l_o = A_i l_i$$

where A_o = Original cross-sectional area

l_o = Original gauge length

l_i = Instantaneous gauge length

$$\therefore \quad \bar{\sigma} = \frac{P}{A_o} \cdot \frac{l_i}{l_o}$$

$$\underline{\bar{\sigma} = \sigma (1 + \varepsilon)} \qquad 1.$$

where ε = Nominal strain

σ = Nominal stress

True (logarithmic) strain $\bar{\varepsilon} = \int_{l_o}^{l_i} \frac{dl}{l}$

$$\bar{\varepsilon} = \ln \frac{l_i}{l_o}$$

$$\underline{\bar{\varepsilon} = \ln (1 + \varepsilon)} \qquad 2.$$

Since $\bar{\sigma} = \frac{P}{A_i}$

$$P = A_i . \bar{\sigma}$$

$$= A_o . \frac{l_o}{l_i} . \bar{\sigma}$$

$$= \frac{A_o . \bar{\sigma}}{1 + \varepsilon}$$

Differentiating,

$$\frac{dP}{d\varepsilon} = A_o \left(\frac{1}{1+\varepsilon} \cdot \frac{d\bar{\sigma}}{d\varepsilon} - \bar{\sigma} \cdot \frac{1}{(1+\varepsilon)^2} \right)$$

At the maximum load, (instability point)

$$\frac{dP}{d\varepsilon} = 0.$$

$$\therefore \quad A_o \left(\frac{1}{1+\varepsilon} \cdot \frac{d\bar{\sigma}}{d\varepsilon} - \bar{\sigma} \cdot \frac{1}{(1+\varepsilon)^2} \right) = 0.$$

$$\therefore \quad \underline{\frac{d\bar{\sigma}}{d\varepsilon} = \frac{\bar{\sigma}}{1+\varepsilon}} \qquad 3.$$

Thus if true stress is plotted against nominal strain, the instability point is found by drawing a tangent to the curve such that the length of the sub-tangent is $(1 + \varepsilon)$

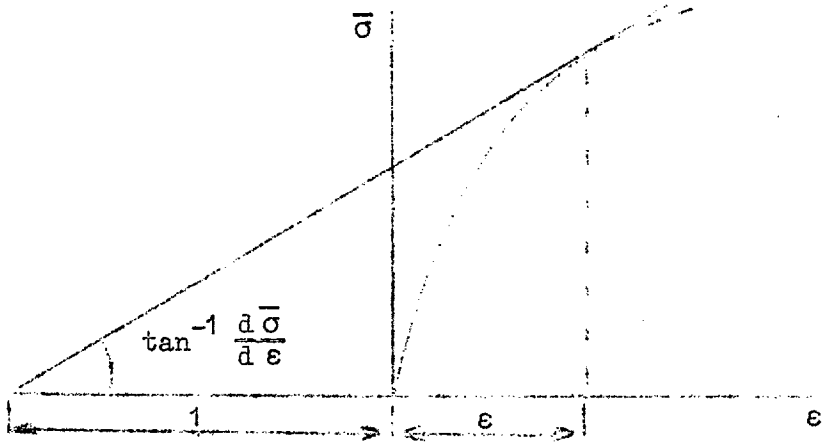

Since $\bar{\varepsilon} = \ln(1+\varepsilon)$ from equation 2

$$\frac{d\bar{\varepsilon}}{d\varepsilon} = \frac{1}{1+\varepsilon}$$

$$\therefore \quad \frac{d\bar{\sigma}}{d\bar{\varepsilon}} = \frac{d\bar{\sigma}}{d\varepsilon} \cdot \frac{d\varepsilon}{d\bar{\varepsilon}}$$

$$= \frac{\bar{\sigma}}{1+\varepsilon} \cdot 1 + \varepsilon$$

$$\underline{\frac{d\bar{\sigma}}{d\bar{\varepsilon}} = \bar{\sigma}} \qquad 4.$$

Thus for a true stress - true strain graph, the instability point is found by constructing a tangent to the curve such that the length of the sub-tangent along the true strain axis is 1.

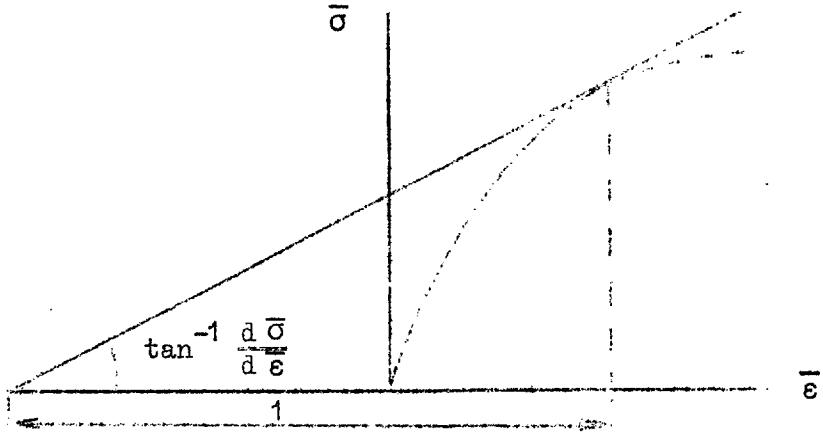

True stress - strain curves may be described by the parabolic equation :-

$$\bar{\sigma} = k \varepsilon^{n} \qquad -(5)$$

where k and n are constants.

This was originally proposed by Ludwik [149], who stated that either true logarithmic strain or nominal strain may be used. Later, Nadai [150] and Pascoe [151] used nominal strain, while Holloman [152], Gensamer [153] and others use logarithmic strain. For small strains, nominal strain and logarithmic strain are almost identical.

Differentiating equation 5, using true strain,

$$\bar{\sigma} = k \bar{\varepsilon}^{n}$$

$$\frac{d\bar{\sigma}}{d\bar{\varepsilon}} = k n \bar{\varepsilon}^{(n-1)}$$

But for instability, $\frac{d\bar{\sigma}}{d\bar{\varepsilon}} = \bar{\sigma}$, from equation 4.

$$\therefore \quad k n \bar{\varepsilon}^{(n-1)} = \bar{\sigma} = k \bar{\varepsilon}^{n}$$

$$\therefore \quad \underline{n = \bar{\varepsilon}} \quad \text{at maximum load} \qquad 6.$$

Also, from $\bar{\sigma} = k \bar{\varepsilon}^{n}$

$$\underline{\log \bar{\sigma} = \log K + n \log \bar{\varepsilon}} \qquad 7.$$

'n' is termed the strain hardening coefficient, and may be evaluated from the slope of the log true stress - log true strain plot, or from the value of true strain at maximum load. It is a measure of the work hardening characteristic and is the limit of uniform strain for any given material which obeys the relationship in equation 5.

Linear log true stress - log true strain plots have been demonstrated for different steels[152], copper alloys[154], silver chloride and some Al alloys[155]. However, non-linear plots have been shown by Carreker and Hibbard[57] for high purity Cu and by Dorn et al[61] for high purity Al and dilute Al alloys.

Other empirical equations for stress-strain curves have been proposed. Generally, these expressions are no better approximations than the simple parabolic expression of Ludwik, and are more complex for theoretical analysis.

A more realistic variation of Ludwik's equation has been proposed by Swift[156].

$$\bar{\sigma} = A (B + \varepsilon)^n \qquad 8.$$

where A, B and n are constants.

This equation is also parabolic.

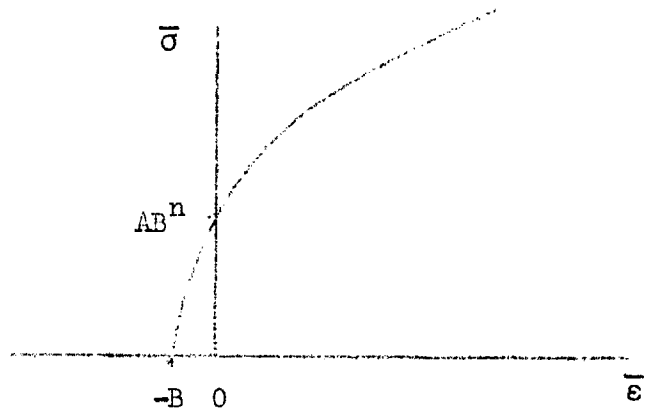

$$\frac{d\bar{\sigma}}{d\bar{\varepsilon}} = n.\ A.\ (B + \varepsilon)^{n-1}$$

$$= \frac{n\bar{\sigma}}{B+\bar{\varepsilon}}$$

But, from equation 4, at instability,

$$\frac{d\bar{\sigma}}{d\bar{\varepsilon}} = \bar{\sigma}$$

$$\therefore \quad \bar{\sigma} = \frac{n.\ \bar{\sigma}}{B + \bar{\varepsilon}} \quad , \text{ and } \quad n = B + \bar{\varepsilon}$$

or, $$\bar{\varepsilon}_{\text{Instability}} = n - B. \qquad 9.$$

Appendix 2.

Calculations from tensile tests on single crystals.

1. The resolved shear stress

$$\tau = \frac{P}{A_o} . \cos \lambda_i . \cos \varphi_i .$$

where, P = load

A_o = original cross-sectional area

λ_i = instantaneous angle between tensile axis and glide direction

φ_i = instantaneous angle between tensile axis and glide plane normal

Thus, the critical resolved shear stress,

$$\tau_o = \frac{P_o}{A_o} . \cos \lambda_o . \cos \varphi_o ,$$

where the subscript 'o' refers to values at the yield point.

For calculating the resolved shear stress on the operative slip plane[55] at other stages of deformation, the following relationship was also used :-

$$\frac{l_i}{l_o} = \frac{\cos \varphi_o}{\cos \varphi_i} = \frac{\sin \lambda_o}{\sin \lambda_i}$$

where, l_o = original gauge length

l_i = instantaneous gauge length.

Now $\frac{l_i}{l_o} = 1 + \varepsilon$ where, ε = tensile strain $= \frac{l_i - l_o}{l_o}$

and $\cos \lambda = (1 - \sin^2 \lambda)^{\frac{1}{2}}$

so that $\cos \lambda_i = (1 - \frac{\sin^2 \lambda_o}{(1+\varepsilon)^2})^{\frac{1}{2}}$

In the present work, resolved shear stress values have been calculated only for single slip deformation, so that $\frac{A_o}{\cos \varphi_i}$ (the area of the slip plane) is constant.

Thus $$\tau = \frac{P}{A_o} \cdot \cos \varphi_o \cdot (1 - \frac{\sin^2 \lambda_o}{(1+\varepsilon)^2})^{\frac{1}{2}} \qquad 1.$$

---

2. Glide strain

This is defined as the relative displacement of two slip planes unit distance apart, and is given by (55)

$$a = \frac{1}{\cos \varphi_o} \cdot [\{(1+\varepsilon)^2 - \sin^2 \lambda_o\}^{\frac{1}{2}} - \cos \lambda_o] \qquad 2.$$

References

1 : ARMSTRONG, R.W. J.Mech. Phys. Solids, 1961, 9, 196.

2 : KAY, D. 'Techniques for Electron Microscopy'. Blackwell, Oxford, 1961. p.103.

3 : HONEYCOMBE, R.W.K. Met. Rev. 1959, 4, No.13.

4 : WILLIAMSON, G.K. and SMALLMAN, R.E. Acta Met., 1953, 1, 487.

5. : BARRETT, C.S. 'Structure of Metals', 2nd ed. McGraw-Hill, New York, 1952, p.492.

6 : ANDERSON, W.A. and MEHL, R.F. Trans. A.I.M.E., 1945, 161, 140.

7 : CULLITY, B.D. 'Elements of X-ray Diffraction', Addison-Wesley, Mass., 1956, p.225.

8 : KELLY, A. and NICHOLSON, R.B. Progress in Materials Science, 1963, 10, No.3.

9 : THOMAS, G. and WHELAN, M.J. Phil. Mag. 1959, (8), 4, 511.

10 : EMBURY, J.D. and NICHOLSON, R.B. 5th International Congress for Electron Microscopy, Academic Press, New York, 1962. J1.

11 : GUINIER, A. Acta Cryst., 1952, 5, 21.

12 : NICHOLSON, R.B. and NUTTING, J. Phil. Mag. 1958, (8), 3, 531.

13 : SILCOCK, J.M., HEAL, T.J. and HARDY, H.K. J. Inst. Metals, 1953-4, 82, 239.

14 : NICHOLSON, R.B., THOMAS, G. and NUTTING, J. J. Inst. Metals, 1958-9, 87, 429.

15 : THOMAS, G. and NUTTING, J. The Mechanism of Phase Transformations in Metals. Institute of Metals. 1956. p.57.

16 : THOMAS, G. and NUTTING, J. Acta. Met., 1959, 7, 515.

17 : NICHOLSON, R.B. 'Electron Microscopy and Strength of Crystals', Wiley, New York, 1963, Chapter 18.

18 : HARDY, H.K. J. Inst. Metals, 1954-5, 83, 17.

19 : SILCOCK, J.M. J. Inst. Metals, 1960-1, 89, 203.

20 : GEROLD, V. and HABERKORN, H. Z. Metallk, 1959, 50, 568.

21 : BROOK, G.B. Fulmer Research Institute, Special Report No.3, 1965.

22 : BAGARYATSKY, Y.A. Doklady Akad. Nauk S.S.S.R., 1952, 87, 559. (Fulmer Research Institute Translation No.55)

23 : WILSON, R.N. and PARTRIDGE, P.G. Acta Met., 1965, 13, 1321.

24 : VAUGHAN, D. Unpublished work.

25 : GEISLER, A.H. 'Phase Transformation in Solids', Wiley, New York, 1951.

26 : HARDY, H.K. J. Inst. Metals, 1951, 79, 321.

27 : DEN-HUGHES, D. and ROBERTSON, W.D. Acta Met., 1960, 8, 156.

28 : BYRNE, J.G., FINE, M.E. and KELLY, A. Phil. Mag., 1961, (8), 6, 1119.

29 : BOMAR, L.G. Ph.D. Thesis, Univ. Cambridge, 1962.

30 : CORDEROY, D.J.H. and HONEYCOMBE, R.W.K. J. Inst. Metals, 1964-5, 93, 432.

31 : MATSUURA, K., IZUMI, S. and KODA, S. J. Phys.Soc., Japan, 1958, 13, 318.

32 : MATSUURA, K. and KODA, S. J. Phys. Soc., Japan, 1960, 15, 195.

33 : SHAW, R.B., SHEPARD, L.A., STARR, C.D. and DORN, J.E. Trans. A.S.M., 1953, 45, 249.

34 : HART, E.W. 'Relation of Properties of Microstructure'. A.S.M., Cleveland, Ohio, 1953. p.95.

35 : CARLSEN, K.M. and HONEYCOMBE, R.W.K. J. Inst. Metals, 1954-5, 83, 449.

36 : GREETHAM, G. and HONEYCOMBE, R.W.K. J. Inst. Metals, 1960-1. 89, 13.

37 : PRICE, R.J. and KELLY, A. Acta Met., 1964, 12, 159.

38 : MATSUURA, K. and KODA, S. Proc. of the Int. Conf. on Crystal Lattice Defects, J. Phys. Soc., Japan, 1963, 18, Suppl. 1, p.50.

39 : KELLY, A., LASSILA, A. and SATO, S. Phil. Mag., 1959, (8), 4, 1260.

40 : PRICE, R.J. and KELLY, A. Acta Met. 1963, 11, 915.

41 : DeLUCA, R. and BYRNE, J.G. Acta Met. 1965, 13, 1187.

42 : PHILLIPS, V.A. J. Inst. Metals, 1952-3, 81, 649.

43 : McREYNOLDS, A.W. Trans. A.I.M.E., 1949, 185, 32.

44 : KRUPNIK, N. and FORD, H. J. Inst. Metals, 1952-3, 81, 601.

45 : PHILLIPS, V.A., SWAIN, J.A. and EBORALL, R. J. Inst. Metals, 1952-3, 81, 625.

46 : SHERBY, O.D., ANDERSON, R.A. and DORN, J.E. Trans. A.I.M.E. 1951, 191, 643.

47 : WESTWOOD, A.R.C. and BROOM, T. Acta Met., 1957, 5, 249.

48 : COTTRELL, A.H. Phil. Mag., 1953, (7), 44, 829.

49 : SPERRY, P.R. Acta Met., 1963, 11, 153.

50 : WRIGHT, J.C., TURNER, M.S. and DAVIES, A.L. J.Inst.Metals, 1961-2, 20, 369.

51 : THOMAS, A.T. Acta Met., 1966, 14, 1363.

52 : MATSUURA, K., HAMAGUCHI, and KODA, S. J. Phys. Soc., Japan, 1957, 12, 1424.

53 : MATSUURA, K., NAGASAKI, and KODA, S. Nippon Kuzoku Gakkai-Si, 1957, 21, 618 .

54 : KELLY, A. and CHIOU, C. Acta Met. 1958, 6, 565.

55 : SCHMID, E. and BOAS, W. 'Plasticity of Crystals'. Hughes, London, 1950.

56 : ROSI, F.D. and MATHEWSON, C.H. Trans. A.I.M.E., 1950, 188, 1159.

57 : CARREKER, R.P. and HIBBARD, W.R. Acta Met., 1953, 1, 656.

58 : McLEAN, D. 'Mechanical Properties of Metals', Wiley, New York, 1962.

59 : MATSUURA, K. and KODA, S. Phil.Mag., 1961, (8), 6, 1531.

60 : DASH, J. and FINE, M.E. Acta Met., 1961, 9, 149.

61 : DORN, J.E., PIETROKOWSKY, P. and TIETZ, T.E. Trans.A.I.M.E. 1950, 188, 933.

62 : HONEYCOMBE, R.W.K. Progress in Materials Science, 1961, 2, p.93.

63 : COTTRELL, A.H. and STOKES, R.J. Proc. Roy. Soc. A. 1955, 233, 17.

64 : KELLY, A. Acta Met., 1959, 7, 811.

65 : THOMAS, G. and NUTTING, J. J. Inst. Metals, 1957-8, 86, 7.

66 : THOMAS, G. and NUTTING, J. J. Inst. Metals, 1956-7, 85, 1.

67 : SILCOCK, J.M. Acta Met., 1960, 8, 589.

68 : KODA, S. and TAKEYAMA. J. Inst. Metals, 1957-8, 86, 277.

69 : NICHOLSON, R.B., THOMAS, G. and NUTTING, J. Acta Met., 1960, 8, 172.

70 : NICHOLSON, R.B. and NUTTING, J. Acta Met., 1961, 9, 332.

71 : FORSYTH, P.J.E. and WILSON, R.N. J. Inst. Metals, 1963-4, 92, 82.

72 : LERINMAN, R.M. SHCHEGOLOVA, T.V., PAVLOVA, G.V. and ADOLINA, T.I. The Physics of Metals and Metallography. 1964, 18, No.4, 139.

73 : SWANN, P.R. 'Electron Microscopy and Strength of Crystals'. Wiley, New York. 1963, Chapter 3.

74 : ASHBY, M. Z. Metallk., 1964, 55, 5.

75 : ASHBY, M. and SMITH, G.C. Phil.Mag., 1960, (8), 5, 298.

76 : KODA, S., MATSUURA, K., and TAKAHASHI, S. J. Inst. Metals, 1962-3. 21, 229.

77 : BOMAR, L.G. and KELLY, A. 5th International Congress for Electron Microscopy, Academic Press, New York, 1962, K.11.

78 : POLLARD, G. and NUTTING, J. J. Inst. Metals, 1964-5, 93, 464.

79 : HIRSCH, P.B. 'The Relation between the structure and Mechanical Properties of Metals'. N.P.L. Symposium, No.15 1963. p.39.

80 : WILSON, R.H. 5th International Congress for Electron Microscopy, Academic Press, New York, 1962. K - 3.

81 : MOTT, N.F. and NABARRO, F.R.N. Proc. Phys. Soc., 1940, 52, 86, and Rep. Conf. Strength of Solids, Physical Society, 1948, p.1.

82 : OROWAN, E. Symposium on Internal Stresses in Metals and Alloys, Institute of Metals, 1948, p.451.

83 : COTTRELL, A.H. 'Dislocations and Plastic Flow in Crystals'. O.U.P., 1953.

84 : ANSELL, G.S. and LENEL, F.V. Acta Met., 1960, 8, 612.

85 : FLEISCHER, R.L. Acta Met., 1960, 8, 598.

86 : FLEISCHER, R.L. 'Electron Microscopy and Strength of Crystals'. Wiley, New York, 1963. Chap. 23.

87 : SEEGER, A. 'Dislocations and Mechanical Properties of Crystals'. Wiley, New York, 1956.

88 : HIRSCH, P.B. and KELLY, A. Phil. Mag., 1965, 12, 881.

89 : KELLY, A. Phil. Mag., 1958, (8), 3, 1472.

90 : WILLIAMS, R.O. Acta Met. 1957, 5, 385.

91 : JONES, R.L. Acta Met., 1966, 14, 81.

92 : BETON, R.H. and ROLLASON, E.C. J. Inst. Metals, 1957-8, 86, 77.

93 : KELLY, A. and FINE, M.E. Acta Met., 1957, 5, 365.

94 : KELLY, A. discussion to Fleischer, R.L. reference (84).

95 : KELLY, A. 'Electron Microscopy and Strength of Crystals', Wiley, New York, 1963, Chap.22.

96 : DEW-HUGHES, D. and ROBERTSON, W.D. Acta Met., 1960, 8, 147.

97 : PRESTON, O. and GRANT, N.J. Trans. A.I.M.E., 1961, 221, 164.

98 : ANSELL, G.S. and HIRSCHHORN, J.S. Acta Met., 1965, 13, 572.

99 : HIRSCH, P.B. J. Inst. Metals, 1957-8, 86, 13.

100: FISHER, J.C., HART, E.W. and PRY, R.H. Acta Met., 1953, 1, 336.

101: TIPPER, C.F. Metallurgia, 1949, 39, 133.

102: PUTTICK, K.E. Phil. Mag., 1959, (8), 4, 464.

103: ROGERS, H.C. Trans. A.I.M.E., 1960, 218, 498.

104: BEEVERS, C.J. and HONEYCOMBE, R.W.K. Phil. Mag., 1962, 7, 763.

105: COTTRELL, A.H. 'Fracture', Wiley, New York, 1959, p.20.

106: CHIN, G.Y., HOSFORD, W.F. and BACKOFEN, W.A. Trans. A.I.M.E., 1964, 230, 437.

107: RYDER, D.A. and SMALE, A.C. 'Fracture in Solids', A.I.M.E. Met. Conf. Series No.20., Wiley, New York, 1963, p.237.

108: CRUSSARD, C., PLATEAU, J., TAMHANKAR, R., HENRY, G. and LAJEUNESSE, D. 'Fracture', Wiley, New York, 1959, p.524.

109: ELAM, C.F. Proc. Roy. Soc. A., 1927, 115, 133.

110: BEEVERS, C.J. and HONEYCOMBE, R.W.K. 'Fracture', Wiley, New York, 1959, p.474.

111: PRICE, R.J. and KELLY, A. Acta Met., 1964, 12, 979.

112 : GHATE, V.B. and WEST, D.R.F. Metallurgia, 1961, 51, 269.

113 : ROHNER, F. J. Inst. Metals, 1947, 73, 285.

114 : OROWAN, E. Report on Progress in Physics, 1948, 12, 185.

115 : SEN, N. Ph.D. Thesis, 1967, London.

116 : HUME-ROTHERY, W. Atomic Theory for Students of Metallurgy. Institute of Metals, 1955.

117 : KOCKS, U.F., Acta Met., 1966, 14, 1629.

118 : JONES, R.L. and KELLY, A. Acta Met. 1967, 15, 656.

119 : NABARRO, F.R.N., Proc. Phys. Soc. 1946, 58, 6, p.669.

120 : PEARSON, W.B. A Handbook of Lattice Spacings and Structures of Metals & Alloys. Pergamon, London, 1958.

121 : TEGART, W.J.Mc.G., Elements of Mechanical Metallurgy. McMillan, London, 1966.

122 : BEEVERS, C.J. and HONEYCOMBE, R.W.K. Acta. Met. 1962, 10, 17.

123 : WILSON, R.N. and FORSYTH, P.J.E. J.Inst. Metals, 1966, 94, 8.

124 : TAYLOR, G.I. J. Inst. Metals, 1938, 62, 307.

125 : BISHOP, J.F.W. and HILL, R. Phil. Mag. 1951, 42, 414 and 1298.

126 : KOCKS, U.F., Acta. Met. 1958, 6, 85.

127 : HOWE, S. and ELBAUM, C. Phil. Mag. 1961, 6, 37.

128 : RICHARDS, T. Ll. Rheologica Acta 1962, Bd.2.,1.

129 : HOSFORD, W.F., Acta. Met., 1966, 14, 1085.

130 : KOCKS, U.F. and BROWN, T.J. Acta. Met. 1966, 14, 87.

131 : KOCKS, U.F. Acta Met. 1960, 8, 345.

132 : KOCKS, U.F. Acta Met. 1964, 12, 849.

133 : LIN, T.H. J. Mech. Phys, Solids, 1964, 12, 391.

134 : BUDIANSKY, B. and WU, T.T. Proc. 4th U.S. Nat. Congr. Appl. Mech. 1962. p.1175.

135 : MUKHERJEE, A.K., MOTE, J.D. and DORN, J.E. Trans. Met. Soc. A.I.M.E., 1965, 233, 1559.

136 : COTTRELL, A.H. The Relation between the Structure and Mechanical Properties of Metals, N.P.L. Symp. No.15. H.M.S.O. London, 1963 p.456.

137 : JOHNSTON, W.G. and GILMAN, J.J. J. Appl. Phys. 1959, 30, 129.

138 : JOHNSTON, W.G. J. Appl. Phys. 1962, 33, 2716.

139 : CHRISTIAN, J.W. The Theory of Transformations in Metals and Alloys. Pergamon, London, 1965.

140 : WILCOX, B.A. and SMITH, G.C. Acta Met. 1964, 12, 371.

141 : BAILEY, D.J., FLANAGAN, W.F. and MILLER, G.E. Acta Met., 1965, 13, 436.

142 : ROSI, F.D. and ABRAHAMS, M.S. Acta Met., 1960, 8, 807.

143 : ROGERS, H.C. Acta Met., 1959, 7, 750.

144 : BEACHEM, C.D., Trans. A.S.M., 1963, 56, 318.

145 : FORSYTH, P.J.E. and RYDER, D.A. Metallurgia, 1961, 63, 117.

146 : RYDER, D.A. and VIAN, R.E. J. Inst. Metals 1961 - 2, 90, 383.

147 : ARMSTRONG, R., CODD, I., DOUTHWAITE, R.M. and PETCH, N.J. Phil. Mag., 1962, 7, 45.

148 : CARREKER, R.P. and HIBBARD, W.R. Trans. A.I.M.E., 1957, 209, 1157.

149 : LUDWIK, P. Elemente der Technologischen Mechanik, Springer, Berlin, 1909.

150 : NADAI, A. Plasticity, McGraw-Hill, New York, 1931.

151 : PASCOE, K.J. An introduction to the Properties of Engineering Materials, Blackie, London, 1961.

152 : HOLLOMAN, J.H. Trans. A.I.M.E. 1945, 162, 268.

153 : GENSAMER, M. Trans. A.I.M.E. 1938, 128, 104.

154 : FRENCH, R.S. and HIBBARD, W.R. Trans. A.I.M.E., 1950, 188, 53.

155 : BRITTAIN, J.O. Modern Applications of Theories of Elasticity and Plasticity to Metals, Instron Eng. Corp. Publication M.5. 1960.

156 : SWIFT, H.W. J. Mech. Phys. Solids, 1952, 1, 1.

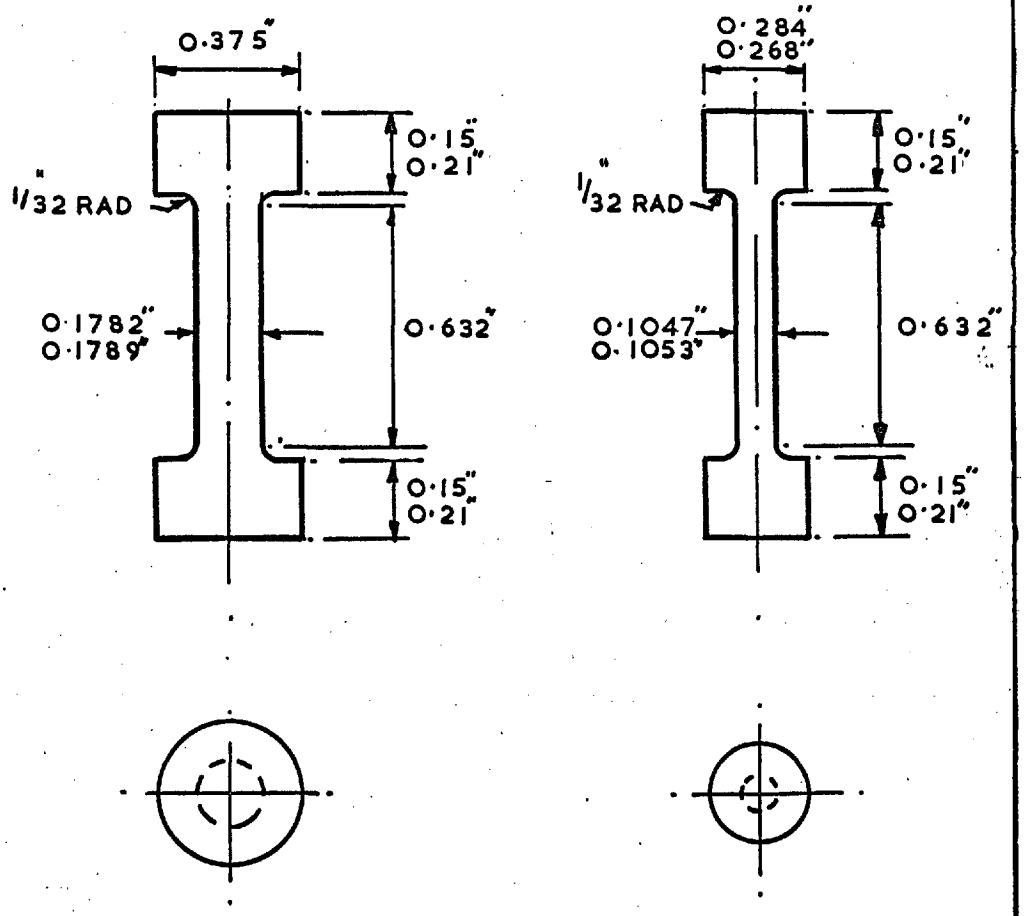

POLYCRYSTAL SPECIMEN.

SINGLE CRYSTAL SPECIMEN.

FIG. 2.
TENSILE TEST SPECIMENS.

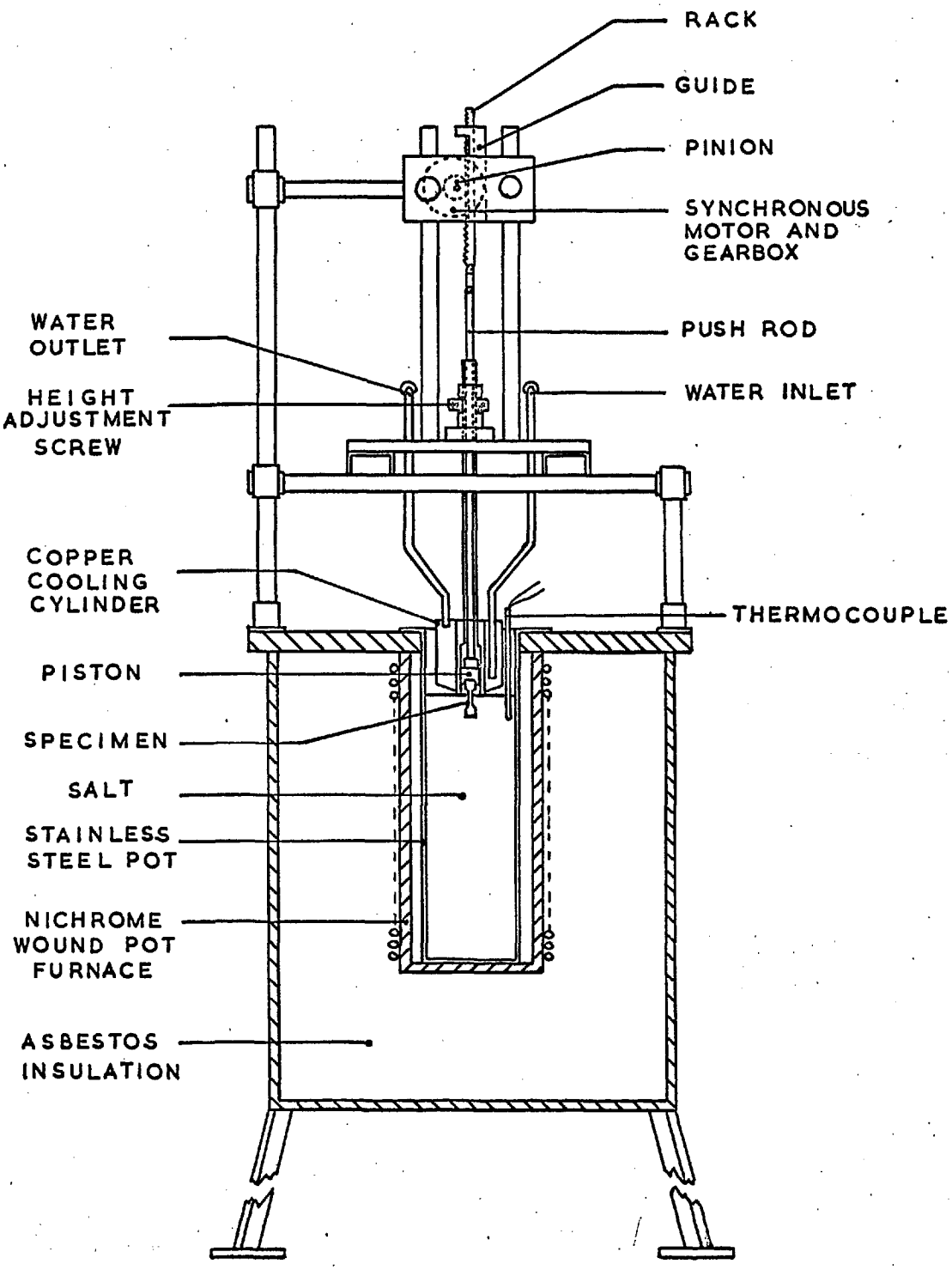

FIG.3

THE STRAIN - ANNEAL SALT BATH.

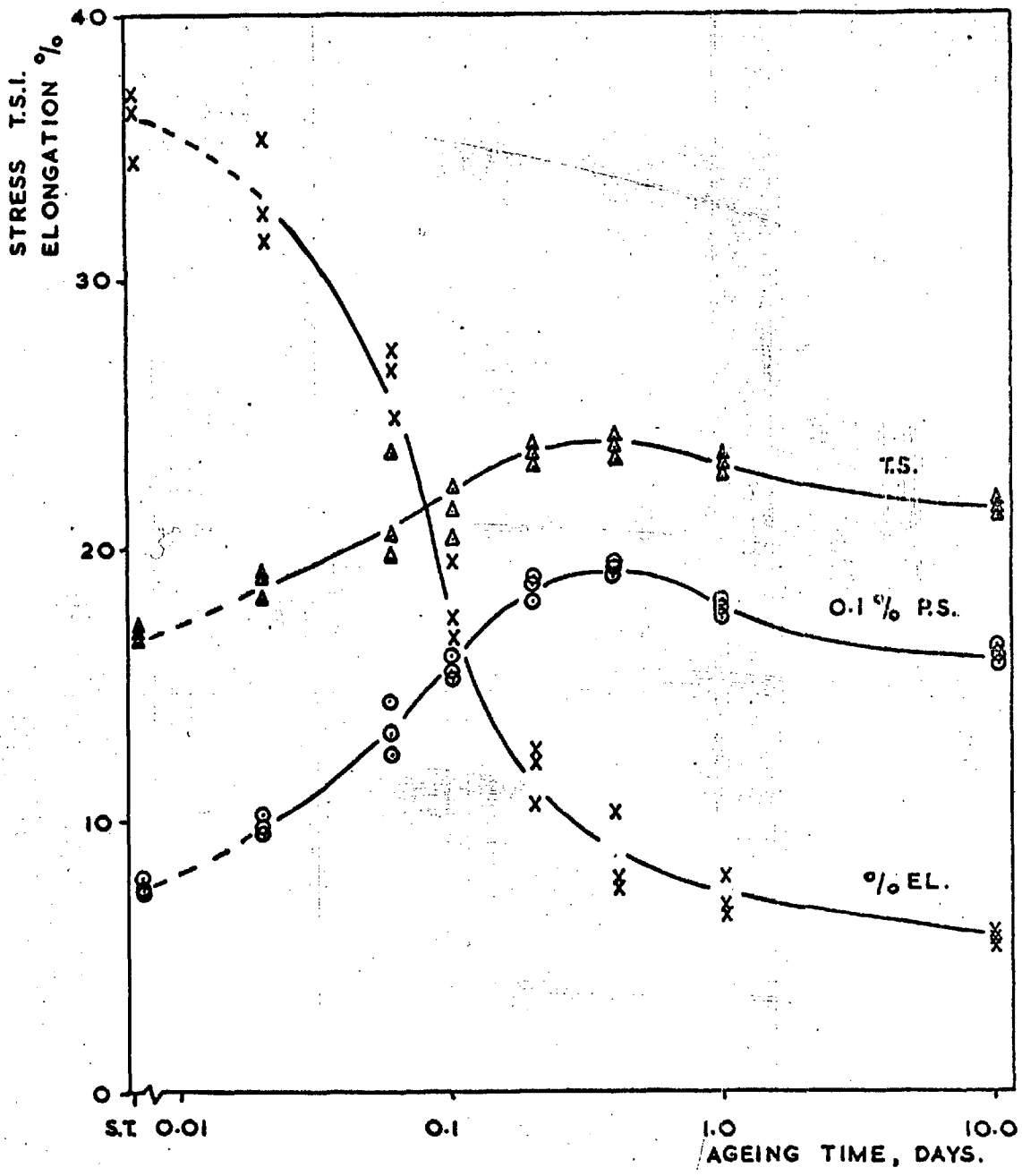

FIG. 4

AGEING CURVES OF 0·1% PROOF STRESS TENSILE STRENGTH AND % ELONGATION FOR 7:1 Cu:Mg ALLOY TESTED AT 295°K.

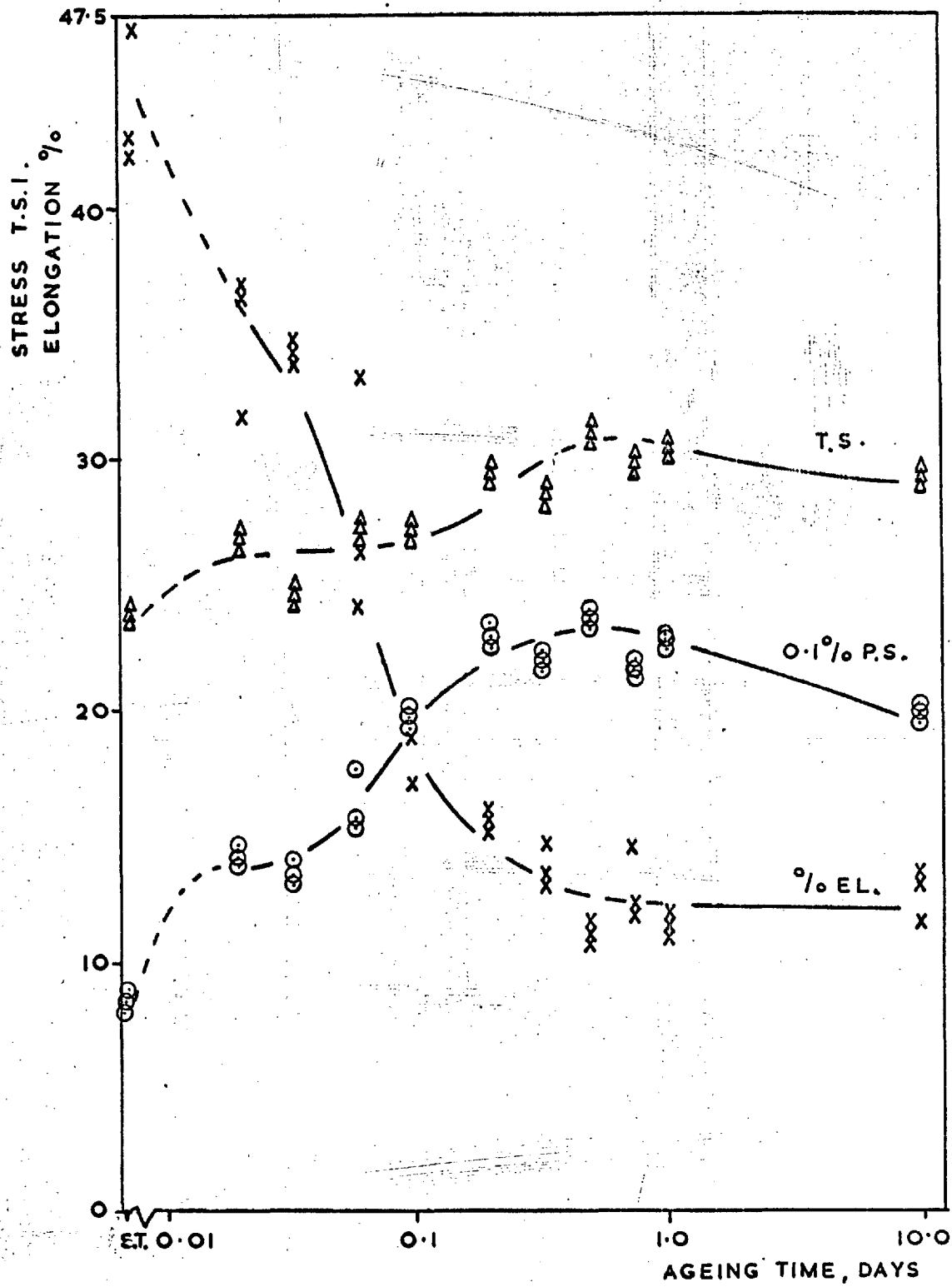

FIG. 5

AGEING CURVES OF 0·1% PROOF STRESS, TENSILE STRENGTH AND % ELONGATION FOR 7:1 Cu. : Mg ALLOY TESTED AT -196°C.

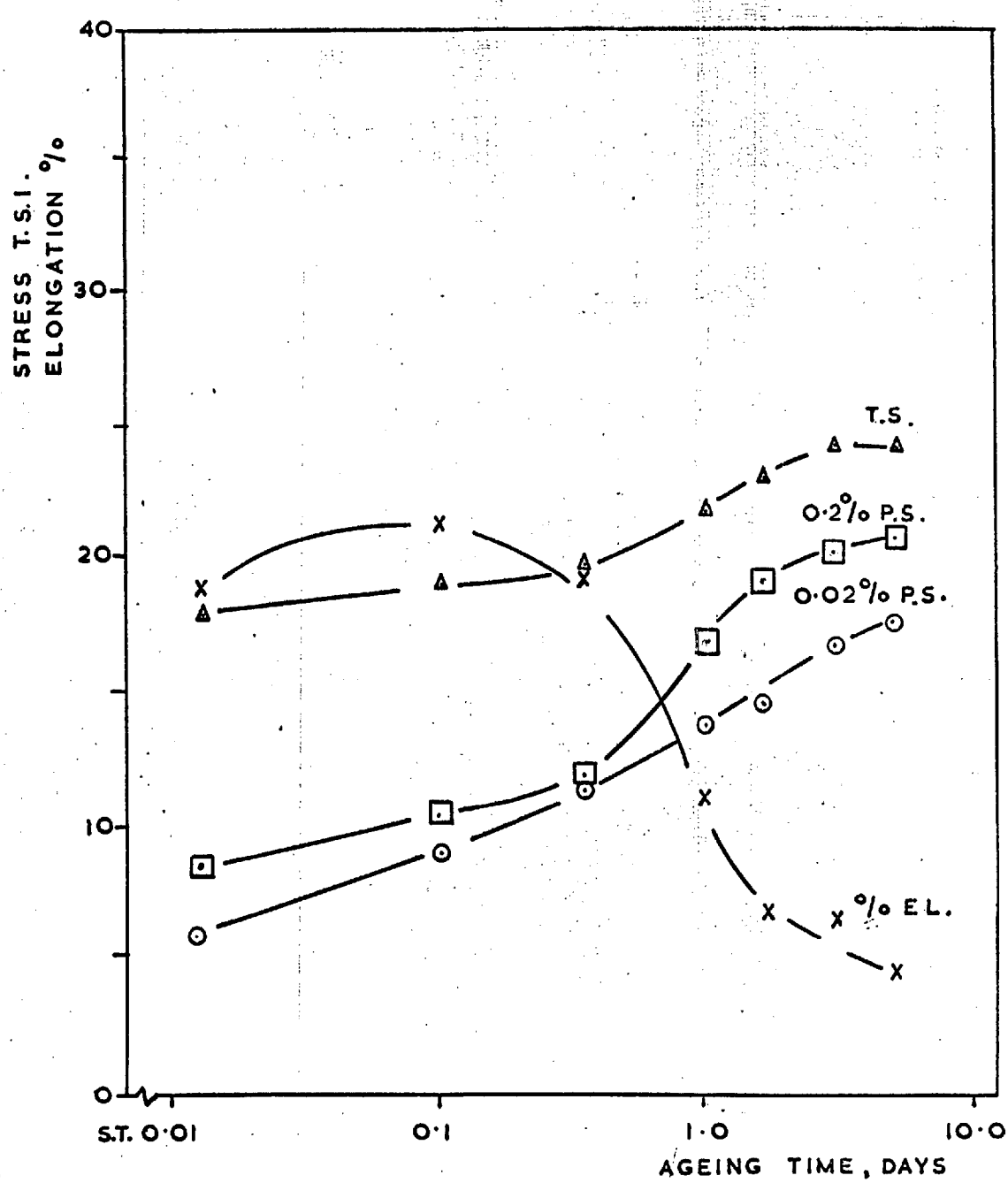

FIG. 6

AGEING CURVES OF PROOF STRESS TENSILE STRENGTH AND % ELONGATION FOR AL, 3·99 wt % Cu, 0·53 wt % Mg ALLOY, TESTED AT ROOM TEMPERATURE; (REF. 110).

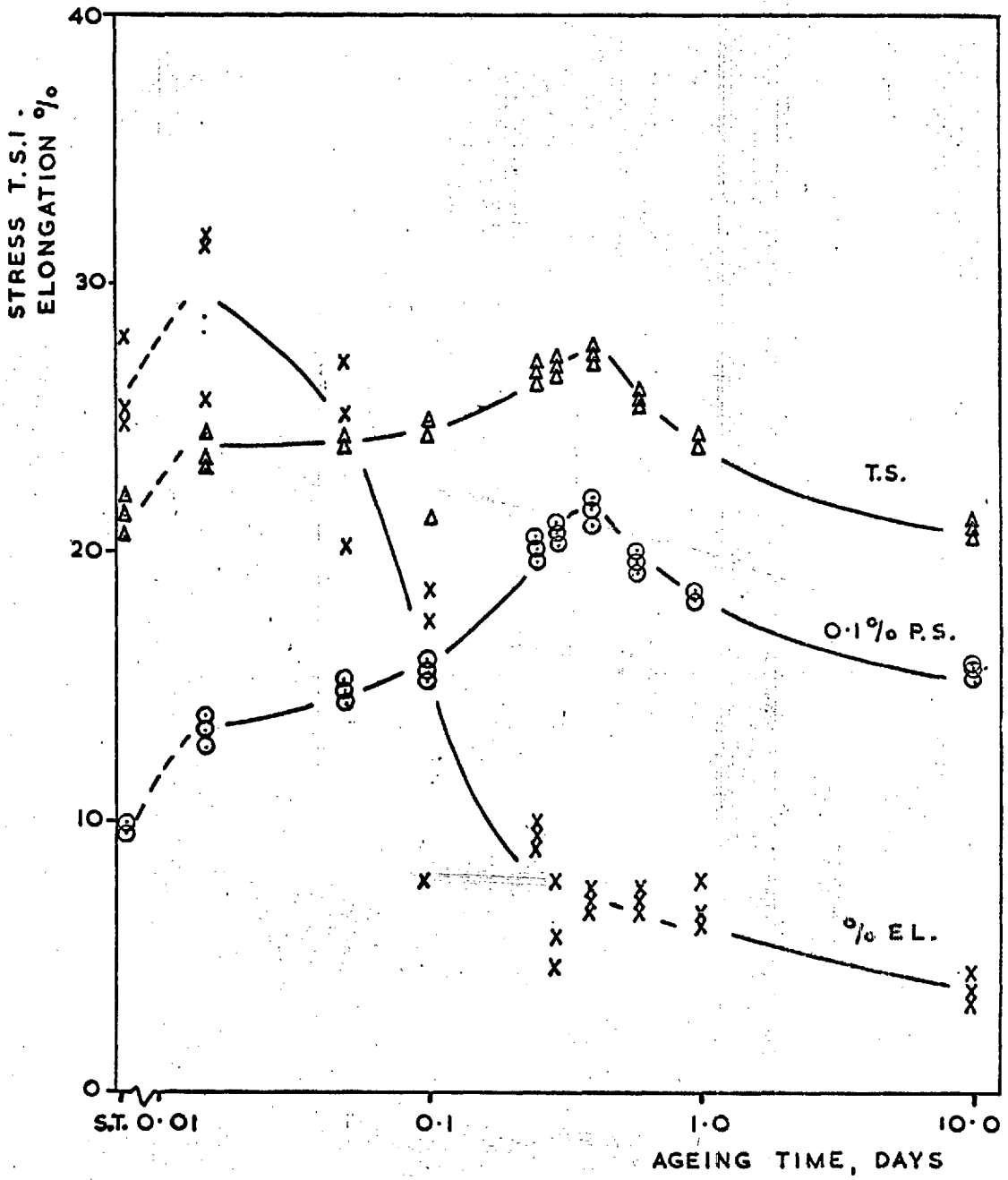

FIG. 7

AGEING CURVES OF 0·1% PROOF STRESS, TENSILE STRENGTH AND % ELONGATION FOR 2·2:1 Cu : Mg ALLOY TESTED AT 295°K.

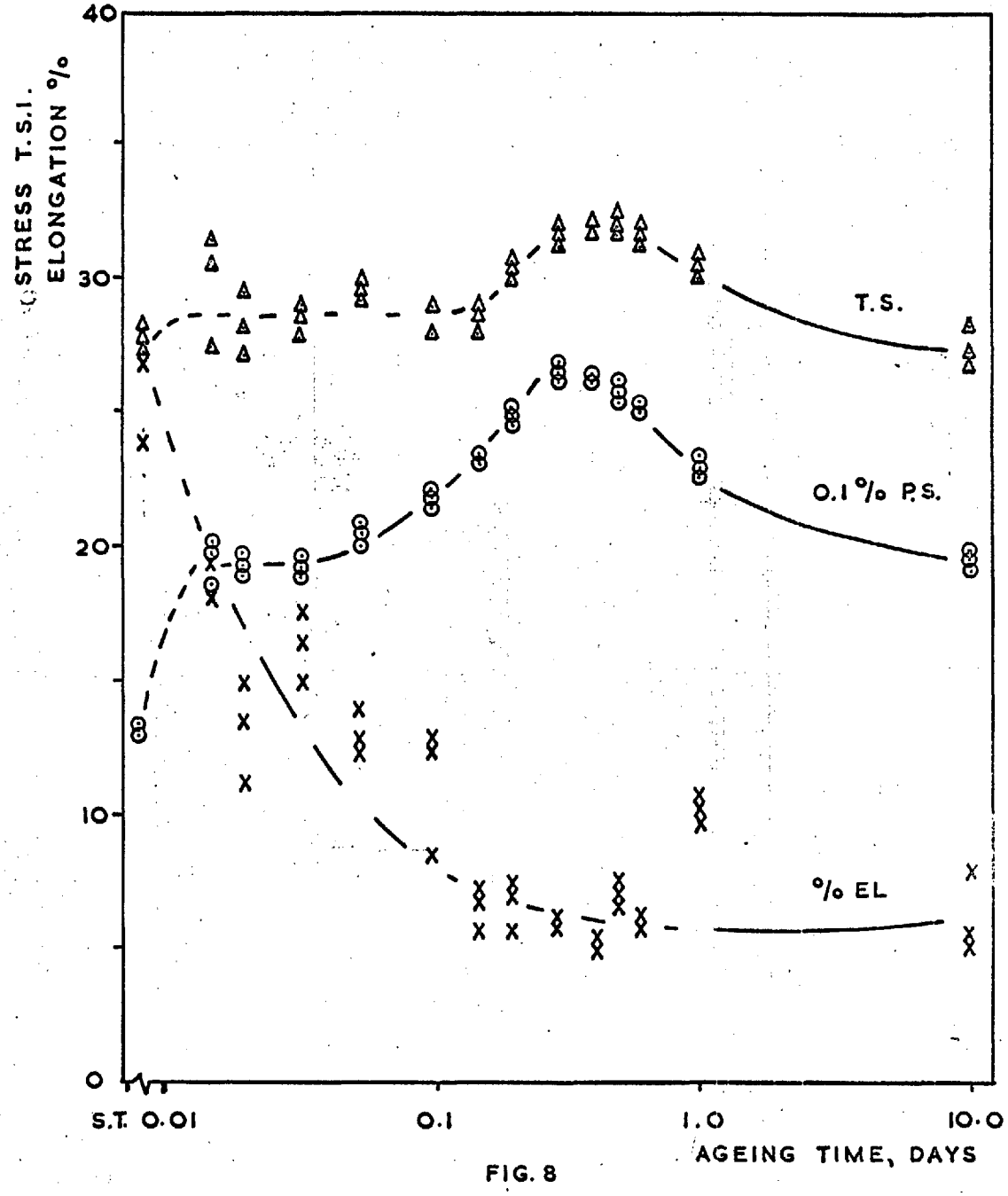

FIG. 8

AGEING CURVES OF 0·1% PROOF STRESS, TENSILE STRENGTH AND % ELONGATION FOR 2.2:1, Cu:MG ALLOY TESTED AT 77°K.

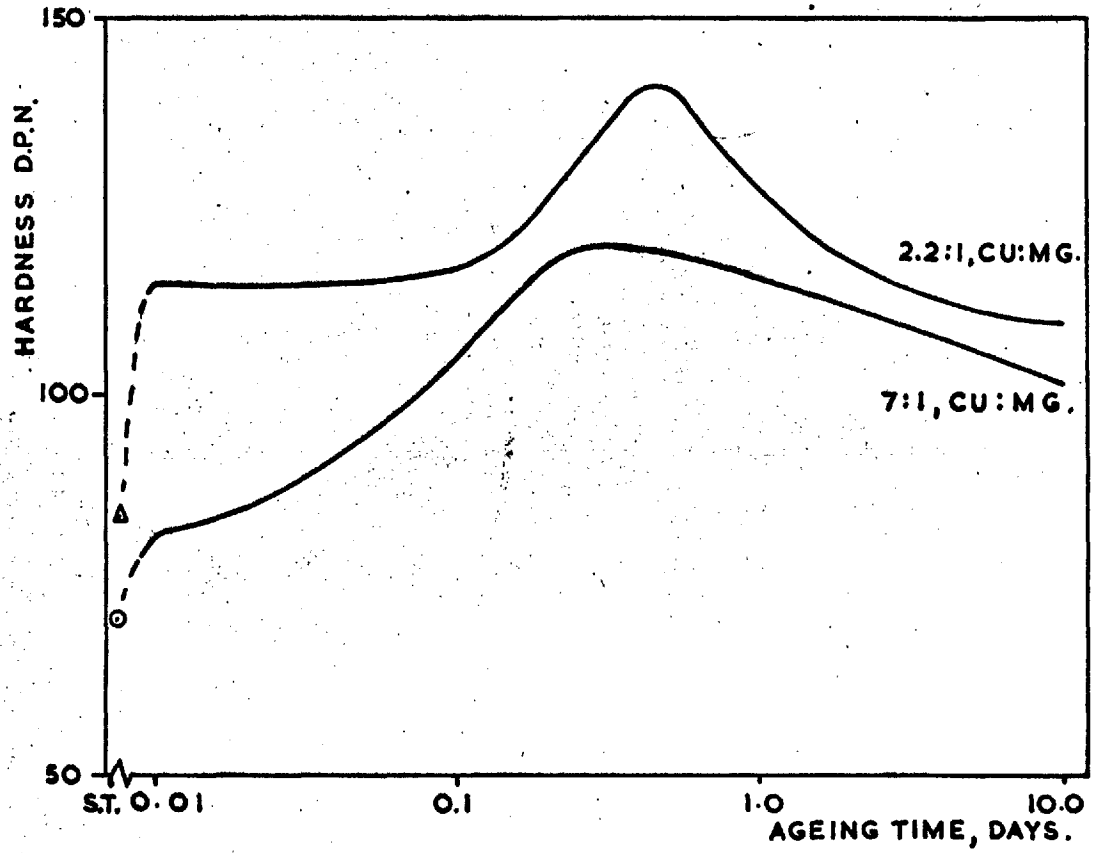

FIG. 9.

HARDNESS-AGEING CURVES FOR 2.2 : 1 & 7 : 1 Cu : Mg ALLOY, AGED AT 190°C, FROM HARDY (18)

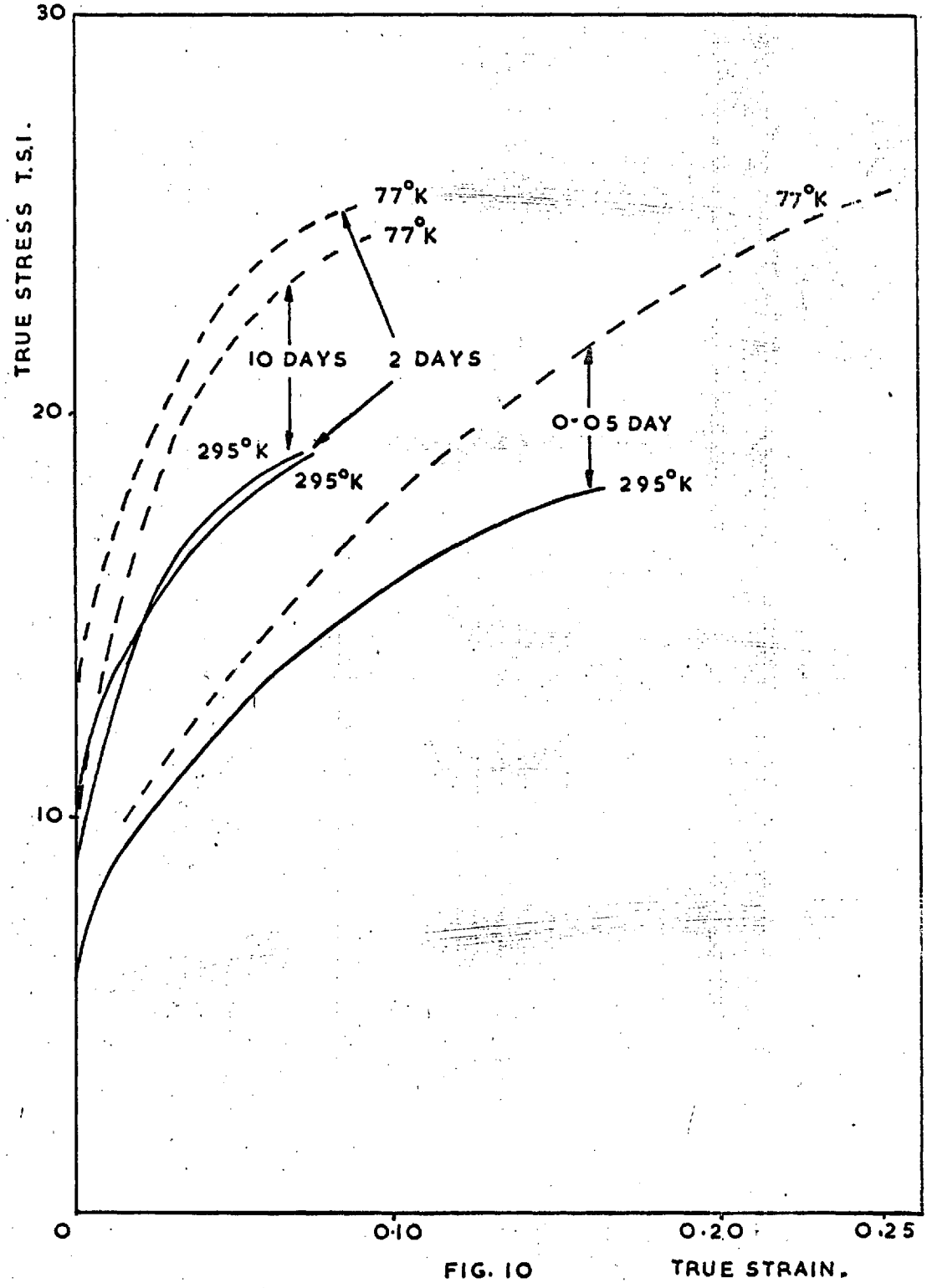

FIG. 10

TRUE STRESS -TRUE STRAIN CURVES FOR AL 3·5wt% Cu ALLOY.

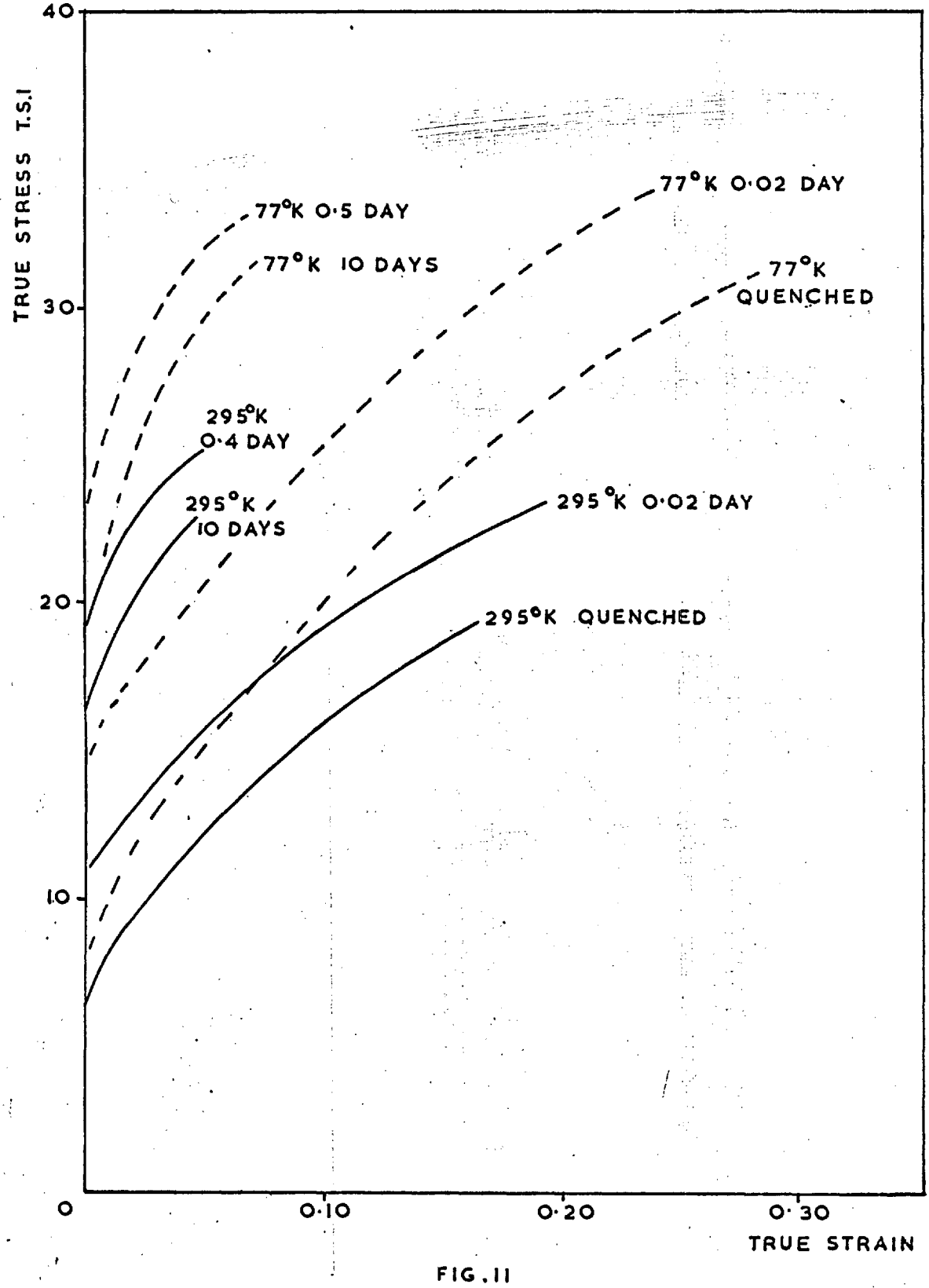

FIG. 11

TRUE STRESS–TRUE STRAIN CURVES FOR 7:1 Cu : Mg ALLOY

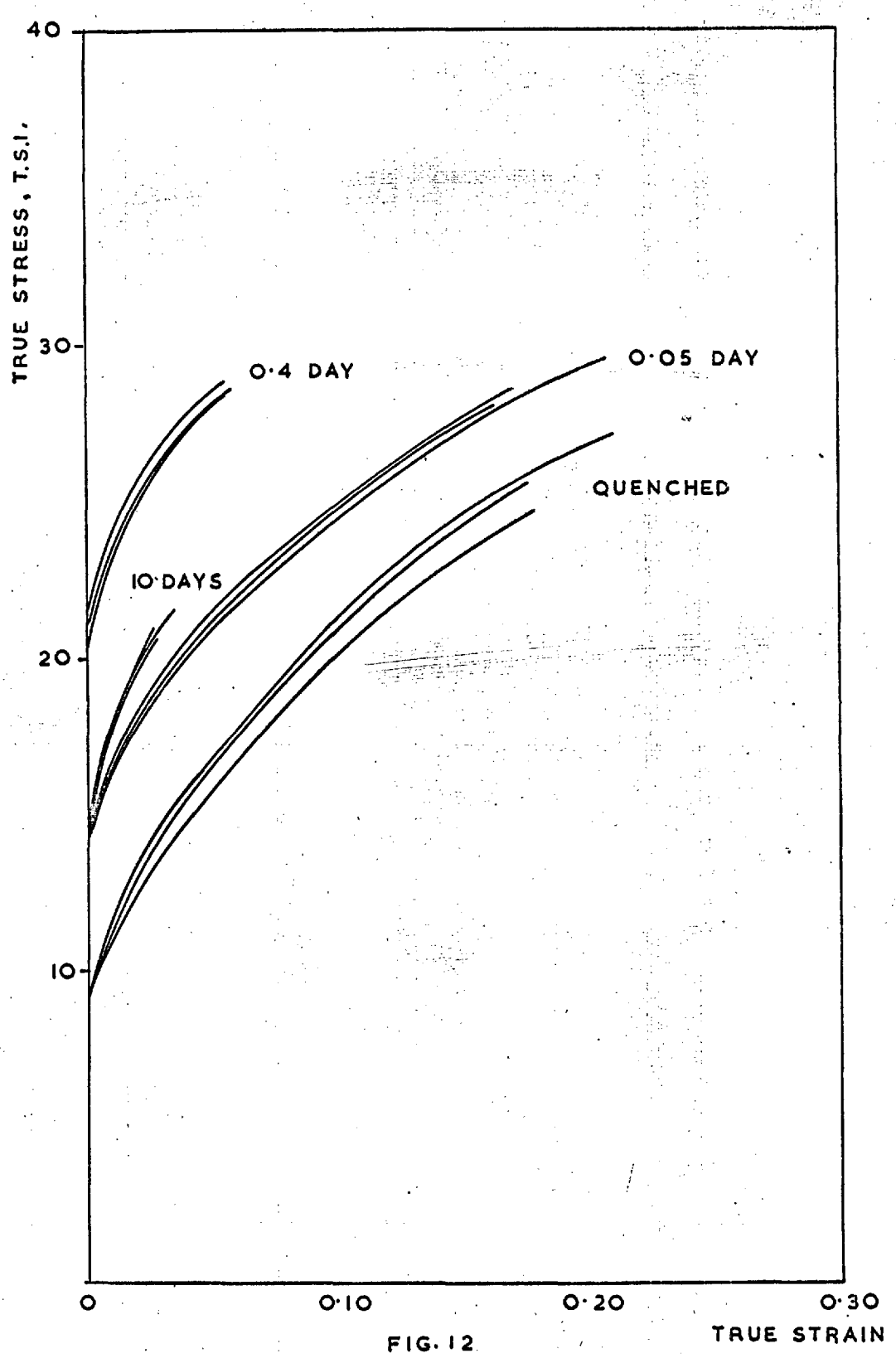

FIG. 12

TRUE STRESS - TRUE STRAIN CURVES FOR 2·2:1 Cu:Mg ALLOY TESTED AT 295°K.

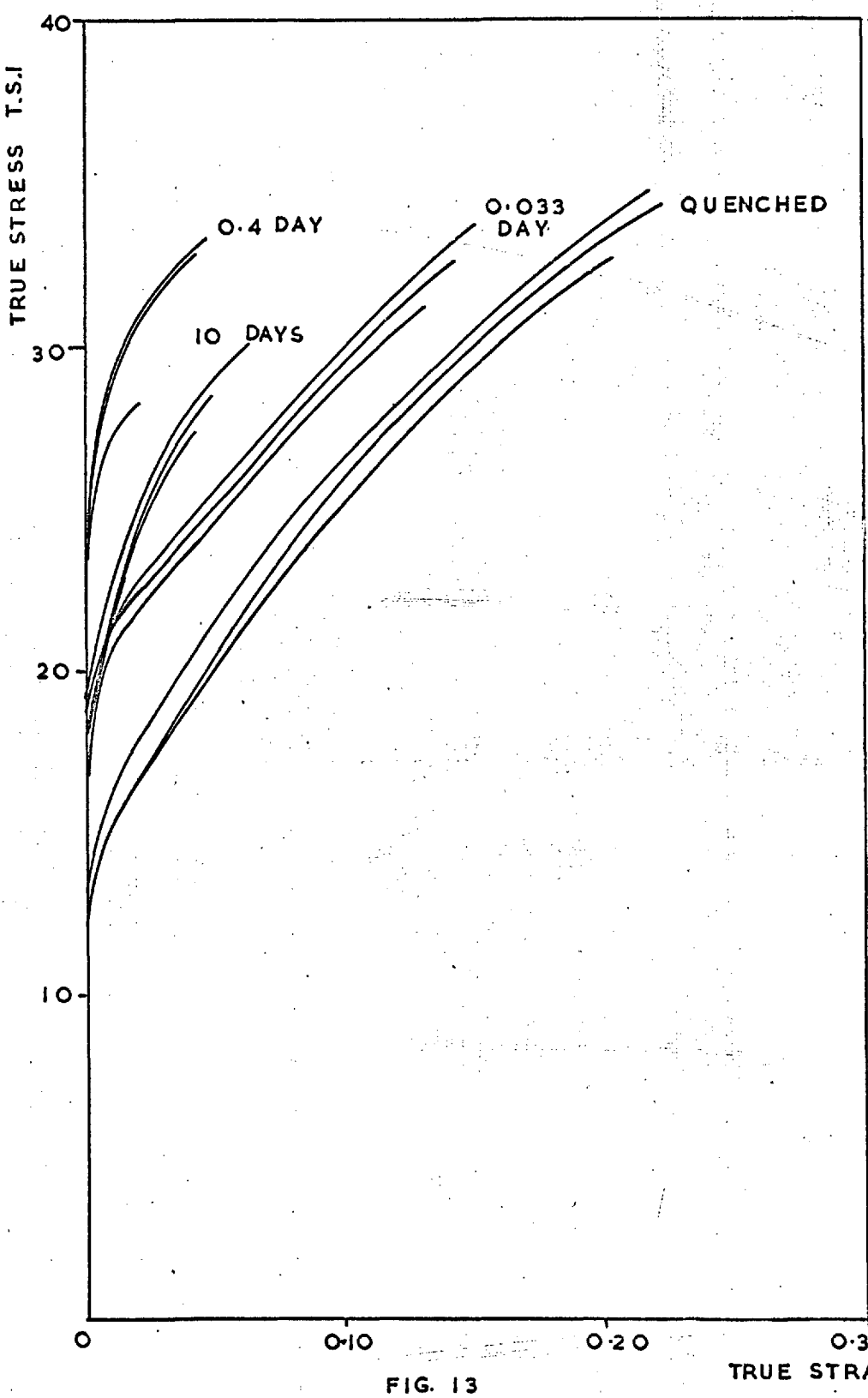

FIG. 13

TRUE STRESS-TRUE STRAIN CURVES FOR 2:2:1 Cu : Mg ALLOY TESTED AT 77°K.

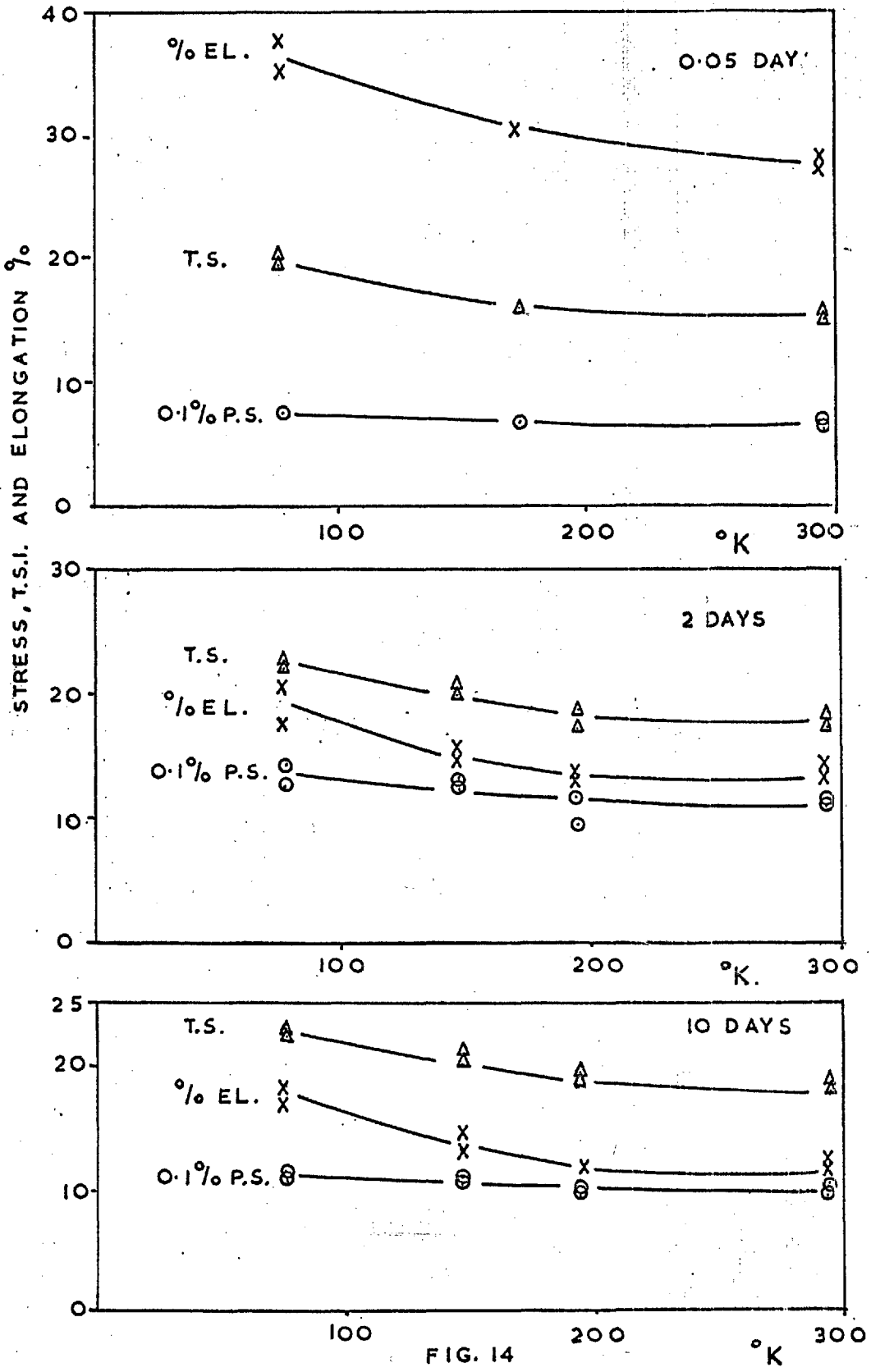

FIG. 14

THE TEMPERATURE DEPENDENCE OF THE MECHANICAL PROPERTIES OF AL 3·5 wt % Cu ALLOYS.

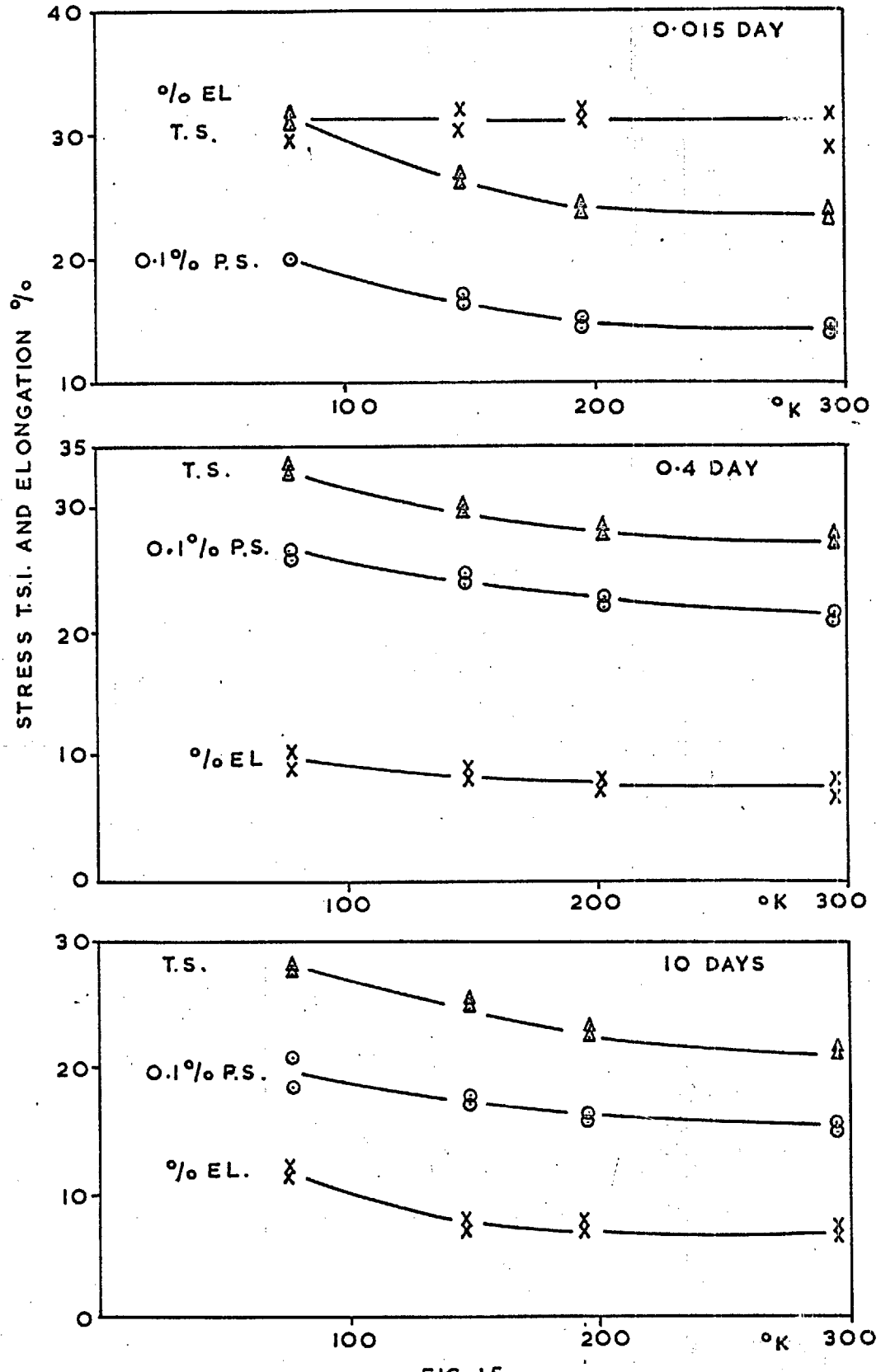

FIG. 15

THE TEMPERATURE DEPENDENCE OF THE MECHANICAL PROPERTIES OF 2:2:1 Cu:Mg ALLOYS

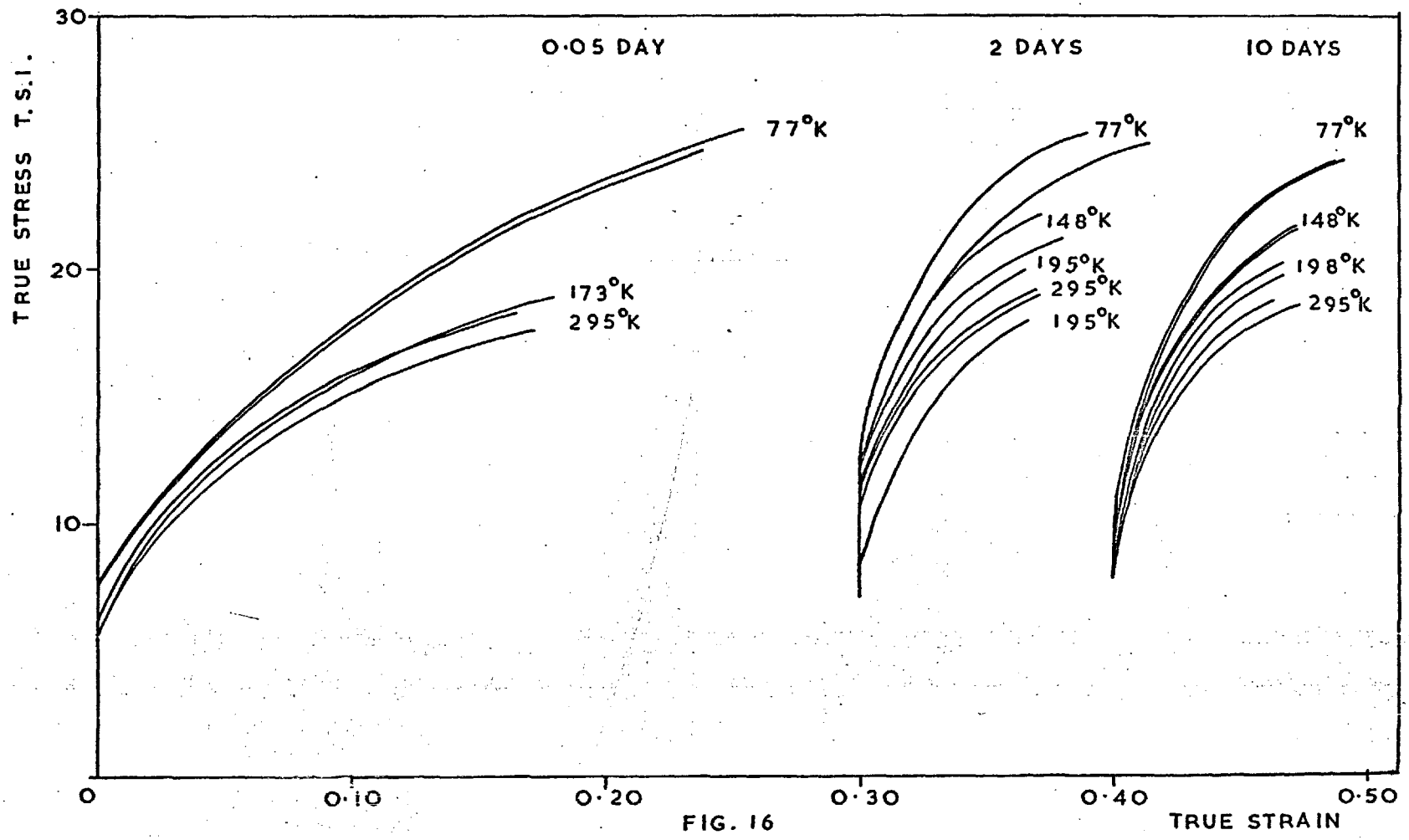

FIG. 16

TRUE STRESS - TRUE STRAIN CURVES FOR AL 3·5 wt % Cu ALLOYS.

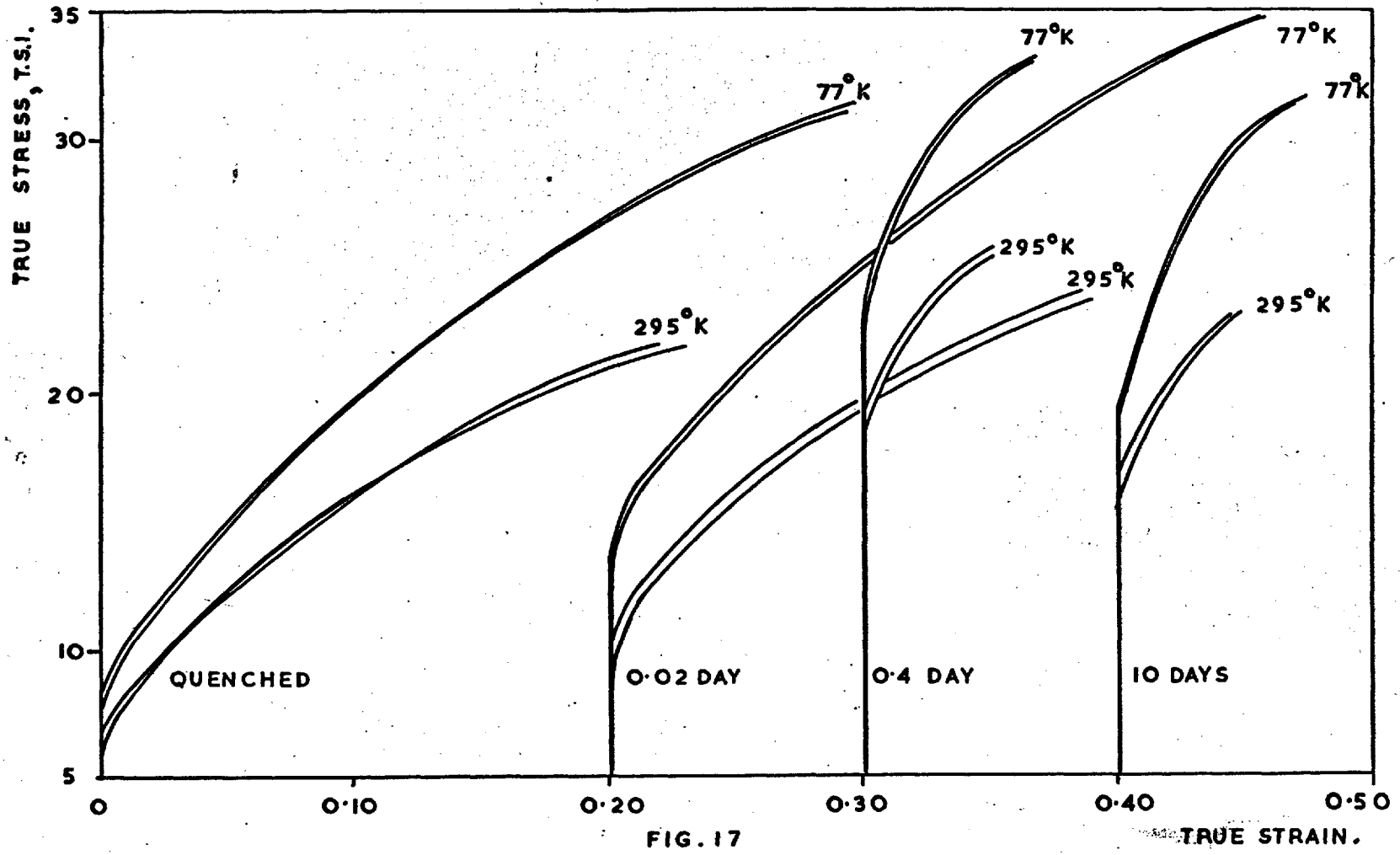

FIG. 17

TRUE STRESS -TRUESTRAIN CURVES FOR 7:1 Cu : Mg ALLOY.

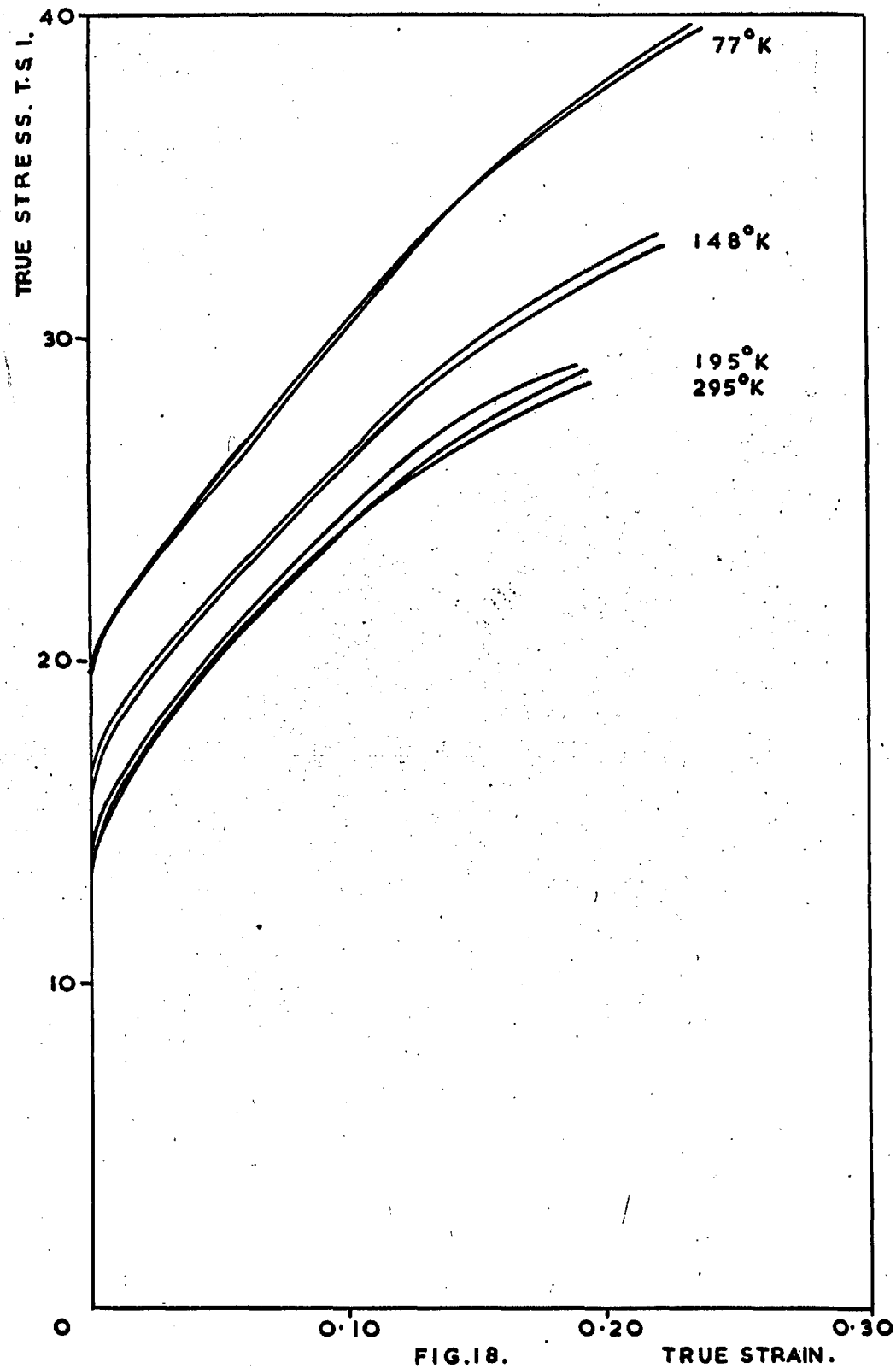

FIG.18.

TRUE STRESS - TRUE STRAIN CURVES FOR 2·2:1 Cu:Mg ALLOYS AGED FOR 0·015 DAYS AT 190°C.

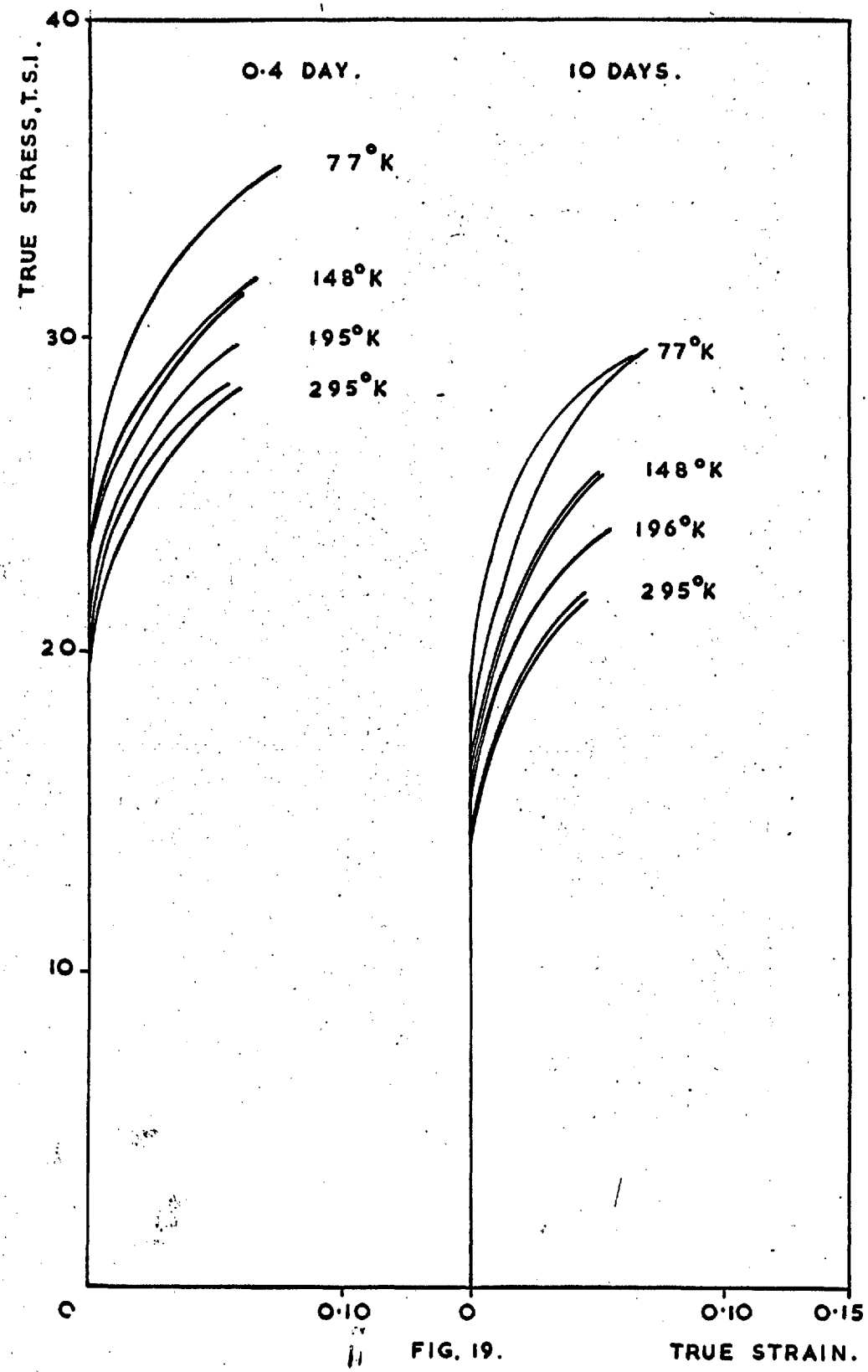

FIG. 19.

TRUE STRESS - TRUE STRAIN CURVES FOR 2·2 11 Cu:Mg ALLOYS AGED FOR 0·4 DAYS AND 10 DAYS AT 190°C.

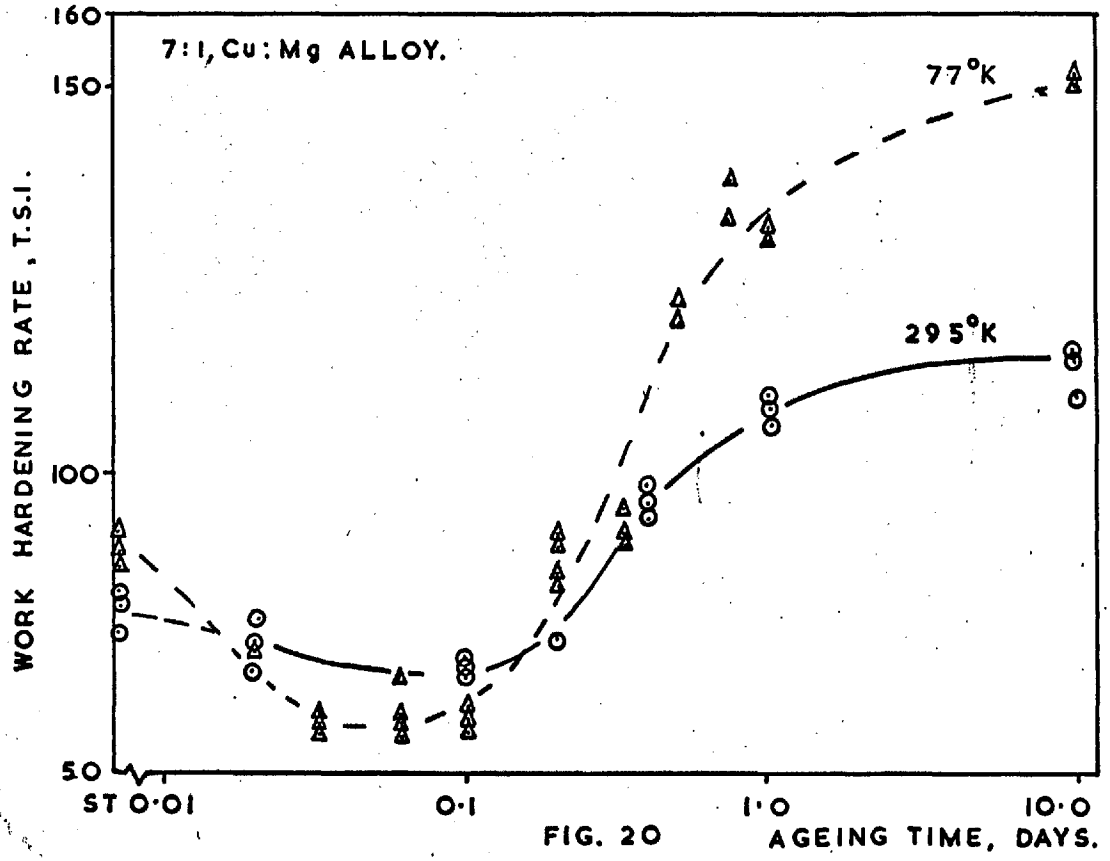

FIG. 20

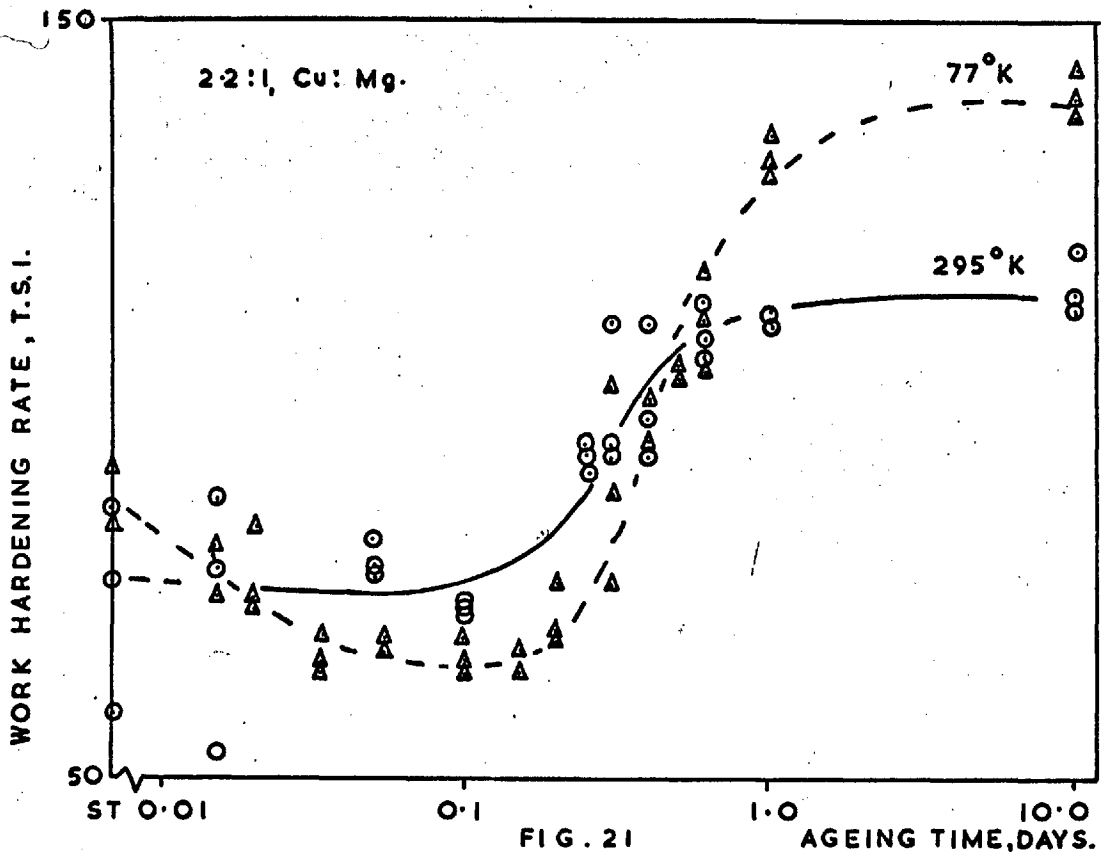

FIG. 21

THE WORK HARDENING RATE $\left(\frac{\sigma 0{\cdot}0376 - \sigma 0{\cdot}0188}{0{\cdot}0188}\right)$ OF 7:1 Cu:Mg & 2·2:1 Cu:Mg ALLOYS.

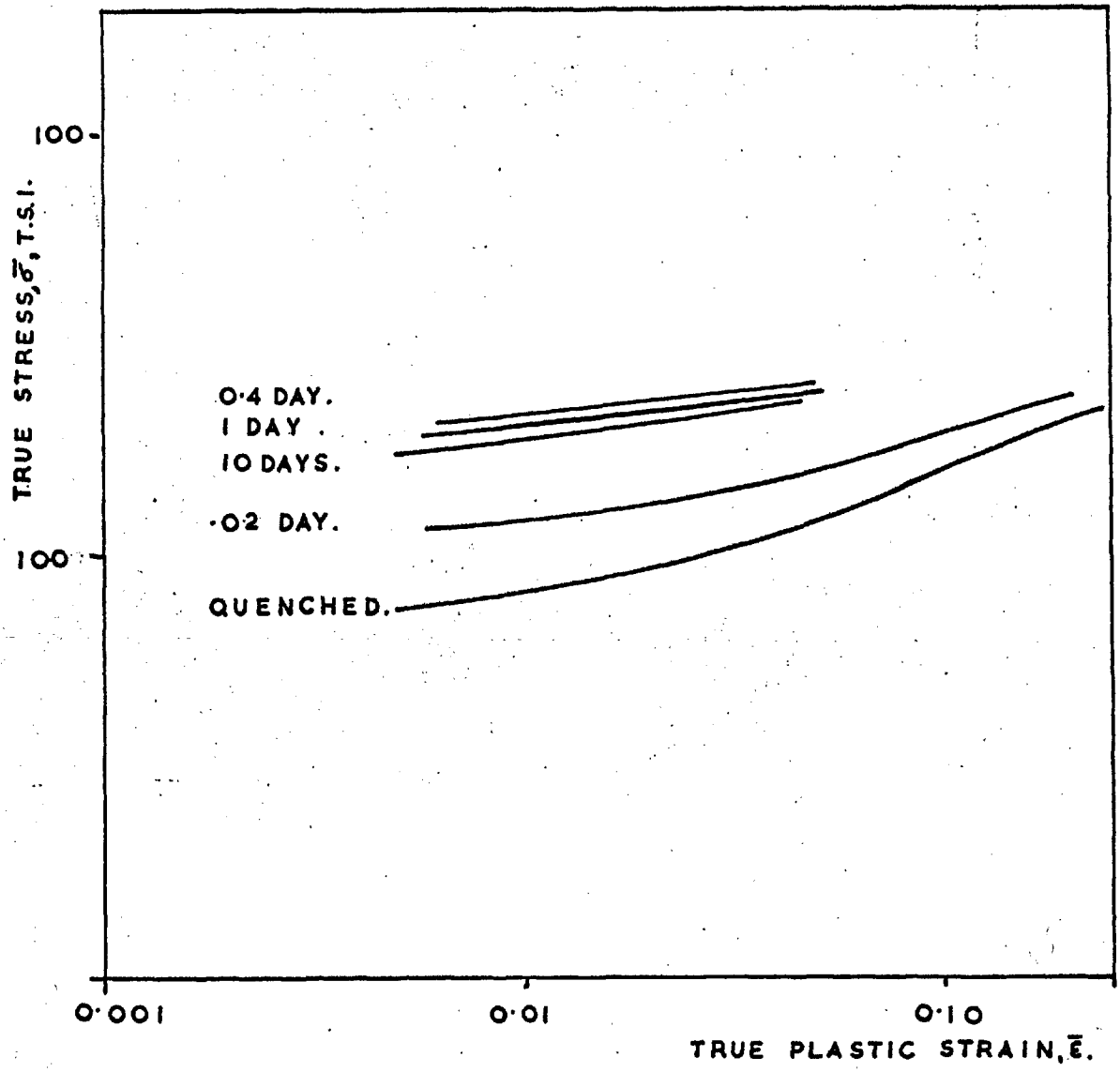

FIG. 22

TRUE STRESS -TRUE STRAIN CURVES FOR 7:1 Cu: Mg ALLOY TESTED AT 295°K.

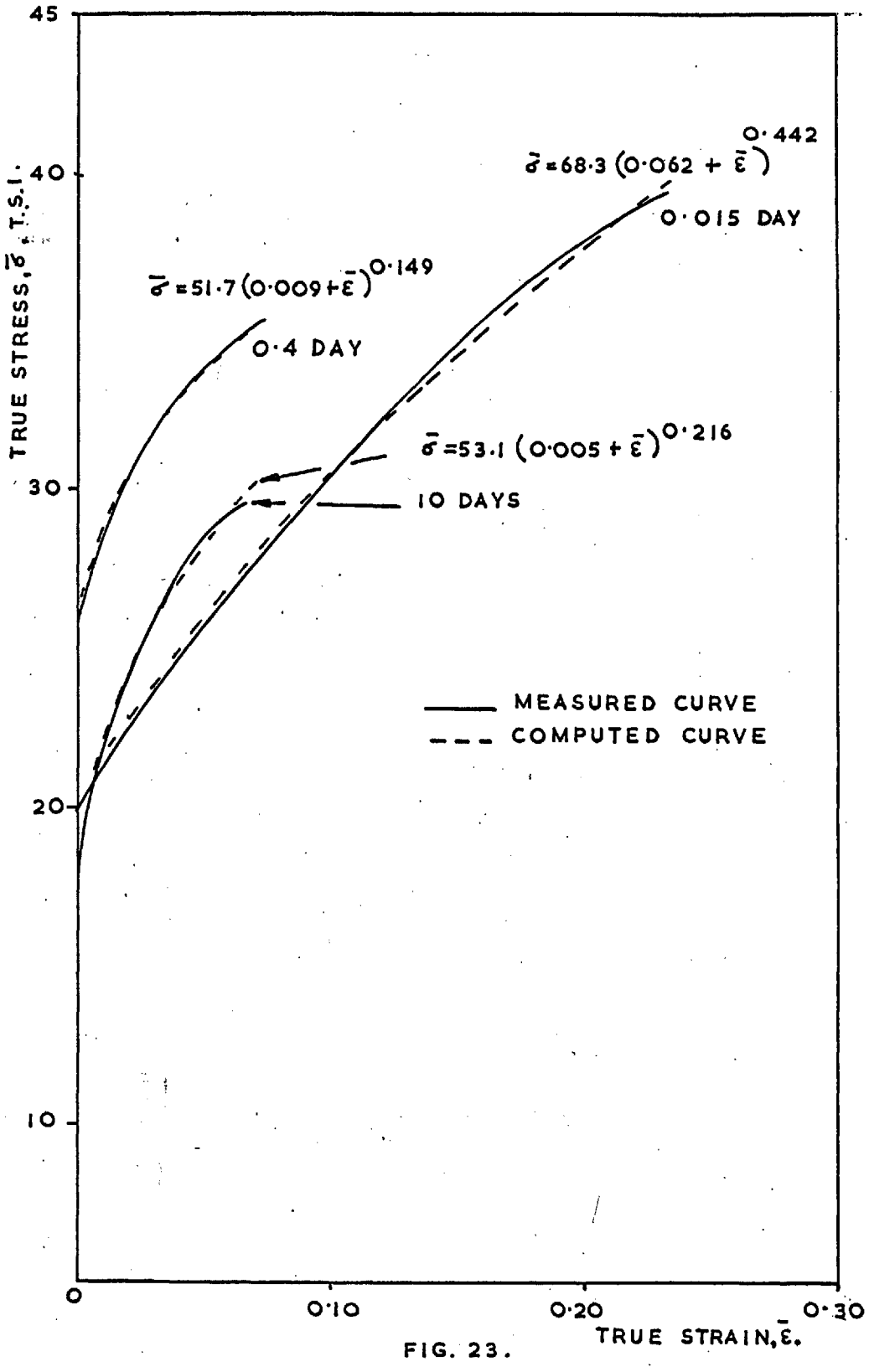

FIG. 23.

MEASURED & COMPUTED TRUE STRESS - TRUE STRAIN CURVES FOR 2·2:1, Cu : Mg ALLOYS TESTED AT 77°K.

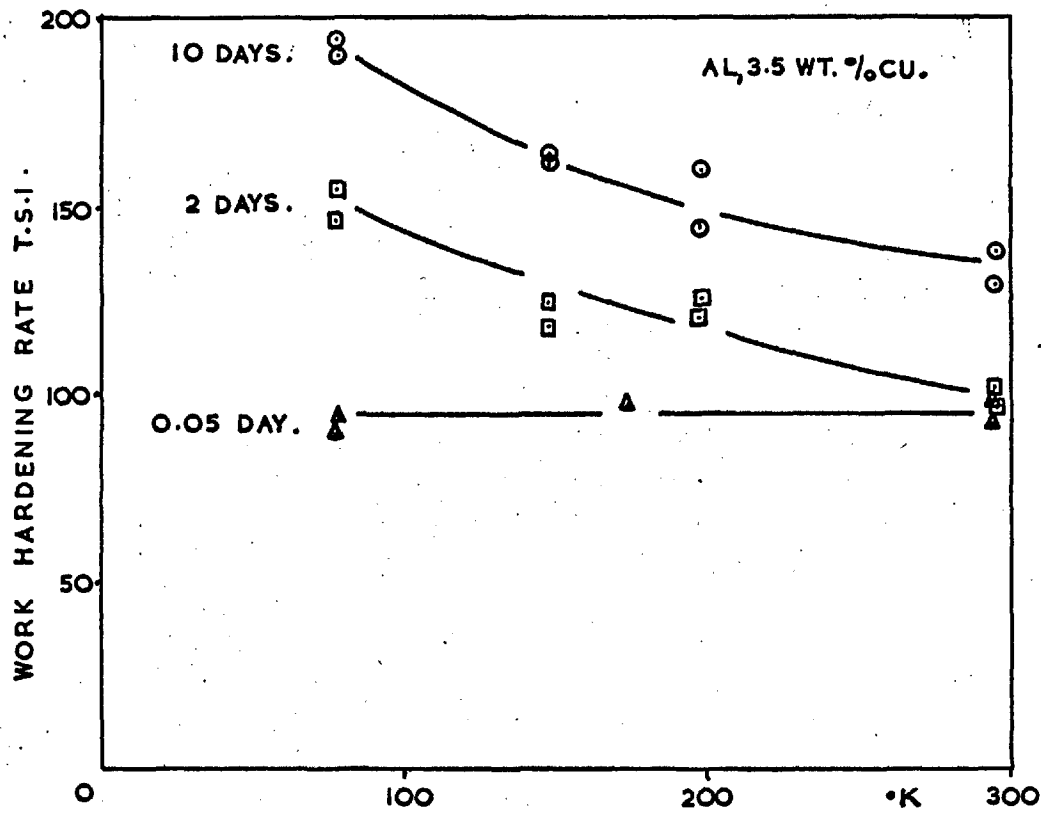

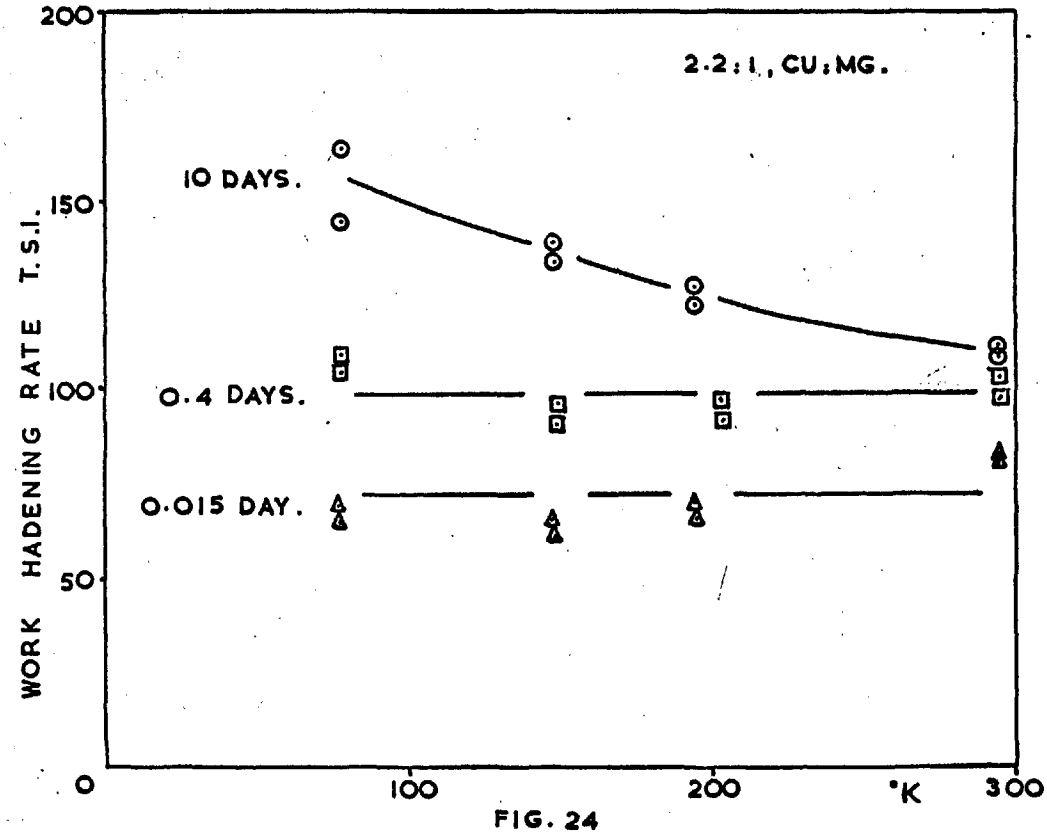

FIG. 24

THE TEMPERATURE DEPENDENCE OF THE WORK HARDENING RATE OF AL, 3·5 % Cu AND 2·2:1 Cu: Mg ALLOYS.

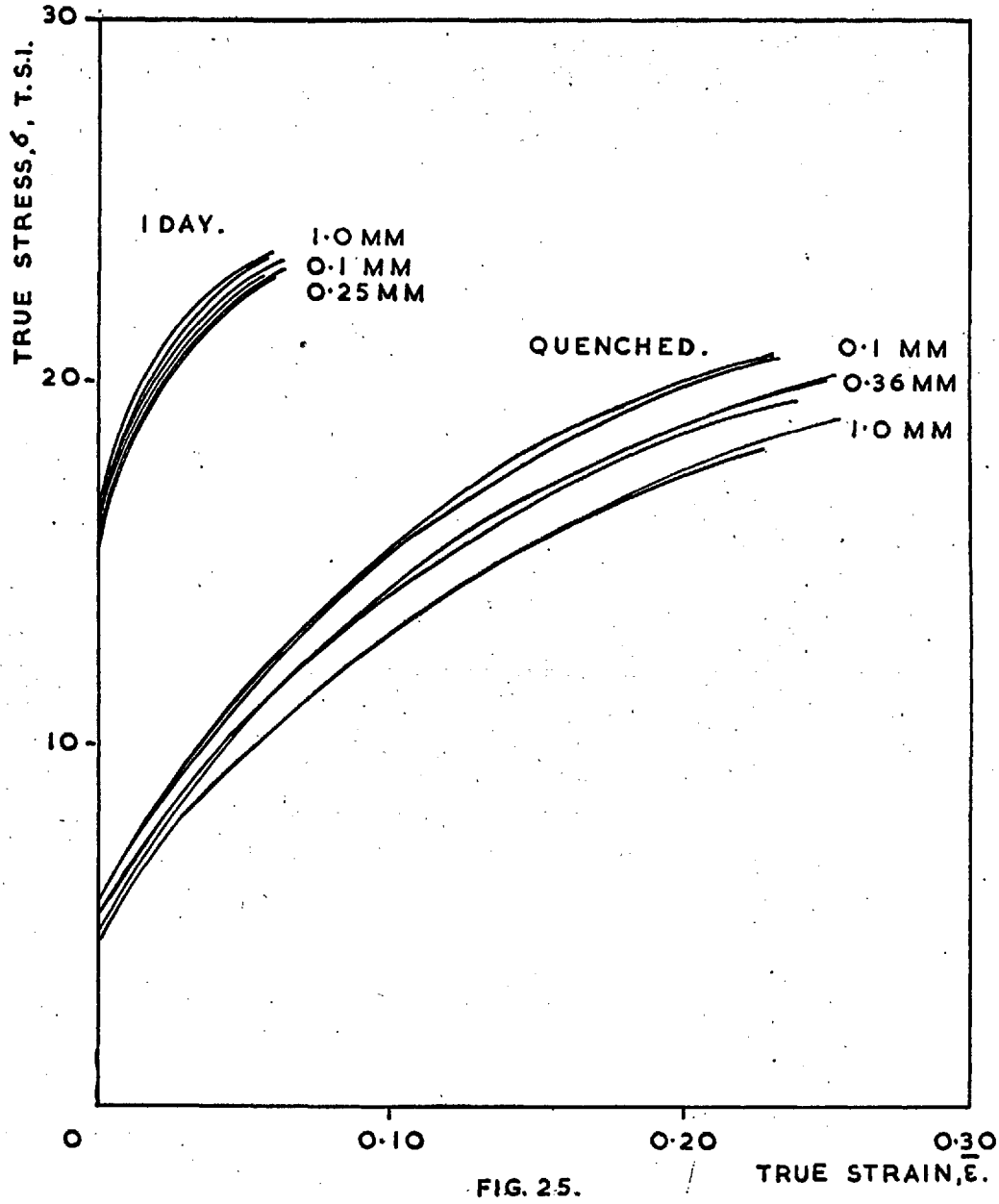

FIG. 25.

TRUE STRESS - TRUE STRAIN CURVES FOR 7:1 Cu: Mg ALLOYS OF DIFFERENT GRAIN SIZE TESTED AT 295°K.

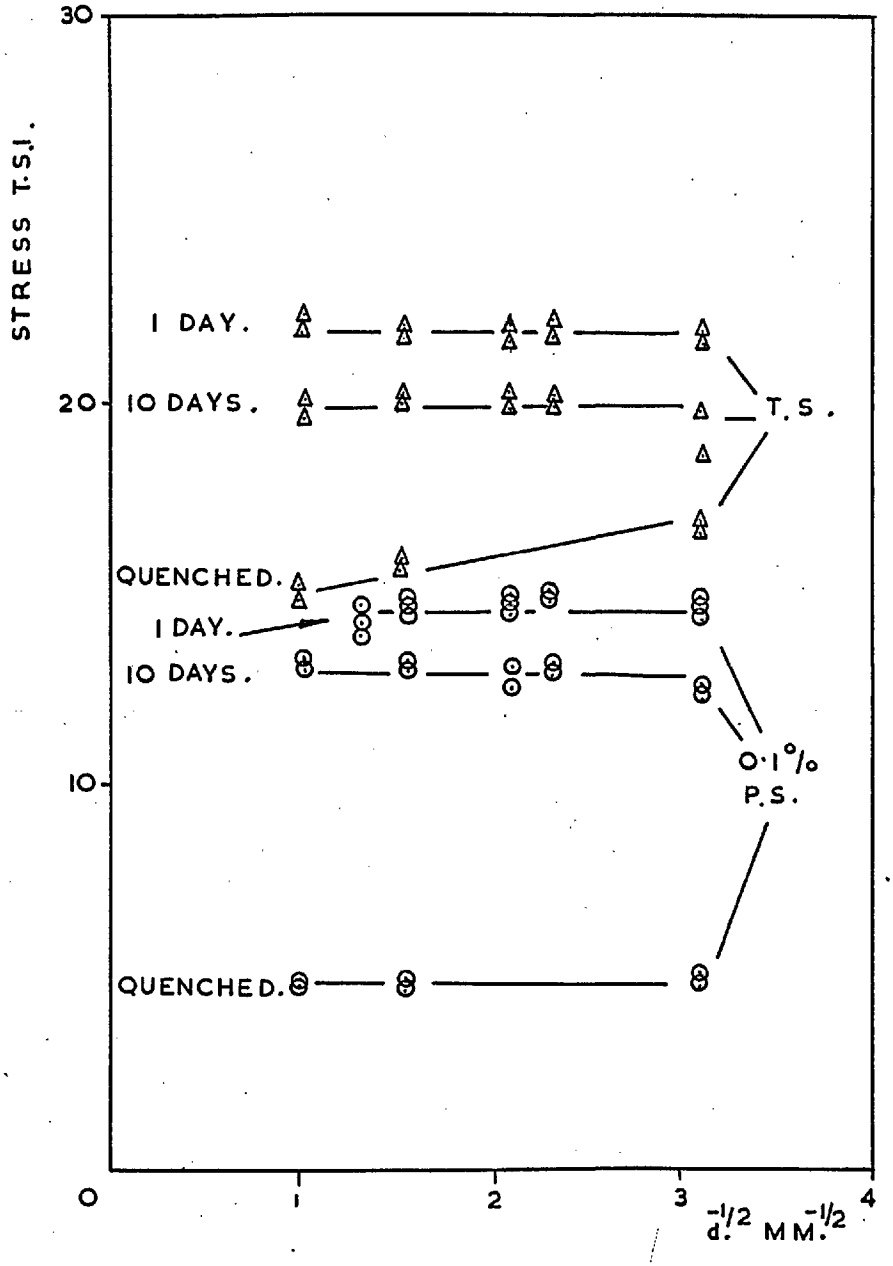

FIG. 26.

THE GRAIN SIZE DEPENDENCE OF 0·1 % PROOF STRESS AND TENSILE STRENGTH FOR 7:1, Cu : Mg ALLOY.

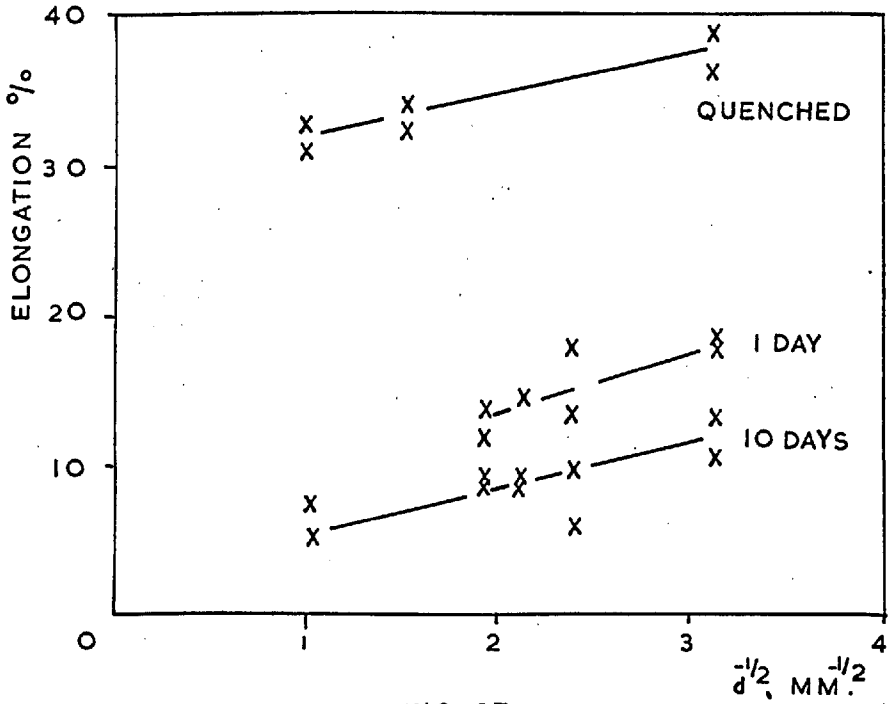

FIG. 27

THE GRAIN SIZE DEPENDENCE OF DUCTILITY FOR 7:1 Cu : Mg ALLOY.

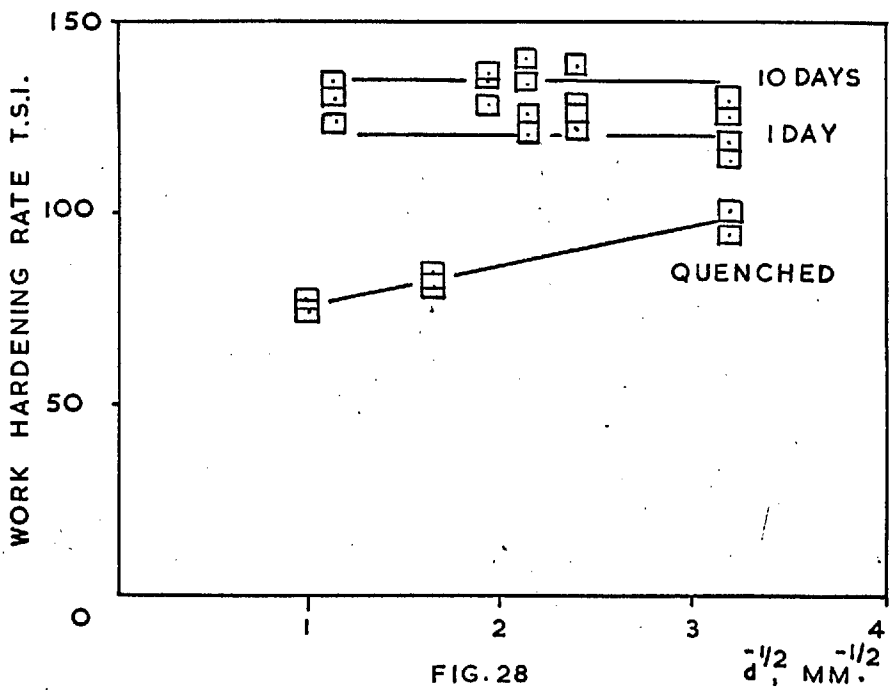

FIG. 28

THE GRAIN SIZE DEPENDENCE OF WORK HARDENING RATE FOR 7:1 Cu : Mg ALLOY.

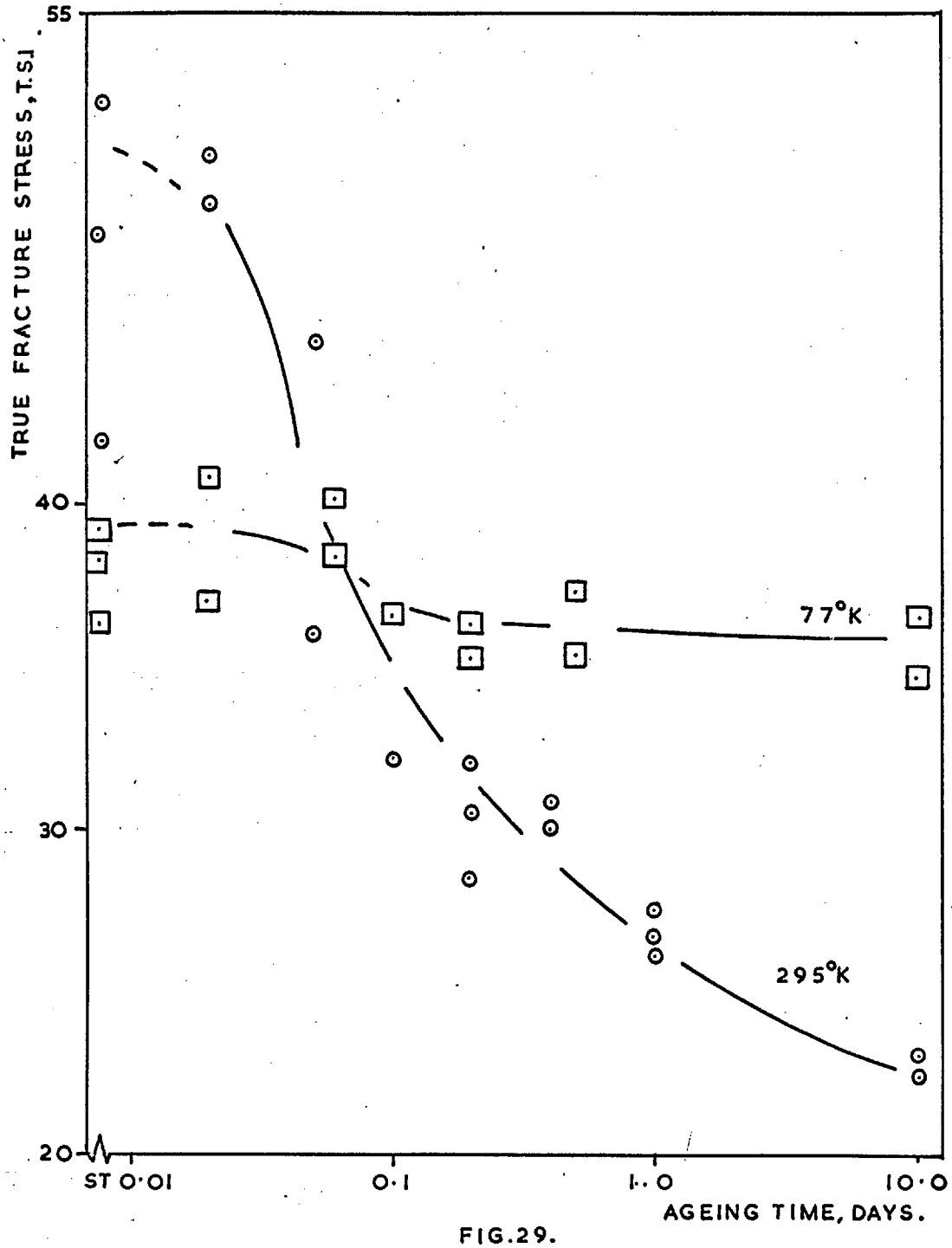

FIG.29.

TRUE FRACTURE STRESS AGEING CURVES FOR 711, Cu : Mg ALLOY.

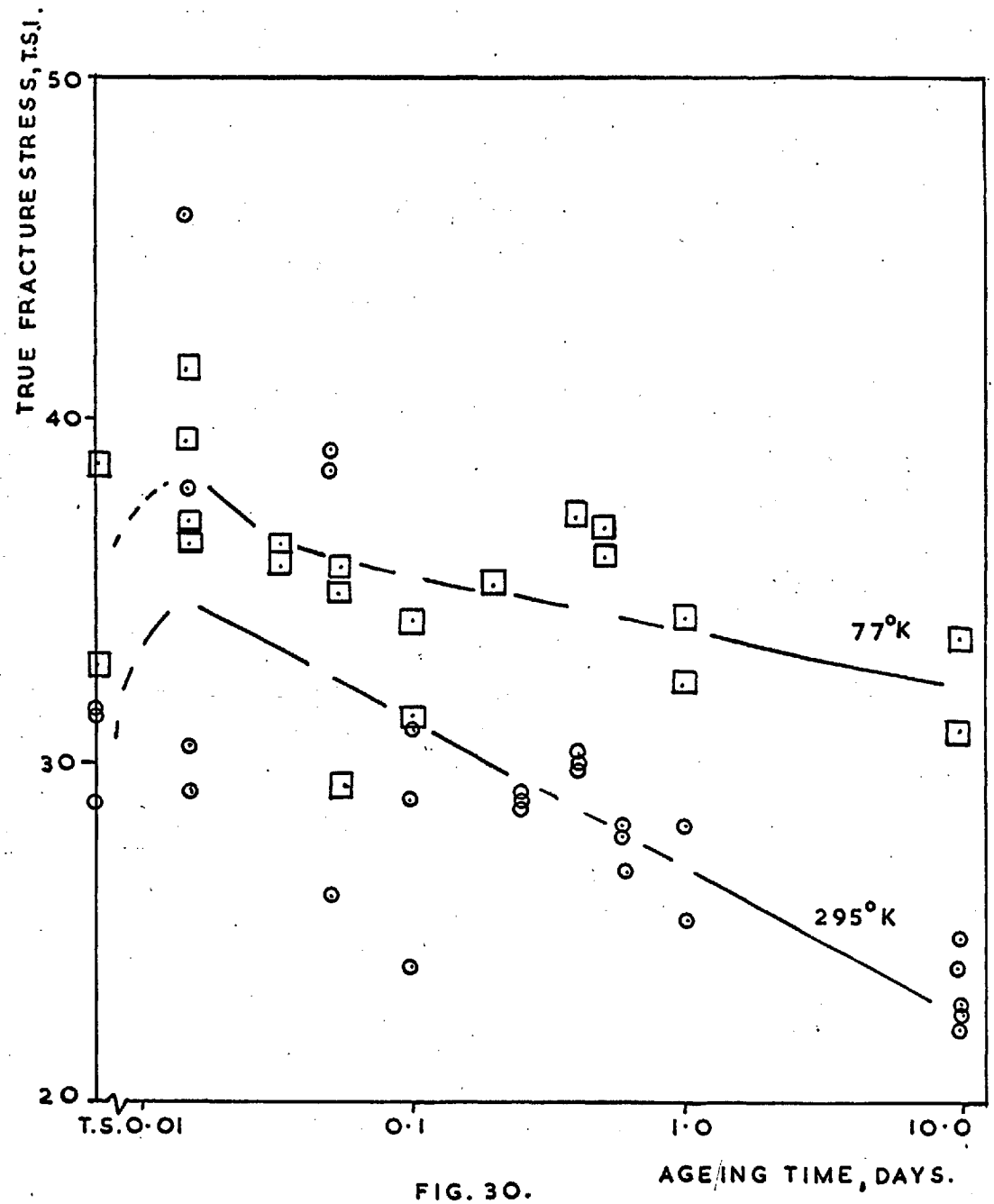

FIG. 30.

TRUE FRACTURE STRESS AGEING CURVES FOR 2:2:1, Cu: Mg ALLOY.

(a) 7:1,Cu:Mg alloy
As-quenched.
Tested at 295°K X6

(b) 7:1, Cu:Mg alloy
Aged for 0.02 day
Tested at 295°K X6

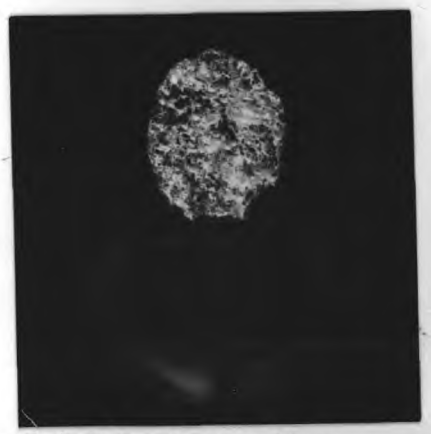

(c) 7:1, Cu:Mg alloy
Aged for 0.06 day
Tested at 295°K X6

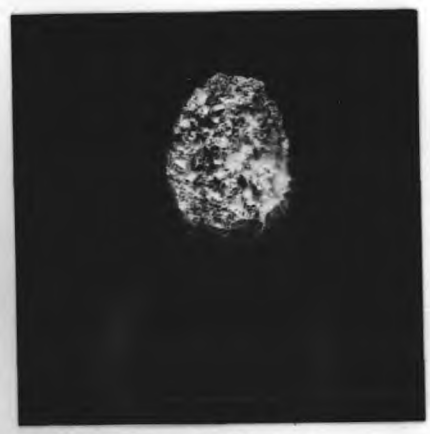

(d) 7:1. Cu:Mg alloy
Aged for 0.1 day.
Tested at 295°K X6

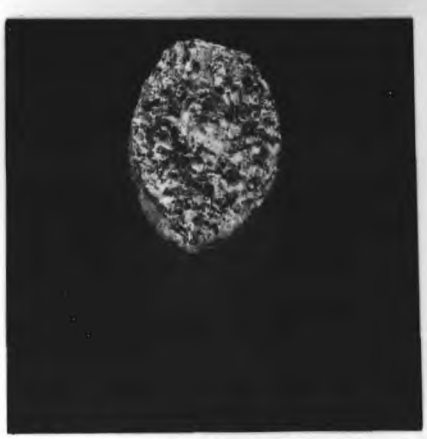

(e) 7:1. Cu:Mg alloy
Aged for 0.4 day
Tested at 295°K X6

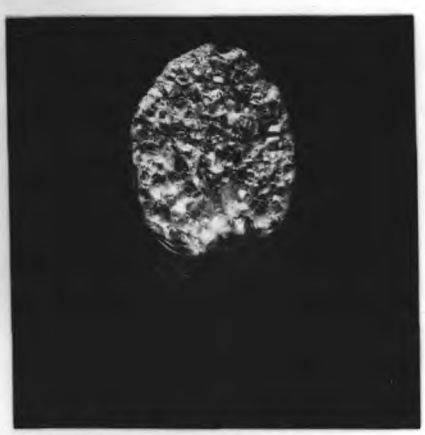

(f) 7:1, Cu:Mg alloy
Aged for 10 days
Tested at 295°K X6

Fig. 31

(a) 7:1, Cu:Mg alloy.
As-quenched
Tested at 77°K X6

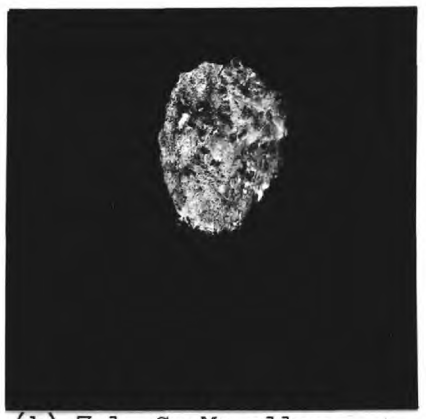

(b) 7:1, Cu:Mg alloy.
Aged for 0.02 day
Tested at 77°K X6

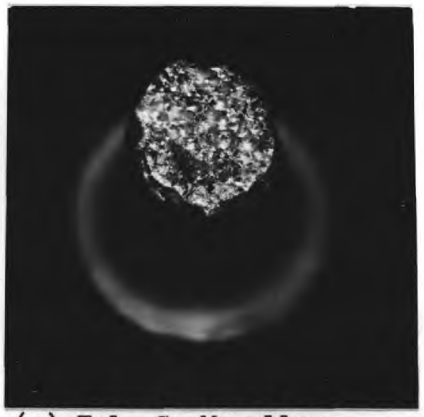

(c) 7:1, Cu:Mg alloy.
Aged for 0.1 day
Tested at 77°K. X6

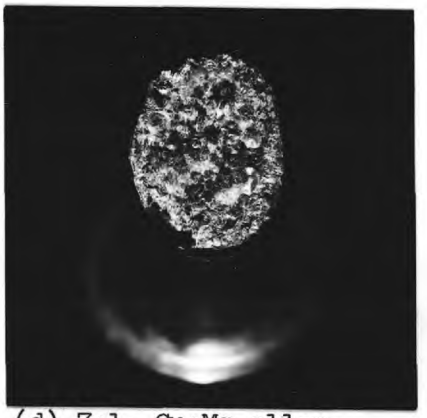

(d) 7:1, Cu:Mg alloy.
Aged for 0.5 day.
Tested at 77°K X6

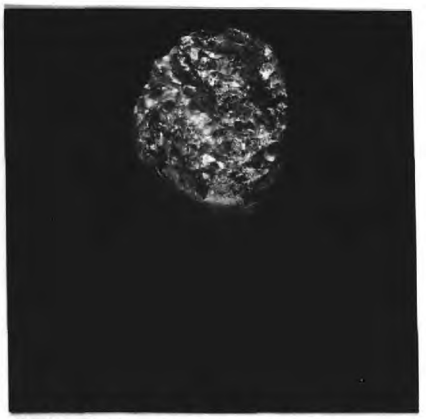

(e) 7:1, Cu:Mg alloy.
Aged for 10 Days.
Tested at 77°K X6

Fig. 32

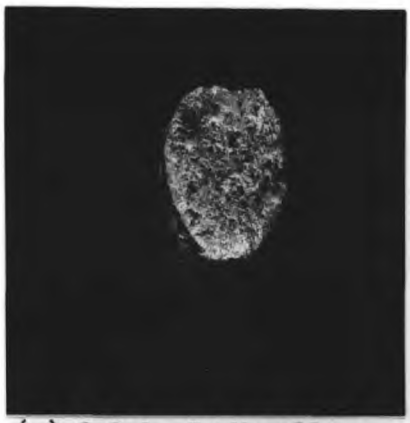

(a) 2.2:1, Cu:Mg alloy.
As-quenched
Tested at 295°K X6

(b) 2.2:1, Cu:Mg alloy.
Aged for 0.015 day
Tested at 295°K X6

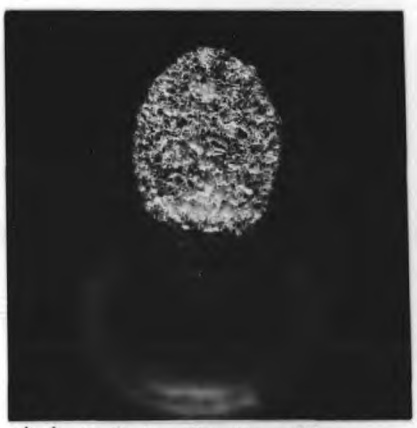

(c) 2.2:1, Cu:Mg alloy.
Aged for 0.1 day.
Tested at 295°K X6

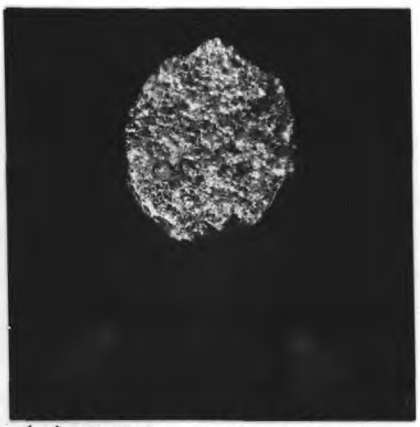

(d) 2.2:1, Cu:Mg alloy.
Aged for 0.4 day.
Tested at 295°K X6

(e) 2.2:1, Cu:Mg alloy.
Aged for 10 days.
Tested at 295°K X6

Fig. 33.

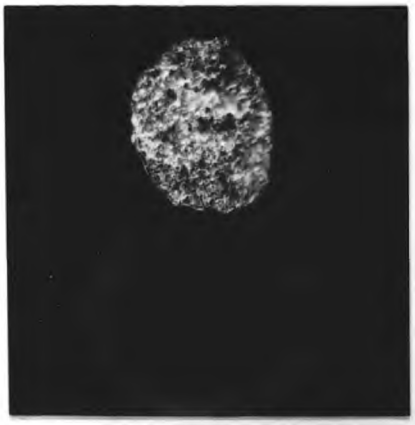

(a) 2.2:1, Cu:Mg alloy.
As quenched.
Tested at 77°K. X6

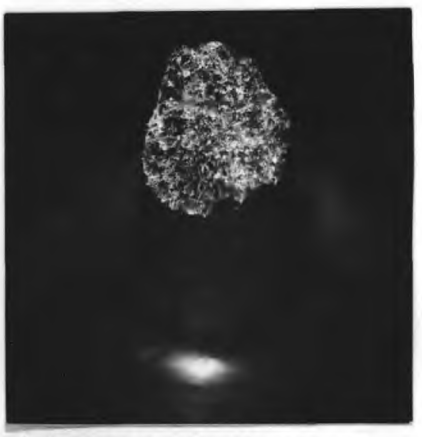

(b) 2.2:1, Cu:Mg alloy.
Aged for 0.015 day.
Tested at 77°K X6

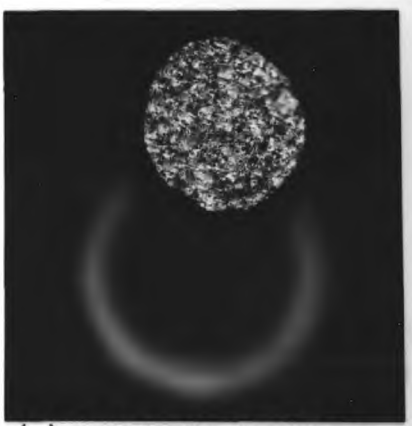

(c) 2.2:1, Cu:Mg alloy.
Aged for 0.054 day.
Tested at 77°K. X6

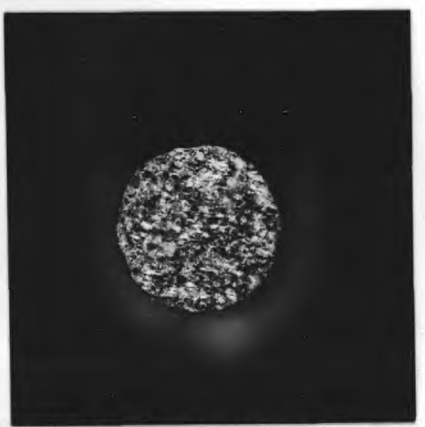

(d) 2.2:1, Cu:Mg alloy.
Aged for 0.2 day.
Tested at 77°K X6

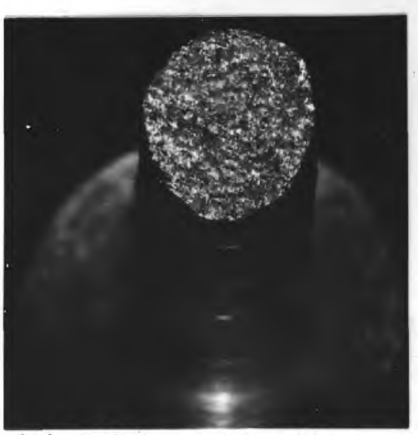

(e) 2.2:1, Cu:Mg alloy.
Aged for 0.4 day.
Tested at 77°K X6

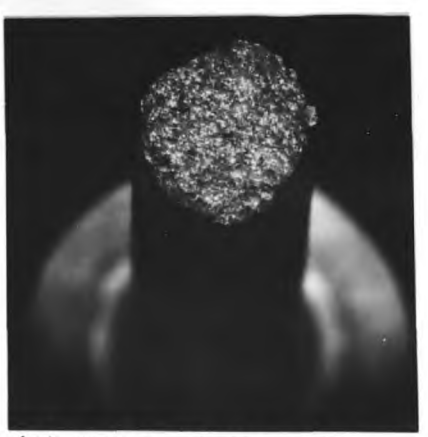

(f) 2.2:1, Cu:Mg alloy.
Aged for 10 days.
Tested at 77°K X6

Fig. 34

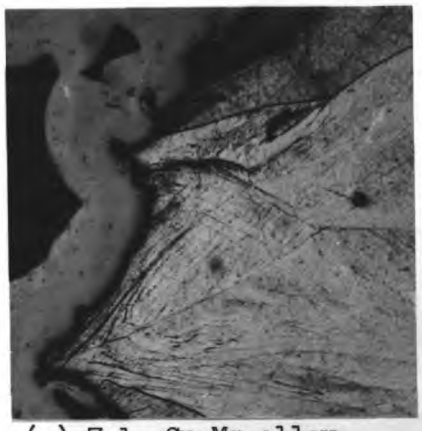

(a) 7:1, Cu:Mg alloy.
Aged for 0.06 day.
Tested at 295°K X100

(b) 7:1, Cu:Mg alloy.
Aged for 0.2 day.
Tested at 295°K x100

(c) 7;1, Cu:Mg alloy.
Aged for 0.4 day.
Tested at 295°K x50

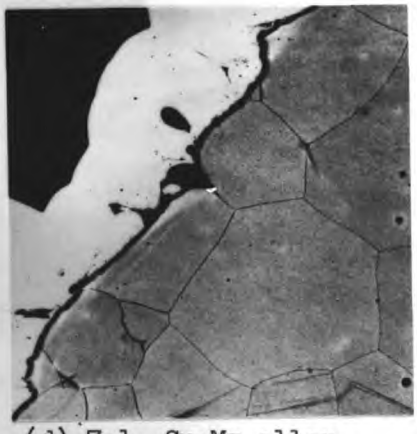

(d) 7:1, Cu:Mg alloy.
Aged for 10 days.
Tested at 295°K. x50

(e) 7:1, Cu:Mg alloy.
Aged for 0.5 day.
Tested at 77°K x50

Fig. 35

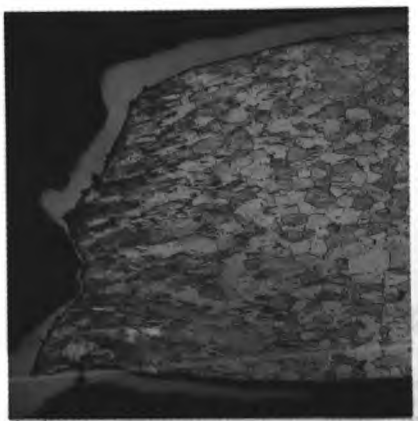

(a) Aged for 0.015 day.
Tested at 295°K x10

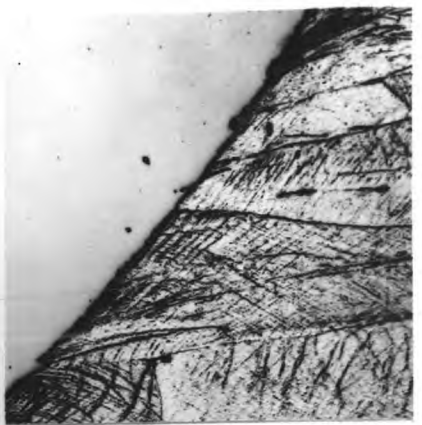

(b) Aged for 0.015 day.
Tested at 295°K x150

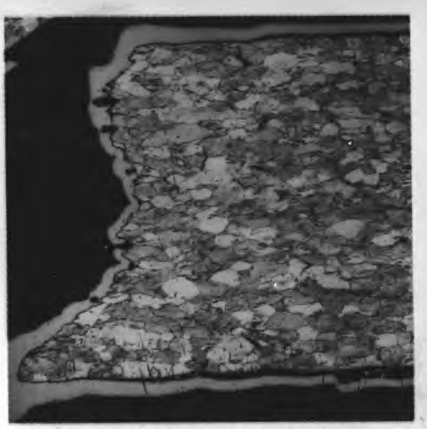

(c) Aged for 0.015 day,
Tested at 77°K x10

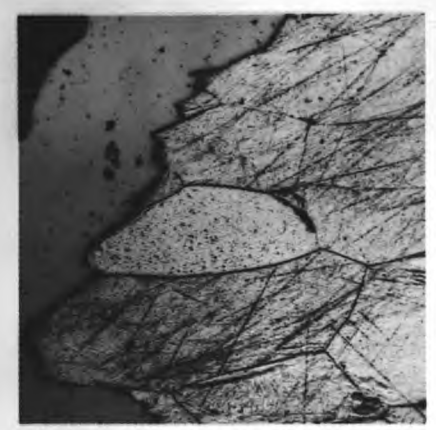

(d) Aged for 0.015 day.
Tested at 77°K x150

Fig. 36

Sections through the fractures of 2.2:1, Cu:Mg alloys

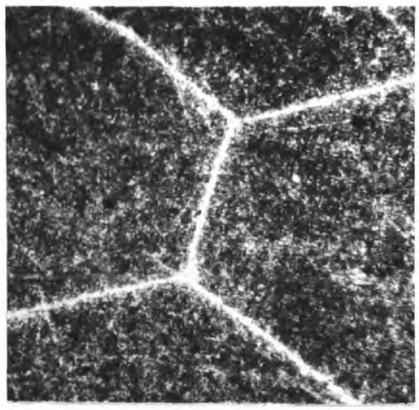

(a) Aged for 0.4 day.
Tested at 77°K x700

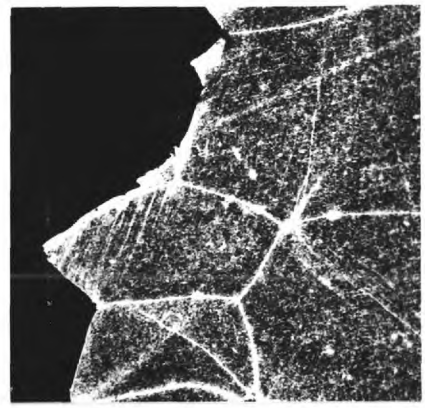

(b) Aged for 0.4 day.
Tested at 295°K x150

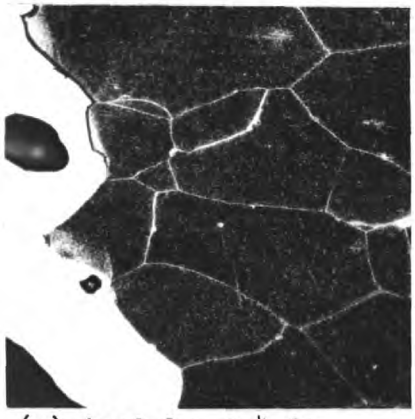

(c) Aged for 0.4 day.
Tested at 77°K x150

(d) Aged for 10 days.
Tested at 77°K X150

Fig. 37

Sections through the fractures of 2.2:1, Cu:Mg alloys

(a) As-quenched x 6000

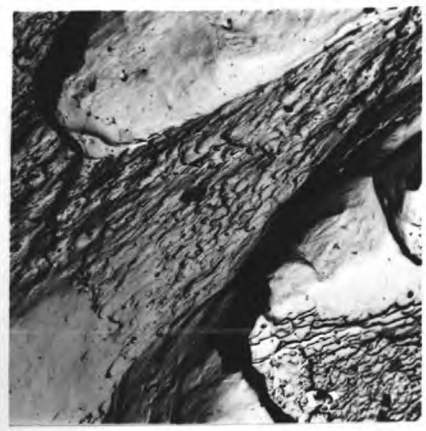

(b) Aged for 0.5 day x 4000

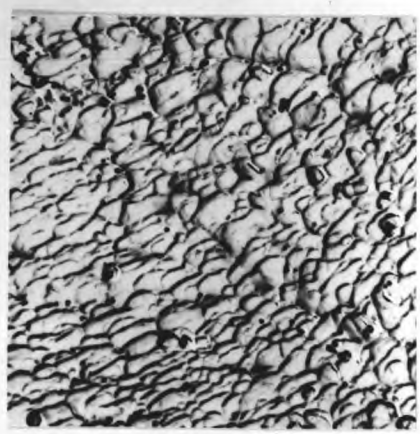

(c) Aged for 10 days X 8000

Fig. 38

Fractographs of 7:1, Cu:Mg alloys tested at 77°K

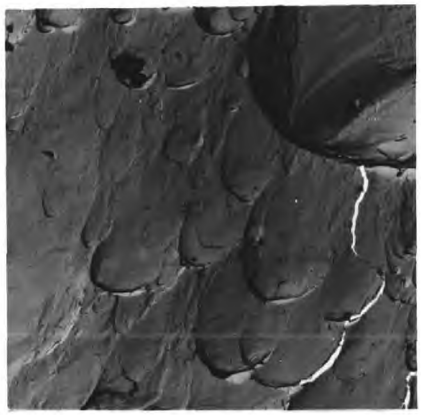

(a) As-quenched. x 6000

(b) Aged for 0.015 day
x 4000

(c) Aged for 0.4 day.
x 6000

(d) Aged for 10 days.
x 8000

Fig.39

Fractographs of 2.2:1, Cu:Mg alloys tested at 295°K

(a) As-quenched. x 6000

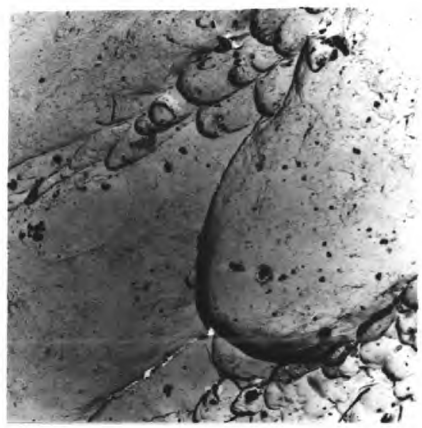

(b) Aged for 0.015 day. x 4000

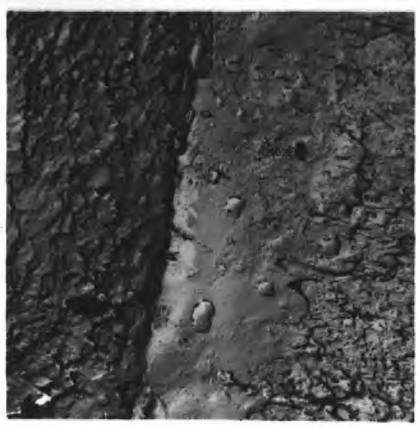

(c) Aged for 0.4 day x 6000

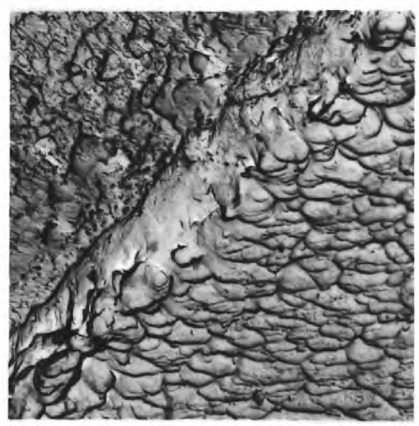

(d) Aged for 10 days x 6000

Fig. 40

Fractographs of 2.2:1, Cu:Mg alloys tested at 77°K

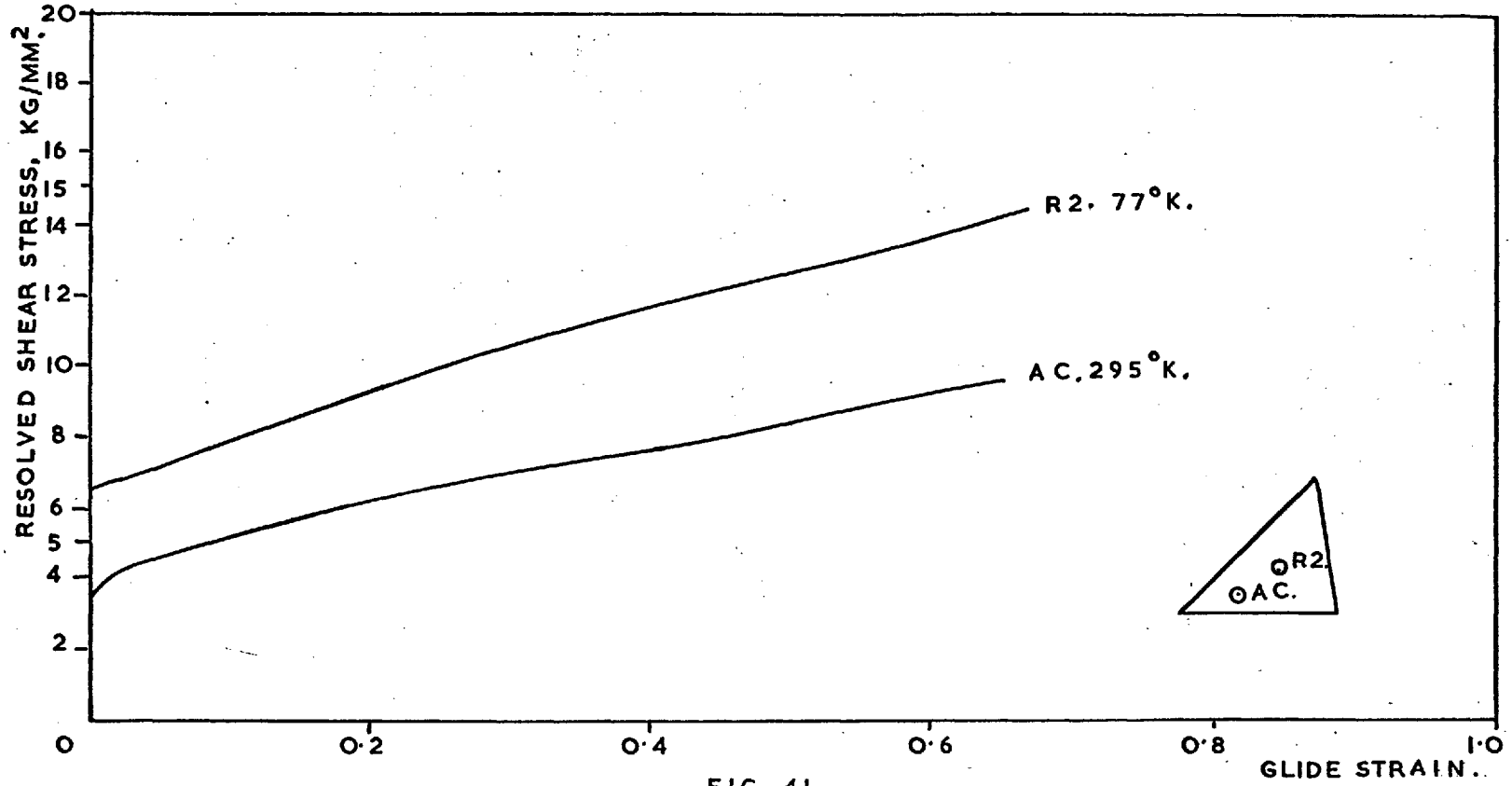

FIG. 41.

RESOLVED SHEAR STRESS - GLIDE STRAIN CURVES FOR QUENCHED 7:1, Cu : Mg ALLOYS.

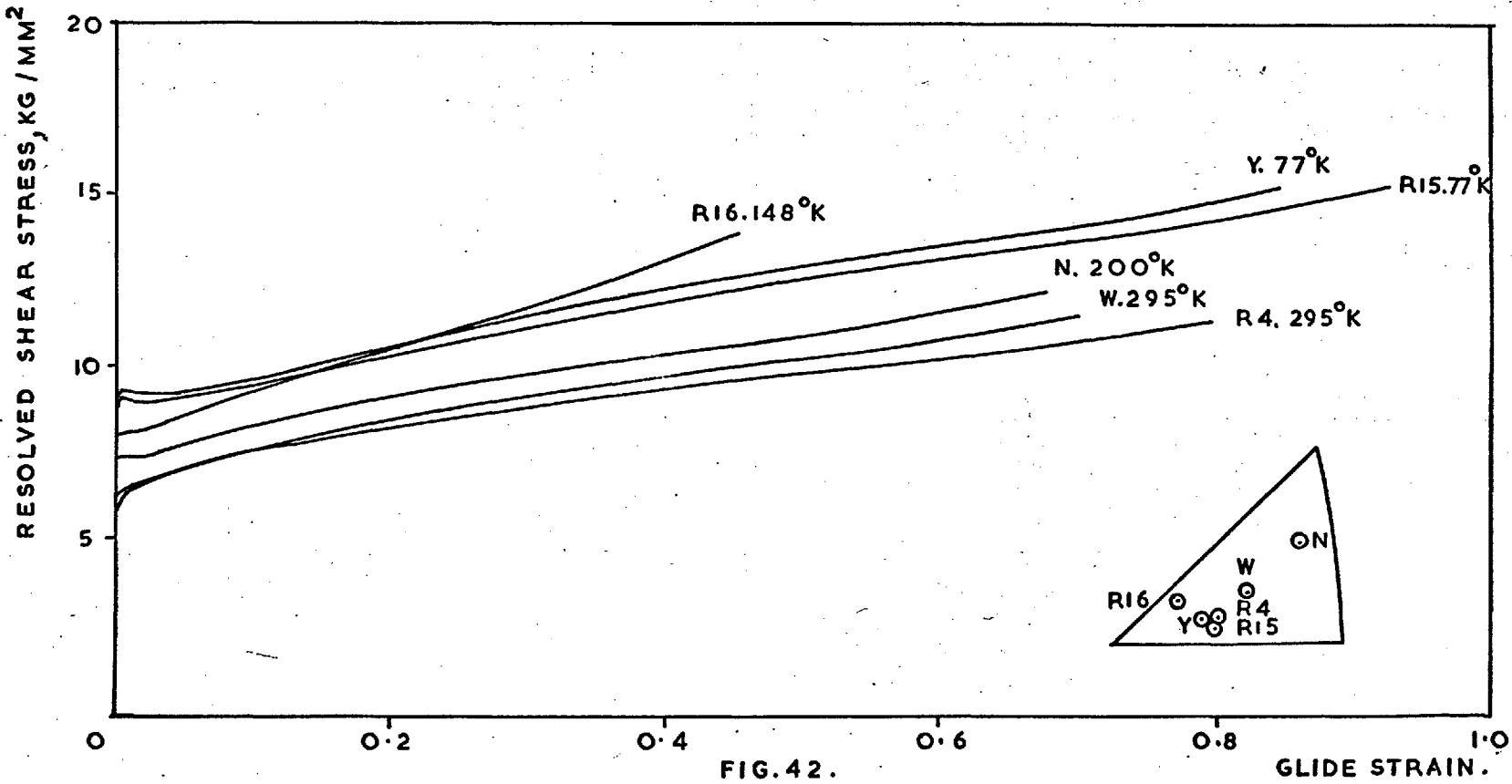

FIG. 42.

RESOLVED SHEAR STRESS – GLIDE STRAIN CURVES FOR 7:1, Cu : Mg ALLOYS AGED FOR 0·01 DAY AT 190°C.

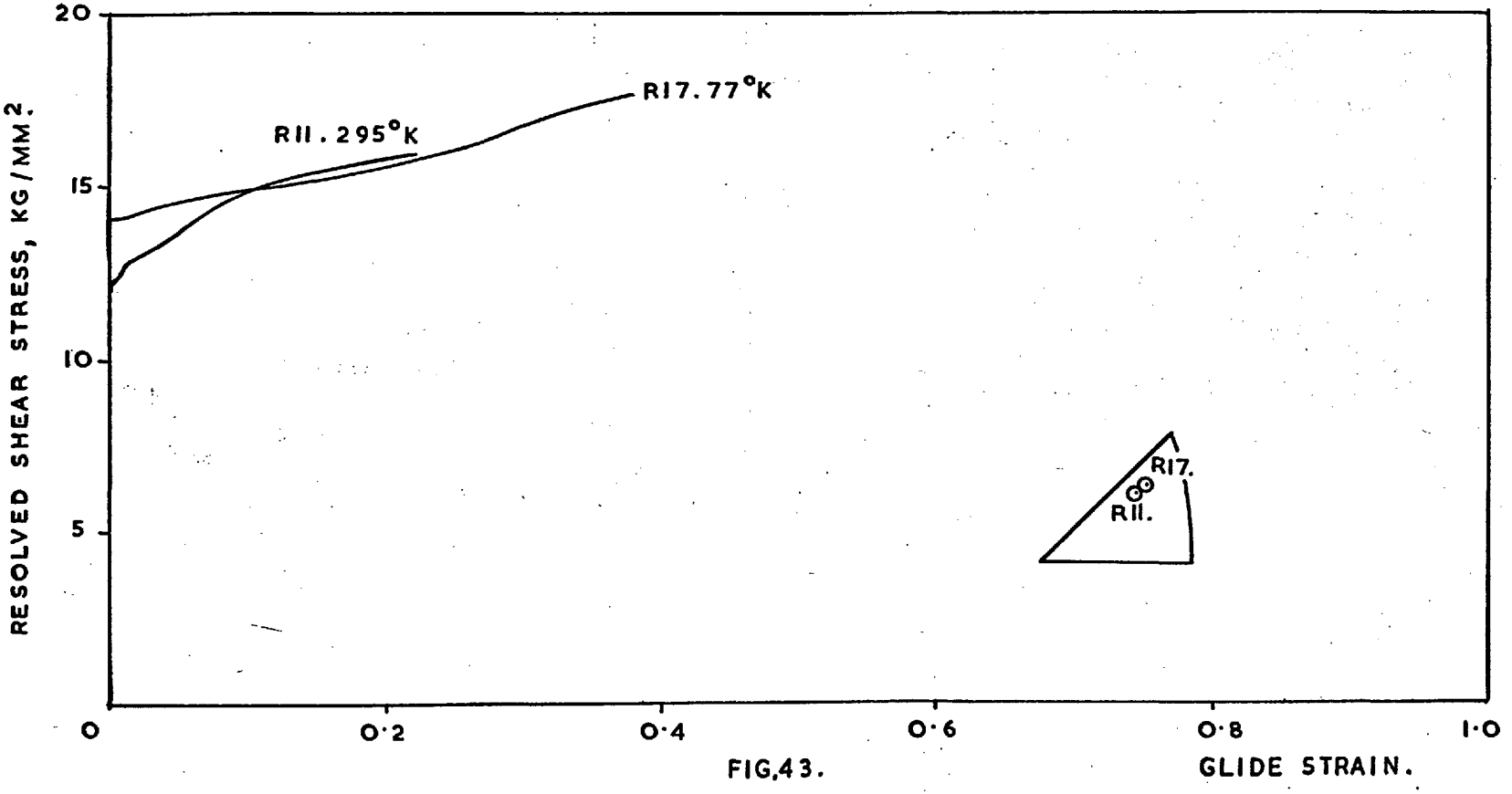

FIG.43.

RESOLVED SHEAR STRESS – GLIDE STRAIN CURVES FOR 7:1 Cu : Mg ALLOYS, AGED FOR 0·1 DAY AT 190°C.

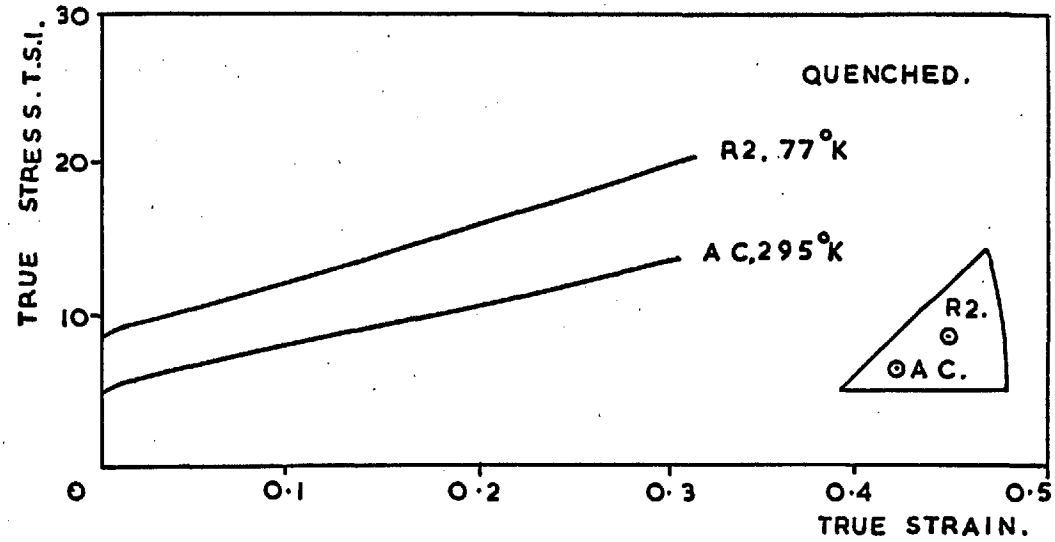

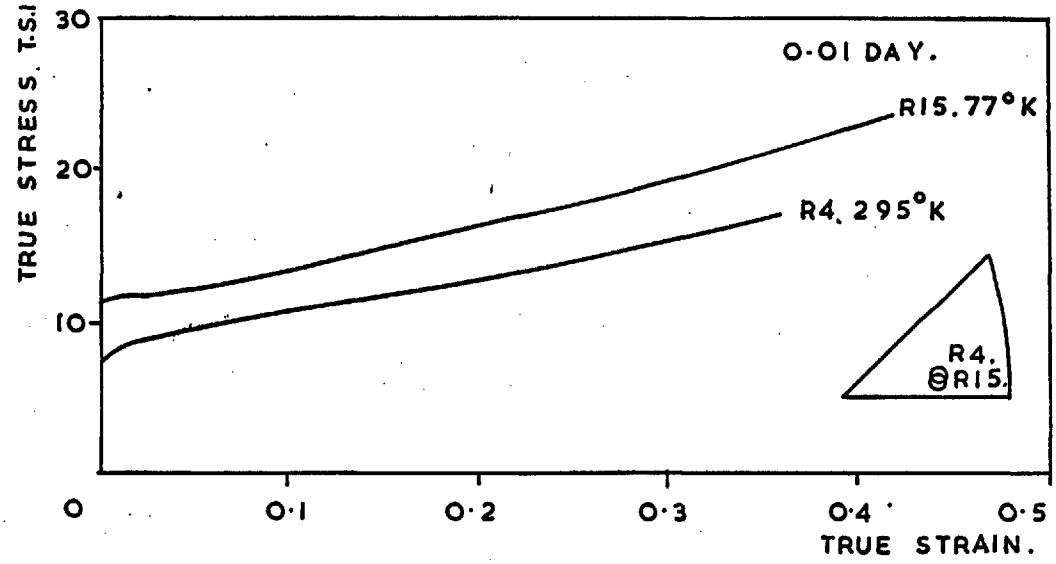

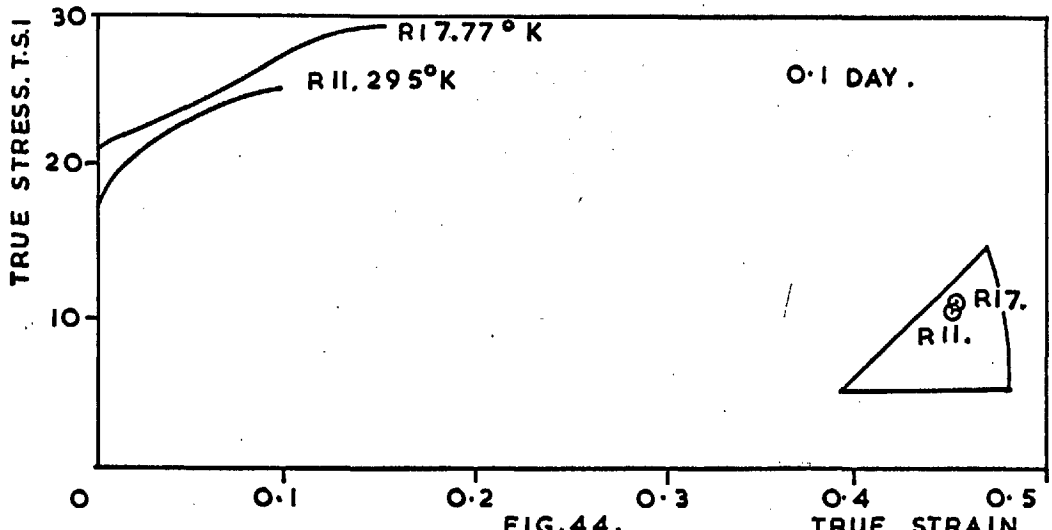

FIG. 44.

TRUE STRESS – TRUE STRAIN CURVES FOR 7:1 Cu : Mg ALLOY.

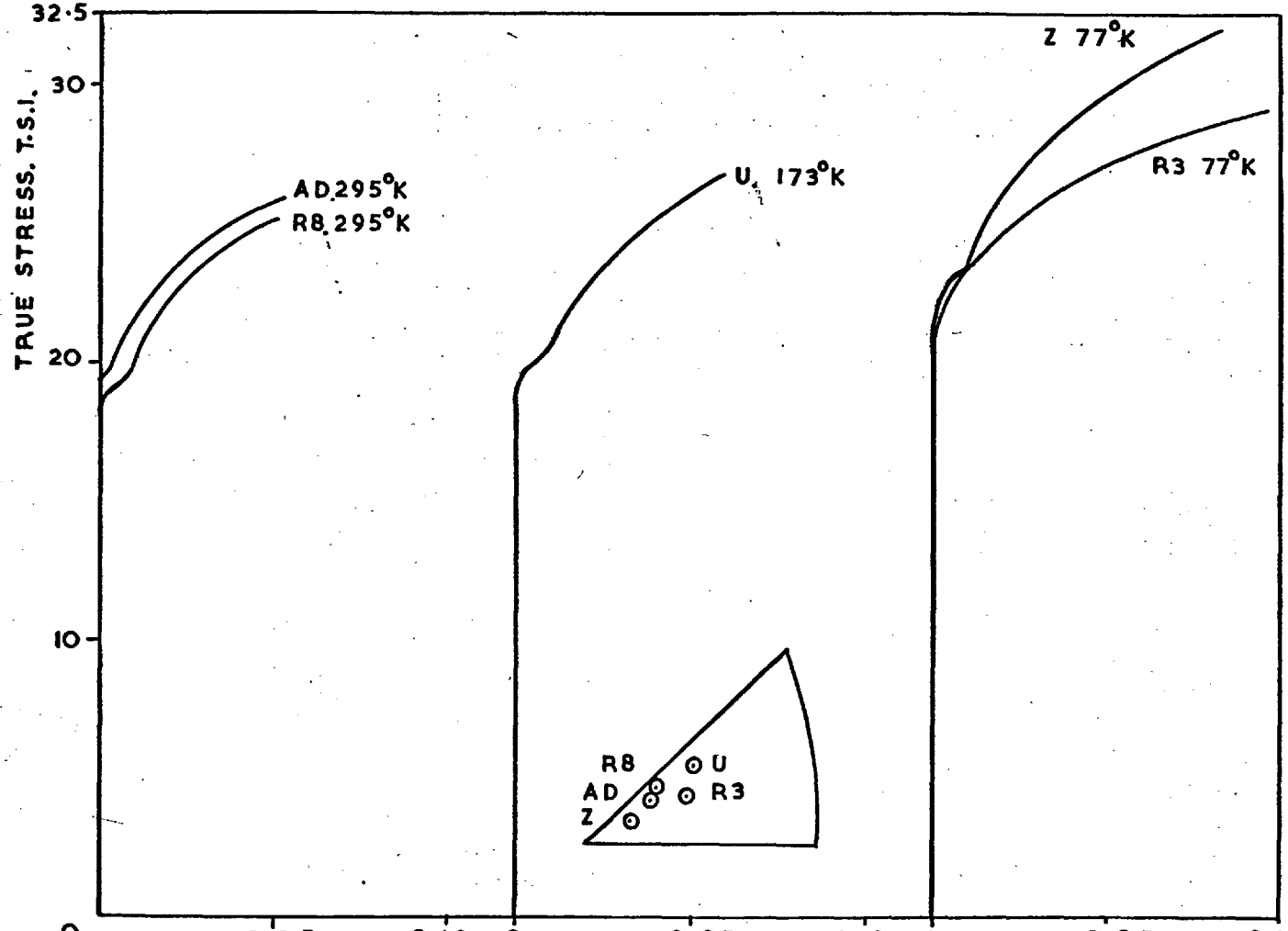

FIG.45

TRUE STRESS-TRUE STRAIN CURVES FOR 7:1 Cu: Mg CRYSTALS AGED FOR 0·5 DAYS AT 190°C.

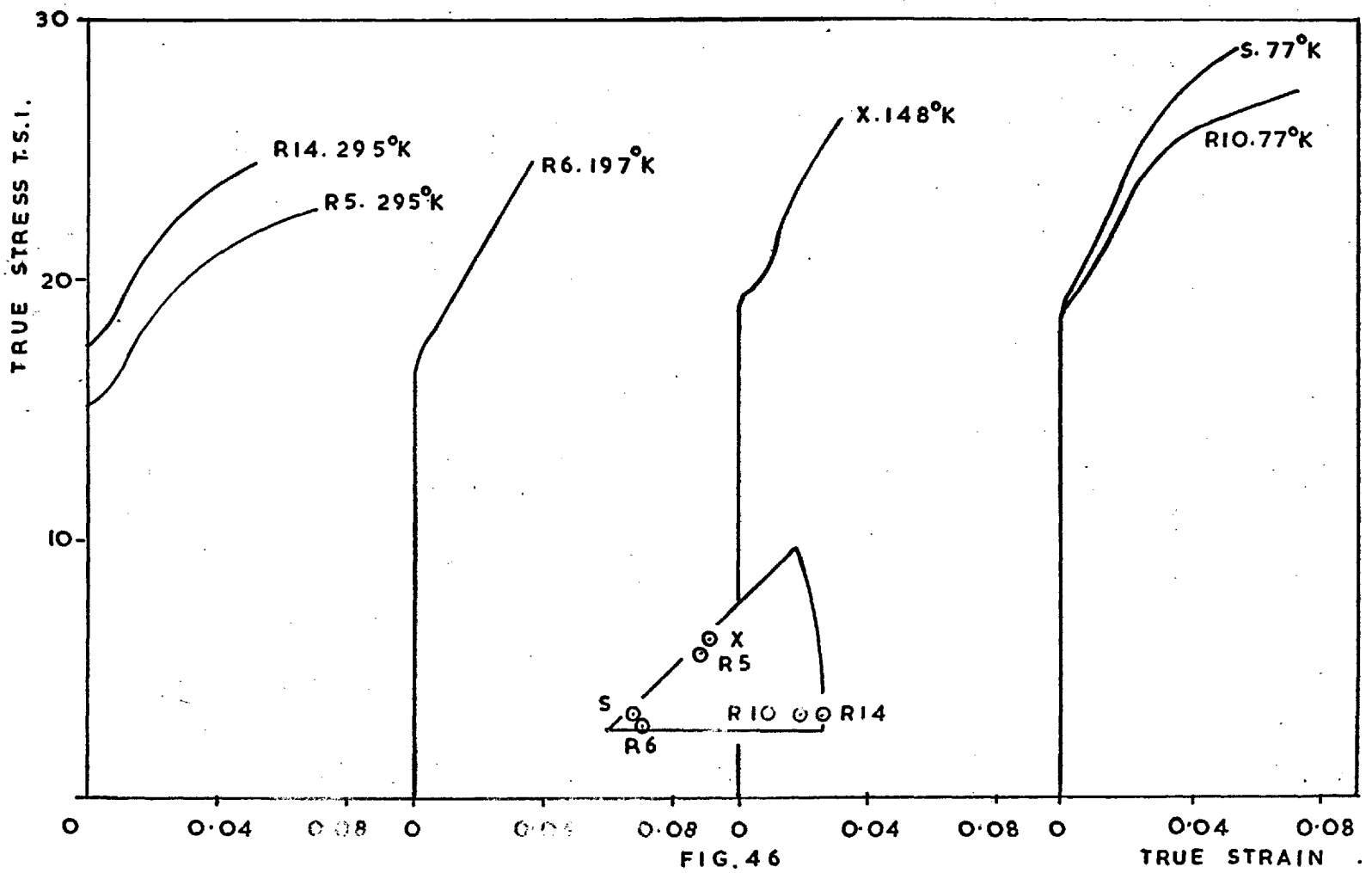

FIG. 46

TRUE STRESS - TRUE STRAIN CURVES FOR 7:1 Cu:Mg ALLOYS FOR 10 DAYS AT 190°C.

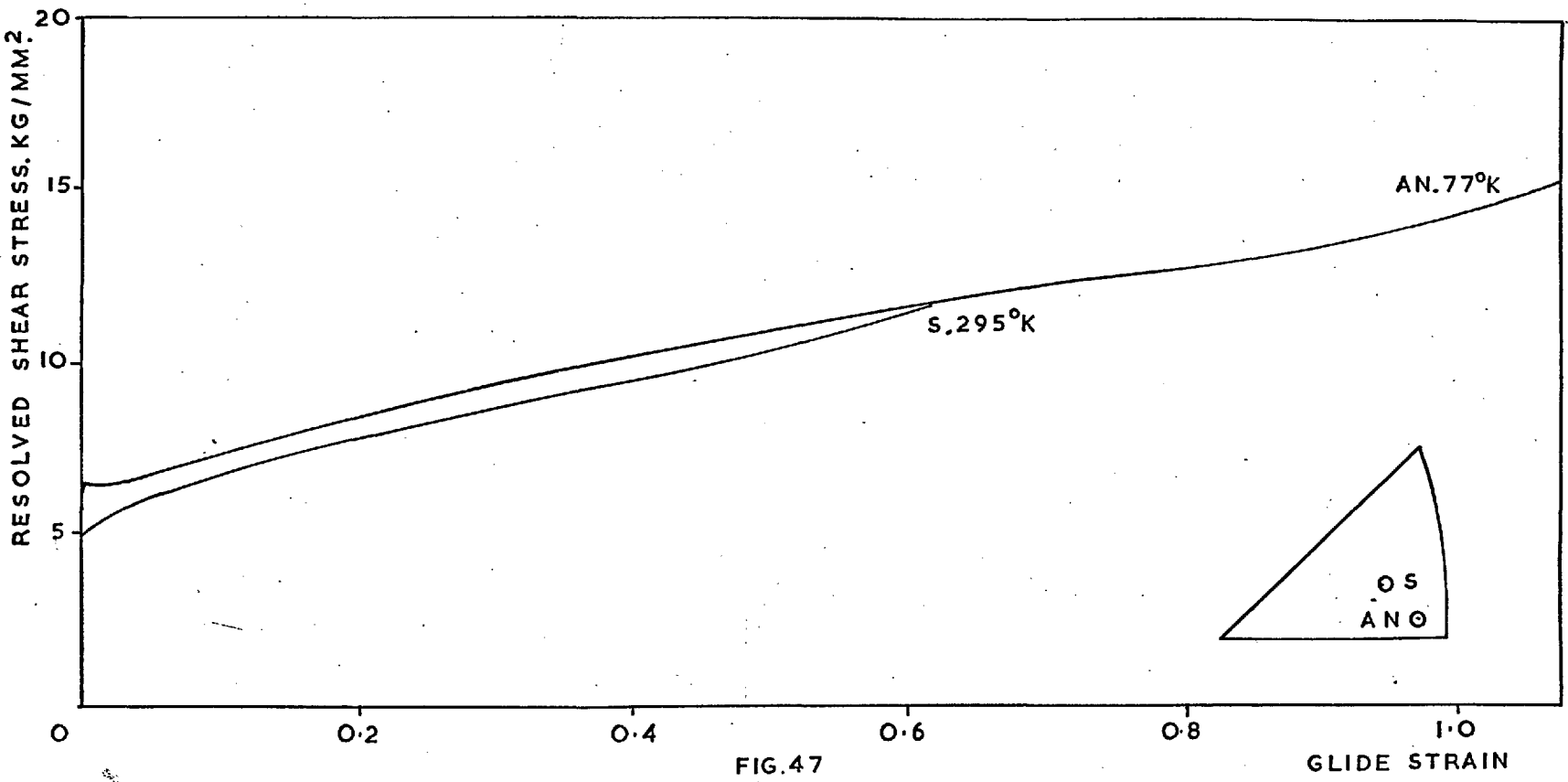

FIG. 47

RESOLVED SHEAR STRESS - GLIDE STRAIN CURVES FOR QUENCHED 2·2:1 Cu:Mg ALLOYS.

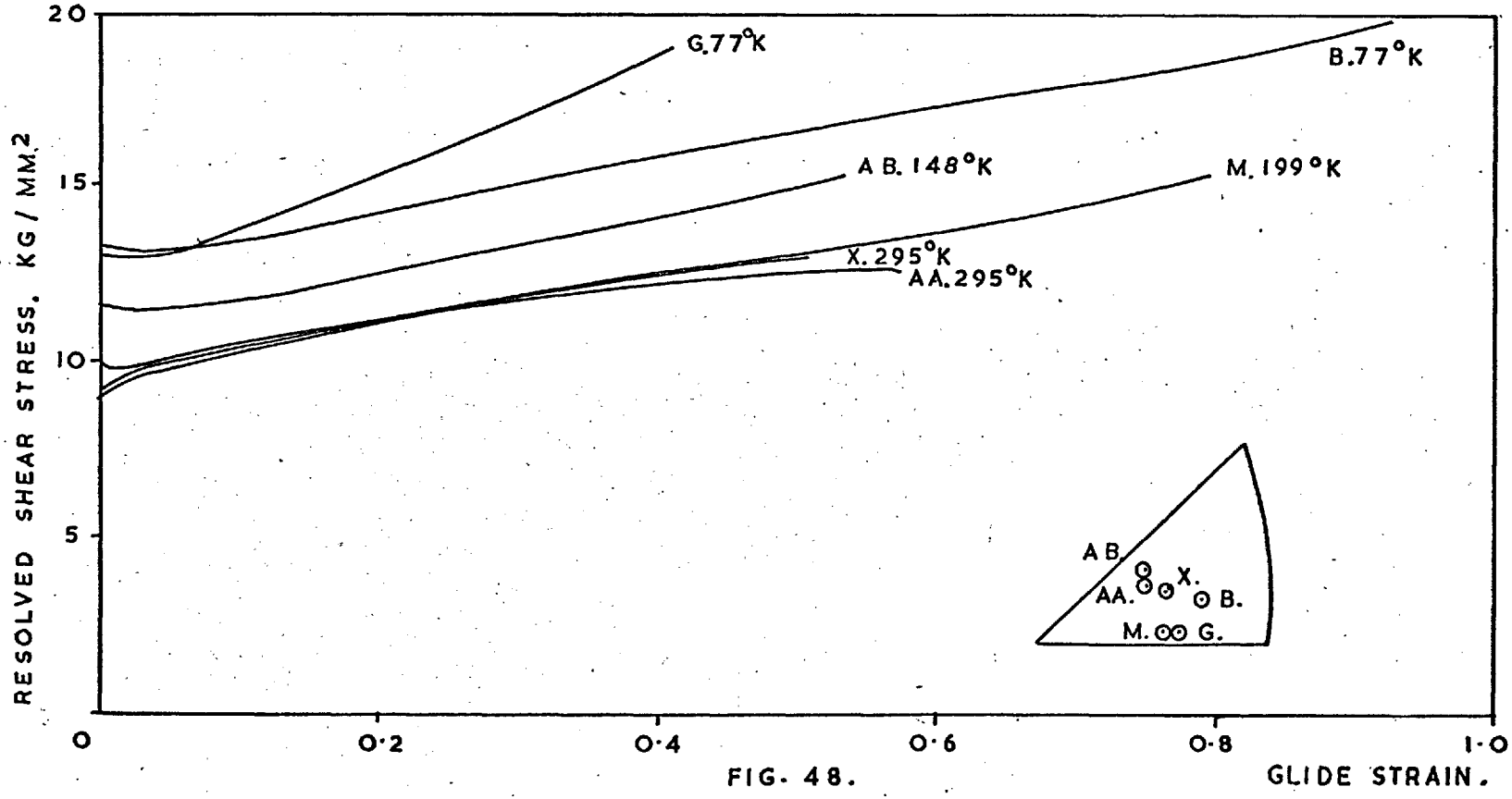

FIG. 48.

RESOLVED SHEAR STRESS - GLIDE STRAIN CURVES FOR 2:2:1, Cu:Mg ALLOYS AGED FOR 0·015 DAY AT 190°C.

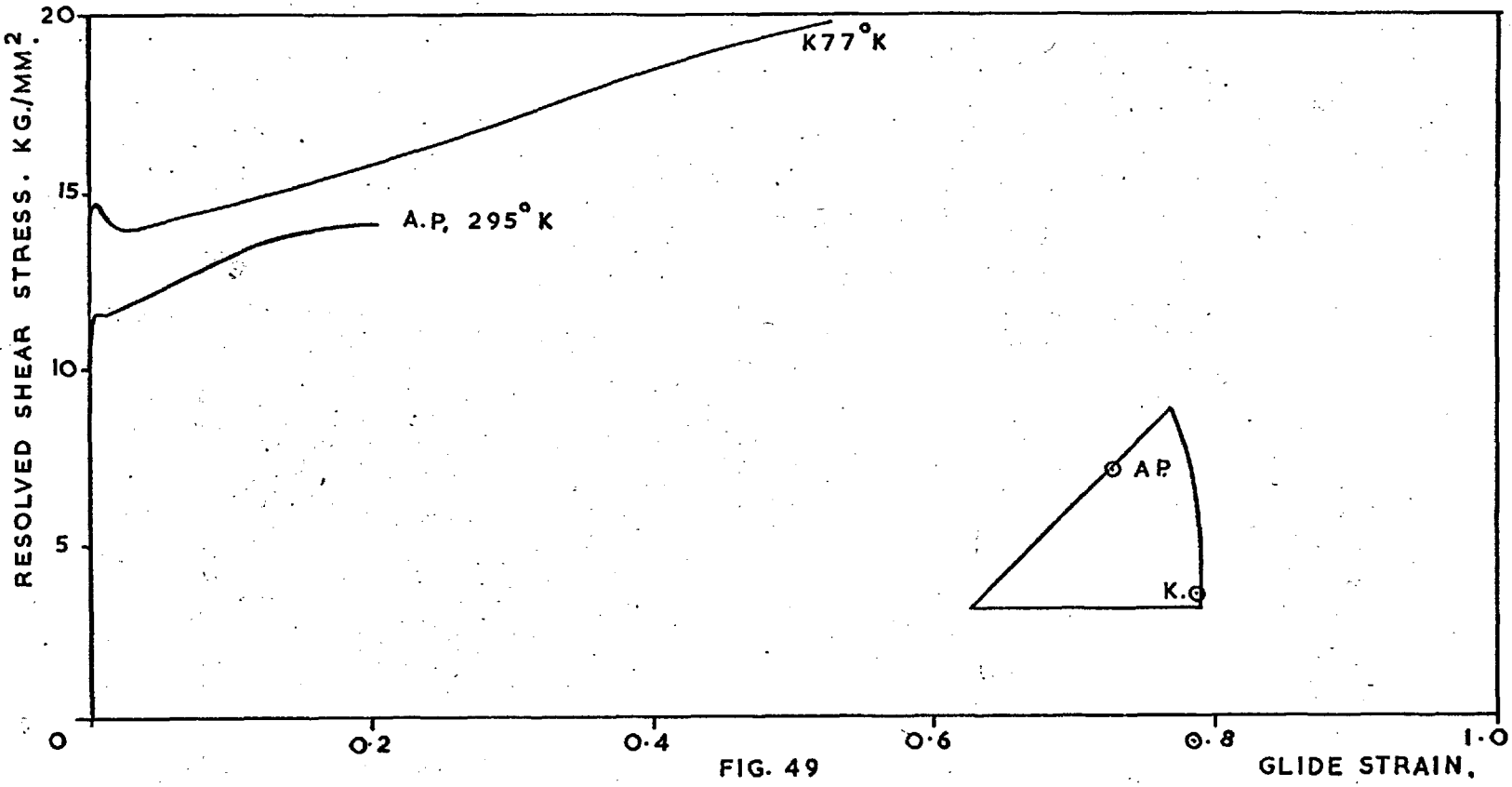

FIG. 49

RESOLVED SHEER-STRESS GLIDE STRAIN CURVES FOR 2·2!1, Cu: Mg ALLOYS AGED FOR 0·1 DAYS AT 190°C.

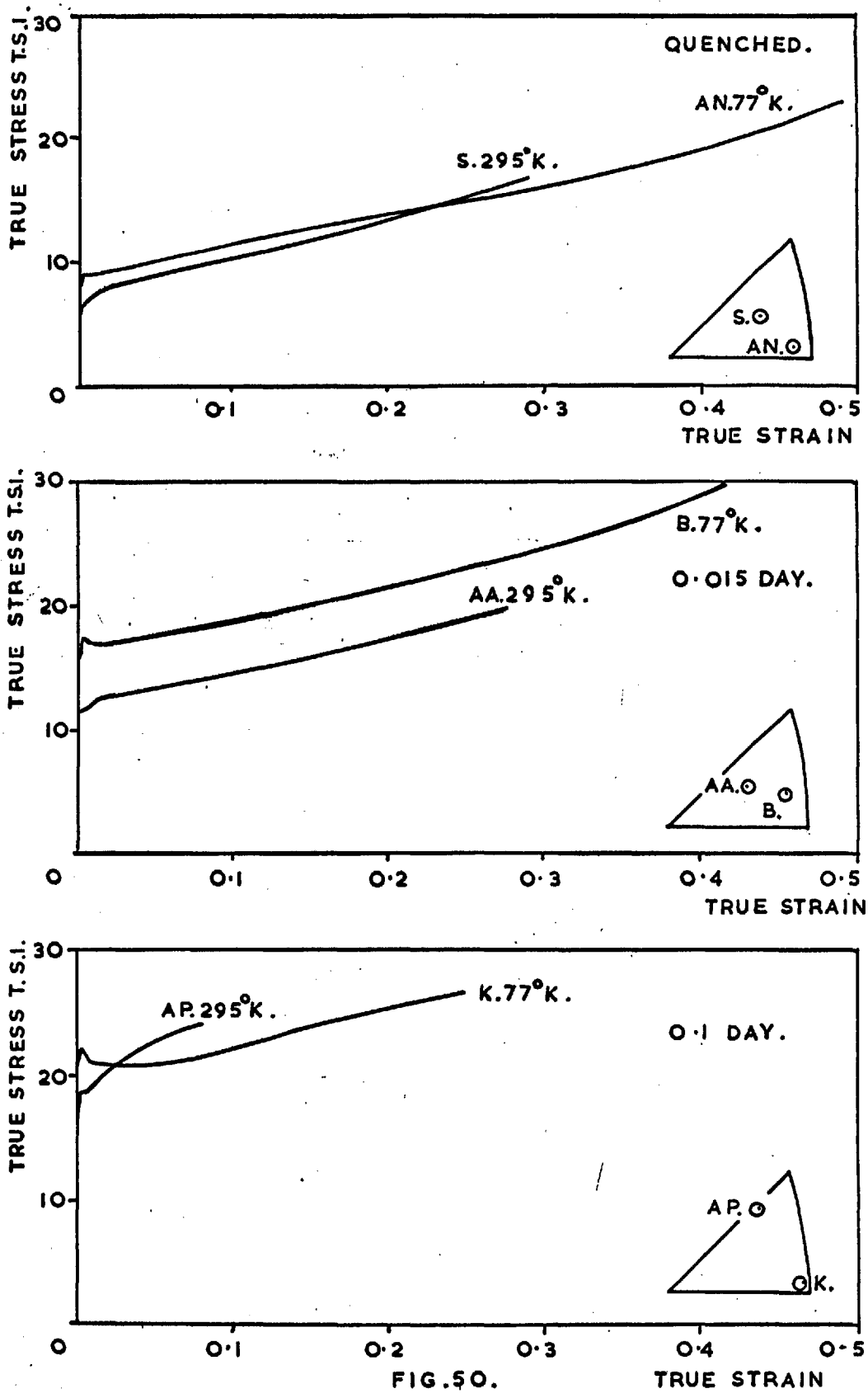

FIG. 50.

TRUE STRESS-TRUE STRAIN CURVES FOR 2·2 11, Cu: Mg ALLOY.

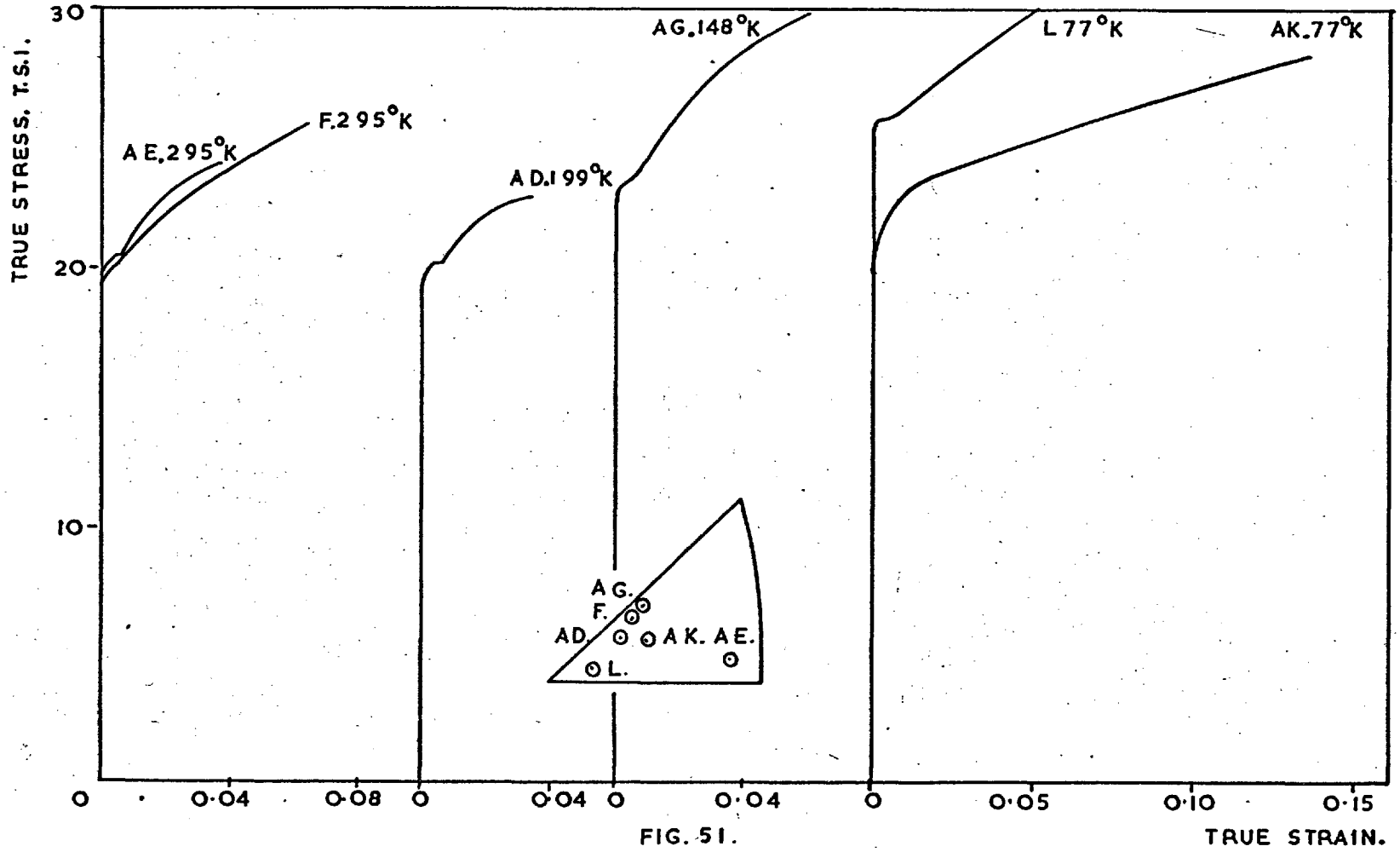

FIG. 51.

TRUE STRESS - TRUE STRAIN CURVES FOR 2·2:1, Cu:Mg ALLOYS AGED FOR 0·4 DAY AT 190°C.

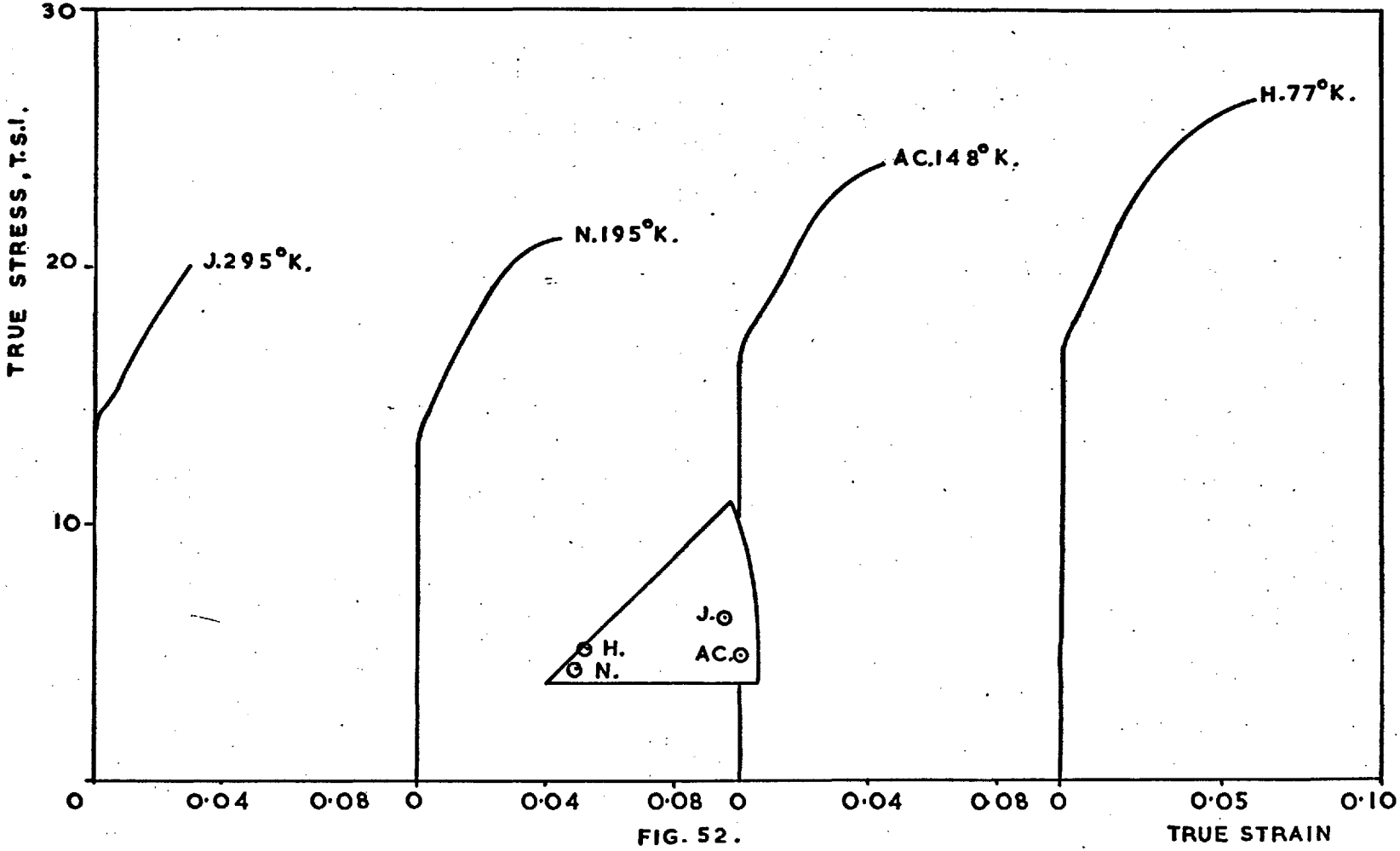

FIG. 52.

TRUE STRESS —TRUE STRAIN CURVES FOR 2:2:1, Cu : Mg ALLOYS AGED FOR 10 DAYS AT 190°C.

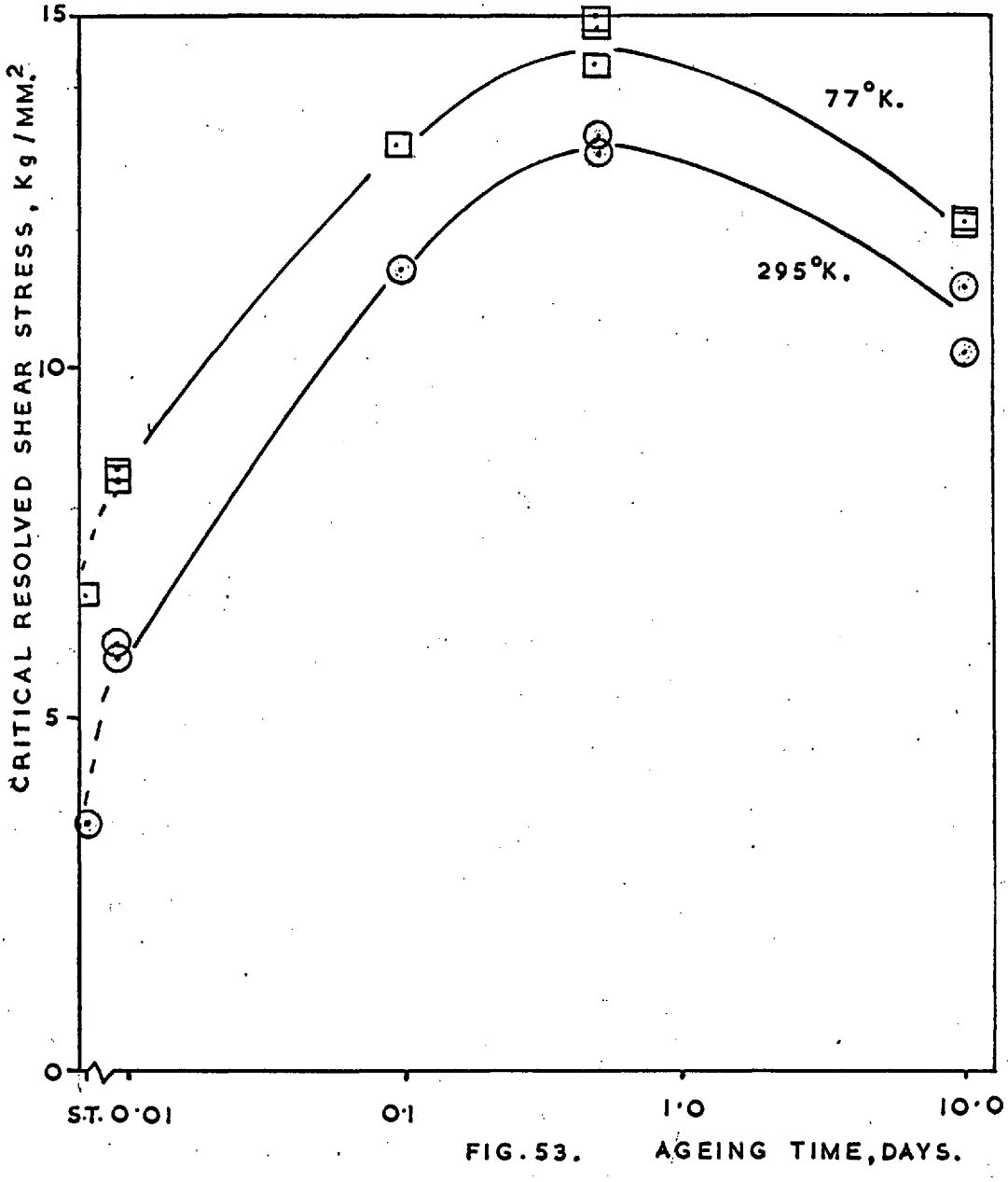

FIG. 53.

C.R.S.S. AGEING CURVES FOR 7:1 Cu: Mg ALLOY.

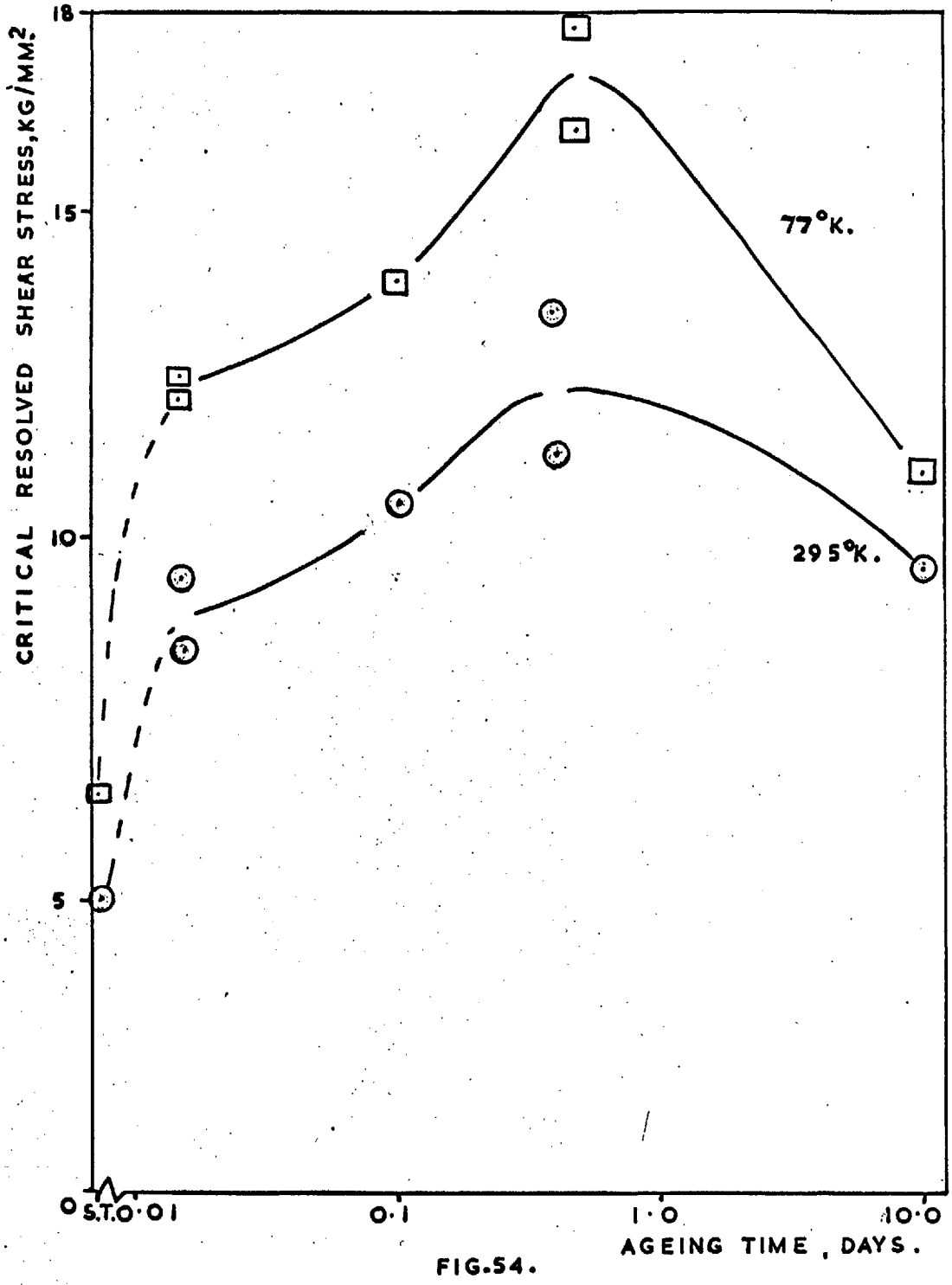

FIG.54.

C.R.S.S. - AGEING CURVES FOR 2·2:1, Cu: Mg ALLOY.

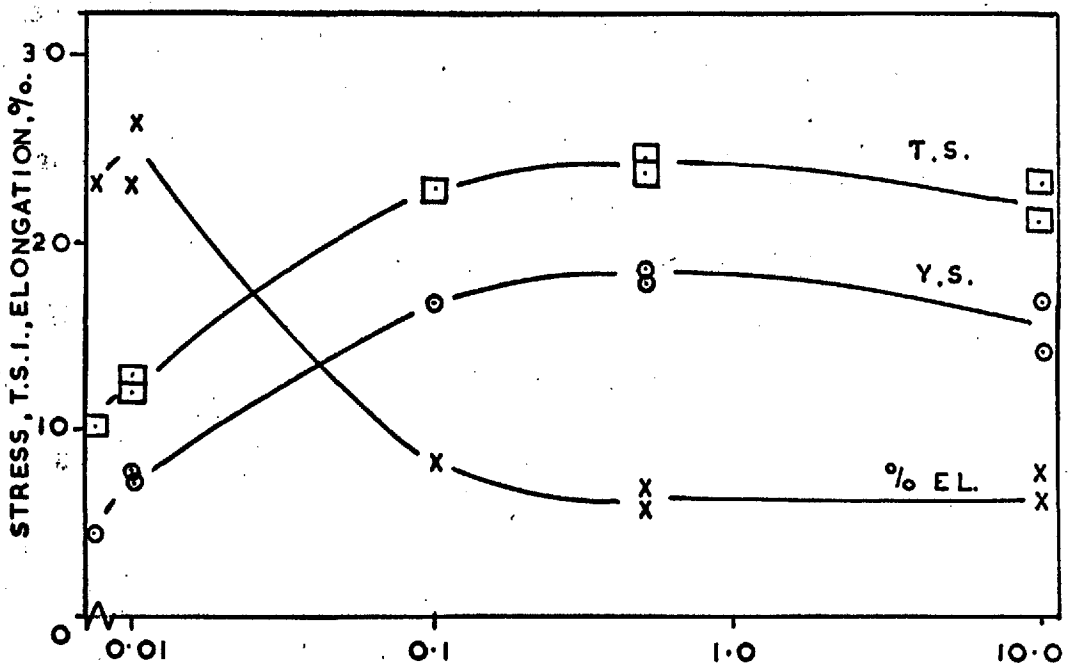

FIG. 55.

MECHANICAL PROPERTIES OF 7:1 Cu: Mg ALLOYS, TESTED AT 295°K.

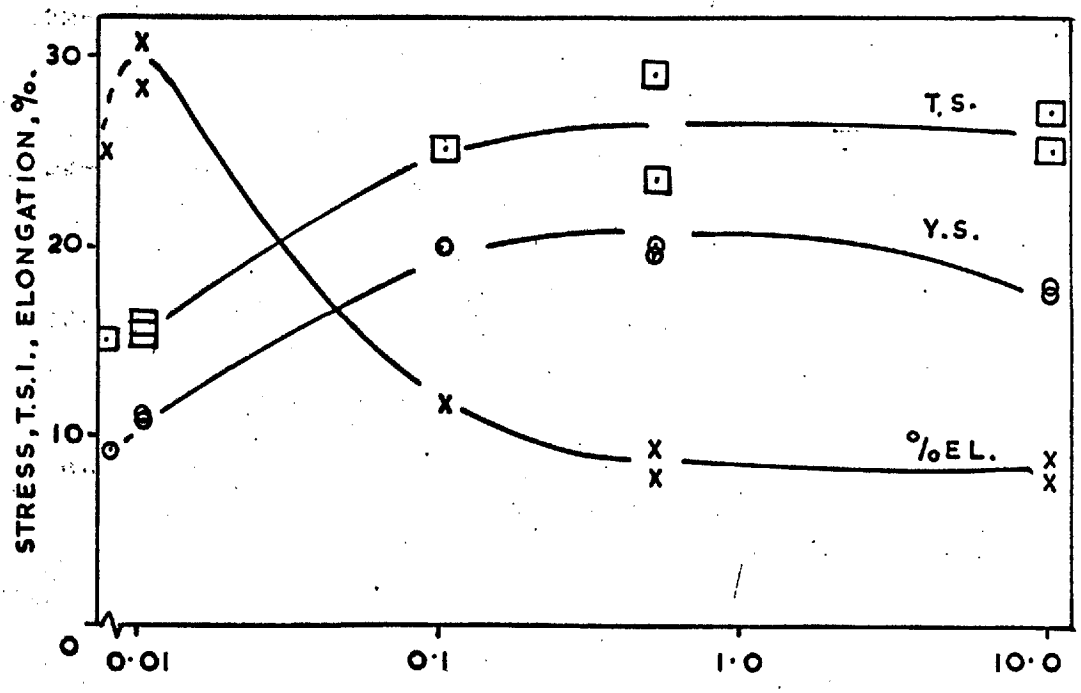

FIG. 56.

MECHANICAL PROPERTIES OF 7:1 Cu: Mg ALLOY, TESTED AT 77°K.

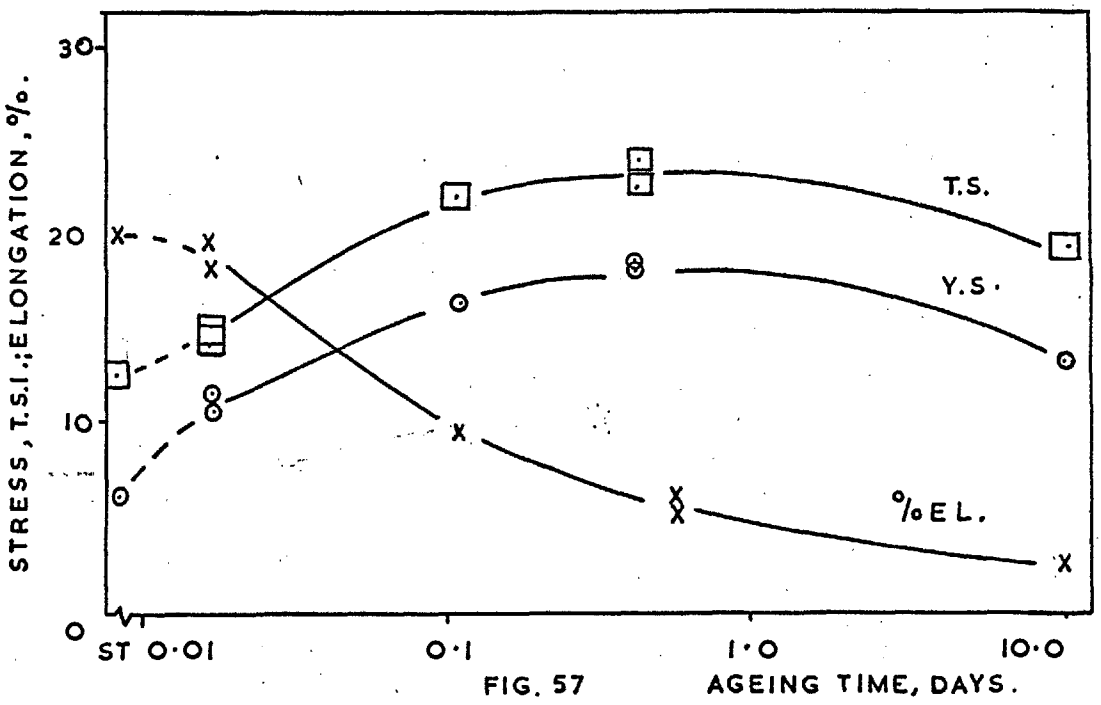

FIG. 57

MECHANICAL PROPERTIES OF 2·2:1 Cu: Mg ALLOYS TESTED AT ROOM TEMPERATURE.

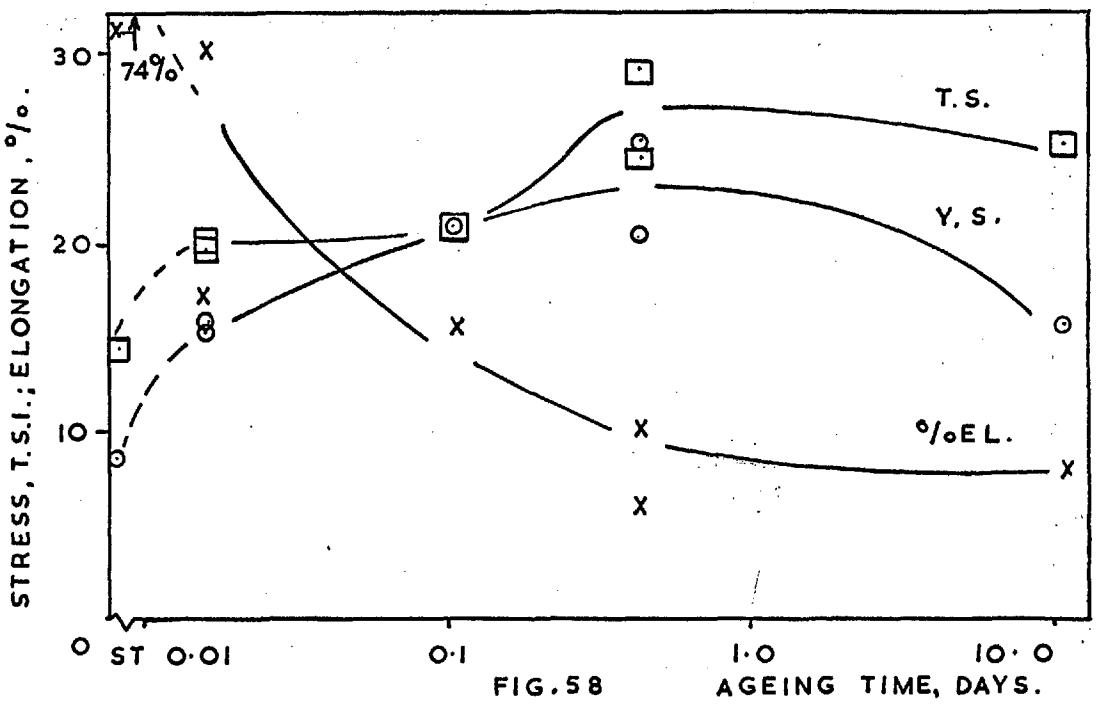

FIG. 58

MECHANICAL PROPERTIES OF 2·2:1, Cu:Mg ALLOYS TESTED AT -196°C.

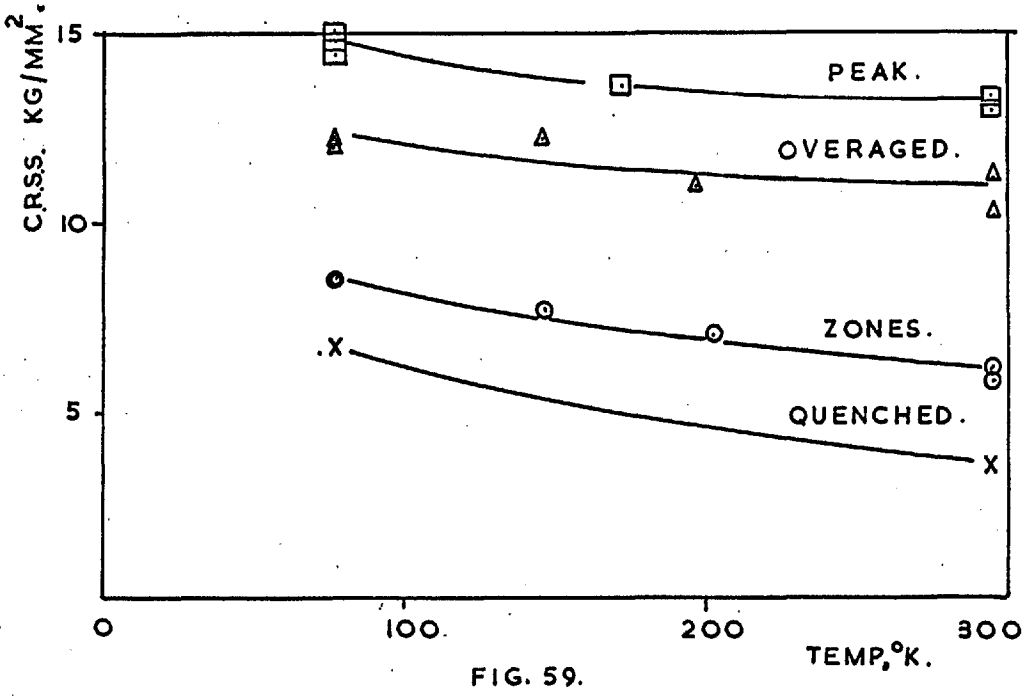

FIG. 59.

THE TEMPERATURE DEPENDENCE OF THE C.R.S.S. FOR SINGLE CRYSTALS OF 7:1, Cu : Mg ALLOY.

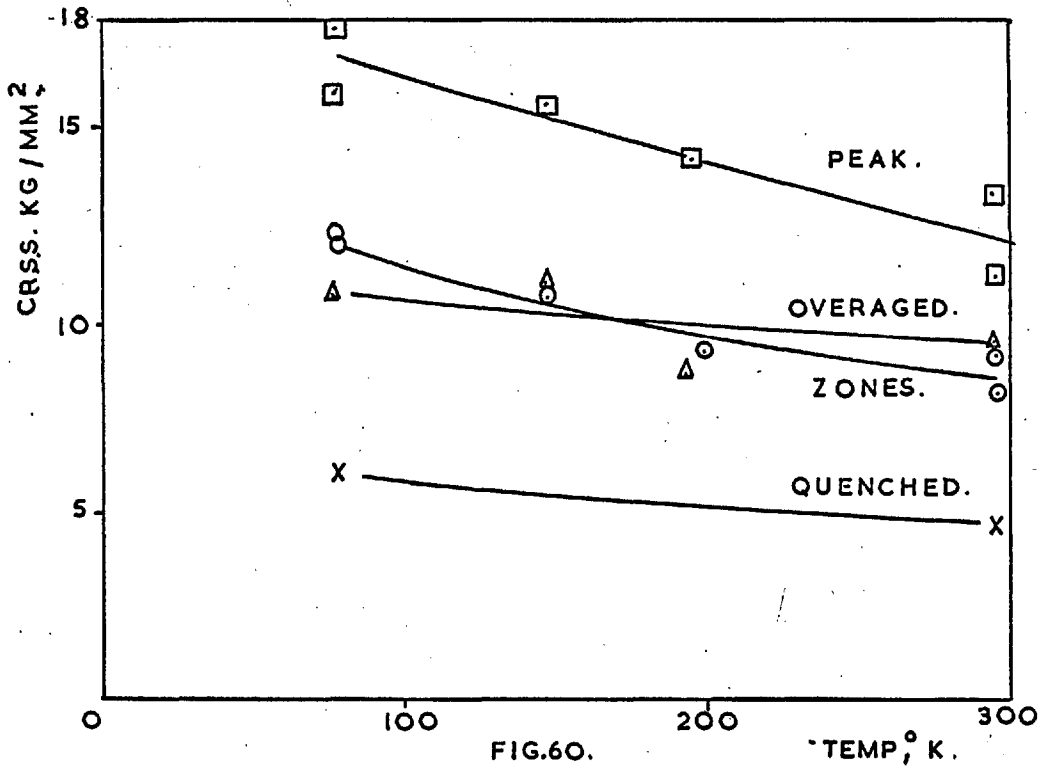

FIG.60.

THE TEMPERATURE DEPENDENCE OF THE C.R.S.S. FOR SINGLE CRYSTALS OF 2·2 :1, Cu : Mg ALLOY.

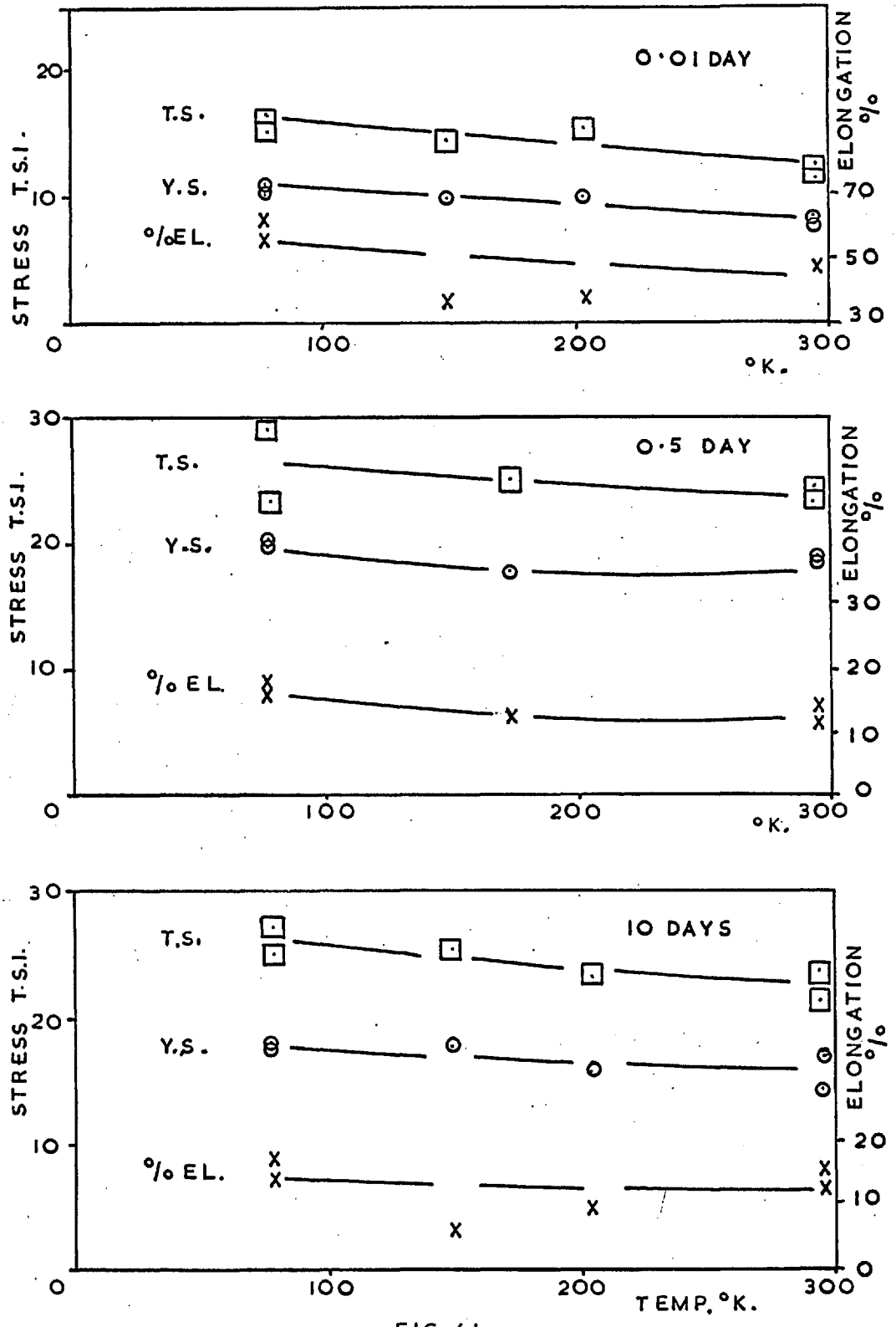

FIG, 61

THE TEMPERATURE DEPENDENCE OF THE MECHANICAL PROPERTIES OF 7:1 Cu:Mg CRYSTALS.

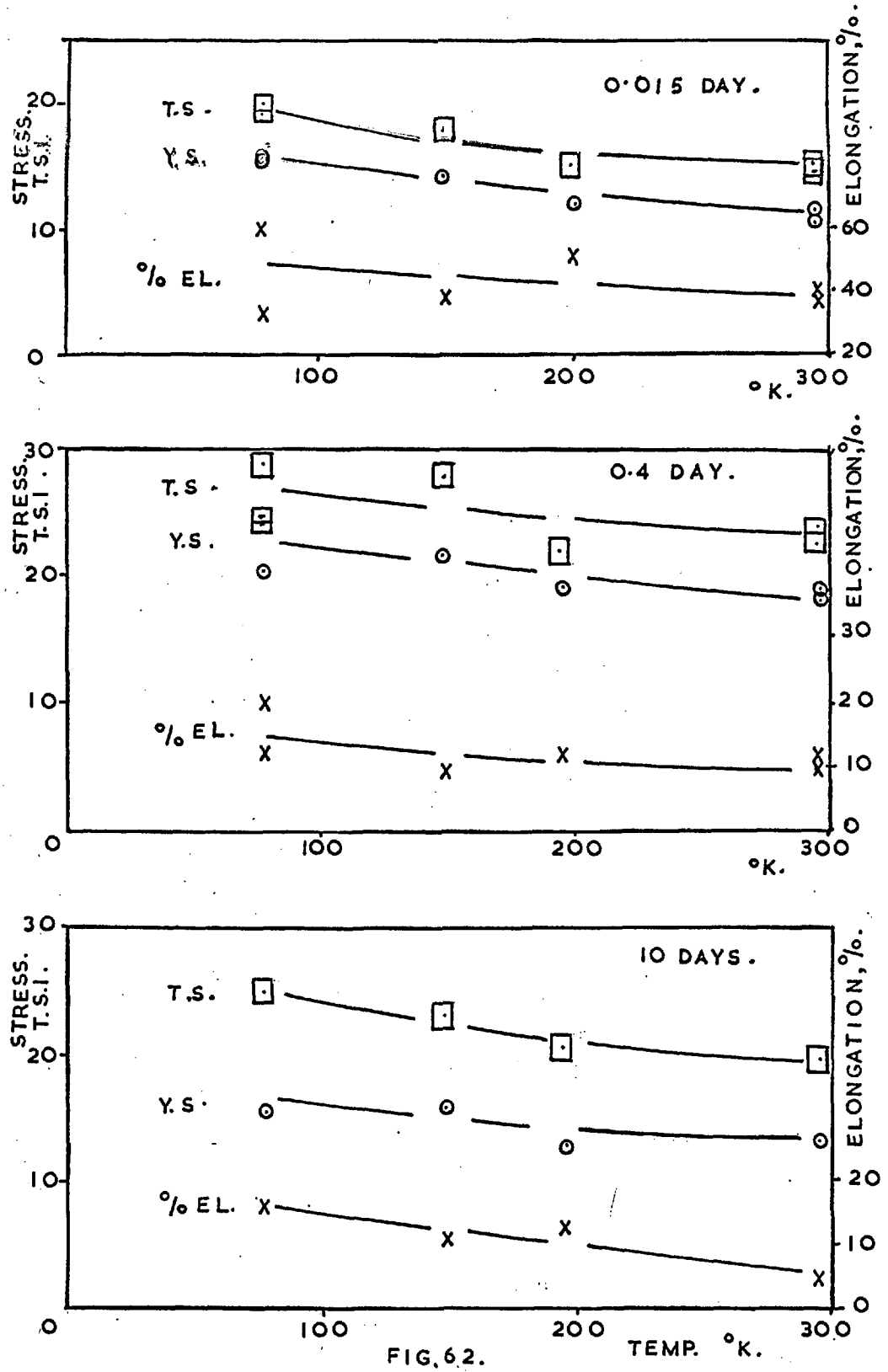

FIG. 6.2.

THE TEMPERATURE DEPENDENCE OF THE MECHANICAL PROPERTIES OF 2·2 : 1 , Cu : Mg CRYSTALS.

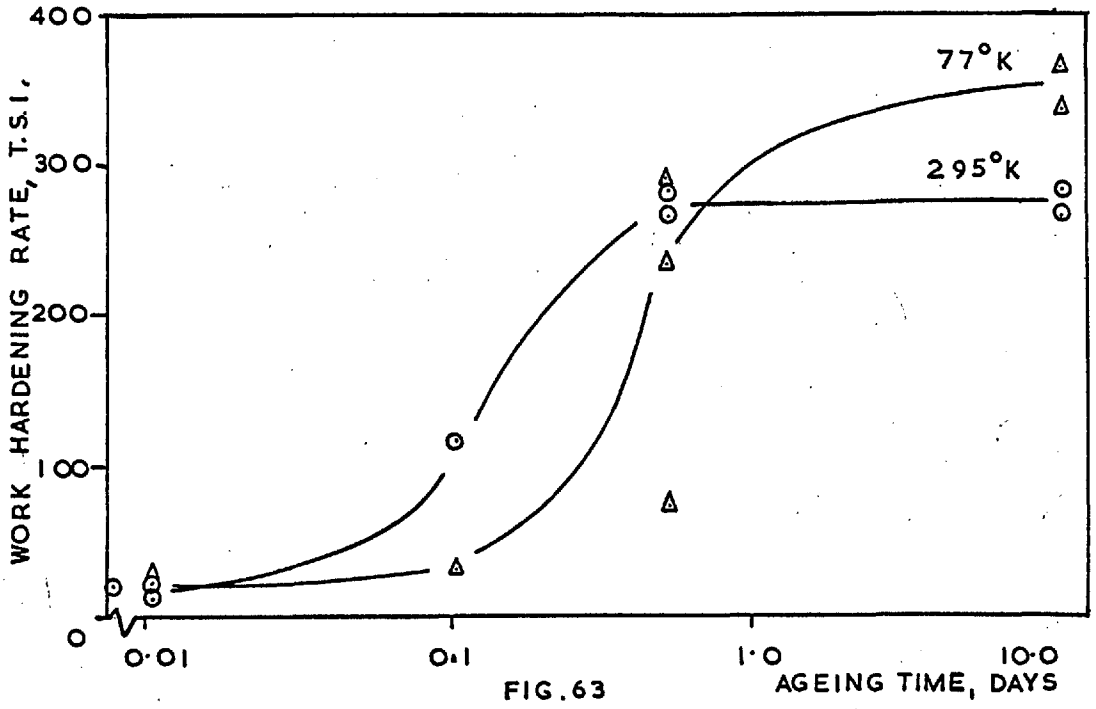

FIG. 63

WORK HARDENING RATE $\left(= \frac{\sigma 0{\cdot}0188 - \sigma\, 0{\cdot}0094}{0{\cdot}0094}\right)$ OF 7:1, Cu: Mg CRYSTALS.

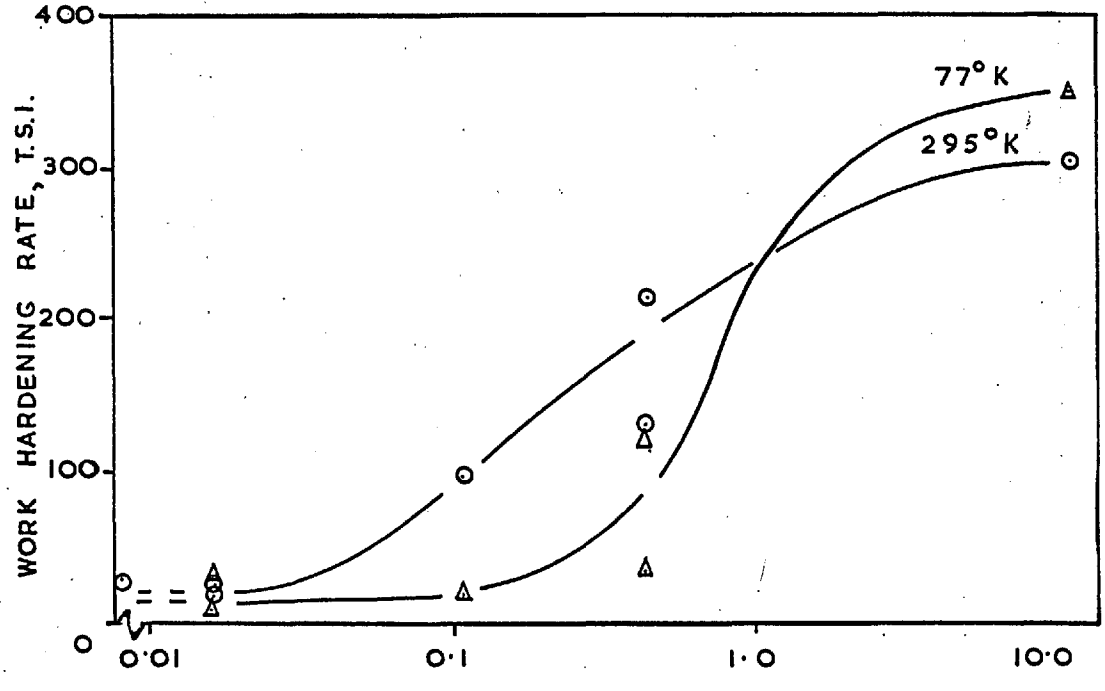

FIG. 64.

WORK HARDENING RATE $\left(= \frac{\sigma 0{\cdot}0188 - \sigma\, 0{\cdot}0094}{0{\cdot}0094}\right)$ FOR 2·2:1, Cu : Mg CRYSTALS.

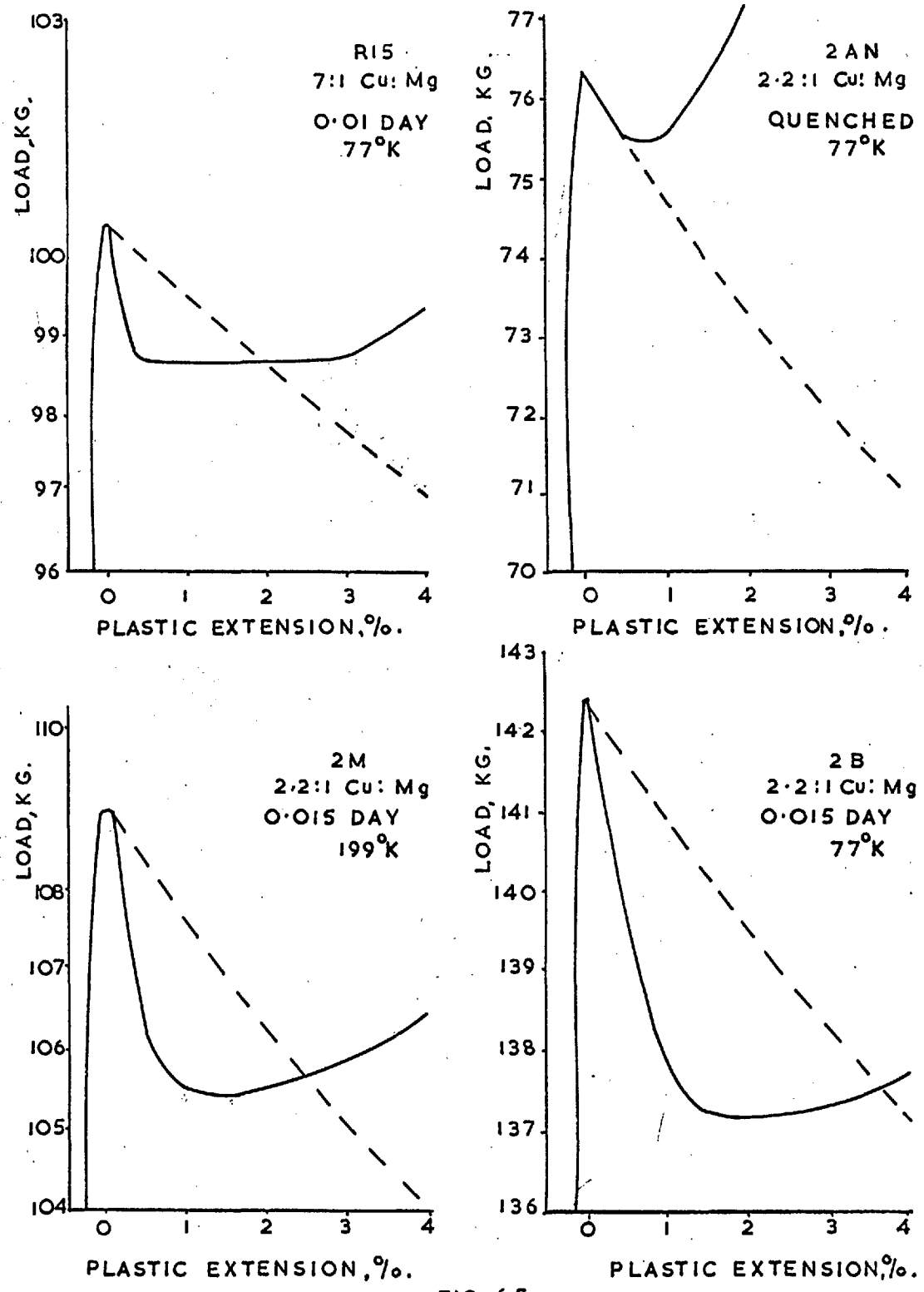

FIG. 65.

YIELD POINTS IN SOME 7:1 Cu: Mg & 2·2:1 Cu: Mg CRYSTALS.

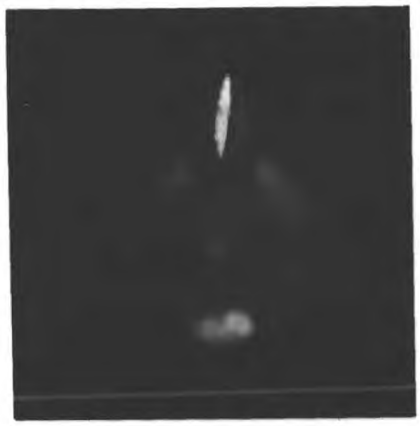

(a) As-quenched x 5

(b) Aged for 0.01 day. x 5

(c) Aged for 0.5 day. x 5

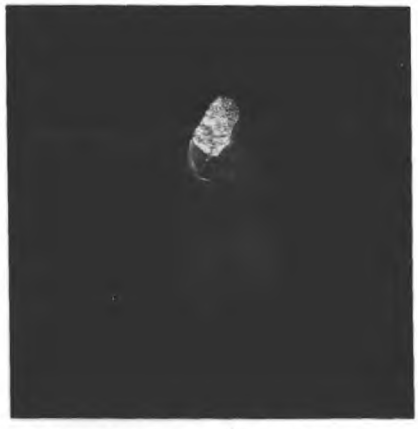

(d) Aged for 10 days. x 5

Fig. 66

7:1, Cu:Mg alloy single crystal fractures, tested at 295°K

(a) Aged for 0.01 day.
x 5

(b) Aged for 0.5 day.
x 5

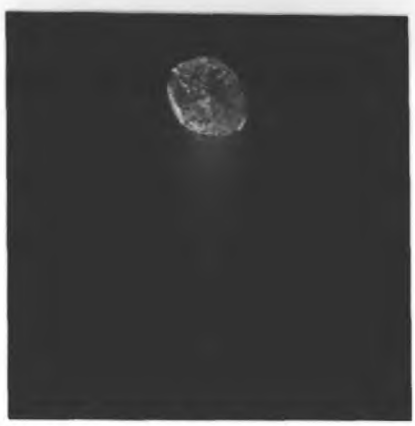

(c) Aged for 10 days.
x 5

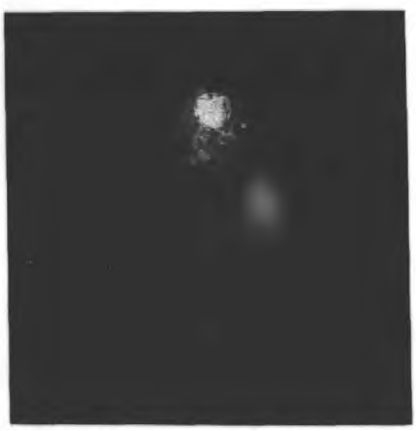

(d) Aged for 10 days.
x 5

Fig. 67

7:1, Cu:Mg alloy single crystal fractures, tested at 77°K

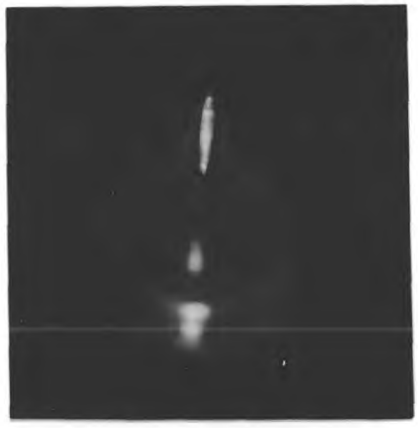

(a) As-quenched x 5

(b) Aged for 0.015 day. x 5

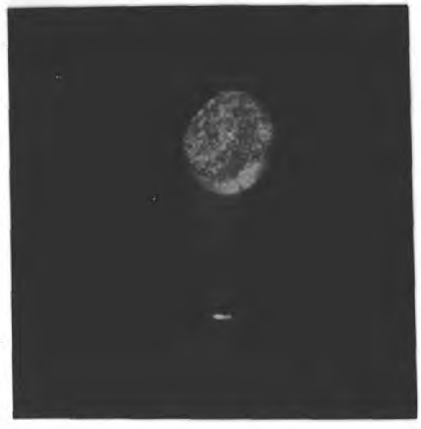

(c) Aged for 0.4 day. x 5

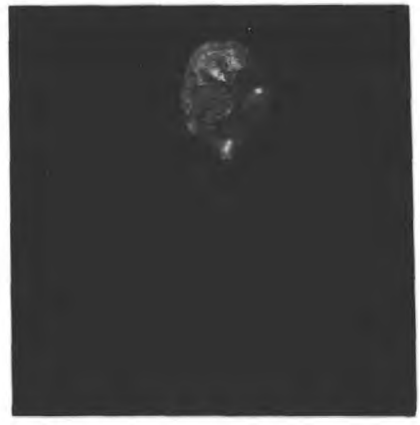

(d) Aged for 10 days. x 5

Fig. 68

2.2:1, Cu:Mg alloy single crystal fractures, tested at 295°K

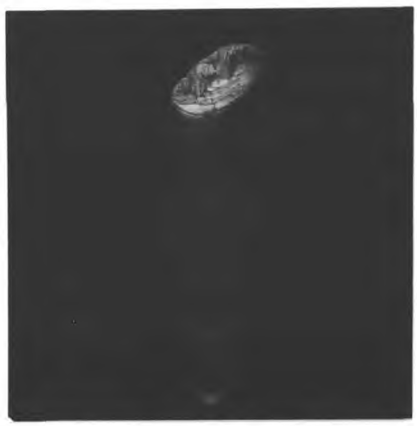

(a) As-quenched. x 5

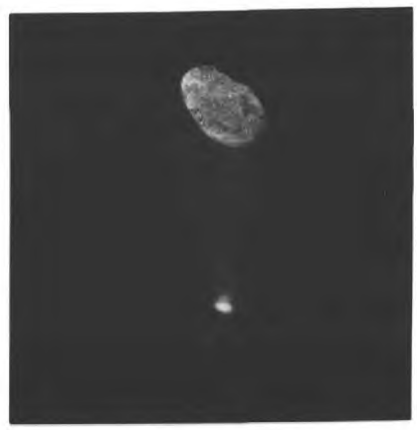

(b) Aged for 0.015 day. x 5

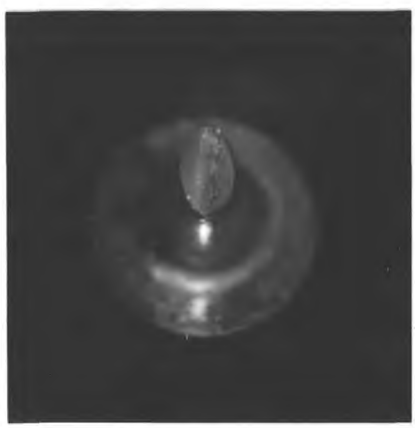

(c) Aged for 0.4 day. x 5

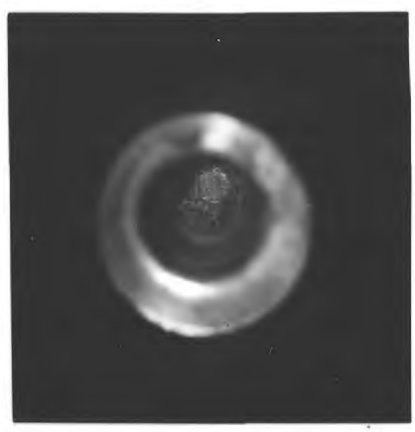

(d) Aged for 10 days. x 5

Fig. 69

2.2:1, Cu:Mg alloy single crystal fractures, tested at 77°K

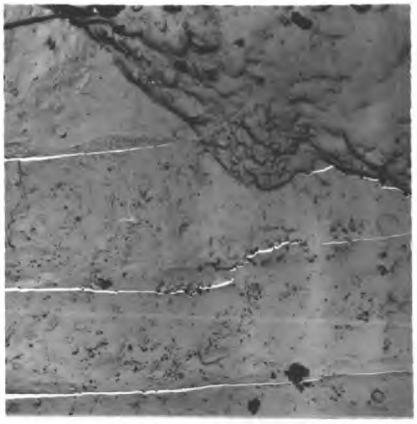

(a) Aged for 0.015 day.
Tested at 148°K
x 2500

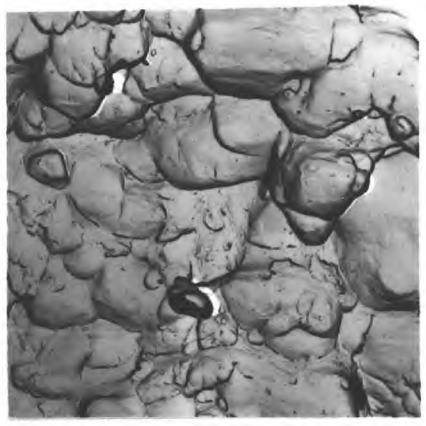

(b) Aged for 0.15 day
Tested at 148°K.
x 6000

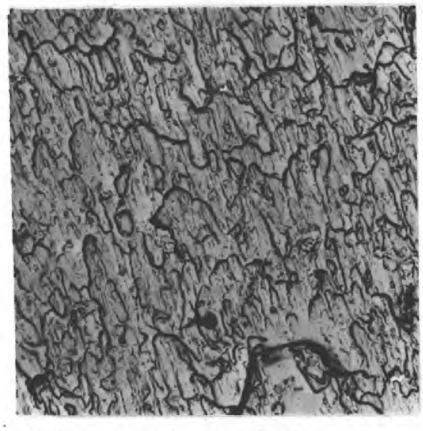

(c) Aged for 0.4 day.
Tested at 173°K
x 6000

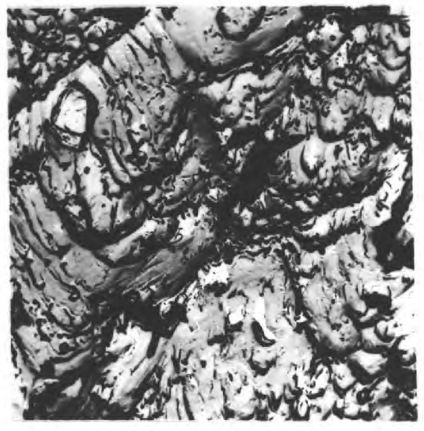

(d) Aged for 10 days.
Tested at 173°K
x 6000

Fig. 70

Fractographs of 2.2:1, Cu:Mg alloy crystals

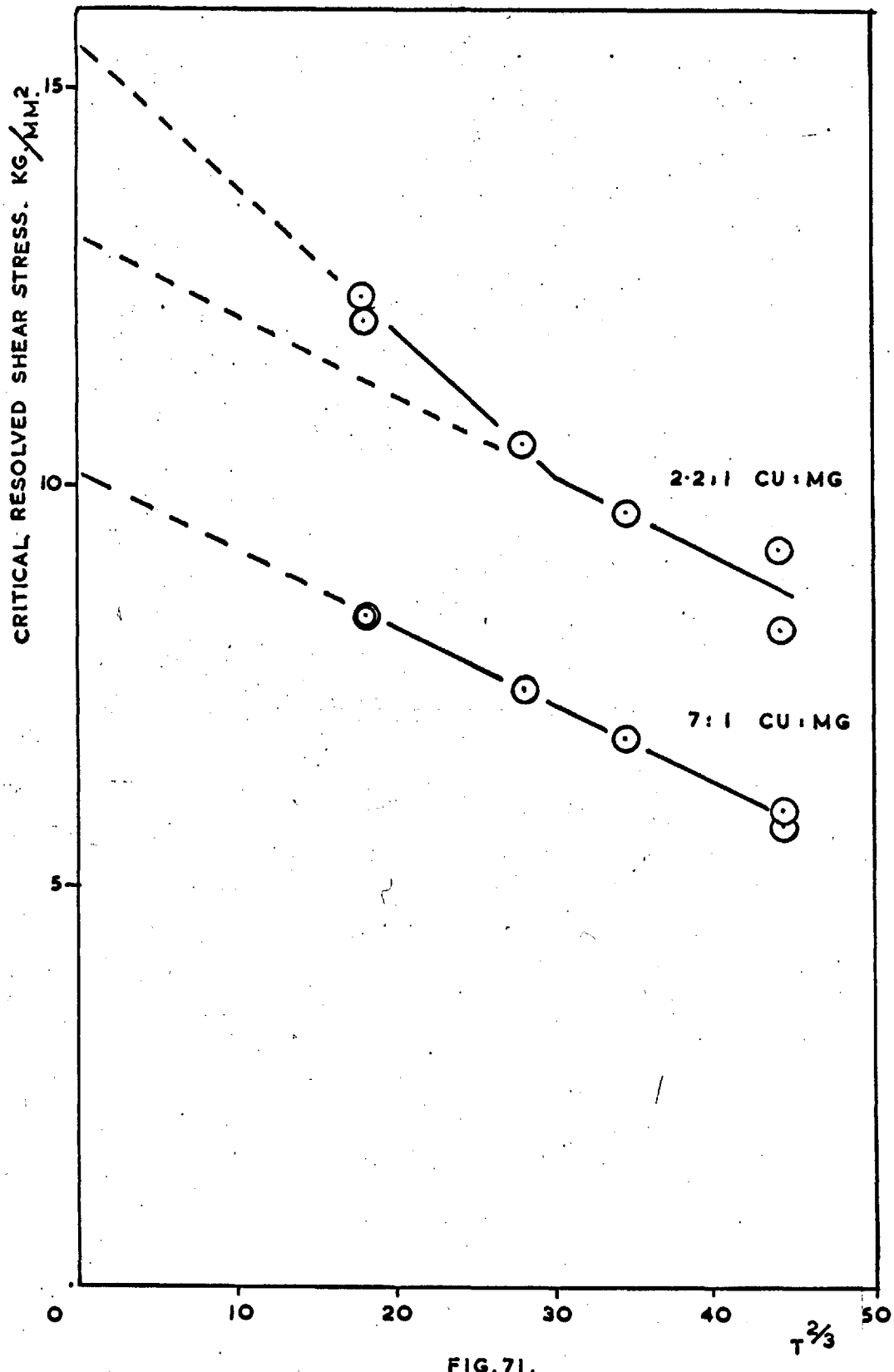

FIG. 71.

$T^{2/3}$ DEPENDENCE OF CRITICAL RESOLVED SHEAR STRESS.

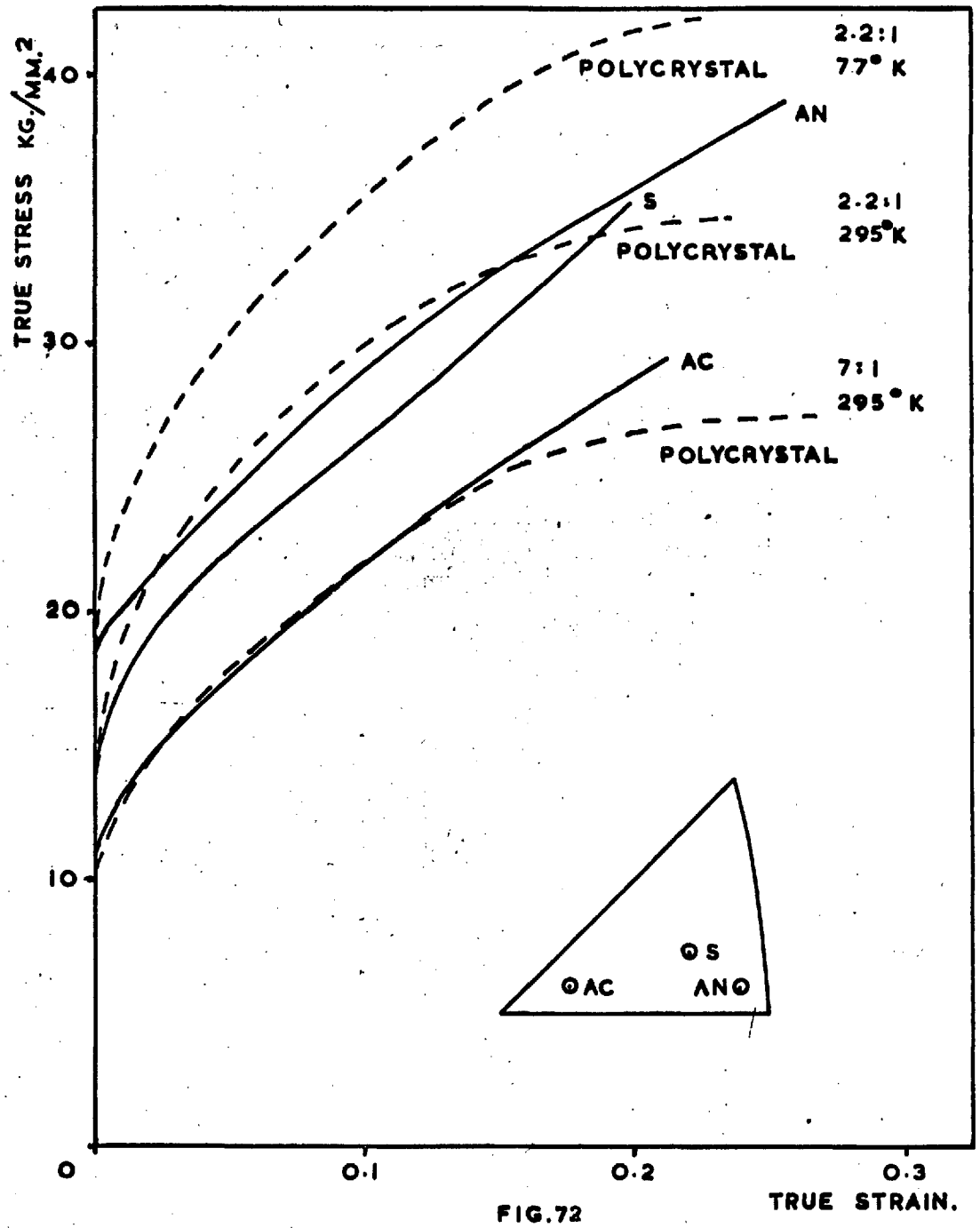

FIG.72

THE COMPARISON BETWEEN AGGREGATE AND POLYCRYSTAL STRESS-STRAIN CURVES FOR AS-QUENCHED ALLOYS.

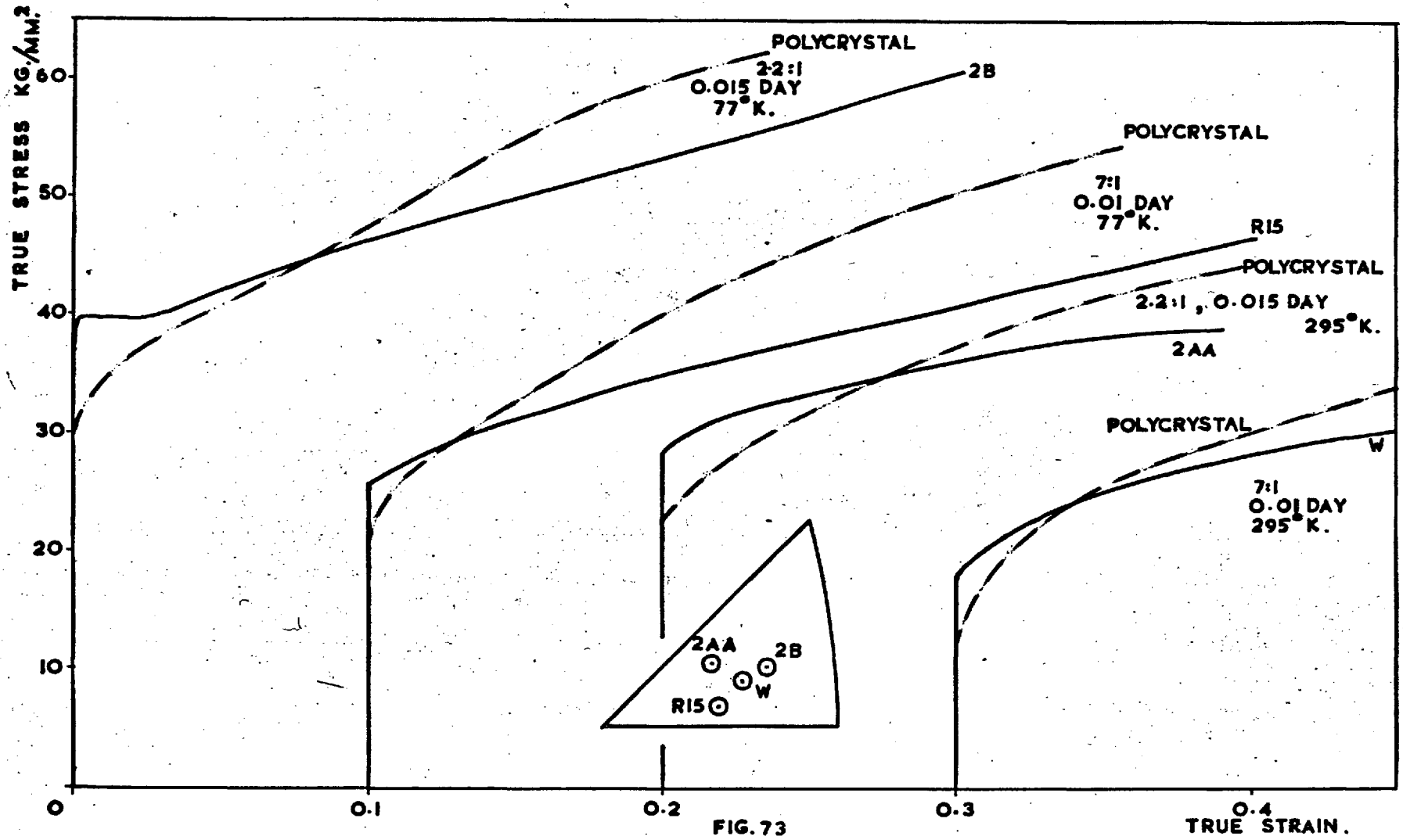

FIG. 73

THE COMPARISON BETWEEN AGGREGATE AND POLYCRYSTAL STRESS-STRAIN CURVES FOR LIGHTLY-AGED ALLOYS.

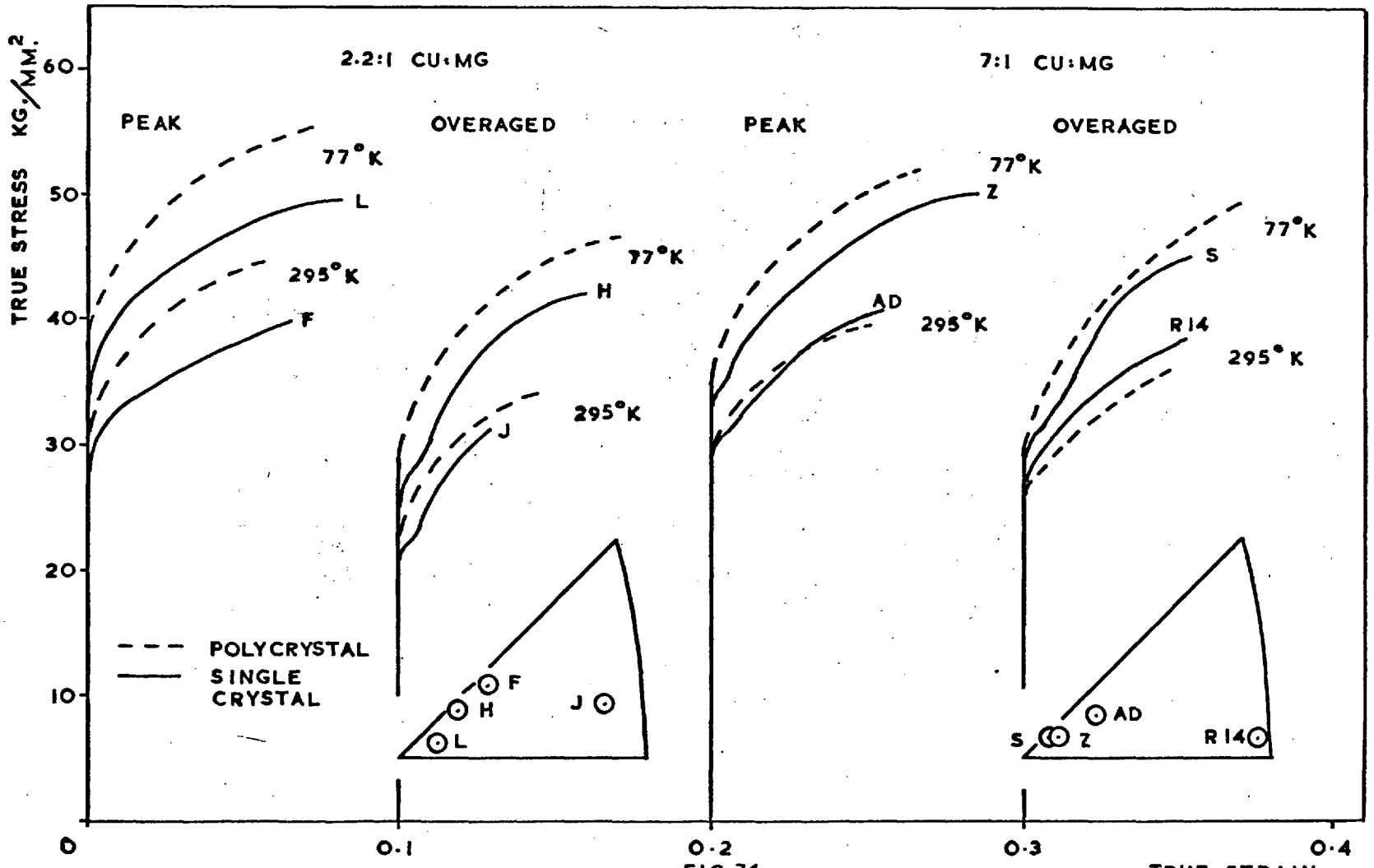

FIG.74

THE COMPARISON BETWEEN TRUE STRESS - TRUE STRAIN CURVES FOR PEAK AND OVERAGED SINGLE CRYSTALS AND POLYCRYSTALS.

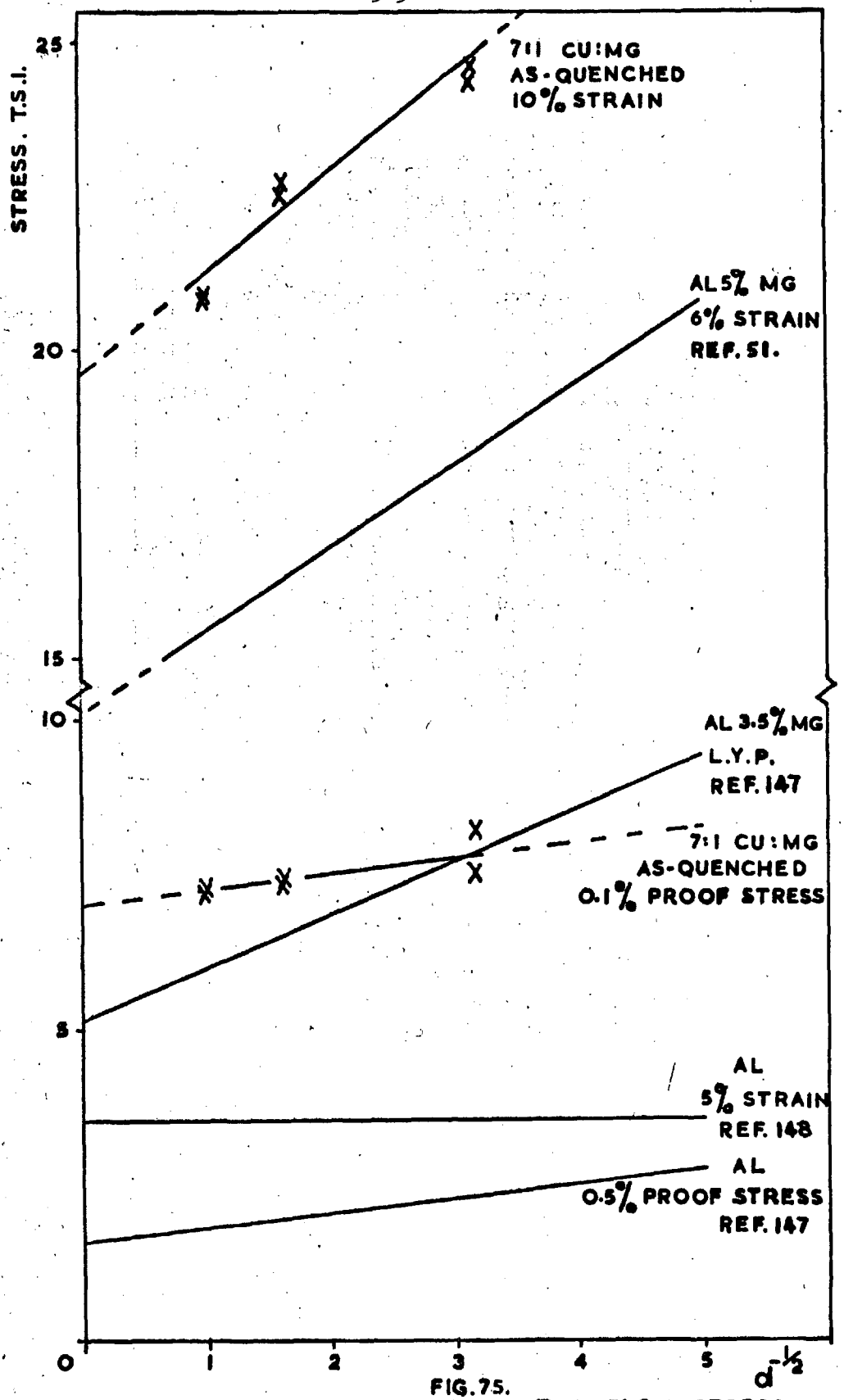

FIG. 75.
THE GRAIN SIZE DEPENDENCE OF THE FLOW STRESS.

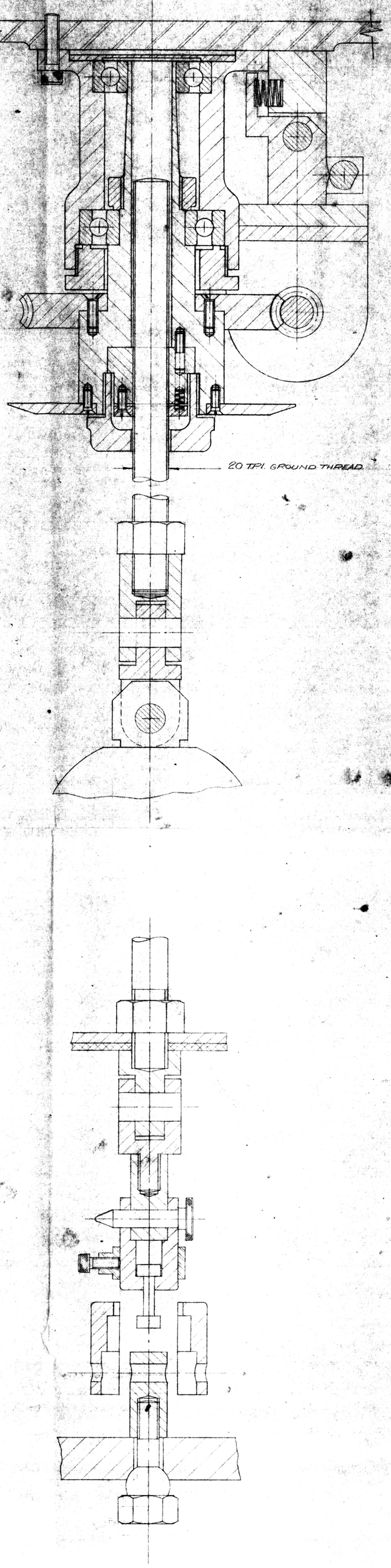

LONGITUDINAL SECTION ON ℄ THROUGH STRAINING MECHANISM.
(SCALE :- FULL SIZE)

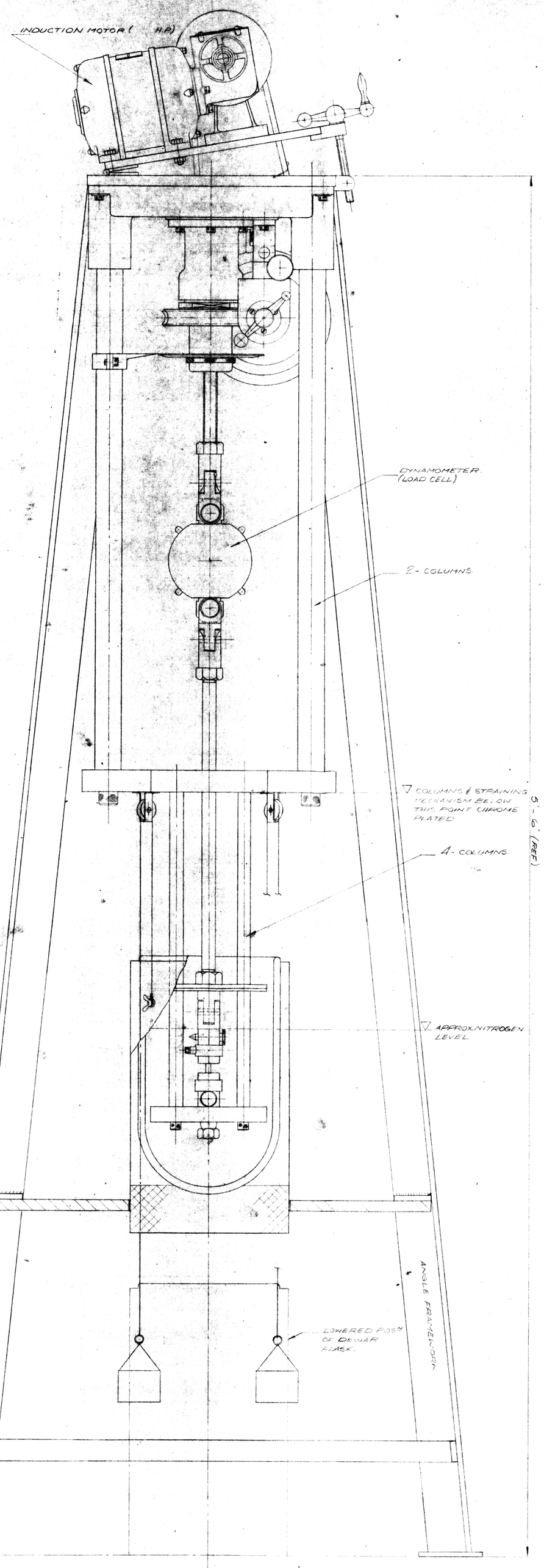

ELEVATION WITH PAIR OF LEGS OMITTED FOR CLARITY.
(SCALE :- 3/8 x FULL SIZE)

CURRY F.R. Ph.D.

FIG.1.

TENSILE TESTING MACHINE